Synaptic and non-synaptic communication between neurons and oligodendrocyte precursor cells in the somatosensory cortex

Paloma P. Maldonado Maldonado Rojas

THÈSE DE DOCTORAT

UNIVERSITÉ PARIS DESCARTES
École doctorale Génétique Cellules Immunologie Infectiologie Développement

Présentée par
Paloma P. Maldonado Rojas

Sujet de la thèse :

Communication synaptique et non-synaptique entre neurones et cellules précurseurs d'oligodendrocytes dans le cortex somatosensoriel

Pour obtenir le grade de
DOCTEUR de l'UNIVERSITÉ PARIS DESCARTES

Sous la direction de **María Cecilia Angulo**

Devant un Jury composé de :

M.	Charbel	MASSAAD	Président du Jury
M.	Christian	GIAUME	Rapporteur
Mme.	Maria	KUKLEY	Rapporteuse
M.	Tommaso	FELLIN	Examinateur
Mme.	María Cecilia	ANGULO	Examinatrice

Contents

Abstract/Résumé

Oligodendrocyte precursor cells (OPCs) are the main source of myelinating oligodendrocytes during postnatal development. These progenitors, identified by the expression of the proteoglycan NG2, are extremely abundant before myelination, but also persist in the mature brain. Similarly to other non-neuronal cells they express a wide range of ionic and ligand-gated ion channels. However, they are unique by their ability to receive truly glutamatergic and GABAergic synaptic contacts from neurons.

During this thesis, we characterized the electrophysiological properties of OPCs during the postnatal development of the mouse somatosensory cortex (first postnatal month). By performing patch-clamp recordings, single-cell RT-PCR analyses and pharmacological approaches, we found that outwardly rectifying I-V curves become linear during development, as the result of an upregulation of Kir4.1 potassium channels. Endowed with these channels, adult OPCs are able to sense local extracellular potassium increases generated by neuronal activity. This developmental upregulation of Kir4.1 channels in OPCs revealed that these cells gain physiological properties during development, conferring them the capacity to communicate with neurons, *via* a non-synaptic potassium-mediated mechanism. This developmental change also supports the view that OPCs are probably more than simple progenitors.

In the second part of this thesis, we were interested in study the connectivity patterns underlying the GABAergic interneuron-OPC network in the young somatosensory cortex (second postnatal week). First, we took advantage of the high lateral and axial precision of one-photon holographic photolysis to stimulate GABAergic interneurons at a single cell resolution in order to evoke an action potential. We then used this technique to map the connectivity between interneurons and OPCs. We found that the connectivity probability of OPCs was around half less than that of pyramidal cells and involved more local microcircuits. In addition, by performing paired-recordings, OPCs showed to be transiently contacted by fast-spiking (FSI) and non-fast-spiking (NFSI) interneurons, through single or double release sites. Interestingly, postsynaptic sites containing $GABA_A$ receptors with the $\gamma 2$ subunit were predominantly connected by FSI, indicating that these cells provide a specific input to OPCs. Here we described for the first time the emergence of specific cortical network between neurons and non-neuronal cells.

In conclusion, this thesis contributed to get a better understanding of the different modes of communication between neurons and OPCs and the establishment of new signaling mechanisms used by neurons to control the activity of these precursors.

Keywords: NG2 cells, oligodendrocyte precursors cells, neuron-OPC interactions, $GABA_A$ receptors, non-synaptic communication, holographic photolysis.

Les cellules précurseur d'oligodendrocytes (CPOs) représentent la majeure source d'oligodendrocytes myélinisants durant le développement post-natal. Ces progéniteurs, identifiés par l'expression du protéoglycane NG2, sont non seulement extrêmement abondants avant la myélinisation, mais ils persistent aussi dans le cerveau mature. À l'instar d'autres cellules non-neuronales, elles expriment un large panel de canaux ioniques et de récepteurs pour des neurotransmetteurs. Cependant, ils sont uniques de part leur capacité à recevoir de véritables contacts synaptiques neuronaux glutamatergiques et GABAergiques.

Durant cette thèse, nous avons caractérisé les propriétés électrophysiologiques des CPOs durant le développement post-natal du cortex en champ de tonneaux de la souris (premier mois post-natal). En effectuant des enregistrements de patch-clamp, des analyses par RT-PCR sur cellule unique et des analyses pharmacologiques, nous avons observé que la courbe I-V à rectification sortante devient linéaire durant le développement, résultant d'une régulation positive de l'expression des canaux potassiques de type Kir4.1. Dotés de ces canaux, les CPOs adultes sont capables de détecter les augmentations locales de potassium extracellulaire générées par l'activité neuronale. Cette régulation positive développementale des canaux Kir4.1 dans les CPOs révèle que ces cellules ont un gain de fonction durant le développement, leur conférant la capacité de communiquer avec les neurones *via* un mécanisme non-synaptique lié au potassium. Ce changement développemental soutient aussi l'idée que les CPOs sont probablement plus que des progéniteurs.

Dans la deuxième partie de cette thèse, nous nous sommes intéressés à l'étude des patrons de connectivité du réseau GABAergique interneurones-CPOs dans le cortex en champ de tonneaux jeune (deuxième semaine post-natale). Dans un premier temps, nous avons tiré avantage de la haute précision latérale et axiale de la photolyse holographique en mono-photon pour stimuler les interneurones GABAergiques avec une résolution à l'échelle de la cellule, de manière à évoquer un potentiel d'action. Nous avons ensuite utilisé cette technique pour cartographier la connectivité entre interneurones et CPOs. Nous avons trouvé que la probabilité de connexion des CPOs est près de moitié moins que celle des cellules pyramidales, et implique plutôt une microcircuitrie locale. De plus, en effectuant des enregistrements pairés, nous avons observé que les CPOs sont contactés transitoirement par des interneurones à décharge rapide et à décharge régulière. Ces connections se caractérisents pour la présence d'un ou deux

sites de libération uniquement. Étonnamment, les sites post-synaptiques contenant des récepteurs $GABA_A$ avec la sous-unité $\gamma 2$ sont principalement connectés par les interneurones à décharge rapide, indiquant que ces cellules constituent une afférence spécifique auprès des CPOs. Ici nous décrivons pour la première fois l'émergence de réseaux corticaux spécifiques entre neurones et cellules non-neuronales.

Mots clés: cellules NG2, précurseurs d'oligodendrocytes, interactions neurones-cellules NG2, récepteurs $GABA_A$, communication non-synaptique, photolyse holographique.

Acknowledgments

I would like to thank:
María Cecilia Angulo
My family and friends
Fernando Ortiz
David Orduz
Maddalena Balia
Mateo Vélez- Fort
Eirini Papagiakoumou
Past and present members of the U603
The members of my jury
The ENP staff

Preface

> *Hitherto, gentlemen, in considering the nervous system, I have only spoken of the really nervous parts of it. But if we would study the nervous system in its real relations in the body, it is extremely important to have a knowledge of that substance also which lies between the proper nervous parts, holds them together and gives the whole its form in a greater or less degree*

Words of the German pathologist Rudolf Virchow, from the 13th lecture entitled "Spinal cord and the Brain" (April, 1858), establishing a difference between neuronal elements and supportive tissue (Kettenmann and Verkhratsky, 2008). Nowadays, the cells of this supportive tissue termed by Virchow nervenkitt (nerve-cement) are called glial cells from the greek $\gamma\lambda\acute{\iota}\alpha$ (glue). The rich diversity in their morphology, function and interaction with neurons in the central nervous system (CNS) permits recognition and classification of glia into three main different types: astrocytes, oligodendrocytes and microglia. However, the borderline between one cell-type and another has not been always easy to define, especially because some glial cells share similar properties (Kettenmann and Verkhratsky, 2008). Moreover, this difficulty exists when defining what it is a glial cell and what it is not. In any case, due to their abundance and their presumed role of glue they were considered passive cells until electrophysiological and imaging techniques, developed for neurons in a first instance, were implemented and used to study glial cell properties. Perhaps one of the most striking finding is that glia cells share similar cellular components with neurons that allow them to interact and communicate with each other.

In the early 80's a new non-neuronal cell was characterized in the CNS by properties that enable interactions with neurons in a way never described before. The main function attributed to these cells was their ability to generate oligodendrocytes, therefore consider as a progenitor cell and for this reason, called oligodendrocyte precursor cells (OPCs). However, emerging evidence has suggested that these cells behave not only as progenitors, but also as glia cells.

The main purpose of this thesis was to characterize the interactions between neurons and OPCs, questioning the vision of OPCs as only progenitor cells and providing more

proves to consider them as the fourth glia cell-type in the CNS, and at the same time to combine conventional with non-conventional techniques to study these interactions.

Part I

Introduction

Chapter 1

Oligodendrocyte Precursor Cells (OPCs)

Much evidence has been assembled to define what an OPC is and what differentiate it from other glia. This first section describes these main lines of evidence, with emphasis on its electrophysiological properties, because they confer the ability to interact with neurons, a topic discussed in detail in the next section. In spite of several names given to OPCs, I will always refer to them as OPCs, namely $NG2^+$ cells *in situ*, unless otherwise indicated.

1.1 The discovery

The use of antigens as markers to identify different types of cells is a helpful strategy to map the lineage of cells. With this aim, Stallcup and Cohn (1976) classified cells lines from nitrosoethylurea-induced tumors into neurons or glia based on their excitability, sodium and potassium conductances. Under this criteria, they found cells with a Neural (N), Glial (G) or intermediate phenotype (Neuronal-Glia, NG) (Stallcup and Cohn, 1976). In order to characterize these NG cells, antisera were generated by injecting NG-phenotype cells into rabbits and purified by absorption. Cross-absorbed antisera recognized cell lines with intermediate properties (Wilson et al., 1981). Further works identified the molecular structure of the protein recognized by the antisera, the NG cell-surface molecule (see section 1.2).

Years later, these cells were associated with smooth protoplasmic astrocytes showing NG2 immunolabeling detected with light and electron microscopy, but lacking glial fibrillary acidic protein (GFAP) and S-100, in the molecular layer of the rat cerebellum (Levine and Card, 1987). Nevertheless, their phenotype *in vitro* showed a degree of

plasticity. Cerebellar cells cultured in the absence of serum resembled protoplasmic astrocytes ($GFAP^-$ and GS^-; glutamine synthetase). However, when cultured in the presence of serum they resembled type II astrocytes ($GFAP^+$) (Levine and Stallcup, 1987).

Some years before Levine and Stallcup (1987) described this new cell type with plastic phenotype, also Raff and Miller (1983) characterized 7-day-old rat optic nerve cells that differentiated into type II astrocytes if cultured in the presence of fetal calf serum, or into oligodendrocytes if cultured in the absence of serum. These cells, expressing the ganglioside A2B5, were called O2A cells. Further studies by Stallcup demonstrated that cultured optic nerve O2A $A2B5^+$ cells were also $NG2^+$, allowing him to speculate that cerebellar $NG2^+$ cells and O2A cells were the same cells, however, behaving somehow differently. For this reason, he analyzed the expression of NG2 in cultured O2A cells of the optic nerve. Optic nerve O2A $A2B5^+$ $NG2^+$ cells expressed GS, an oligodendrocyte specific marker, absent in cerebellar $NG2^+$ cells in the same conditions (serum-free), as mentioned before. NG2 and GS were only transiently co-expressed, so when fully developed into oligodendrocytes these cells were $NG2^-$ (Stallcup and Beasley, 1987). In fact this loss of NG2 expression before the end of differentiation to oligodendrocytes is the main reason why it has been so hard to demonstrate *in vivo* that the cells described by Raff and Stallcup are OPCs.

Immunolabeling for NG2 have allowed for the observation that OPCs are widely spread and have different morphology in the grey and white matter. In general, they are characterized by a stellate shape with a centrally located soma, from which several long, slender primary processes extend and bifurcate one, two or more times. However, in the grey matter, their arborization tends to be symmetrical and forms connections with neurons, whereas in the white matter, the arborization tends to be polarized along the axons and their processes intermingle with those of astrocytes and oligodendrocytes (Butt et al., 2005).

1.2 The proteoglycan NG2

The epitope NG2 is a chondroitin sulfate proteoglycan of 500 kDa, with a core of 300 kDa (Figure 1.1)(Stallcup et al., 1983). From its amino acid sequence, it is known to have a single membrane-spanning molecule, with a large extracellular domain containing a N-terminal domain stabilized by disulfate bonds; a type VI collagen-binding site; a single chondroitin sulfate chain and a globular domain with at least 2 sites of proteolytic processing. The transmembrane domain of 24 amino acid residues links the extracellular domain with the cytoplasmic tail. This latter contains a PDZ binding motif, a proline rich segment and several potential sites for threonine phosphorylation (Nishiyama et al., 1991; Stallcup, 2002). These domains are represented in figure 1.1.

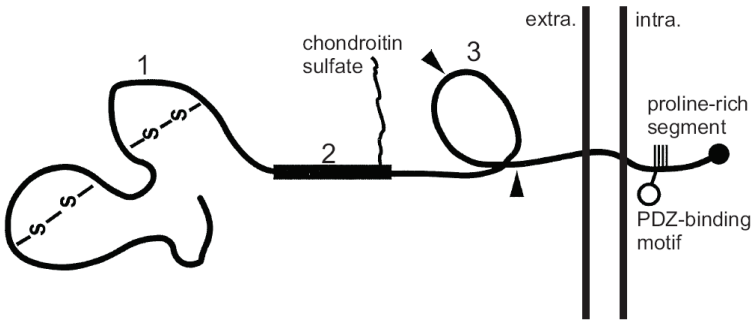

Figure 1.1: **Structure of the transmembrane proteoglycan NG2.**
1, N-terminal globular domain, stabilized by disulfide bonds. 2, central domain: VI collagen-binding site (bold segment) and a single chondroitin sulfate chain. 3, membrane-proximal globular domain, containing proteolytic sites (head arrows). Adapted from Stallcup (2002).

The elucidation of the NG2 structure allowed definition of its interactions with the extracellular and intracellular partners shedding light on its possible functions. The proteoglycan contributes to processes such as cell proliferation and cell motility, which are crucial for the cell functioning. This contribution is possible, on one hand, because the NG2 is capable of binding both growth factors: basic fibroblast growth factor (bFGF) and platelet-derived growth factor α (PDGFα), through interaction with its core (Goretzki et al., 1999). These are critical mitogens for OPCs, which proliferate in response to them (Nishiyama et al., 1996). On the other hand, the NG2 can interact with some extracellular matrix components, for example the type IV collagen, promoting cell spreading and cell motility. This probably occurs due to transmembrane signaling events that lead to dynamic rearrangements of the actin cytoskeleton (Fang et al., 1999). Furthermore, a recent study has revealed that NG2 regulates the OPC polarity, necessary to direct migration through the interaction between its PDZ-binding motif and the RhoAGTPase, a small protein of the G-protein signaling (Binamé et al., 2013). Through this same binding motif, the NG2 can also interact with the glutamate receptor interaction protein 1 (GRIP1); the latter acts as a molecular link between AMPA receptors and the proteoglycan NG2 *in vitro* (Stegmüller et al., 2003; Trotter et al., 2010). Although, this complex has not been observed *in vivo* yet.

1.3 Other markers

Though important for OPCs, the proteoglycan NG2 does not exclusively mark these cells. Indeed, NG2 is also expressed by other cell types such as developing mesenchymal cells in the cartilage, muscle and bone and pericyte/smooth muscle cell in the vasculature (Stallcup, 2002). For this reason, the most specific marker that allows for the unequivocally identification of OPCs is the PDGFα receptor. The expression of

OPC	Astrocyte	Oligodendrocyte	Microglia
NG2	GFAP	O4	F4/80
PDGFαR	GLAST	Olig2	CD11b/CD18
Olig2	GS	SOX10	ILB4
SOX10	S100β	Galactocerebroside	Iba1
		MBP	

Table 1.1: **Principal markers of the fourth main glia cells**. From Nishiyama et al. (2009); Kettenmann et al. (2011).

this receptor is visible in the ventral ventricular regions of the embryonic spinal cord and in the subventricular zone (SVZ) of the embryonic and postnatal animals prior to the expression of NG2 (Nishiyama et al., 1996). Other markers less specific are Olig2 and SOX10 (see Table 1.1)(reviewed by Nishiyama et al., 2009).

Table 1.1 summarizes the principal markers related to OPCs and shows that these cells are antigenically distinct from astrocytes, oligodendrocytes and microglia.

1.4 Origin and fate of OPCs

By using a cre-lox fate mapping approach, it has been shown that OPCs are generated from three temporally sequenced migrating waves in the embryonic telencephalon (Figure 1.2). A first wave (embryonic day 12.5, E12.5) from the medial glanglionic eminence (MGE) and anterior entopeduncular area (AEP); a second wave (E15.5) from the lateral and/or caudal ganglionic eminences (LGE and CGE); and finally, a third wave (E16) that arises in the cortex (Kessaris et al., 2006).

Figure 1.2: **Origin of forebrain OPCs.**
Three sequential waves of OPCs from the telencephalic ventricular zone. The colors indicate different populations. MGE, medial glanglionic eminence; AEP, anterior entopeduncular area; LGE, lateral ganglionic eminence; CGE, caudal ganglionic eminence. Adapted from Kessaris et al. (2006).

In postnatal stages, OPCs are widely distributed in the whole brain. Although the

OPC density decreases with development (Vélez-Fort et al., 2009), they still comprise 8-9% of the total cell population in the adult white matter and 2-3% of total cells in the adult grey matter (Dawson et al., 2003). Moreover, by cumulative bromodeoxyuridine labeling (BrdU, an analogue of thymidine that is incorporated in the DNA during replication), it has been possible to determine the number of dividing OPCs. For all rat adult brain regions tested (cortex, hippocampus and *corpus callosum*), 70-75% of the $BrdU^+$ cells were $NG2^+$ and 1-4% of them divided over the course of 2 hours (Dawson et al., 2003). These results indicate that OPCs represent the major cycling cell type in the adult rodent brain.

Before the evidence that OPCs were a proliferative population of cells, able to respond to proliferative agents as PDGFα (Richardson et al., 1988; Noble and Murray, 1984), these cells were associated to different differentiation capabilities during development. This have generated large controversies in the field. The idea that OPCs have a plastic fate arises first from cultured O2A cells that generate astrocytes or oligodendrocytes according to the cultured medium. However, cultured systems do not necessarily reflect a situation *in vivo* and thus gave only indirect evidence of possible different OPC fates. By performing experiments utilizing BrdU, it is possible to recognize OPCs during cell division. Experiments performed using this methodology, revealed that the majority of proliferating cells of the spinal cord were immature glial progenitors ($NG2^+$ cells) and persisted as immature glial progenitors during four weeks post-BrdU injection. Moreover, at four-week post-injection, 10% of the dividing cells expressed markers for astrocytes and oligodendrocytes (Horner et al., 2002). However, this study only shows a correlation between the number of proliferating OPCs and newly generated oligodendrocytes/astrocytes, lacking a direct trace of the OPC fate. In addition, cultured OPCs under certain extracellular signals give rise not only to astrocytes and oligodendrocytes, but also to neurons, leading to call them "multipotential" CNS stem cells (Kondo and Raff, 2000).

To determine more directly the identity and fate of OPCs, a lineage-tracing method using the cre/lox approach is needed. When the Cre enzime is expressed under the OPC promoter in transgenic mice with a determined flox reporter line, the expression of the reporter gene is permanently activated in OPCs and their progeny. This technique revealed that during development, oligodendrocytes of both grey and white matters of the forebrain and the spinal cord derived from OPCs (Zhu et al., 2008a,b). In the same studies, the authors also demonstrated that OPCs gave rise to a subset of protoplasmic astrocytes. Nevertheless, this capacity of OPCs to generate astrocytes is restricted to embryonic states (Zhu et al., 2011). Conversely, in the adult, OPCs only generate oligodendrocytes and this has been confirmed by several groups, using different promoters for OPC identification: PDGFαR-Cre (Kang et al., 2010), NG2-Cre (Zhu et al., 2011), Olig2-Cre (Dimou et al., 2008).

After initial evidence of neurogenesis from OPCs, two fate mapping studies also showed the generation of projecting neurons in the piriform cortex (Rivers et al., 2008) and

of immature neurons in the ventral forebrain, dorsal cerebral cortex and hippocampus (Guo et al., 2009). Some of the above cited studies also evaluated neurogenesis from OPCs (Kang et al., 2010; Zhu et al., 2008b, 2011), but they did not find any evidence of OPC-derived neurons. No consensus has been established on this issue and these discrepancies are still unresolved. However, the expression of the reporter on neurons could be explained by (1) ectopic expression of Cre, labeling other cells rather than the targeted ones, or (2) it is possible that NG2 and PDGFα receptor is expressed in SVZ and hippocampal stem cells expressing the reporter (Belachew et al., 2003; Aguirre and Gallo, 2004; Aguirre et al., 2004) given rise to a population of neurons. Future experiments should help to clarify thus point.

1.5 Self-renewal population of OPCs in the normal and injured brain

By their abundance and widespread distribution in the whole CNS, OPCs constitute the most important proliferative cell population of the brain. The length of the cell cycle of OPCs vary with the age and the brain region (Table 1.2). Similar values have been observed by Kukley and Dietrich (2009); Simon et al. (2011); Hughes et al. (2013).

Brain region	PN6	PN60	PN240	PN540
corpus callosum	1.7±0.2	9±2	72±21	75±18
cortex	2±0.2	18±3	76±28	170±54

Table 1.2: **OPC cycling time (in days) during postnatal development according to the brain region.** From Psachoulia et al. (2009).

This capacity of renewal arises many questions on the mechanisms that maintain OPC density and distribution in the brain. Only recently, these mechanisms started to be elucidated. Notably, time-lapse two-photon imaging experiments in the adult demonstrated that the control of OPC population is, at least partly, determined by self-repulsion (Hughes et al., 2013). Indeed, OPCs survey their environment by filipodia motion and cone extension. In the adult hypothalamus, all OPCs are able to proliferate and restore OPC population after a mitotic blockade. Interestingly, the repopulation derives exclusively from OPC resident cells (Robins et al., 2013).

Proliferation is an important feature of OPCs during the first postnatal month since these cells generate myelinating oligodendrocytes. However, the reasons why these cells continue to cycling in the normal adult brain when myelination is complete are less understood. There are two alternatives that could explain this OPC renewal; one possibility is that OPCs generate oligodendrocytes to myelinate unmyelinated axons in regions such as subcortical white matter or cortical grey matter; or, to remodel existing myelinated axons, in regions where changes in the neuronal plasticity are required.

Young et al. (2013) has investigated these alternatives and they have found that OPCs generate oligodendrocytes in regions where myelination occurs in a large majority of axons, like the 4-month-old optic nerve, suggesting that newly generated oligodendrocytes are implicated in myelin remodeling. Moreover, new oligodendrocytes produce more and shorter internodes than oligodendrocytes produced at early stages of development. The diminished internode length could influence, along with other factors, the axonal speed conduction (Young et al., 2013). It is not excluded, however that, in addition, to myelin remodeling, OPCs reside in the adult brain to play undiscovered roles.

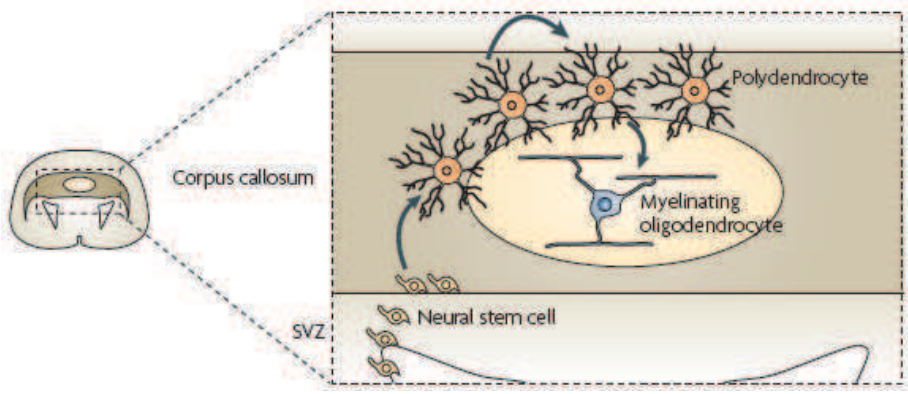

Figure 1.3: **Schematic representation of events occurring during a demyelination lesion in the *corpus callosum*.**
Diagram of a coronal section of the brain with *corpus callosum* in dark brown (left). A demyelinating lesion is represented by a yellow oval. A magnification of the lesion (right) shows proliferation of resident OPCs followed by differentiation into oligodendrocytes and/or SVZ progenitor mobilization to the lesion. From Nishiyama et al. (2009).

The dynamic of oligodendrocyte generation has been also evaluated in injury conditions, since it is not clear if in demyelinating diseases such as multiple sclerosis (MS), the failure of remyelination is due to impairment in OPC recruitment and/or differentiation (Franklin and Ffrench-Constant, 2008). After demyelinating lesions, OPCs proliferate and generate remyelinating oligondendrocytes (Reynolds et al., 2002; Watanabe et al., 2002; Polito and Reynolds, 2005). Indeed, following demyelination, resident OPCs or those recruited from the SVZ (Menn et al., 2006) proliferate around the lesion and differentiate into oligodendrocytes (Figure 1.3) (reviewed by Nishiyama et al., 2009). In the proliferation stage, OPCs re-enter the G1 phase very fast and the length-time of the cycle is shortened (Simon et al., 2011). This explains the three-fold increase in OPC density (Figure 1f, Sahel et al., Annex). Immediately after lesion, OPCs reorient and extend their processes toward the injured region; this process is followed by migration to the lesion ensuring an efficient replacement of oligodendrocytes (Hughes et al., 2013). Although a lesion generates a general gliosis, there are evidences that astrogliosis come from a resident pool of astrocytes or from migration of ependymal zone stem cells and not from OPCs (Dimou et al., 2008; Tripathi et al., 2010).

1.6 Physiological properties

Glial cells are often electrically coupled, have more negative resting membrane potential (E_m) than neurons, have a predominantly potassium membrane permeability and are considered as non-excitable cells (Barres, 1991). In this section, we will see how many of these features are or not shared by OPCs.

1.6.1 Intrinsic membrane properties

The study of the electrophysiological properties of specific glial cell types has not been easy for two main reasons: they are relatively small cells and it is difficult to distinguish one cell type from another. Some of these problems have been overcome by the development of the patch-clamp technique and the use of transgenic mice where the glia of interest specifically expresses a fluorescent protein.

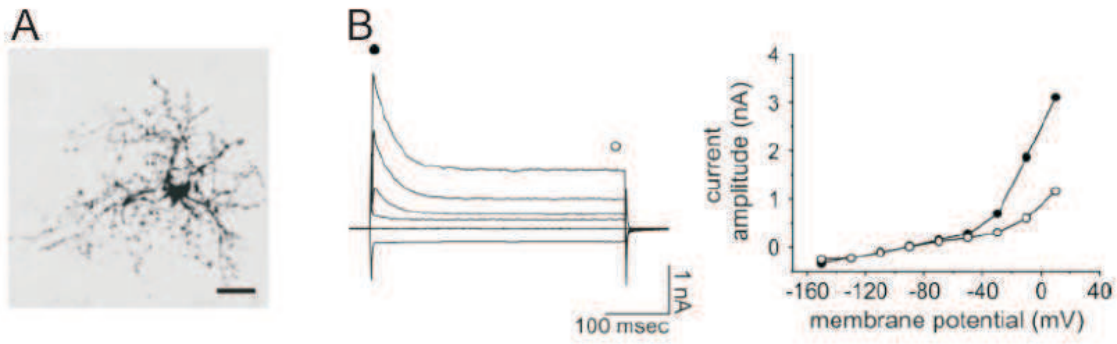

Figure 1.4: **Electophysiological profile of a hippocampal OPC.**
A. Confocal image of a recorded OPC loaded with biocytin and revealed with streptavidin coupled to a fluorescent dye. Scale bar, 20 μm.
B. Current responses elicited, in the same OPC held at -90 mV, by voltage steps from -150 mV to +10 mV (left). IV curve of currents at the peak (black circle) and at the steady state (open circle). From Vélez-Fort et al. (2009).

Although the identity of OPCs has been controversial in the past, they exhibit a characteristic electrophysiological profile (Figure 1.4.) One major characteristic that distinguishes these cells from protoplasmic astrocytes is their lack of cell-to-cell dye coupling. The absence of biocytin-labeled networks of OPCs strongly suggests that these cells are not coupled by gap junctions (Figure 1.5) (Lin and Bergles, 2002; Giaume and Naus, 2013; Vélez-Fort et al., 2009). In addition, connexins 30 and 47, well described markers for astrocytes and oligodendrocytes, respectively, are very poorly expressed in OPCs according to a transcriptome assay (Cahoy et al., 2008).

In acute slices, OPC membrane properties seem to vary according to the brain re-

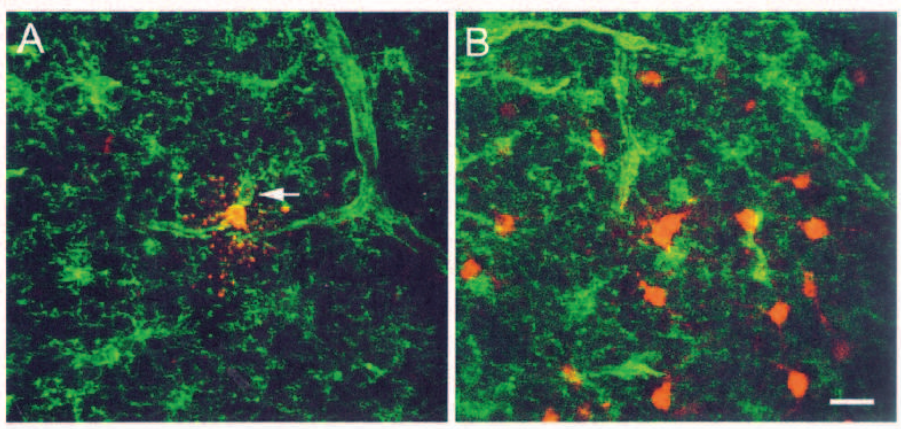

Figure 1.5: **Comparison of dye coupling between OPCs and astrocytes in the hippocampus.**
A. OPC loaded with biocytin, revealed with Cy5-streptavidin and identified by immunostaining against the NG2 protein (green). The arrow indicates no dye coupling between the cells.
B. Astrocyte loaded under the same conditions. However, diffusion of biocytin reaches several adjacent cells. Scale bar, 20 μm. From Lin and Bergles (2002).

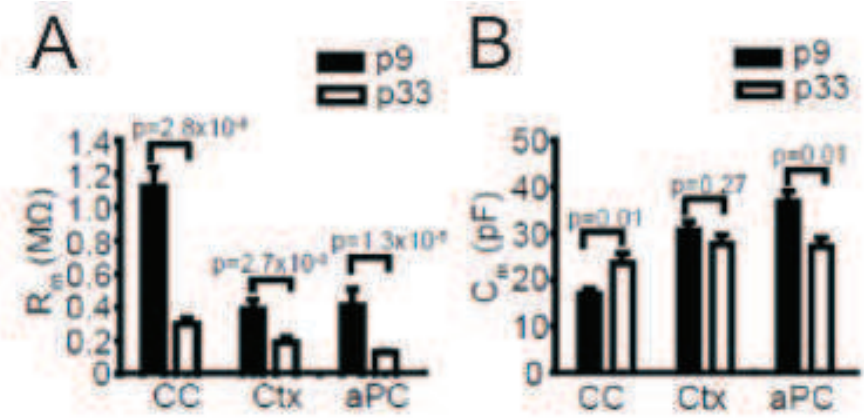

Figure 1.6: **Membrane intrinsic properties of OPCs during development.**
A and B. Membrane resistance (A) and capacitance (B). Comparison between PN9 and PN33 in three different brain regions: CC, *corpus callosum*; Ctx, motor cortex; aPC, anterior piriform cortex. From Clarke et al. (2012).

Brain region	Membrane potential (mV)	Membrane resistance (mΩ)	Membrane capacitance (pF)
white matter	-70±5	≈2500	8±1
grey matter	-87±5	≈500	40±1
Differentiation stage			
OPC	-89±0.4	≈300	20±1.3
Pre-oligodendrocyte	-87±0.9	≈450	74±8.5
Oligodendrocyte	-58±1.7	≈60	48±6.6

Table 1.3: Membrane intrinsic properties of OPCs according to the brain region and at different stage of differentiation from the *corpus callosum*. From Chittajallu et al. (2004); De Biase et al. (2010).

gion, the stage of differentiation (Table 1.3) and the developmental stage (Figure 1.6). Chittajallu et al. (2004) suggest that white and grey matter OPCs represent different developmental stages of the same cell or two subpopulations of OPCs. In any case, the electrophysiological differences between OPCs in different regions probably reflect a different ionic channel composition.

1.6.2 Potassium channels

Outward currents

In the past, OPCs were also called "complex" cells because of their voltage-dependent potassium and sodium currents, different from $GFAP^+$ "passive" astrocytes(Steinhäuser et al., 1992, 1994).

After depolarizing voltage steps, OPCs display a characteristic pattern of voltage-dependent currents. A rapidly inactivating A-type (I_{KA}) and a sustained delayed rectifier type potassium current (I_{KDR}), blocked by 4-aminopyridine (4AP) and tetraethylammonium (TEA), respectively (Figure 1.7 A and B)(Kressin et al., 1995). It is has been shown that cultured OPCs, identified as glia progenitors by the expression of the intermediate filament protein vimentin (Keilhauer et al., 1985), express all RNA transcripts of the voltage-gated potassium channel family Kv1 (from 1.1 to 1.7). However, initial observations showed that only Kv1.4, Kv1.5 and Kv1.6 proteins were expressed and, from them, only homomeric Kv1.5 seemed to be functional (Attali et al., 1997; Schmidt and Eulitz, 1999). Later, it was demonstrated that Kv1.3 was also functionally expressed in OPCs (Chittajallu et al., 2002).

Kv1 channels (for voltage-gated potassium channels) are shaker-type potassium chan-

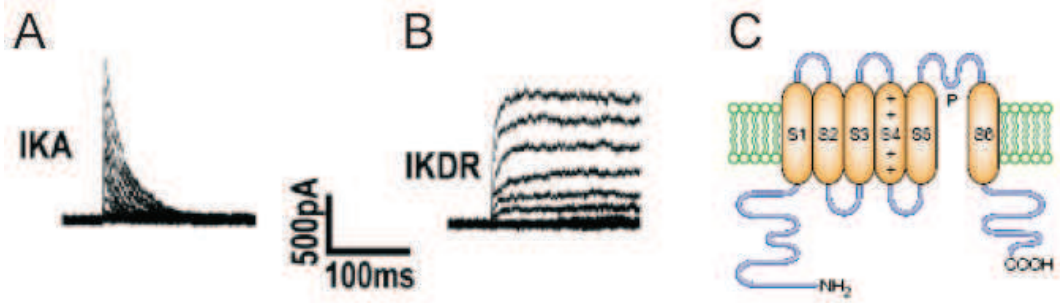

Figure 1.7: **Potassium outward currents of OPCs.**
A and B. Both transient I_{KA} (A) and sustained voltage-dependent I_{KDR} (B) outward currents in an OPC. These currents were deduced from two different voltage step protocols as described in Chittajallu et al. (2002, 2005).
C. Schematic representation of a voltage-gated potassium channel. Note the presence of six differents transmembrane segments (S1-S6). From Choe (2002).

nels, existing as tetramers with each subunit having six transmembrane helices (S1-S6). The pore domain is formed by the S5 and S6 helices and a short loop between them. The S4 domain has positively charged residues that act as a voltage sensor, conferring to the channel the capacity to respond to changes in membrane potential (Figure 1.7 C)(Choe, 2002). In neurons, these channels produce predominately low threshold, rapidly activating, and slowly inactivating currents, and are thus well suited to control subthreshold events such as E_m, subthreshold oscillations, and action potential threshold (Coetzee et al., 1999; Hsiao et al., 2009). In O2A cells, however, delayed rectifier potassium currents are implicated in cell proliferation. Signals that block these potassium currents consequently generate a reduction in the PDGF or bFGF-induced proliferation. These signals can be mediated for example by the activation of AMPA/kainate glutamate receptors that induces increases of intracellular calcium and sodium concentrations and, indirectly, reduces OPC potassium currents, having an anti-proliferative effect (Gallo et al., 1996; Knutson et al., 1997). Moreover, proliferative O2A cells express larger outward-rectifying currents than non-dividing immature and mature oligodendrocytes. In fact, there is an upregulation of potassium currents that occurs in the G1 phase of the cell cycle and reflects a selective increase in expression of the potassium channel subunit Kv1.3 and 1.5 proteins. Nevertheless, the block of Kv1.3-mediated currents inhibits the proliferation, whereas the antisense oligonucleotide for Kv1.5, that causes a reduction in its expression, does not affect O2A cell proliferation (Attali et al., 1997).

Finally, it has been suggested that type-A and delayed rectifying potassium currents of *in situ* CA1 hippocampal OPCs decrease during postnatal development (Kressin et al., 1995), but no evidence exists showing that this phenomenon is a general feature of OPCs in other brain regions. Moreover, delayed rectifying potassium currents of OPCs are larger compared to those of $O4^+$ pre-oligodendrocytes in subcortical white matter (PN4-PN7). Conversely, I_{KA} currents remain the same in both cell types (Chittajallu

et al., 2005). In addition, inactivating I_{KA}, I_{KDR} and inward type potassium currents are larger in grey matter compare to white matter (Chittajallu et al., 2004).

Inward currents

In addition to outward currents, OPCs exhibit inward rectifying currents visible after hyperpolarizing voltage steps (Steinhäuser et al., 1992; Kressin et al., 1995). These currents were described for the first time by Barres et al. (1990b) in O2A cells and also reported in other glia cell types such as Müller cells, astrocytes and oligodendrocytes (Barres et al., 1990b,a). The identification of the channel mediating this inward current was achieved in 1995, with the report of a novel ATP-dependent inward rectifier potassium channel predominantly expressed in glial cells, presumably oligodendrocytes (Takumi et al., 1995). This channel was later named Kir4.1 channel (for review on Kir Channels, see Hibino et al., 2010).

As Kv channels, Kir channels are also tetramers, but with only two transmembrane domains and a pore loop between them (Figure 1.8 A). The inward rectification is caused by polyamine or magnesium block, which plug the conduction pathway during depolarization and thereby impede the outward flow of potassium (Figure 1.8 A)(reviewed by Bichet et al., 2003). The Kir4.1 channel subclass is an ATP- and pH-sensitive, weakly rectifying channel (Hibino et al., 2010) known to be mainly expressed in astrocytes, oligodendrocytes and Müller cells of the retina (Poopalasundaram et al., 2000). I will briefly refer to the function of this channel described in glia. I will not discuss the expression of this channel in neurons, since their expression is controversial and has never been confirmed *in situ* (Neusch et al., 2001, for example in spinal cord neurons).

The best characterized role of Kir4.1 channels has been done in astrocytes. The first role assigned to these channels is their participation in keeping E_m close to the reversal potential for potassium. Indeed, a conditional knockout mouse for this channel targeted to astrocytes shows an elevated E_m (Djukic et al., 2007). Nevertheless, the effect of 100 μM barium on E_m of astrocytes is larger than that observed in Kir4.1 knockout mice, suggesting that a Kir4.1 deletion does not change directly astrocyte membrane properties, but possibly affects other channel/transporter function leading indirectly to membrane depolarization (Djukic et al., 2007). The linear I-V relationship in astrocytes also has been associated to high expression of Kir4.1 (Seifert et al., 2009). However, it is not clear if it is the only channel responsible for this linearity, since astrocytes express also the two-pore-domain potassium channels TREK-1 and TWIK-1 (Zhou et al., 2009).

Neuronal activity leads to transient increases in extracellular potassium concentrations, due to the release of potassium during the falling phase of the action potential (Hille, 2001). The major protagonists involved in the potassium clearance are astrocytes,

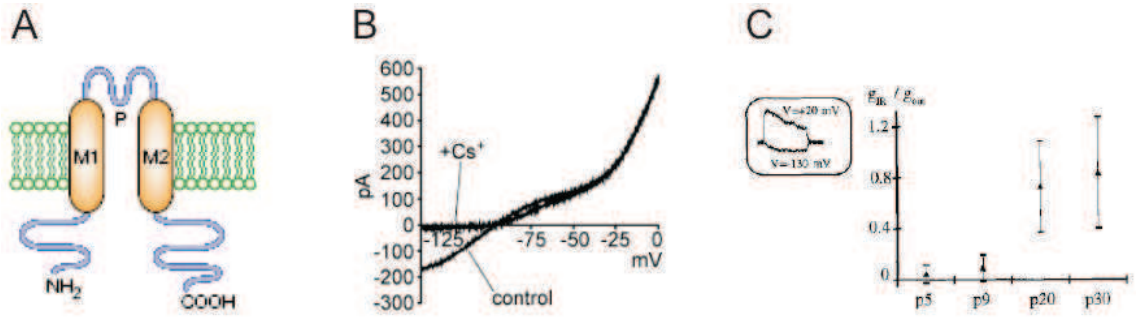

Figure 1.8: **Potassium inward currents of OPCs.**
A. Schematic representation of a Kir potassium channel. Note the presence of only two transmembrane segments separated by a pore loop. From Choe (2002).
B. Ramp protocol showing an inward current identified by its sensitivity to extracellular 5 mM cesium at hyperpolarizing potentials. From Chittajallu et al. (2004).
C. Developmental course of hippocampal complex current phenotype in complex glia. Note that the ratio gIR/gout is increased by the upregulation of inward currents. gIR, maximum inward conductance; gout, maximum outward conductance. From Kressin et al. (1995).

through a process called potassium spatial buffering (Orkand et al., 1966; Kofuji and Newman, 2004, review). Particular characteristics of these cells allow them to perform this function: astrocytes are electrically coupled through gap-junctions forming a continuum (network or syncytium) and they express high levels of channels selectively permeable to potassium. The potassium spatial buffering consists of a potassium flow in astrocytic networks from regions of elevated concentration to regions of lower concentration *via* Kir (probably Kir4.1) channels (Djukic et al., 2007). This is possible because there is a local driving force for potassium created by its concentration increase in the extracellular space. The potassium flow results from the created local potassium potential and the membrane potential of the syncytium (Figure 1.9) (reviewed by Kofuji and Newman, 2004). In addition to this mechanism, there is a specialized form of potassium buffering called potassium siphoning in the retina Müller cells (Karwoski et al., 1989). In the retina, Müller cells are the principal glial cell type. Due to a non-uniform distribution of the Kir4.1 channels in their membrane, the excess of potassium from the inner layer of the retina is siphoned by Müller cells to the vitreous humor (reviewed by Kofuji and Newman, 2004).

As well as in astrocytes and Müller cells, Kir4.1 channels are expressed in oligodendrocytes. Interestingly, a Kir4.1$^{-/-}$ mouse shows impairment of the maturation of oligodendrocyte lineage cells and of myelination. The mice die prematurely (PN8-PN15) and display severe hypomyelination, as well as white-matter vacuolization, incomplete myelin compaction and axonal degeneration in the spinal cord (Neusch et al., 2001). It is noteworthy that the hypomyelination exhibited by the Kir4.1$^{-/-}$ mouse, might be not a direct consequence of the Kir4.1 deficit, but rather a decrease in the number

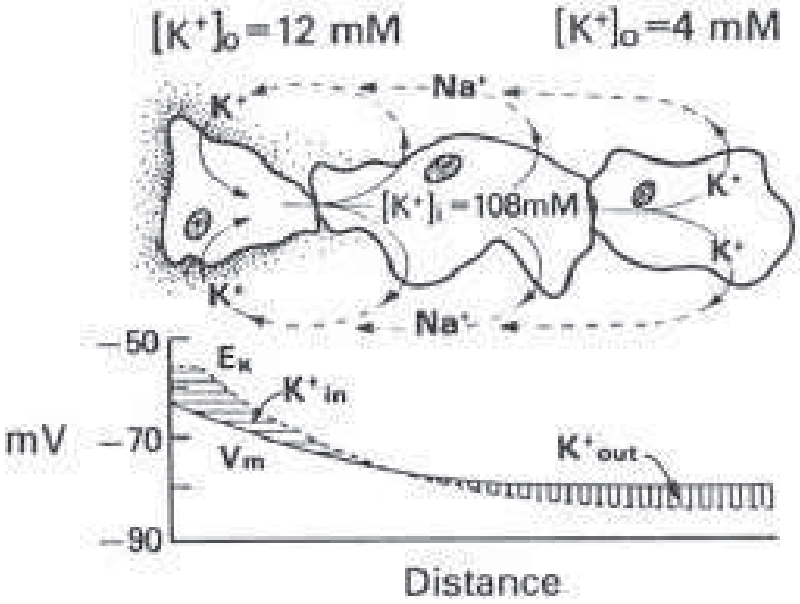

Figure 1.9: **Spatial potassium buffering.**
Schematic representation of potassium buffering mechanism. A local increase of extracellular potassium from 4 mM to 12 mM produces a local depolarization that spreads trough the astrocytic syncytium (top). There is a potassium influx when $V_m < E_m$ and a eflux when $V_m > E_m$ (bottom). From Kofuji and Newman (2004).

of OPCs (denominated complex cells) that lead to a reduction in the normal oligodendrocytes production (Djukic et al., 2007).

In OPCs, small inward currents are sensitive to barium (Kressin 1995), cesium and desipramine (Tang et al., 2009), all antagonists of the Kir4.1 channel, indicating that this current is probably mediated by this channel (Figure 1.8 B). Even if the presence of Kir4.1 has been described in OPCs, in culture and young animals, their expression is weaker compared to that of astrocytes (Tang et al., 2009) and reaches high levels only in differentiated oligodendrocytes (Neusch et al., 2001). Compared to Kv potassium channels, the role of Kir4.1 in OPCs has been poorly described, probably because of its low expression in these cells. Tang et al. (2009) suggested that they may contribute to the OPC resting potassium conductances as well as in astrocytes. The inward current observed by Kressin et al. (1995) in OPCs is upregulated during development (Figure 1.8 C), however, the phenotype of the recorded cells, claimed as complex cells is not completely conclusive, since they also observe a decrease in sodium current amplitudes during development. Indeed, from work of our laboratory and others, we know that OPCs also express sodium currents in the adult (more details in section 1.6.3). Thus, it is plausible that they have recorded both astrocytes and OPCs, and mainly astrocytes in the adult. Further experiments in mature stages are needed in order to evaluate the expression and possible role of these channels in OPCs and how they could determine new features in OPC physiology.

1.6.3 Sodium channels

One of the important hallmarks of OPCs is the expression of sodium voltage-dependent channels (Nav channels). Barres et al. (1989) characterized the sodium currents of the glial progenitor O2A. They observed a current density of 100 pA/pF, similar to that in neurons (in the same conditions), and also similar in terms of voltage dependence, kinetics and TTX sensitivity.

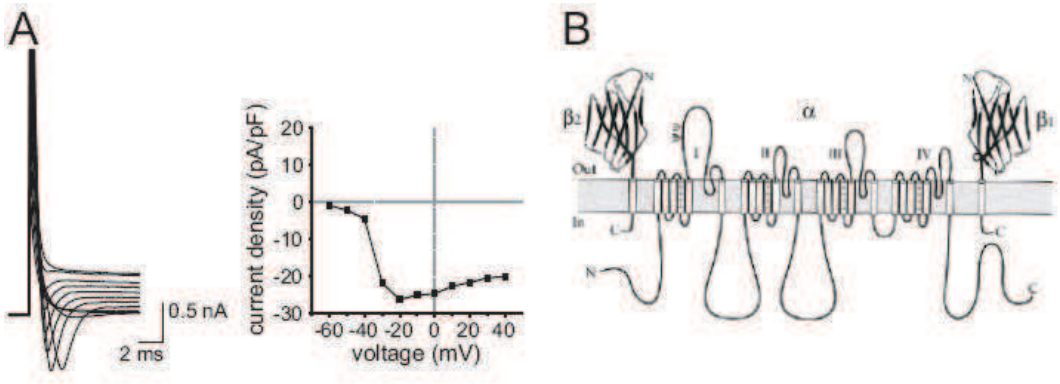

Figure 1.10: **Sodium currents of OPCs.**
A. Schematic representation of a voltage-gated sodium channel. Note the presence of the four domains (I-IV) of the α subunit and the auxiliary subunits β1 and β2. From Hille (2001).
B. Sodium currents elicited, in a OPC (PN6) held at -90 mV, after voltages steps from -60 to +40 mV, recorded with a CsCl-based intracellular solution, containing 4AP and TEACl in a NG2-DsRed transgenic mouse (left). Corresponding I-V curve obtained after leak subtraction (right). From Maldonado et al. (2011, see Annex).

In situ, OPCs expressed variable but lower density currents than O2A cells, but still have fast activation and inactivation kinetics and sensitivity to tetrodotoxin (TTX) (Figure 1.10 A)(Xie et al., 2007). In order to properly study these fast currents, which have a time course of activation/inactivation of 2 ms, Xie et al. (2007) used fresh isolated $NG2^+$ glia and also blocked the potassium conductances. From Table 1.4, it is clear that the current parameters change when the recordings were done in these conditions. The molecular functional identity Nav isoforms present in OPCs have not been identified yet, since the IC_{50} value is higher than those values attributed to any known isoform in the CNS (Xie et al., 2007). However, a mRNA array analyses shows that the subunits Nav1.1, 1.2, 1.3 and Nax are upregulated comparing those in oligodendrocytes (Cahoy et al., 2008; De Biase et al., 2010).

Nav channels are form by α(1-9) and β(1-3) auxiliary subunits. The α subunits comprise four domains (I-IV) that in turn are formed by six transmembrane segments (S1-S6). Between S5 and S6 there is a re-entrant loop, these three elements form the pore. Besides, the S4 segment serves as a voltage sensor (Figure 1.10 B)(Catterall,

	I_{Na} threschold (mV)	I_{Na} peak (mV)	I_{Na} current density (pA/pF)
NG2 glia *in situ* with K^+ conductance	-39.0±4.5	7.0±9.2	15.7±9.4
Freshly isolated NG2 glia with K^+ conductance	-45.0±6.2	-8.3±7.1	9.5±5.3
Freshly isolated NG2 glia with K^+ conductance inhibited	-50.5±10.1	-5.9±10.1	10.3±6.5

Table 1.4: **Sodium currents differences between *in situ* and freshly isolated OPCs.**
$*p<0.05$. From Xie et al. (2007).

2000a). In neurons these channels are responsible for initiation of the action potential (Bean, 2007). Considering this role in neurons and that OPCs also express Nav channels, it seems obvious to test their response under depolarizing current injections (current-clamp). In current-clamp mode, a proportion of mouse OPCs from grey matter at PN5-PN10 displayed a single spike (Figure 1.11)(Chittajallu et al., 2004), but never a train of action potentials as in neurons. The spike described initially by Chittajallu et al. (2004), had a threshold at -26 mV, it was followed by a pronounced hyperpolarization, and some of them also exhibited an after-depolarization. Although sensitive to the sodium channel blocker TTX, this spike was clearly different to a mature neuronal action potential, it had a larger threshold, the peak did not reach the sodium reversal potential and the spike duration was longer. Chittajallu et al. (2004) also studied this spike ability relative to the sodium current amplitude. As expected, the spiking ability was proportional to the magnitude of the sodium currents.

It is noteworthy that the same type of spike was observed by other labs and our group (Ge et al., 2009; De Biase et al., 2010; Maldonado et al., 2011, see Annex). However, in Káradóttir et al. (2008). OPCs of rat cerebellar white matter (PN7-PN12), presumably identified by $NG2^+$ post-immunolabeling, exhibited two different phenotypes: one type expressed sodium currents, generated real action potential discharges like neurons and they were more sensitive to damage caused by stroke; the other type lacked all these features (Karadottir, 2008). Until now, no reports have reproduced these results. Moreover, De Biase et al. (2010), showed that OPCs from diverse mouse brain regions, including the cerebellar white matter, never discharge action potentials. In their own words: "It is possible that the excitable cells described by Káradóttir et al. (2008) correspond to interneurons rather than $NG2^+$ cells". To clarify this issue, Clarke et al. (2012) used a PDGFαR-GFP transgenic mouse that allows identification of cells of the oligodendrocytes lineage and performed NG2 post-immuno labeling for GFP^+ OPC identification. They showed that OPCs in white and grey matters all express sodium channels and approximately 70% of them are able to generate one or few small spikes, but differently from action potentials discharges described by Káradóttir et al. (2008).

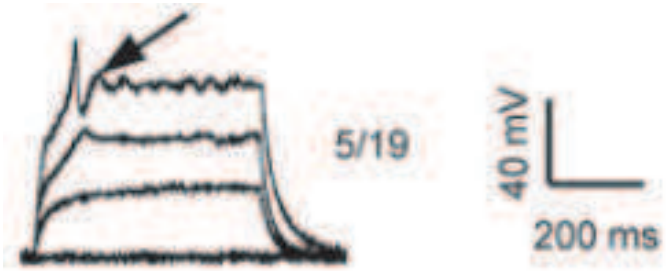

Figure 1.11: **Generation of immature spikes in cortical OPCs.**
Example of membrane responses in a cortical OPC upon depolarizing current injections. In these experiments, 5 out of 19 spiking OPCs displayed a small afte-depolarization (arrow). From Chittajallu et al. (2004).

They state: "The difference in spiking behavior we observed in mouse OPCs compared with rat OPCs (Káradóttir et al., 2008) might reflect the fact that mouse OPCs have a six-fold lower ratio of net inward current to membrane resistance than was found previously for rat INa OPCs" (Clarke et al., 2012). To resolve this controversy, it will be necessary to reproduce the experiments performed in rat white matter cerebellum. Concerning the presence of sodium currents, De Biase et al. (2010) found that all OPCs have sodium currents. Supporting this issue, Kukley et al. (2010), found that the differentiation of OPCs to oligodendrocytes is accompanied with a loss on sodium currents, suggesting that the lack of sodium current in some OPCs correspond to a more mature differentiation stage of OPCs.

In the absence of real neuron-like excitability, sodium channels may play other roles in OPCs. Current knowledge indicates that the expression of sodium currents is related to a +25 mV more depolarized E_m compare to astrocytes that lack sodium currents (Xie et al., 2007). The relative permeability ratio pNa/pK, calculated by Xie et al. (2007) is three-fold higher than that of astrocytes and the potential of the window current (the time where the inactivating current is persistently active) is closer to the E_m, indicating that a persistent sodium component is activated at the OPC E_m. All these data suggest that these currents contribute significantly to the more depolarized E_m of OPCs (Xie et al., 2007).

In an attempt to relate OPC sodium currents with a physiological function, it has also been described that an activation of a persistent sodium current in hippocampal OPCs, due to a GABA-induced depolarization, increases the sodium intracellular concentration. This leads to a reversal activity of a type 1 Na^+/Ca^{2+} exchanger (NCX1), which in turn induces an increase in the intracellular calcium concentration. This increase in calcium concentration promotes OPC migration (Tong et al., 2009).

The expression of sodium currents has been observed throughout postnatal development and in white and grey matters (De Biase et al., 2010; Clarke et al., 2012). Con-

versely, the capability to generate spikes is reduced in later developmental stages, due to the increase of potassium conductances. This was systematically tested and found to be true in the hippocampus, cerebellar molecular layer, *corpus callosum* and cerebellar white matter (De Biase et al., 2010; Kukley et al., 2010; Maldonado et al., 2011, see Annex). However, the current density was downregulated gradually as OPC differentiated to oligodendrocytes, where this sodium current was not observed (De Biase et al., 2010; Kukley et al., 2010; Clarke et al., 2012).

1.6.4 Calcium channels

One major source of intracellular calcium concentration increases ($[Ca^{2+}]i$) in OPCs could be mediated by the activation of voltage-gated calcium channels (VGCCs). As well as Kv and Nav channels, VGCCs channels are voltage-gated channels. VGCCs alike Nav channels comprise four domains (I-IV) and six transmembrane segments (S1-S6) (Figure 1.12 A)(Hille, 2001). However, the channel subunit composition is different: $\alpha\beta1\beta2$ and $\alpha1\alpha2\beta\gamma\delta$, for Nav and VGCCs, respectively (Catterall, 2000b). According to their voltage-gated threshold they can be classified in high voltage-activated (L, P, N-type) and low voltage-activated (T-type) channels (Catterall, 2000b). The first evidence of the existence of these channels suggested that inward movement of calcium ions might be involved in the production of the action potential (Fatt and Katz, 1953). However, their unique role in excitable cells is "to translate the electrical signals into chemical signals" (Hille, 2001).

The expression of VGCCs in OPCs is a matter of debate. Some reports showed that OPCs lack this type of voltage-gated mediated currents (Sontheimer et al., 1989; Ge et al., 2006). Others studies, however, have been unable to exclude it (Hamilton et al., 2010). Finally, reports from Christian Steinhauser's laboratory strongly supports the idea that calcium signals in OPCs are mediated, in part, by VGCCs (Figure 1.12 B). In an early study, they identified low and high-voltage activated calcium currents in grey matter OPCs (Akopian et al., 1996). These two classes of calcium channel were previously observed in O2A cells (Kirchhoff and Kettenmann, 1992; Blankenfeld et al., 1992). By performing single-cell RT-PCR in $NG2^+$ cells in hippocampal slices, a recent study has identified mainly the transcripts for L-type channel isoforms Cav 1.2 and 1.3 and the T-type channel isoforms Cav 3.1 and 3.2 (Haberlandt et al., 2011). P/Q and N-type channel isoforms Cav 2.1 and 2.2 were also present, but were less abundant (Haberlandt et al., 2011).

$[Ca^{2+}]i$ signals constitute a universal signaling system of transduction. The calcium ion has the ability to change the electrostatic field and conformation of proteins, controlling in this way many protein functions (reviewed by Clapham, 2007). Indeed, calcium signaling is related to almost any single cell process from muscle cell contraction, proliferation, migration to cell-to-cell communication (reviewed by Berridge et al.,

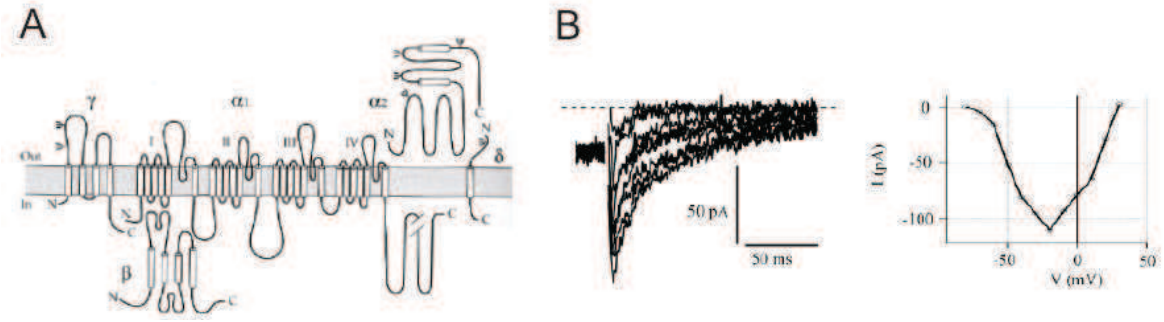

Figure 1.12: **Calcium channels of OPCs.**
A. Schematic representation of a voltage-gated calcium channel. Note presence of four domains of the $\alpha 1$ subunit and the auxiliary subunits: $\alpha 2\beta\gamma\delta$. From Hille (2001).
B. Calcium currents isolated in a OPC by conditioning pre-pulses to -110 and 10 mV and recorded in a sodium and potassium free solution containing sodium and potassium channel blockers (left). Corresponding IV relationships (right). From Haberlandt et al. (2011)

2000). In neurons, in particular, $[Ca^{2+}]$i increases in presynaptic terminals trigger neurotransmitter release; postsynaptically, it activates downstream cascades responsible for modifications in synaptic efficacy (Lisman, 1989) and, in subcellular compartments such as the nucleus, it regulates gene transcription (reviewed by Grienberger and Konnerth, 2012). Different mechanisms can lead to an increase in $[Ca^{2+}]$i: activation of VGCCs, activation of ligand-gated receptors permeable to calcium, activation of transient receptor potential channel (TRP) and the release from endoplasmic reticulum (reviewed by Clapham, 2007). For the propose of this thesis, in the next section I will make reference only to the first two mechanisms mentioned above, because of their main reported implications in OPC physiology.

Calcium signaling

In OPCs, calcium signaling has been implicated in important processes that can result in myelination such as proliferation, motility, migration, differentiation and gene expression. Golli proteins, products of the myelin basic protein gene, modulate calcium uptake via VGCCs, by increasing the size of calcium oscillations observed during the process of extension and retraction of OPC processes that mediates migration in living tissue (Figure 1.13)(Paez et al., 2009). The effect of Golli proteins is exclusive on L-type calcium channels and specifically in OPCs, not in oligodendrocytes (Fulton et al., 2010). A further study of Paez et al. (2011), using golli knockout and overexpressing Golli mice, demonstrate that, in addition to VGCCs, Golli proteins promotes calcium influx *via* store-operated calcium channels (SOCCs) and TRP channels.

It is probably that depolarization induced by activation of ligand-gated receptors leads

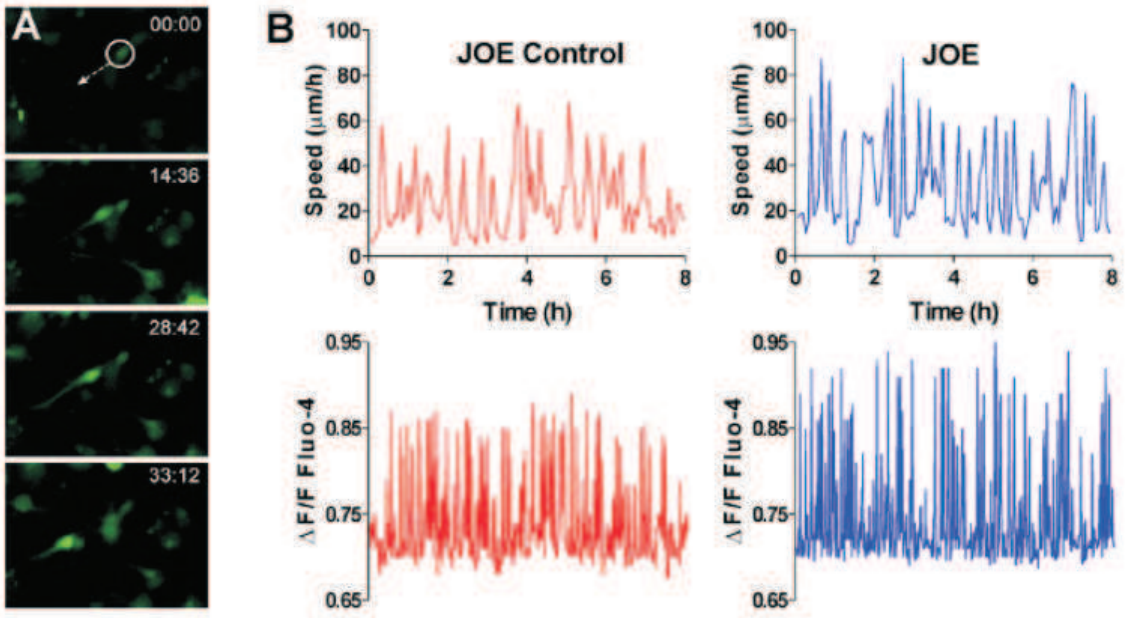

Figure 1.13: **Calcium transients in OPCs during migration.**
A. Time-lapse image of a migrating OPC from primary cultures isolated from a over-expressing Golli J37 protein mouse (JOE mouse).
B. Changes in calcium transients over time in control (red) and JOE mouse (blue). Upward reflections in lines represent elevation of $[Ca^{2+}]i$ in the OPC somata, downward deflections indicate the decrease of calcium levels. Note that the amplitude of calcium oscillations in the JOE mouse are larger compare to the control animal. Adapted from Paez et al. (2009).

to activation of VGCCs in OPCs. These cells express a wide series of ionotropic receptors, mainly glutamate and $GABA_A$ receptors ($GABA_A$Rs). Although this has not been demonstrated directly, here I will discuss the principal lines of evidence that relate activation of ligand-gated receptors, calcium signals and specific functions of OPCs.

Bath application of AMPA receptor (AMPAR) antagonists prevents the proliferation of rat O2A cells and rat cerebellar organotypic slices (Gallo et al., 1996; Yuan et al., 1998). AMPAR-mediated currents lead to a depolarization that causes the upregulation of cyclin-dependent kinase inhibitors, p27 and p21, responsible for cell cycle arrest (Ghiani et al., 1999b,a). Together with this effect, AMPAR activation also prevents the differentiation of O2A cells into oligodendrocytes, but not migration (Gallo et al., 1996).

It has also been described that OPC AMPARs form a complex with αv integrin and the myelin proteolipid protein (PLP). The activation of AMPARs increases the interaction of the receptor subunits with the complex, reducing the binding to the extracellular matrix and enhancing OPC migration. The cell movement was correlated with an increase in intracellular calcium transients *via* a Gi-protein-mediated signaling (Gudz et al., 2006).

Although $GABA_A$Rs in neurons have normally an inhibitory effect by hyperpolarizing the membrane, the activation of $GABA_A$Rs in OPCs induces a depolarization that mediates the activation of either VGCCs (Tanaka et al., 2009; Haberlandt et al., 2011) or a type 1 Na^+/Ca^{2+} exchanger (Tong et al., 2009). This latter promotes OPC dorsorostral migration from the SVZ in neonatal cultured brain slices, as discussed in section 1.6.3 (Tong et al., 2009).

Calcium signals in OPCs have also been associated to the activation of purinergic receptors in the optic nerve (PN12-PN16)(Hamilton et al., 2008) and of α7-containing nicotinic receptors in the hippocampus (Vélez-Fort et al., 2009). Bath application of ATP triggers $[Ca^{2+}]$i increases mediated by P2Y1 and P2X7 receptors. Moreover, axonal electrical stimulation of the optic nerve induces an increase in $[Ca^{2+}]$i in astrocytes that is followed by an increase in OPCs. Since it is known that astrocytes release ATP in response to neuronal activity (Hamilton et al., 2008), one possibility is that astrocytic ATP release could in turn activate OPC purinergic receptors. This work suggests a close interaction between axons, astrocytes and OPCs (Hamilton et al., 2010). Finally, bath application of choline induces increases in $[Ca^{2+}]$i in mouse hippocampal OPCs (7PN-14PN). This signaling was mediated by calcium-permeable α7-containing nicotinic receptors (Vélez-Fort et al., 2009). However, it is still unknown in which conditions these receptors are activated *in vivo.*

In addition to the above referred receptors, other receptors expressed by OPCs could also induce $[Ca^{2+}]$i increases. For example, NMDA receptors (NMDARs) permit the

flow of sodium but can act as a calcium channel as well. All these mechanisms allowing calcium entry are well described for OPCs and correlated with a cellular function, as proliferation, differentiation or migration. However, less is known about the intracellular pathways and the molecular effectors underlying it. Thus, calcium signaling constitutes a mean allowing OPCs to response to their environment.

Chapter 2

Neuron-OPC interactions

Glial cells are able to respond to neuronal activity because they express a large repertoire of ionotropic and metabotropic receptors for neurotransmitters, which are responsible for the activation of receptor-mediated currents and second-messenger pathways, respectively (reviewed by Verkhratsky and Steinhäuser, 2000). Oligodendrocytes and microglia have been long assigned more specialized functions of myelination and defense, respectively, whether astrocytes have been recognized as cells having multiple roles. Astrocytes have attracted the majority of the attention concerning interactions with neurons and modulation of neuronal function, since they are able to respond to neuronal activity in the form of calcium signals leading to gliotransmission (for review see Volterra and Meldolesi, 2005; Perea and Araque, 2005). Nevertheless, there is no evidence that neurons and astrocytes interact *via* classical chemical synapses, therefore neurotransmitters spilling out of the synaptic cleft is likely to be the main signaling mechanism between these two cell types. In this context, when Bergles et al. 2000 described for the first time that OPCs received true functional synaptic contacts from neurons, one of the central dogma of neuroscience stipulating that only neurons have synapses in the CNS, was broken.

2.1 Neuron-OPC synapses

2.1.1 AMPA receptor-mediated synaptic currents

Properties

Characterization of synapses. Rat CA1 hippocampal OPCs (PN12-PN16), present miniature events reflecting the release of a single quantum of neurotransmitter (Figure 2.1 A). OPCs also exhibit evoked excitatory postsynaptic currents (eEPSCs) after electrical Schaffer collateral/commissural fibre stimulation. These currents show paired-pulse facilitation (Figure 2.1 B), are blocked by AMPA/kainate or AMPARs antagonists, NBQX and GYKI 52466, respectively, are potentiated by cyclothiazide and exhibit an inward rectifying I-V relationship in the presence of intracellular spermine. All these results indicate that eEPSCs in hippocampal OPCs are mediated by AMPARs lacking the edited GluR2 subunit, and are thereby permeable to calcium (caAMPARs) (Bergles et al., 2000). It is noteworthy that calcium-impermeable AMPARs are also expressed in OPCs and they contribute to the total AMPAR-mediated synaptic currents (Ge et al., 2009). An estimation of the proportion of caAMPARs durring development in OPCs will be discussed in the next section.

The presence of *bona fide* synapses is confirmed by ultrastructural analyses using electron microscopy, showing direct synaptic junctions between neurons and OPCs, although the post-membrane specializations are thinner than at synapses on dendrites spines (Figure 2.1 C)

Receptor subunit composition. Cultured OPCs express caAMPARs composed by the subunit GluR4 and GluR5, which level (mRNA and protein) are upregulated comparing to those from oligodendrocytes (Itoh et al., 2002). In OPCs, the expression of this type of receptor is dynamic and varies according to different conditions, such as age, brain region and signaling mechanisms. These variables will be described below. In the hippocampus CA1 region, OPC currents induced by stimulation of Schaffer collaterals exhibit a reduction in the I-V rectification between PN8-PN10 and PN13-PN15, and also a reduction in the sensitivity to the synthetic analog of Joro spider toxin, NAS, that selectively blocks caAMPARs (Ge et al., 2006). This indicates a reduction in the caAMPAR-mediated eEPSC during this particular stage of development. Conversely, Ziskin et al. (2007) showed that the currents mediated by caAMPARs in the *corpus callosum* are increased between PN7-PN8 and PN42-PN52. These discrepancies are probably due to the different time-window and brain region analyzed. Finally, it has been shown that the expression and functionality of OPC caAMPARs in the rat optic nerve and cerebellum is a regulated process (Zonouzi et al., 2011). Indeed, caAMPAR-mediated synaptic currents increase after mGluR1/5 receptor agonist (DHPG) application. This change is mainly due to an increase in the receptor conductance and depends on a mechanism involving intracellular calcium increases and the activation of downstream proteins (PI3K, PICK-1 and the JNK pathway). In addition, the expression of auxiliary transmembrane AMPAR regulatory proteins (TARPs) is required for the delivery of caAMPARs at the surface. Conversely, stimulation of OPC P2Y purinergic

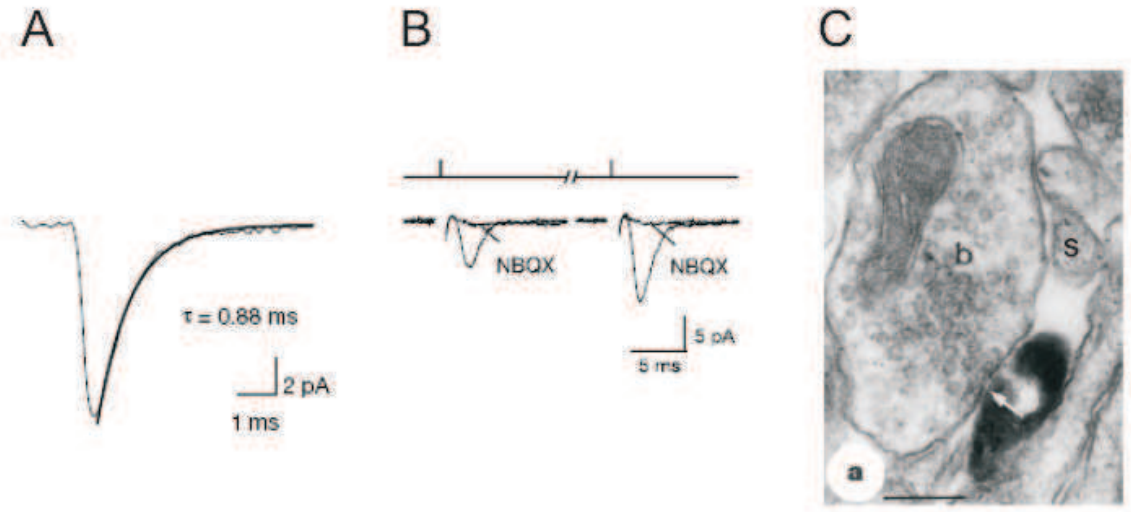

Figure 2.1: **Glutamatergic synapses into hippocampal OPCs.**
A. Average of miniature synaptic events, triggered by pardaxin, a neurotoxine that enhances the frequency of vesicular release. This current was fitted with a single exponential fuction.
B. Paired-pulse stimulation (pulse interval 50 ms). The evoked currents exhibited facilitation and were bloked by NBQX.
C. Electron micrograph of a glutamatergic neuronal terminal contacting a biocytin-labeled OPC (black, peroxidase reaction). Note that the neuronal terminal (b) contacts an OPC (arrow) and, at the same time, a synapse to a dendritic spine (s). Scale bar, 0.2 μm. From Bergles et al. (2000).

receptors decreases the caAMPAR-mediated currents in a calcium dependent manner (Zonouzi et al., 2011).

In conclusion, the regulation of the expression of different types of AMPARs suggests a differential role. Even if the function for this particular type of receptor is still unknown, Ge et al. (2006) demonstrated that evoked theta burst stimulation of Schaffer collaterals in the rat hippocampus induces a long-term potentiation (LTP) of OPC eEPSCs. In contrast to neurons, this glial LTP was independent of NMDARs, but dependent on caAMPARs.

Synaptic characteristics during differentiation. De Biase et al. (2010), by analyzing the gene expression profile database obtained from OPCs, premyelinating oligodendrocytes and mature oligodendrocytes, found that GluR1-4 mRNAs are highly up-regulated in OPCs compare to both premyelinating oligodendrocytes and mature oligodendrocytes. The expression of AMPARs is therefore restricted to the OPC stage. Indeed, once OPCs start to differentiate into oligodendrocytes, their synapses are lost and their AMPARs are downregulated (Figure 2.2) (De Biase et al., 2010; Kukley et al.,

2010). This was also observed in a focal lysolycethin (LPC)-induced demyelinating lesion of *corpus callosum*. After LPC injection, OPCs of the SVZ migrate to the lesion and form glutamatergic synaptic contacts with un- or de-myelinated axons. One week after lesion, differentiated oligodendrocytes also lose their synapses as soon as they start to differentiate (Etxeberria et al., 2010, Sahel et al., Annex).

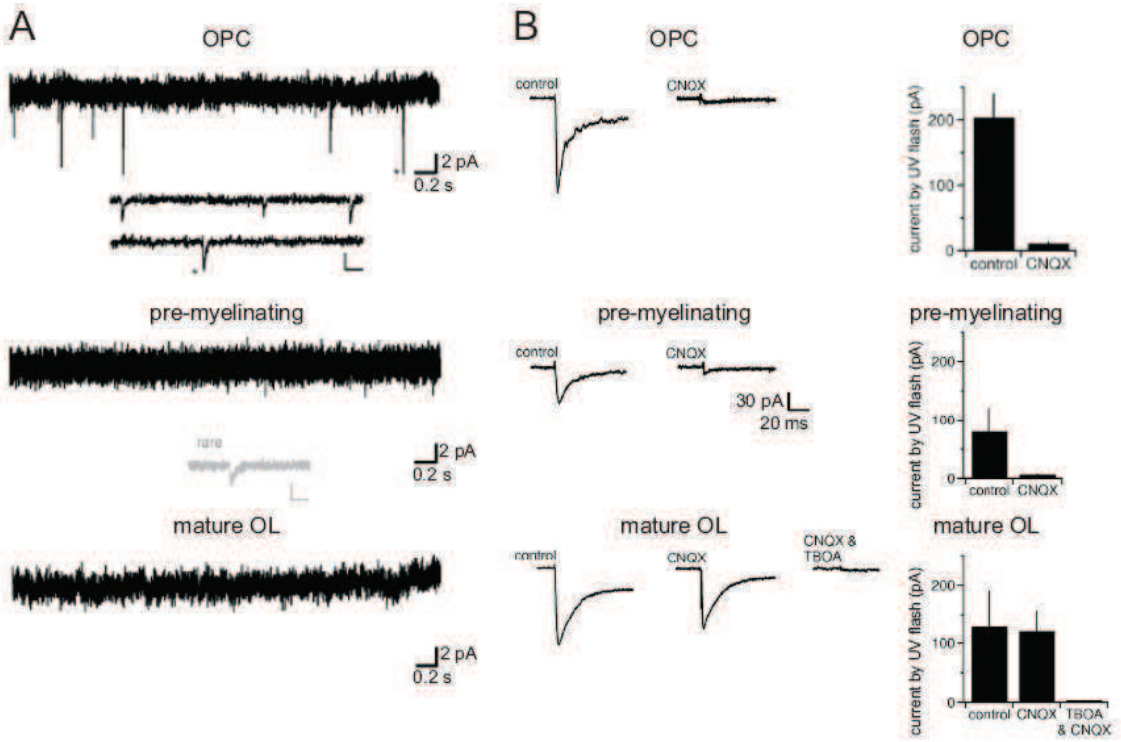

Figure 2.2: **Glutamatergic synaptic inputs in the oligodendrocyte lineage**.
A. Ruthenium red-evoked EPSCs in the presence of $GABA_A$Rs antagonist and TTX from a OPC, a pre-myelinating oligodendrocyte and a mature oligodendrocyte (mature OL) from CA1 *stratum radiatum*. Each type of cell was identified by usign different transgenic mice (NG2cre:Z/EG and PLP-GFP).
B. Currents evoked by glutamate uncaging in the presence of NMDA and $GABA_A$ receptor antagonist (left). Note that even if mature OLs have a considerable response, this current is the result of the glutamate transporter activity (right). It is noteworthy that, even if the currents were not normalized by the cell capacitance in these examples, the decrease in current amplitude between OPCs and pre-oligodendrocytes was also described by De Biase et al. (2010), for normalized currents. Adapted from Kukley et al. (2010).

Synaptic characteristics during development and brain region expression. Noteworthy, OPCs from all ages receive excitatory synaptic inputs (PN5-PN90) (Bergles et al., 2000; Mangin et al., 2008; Ziskin et al., 2007). In particular, spontaneous glutamatergic events in OPCs increase in frequency and amplitude during the first three

postnatal weeks in the hilus of the mouse dentate gyrus, correlating with decreased rise time and decay times (Mangin et al., 2008). Similarly, electrical stimulation of callosal axons generates inward currents in OPCs that increases in amplitude during development and can be elicited in mature stages (Ziskin et al., 2007). Finally, it is important to note that spontaneous and evoked AMPAR-mediated currents were also observed in diverse brain regions and species: rat and mouse CA1 hippocampus (Bergles et al., 2000; Jabs et al., 2005), mouse dentate gyrus (Mangin et al., 2008), mouse cortex (Chittajallu et al., 2004; Mangin et al., 2012), mouse and rat cerebellum (Lin et al., 2005; Káradóttir et al., 2005, 2008), mouse medial nucleus of the trapezoid body (Müller et al., 2009) and mouse and rat *corpus callosum* (Ziskin et al., 2007; Etxeberria et al., 2010; Kukley et al., 2007), meaning that glutamatergic synaptic contacts into OPCs is a common feature of these cells.

Function

One of the most intriguing questions in the field of OPC physiology is the role of neuron-OPC synapses in the CNS. What are they for? Unfortunately, a direct demonstration of their role in the brain does not exist so far. However, some indirect evidence strongly supports the idea that glutamatergic synaptic activity onto OPCs inhibits their proliferative ability. The first indirect evidence comes from results obtained in either O2A cell cultures or organotypic slice cultures where AMPAR activation inhibits the proliferation of $NG2^+$ cells, as discussed in the section 1.6.4 (Gallo et al., 1996; Yuan et al., 1998). A very recent study has given an *in vivo* demonstration of the relationship between the strength of glutamatergic synaptic activity and the rate of OPC proliferation (Mangin et al., 2012). In physiological conditions, layer IV OPCs in the somatosensory cortex display particular spatial cell and synaptic distributions. Layer IV OPCs accumulate mainly in the septa of barrel structures and receive strong synaptic inputs from thalamocortical axons, whereas a low cell density and small synaptic currents are observed in the barrel cores. Mouse sensory deprivation, by removal of the central row of mystacial whiskers early in development, decreases the thalamocortical inputs onto OPCs and increases their proliferation, leading to a more uniform distribution within the central row barrels of deprived mice (Mangin et al., 2012). Interestingly, a similar correlation between a decrease in synaptic activity and an increase in OPC proliferation is observed in a model of LPC-induced demyelination in *corpus callosum*. During the active phase of OPC proliferation in a focal lesion, proliferative OPCs labeled with Edu (a BrdU analog) shows no $vGluT1^+$ contacts, whereas in normal white matter region no proliferative OPCs (OPC Edu^-) show $vGluT1^+$ contacts (Sahel 2013 et al., see Annex).

In spite of these evidences, it has also been observed that OPCs undergoing cell division remain synaptically connected to glutamatergic neurons, as do their progeny, suggesting that dividing OPCs continuously sense neuronal signals (Kukley et al., 2008; Ge

et al., 2009). This observation goes against a role of glutamatergic synapses in inhibiting OPC proliferation and thus diverges from the studies mentioned above. First evidence also showed that electrical stimulation of axons in the developing rat optic nerve leads to an increase in OPC proliferation (Barres and Raff, 1993). If glutamatergic synapses of OPCs are implicated in this process, the result of this early report tends to favor a role of synapses in promoting rather than in inhibiting OPC proliferation. Unfortunately, the cascade of events that occur following axonal stimulation *in vivo* are still elusive and may involve complex signaling mechanisms independent of glutamate.

Taking in account these discrepancies, it is clear that further investigation where OPC glutamatergic synapses are specifically targeted is required in order to determine their role in proliferation as well as other potential roles.

2.1.2 $GABA_A$ receptor-mediated synaptic currents

Properties

Characterization of synapses. Rat CA1 hippocampal OPCs (PN13-PN16), exhibit GABAergic spontaneous synaptic activity as the result of direct synaptic release from adjacent synapses from interneurons. Additionally, miniature GABAergic events reveal that the amount of GABA released from one single synaptic vesicle is enough to induce a fast activation of OPC $GABA_A$Rs, as is the case in neurons (Figure 2.3 A). These cells also exhibit evoked postsynaptic currents after electrical stimulation of interneurons (Lin and Bergles, 2004). In the presence of glutamate receptor antagonists, these currents show paired-pulse depression (Figure 2.3 B), are blocked by GABAAR antagonist SR-95531 and are dependent on both axonal conduction and presynaptic calcium influx. Moreover, GABA should exert a depolarizing effect in OPCs, since the measured reversal potential for the chloride ion comprises values as follows: -43.6 mV (Lin and Bergles, 2004); -30.6 mV (Tanaka et al., 2009) and -44.5 mV (Passlick et al., 2013) and $GABA_A$R activation is associated to $[Ca^{2+}]$i (Vélez-Fort et al., 2010).

Morphologically, inhibitory terminals containing puncta of $GAD65^+$ (an enzyme that catalyzes the conversion of glutamate to GABA) are in close opposition to $NG2^+$ processes of OPC in the /emphstratum radiatum region of the hippocampus. Ultrastructural analysis using electron microscopy reveals synaptic junctions with interneurons. This finding is supported by the presence of pleomorphic vesicles, which typically contain GABA and differ from round vesicles containing glutamate (Figure 2.3 C).

Receptor subunit composition and brain region expression. Balia et al. (2013), by performing single-cell RT-PCR and pharmacological approaches, found that synap-

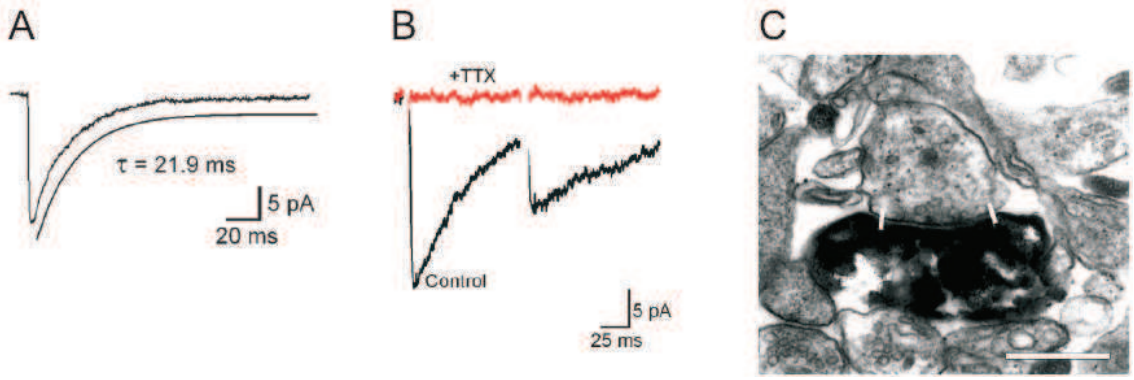

Figure 2.3: **GABAergic synapses into hippocampal OPCs.**
A. Average of miniature synaptic events obtained in the presence of TTX, NBQX and the secretagogue ruthenium red. They are well fitted with a single exponential function.
B. Paired-pulse stimulation. The evoked events exhibited depression and were bloked by TTX.
C. Electron micrograph of a putative GABAergic synaptic junction. The postsynaptic terminal with pleomorphic vesicles, containing probably GABA, contacts an OPC (black, peroxidase reaction). Scale bar, 0.4 μm. From Lin and Bergles (2004).

tic $GABA_A$Rs of OPCs are composed mainly by $\alpha 1$, $\alpha 5$ and $\gamma 2$ subunits in the somatosensory cortex. Interestingly, the expression of $\gamma 2$, a crucial molecular component for the clustering of $GABA_A$Rs at postsynaptic sites in neurons, is downregulated once transient cortical synapses disappear after the second postnatal week in this region (Vélez-Fort et al., 2010; Balia et al., 2013). The presence of $\alpha 1$ and $\gamma 2$ in synaptic $GABA_A$Rs was also confirmed in the hippocampus (Passlick et al., 2013), although $\alpha 5$ was less expressed.

Spontaneous and evoked $GABA_A$R-mediated currents have been observed in diverse brain regions and species including the mouse cortex (Kukley et al., 2008; Ge et al., 2009; Tanaka et al., 2009; Vélez-Fort et al., 2010), mouse dentate gyrus (Mangin et al., 2008), mouse and rat CA1 (Jabs et al., 2005; Lin and Bergles, 2004) and rat cerebellum (Káradóttir et al., 2008). Whether these currents are synaptic or not will be discussed later on.

Function

Although several hints exist on the role of glutamatergic synapses onto OPCs, the role of GABAergic synapses remains a mystery.

If OPC synaptic activity promotes myelination by $GABA_A$R-mediated OPC develop-

ment onto oligodendrocytes, this activity should decrease when the myelination process starts in the postnatal brain. Work from our laboratory supports this hypothesis. Indeed, Vélez-Fort et al. (2010) has observed that OPCs of the mouse barrel cortex are mainly synaptically innervated by GABAergic interneurons and change their mode of transmission from synaptic to extrasynaptic during the first postnatal month, a critical period for myelination (Salami et al., 2003; Bjelke and Seiger, 1989; Maldonado et al., 2011, see Annex). Contrary to glutamate, however, less information exists on the effect of GABA in OPCs and it is thus difficult to hypothesize whether GABAergic synapses might participate either to proliferation or to differentiation. Interestingly, it was recently demonstrated that parvalbumin (PV)-positive interneurons induce a γ2-mediated tonic current in neuronal progenitors radial glia-like cells in the adult hippocampus that maintains their quiescence state and inhibits their self-renewal (Song et al., 2012). By analogy, it is therefore conceivable that GABA and, in particular GABAergic synapses of OPCs, regulate their proliferation using specific local GABAergic microcircuits.

Additionally, it has been proposed that GABA stimulates the production of the neurotrophic factor BDNF and its release by cortical OPCs after ischemia. Although this was not assessed directly, the authors claim that a subpopulation of $Nestin^{+}/NG2^{+}$ glial cells could be implicated in the functional recovery occurring after ischemic injuries (Tanaka et al., 2009).

Finally, as discussed in section 1.6.4, $[Ca^{2+}]$i increases mediated by GABA-induced depolarization has never been observed in physiological conditions, but remain a possibility. Indeed, OPC calcium transients are observed after moderated stimulation of Schaffer collaterals in both soma and processes, however, contrary to astrocytes, they exhibit a rapid run-down after three-pulse stimulation (50 hz)(Figure 2.4)(Honsek et al., 2012). Although the mechanisms mediating $[Ca^{2+}]$i elevation in OPCs were not addressed in this report, GABA and/or glutamate released upon neuronal stimulation may indirectly induce these changes. However, it is important to consider that OPCs have a hyperpolarized E_m (-80 mV to -100 mV), making difficult to reach the threshold of VGCCs. For this, a possibility is that physiological $[Ca^{2+}]$i increases occur very locally at the level of OPC thin processes where GABA might induce strong depolarizations. The employment of 2-photon microscope combine with a suitable calcium-sensitive dye or genetically encoded calcium indicator would be a good alternative to follow GABA-mediated $[Ca^{2+}]$i increases at specific postsynaptic sites.

2.2 Neuron-OPC extrasynaptic communication

Classical synapses are characterized by pre- and post-synaptic specializations: active zones (Couteaux and Pécot-Dechavassine, 1970) and postsynaptic densities (Palay,

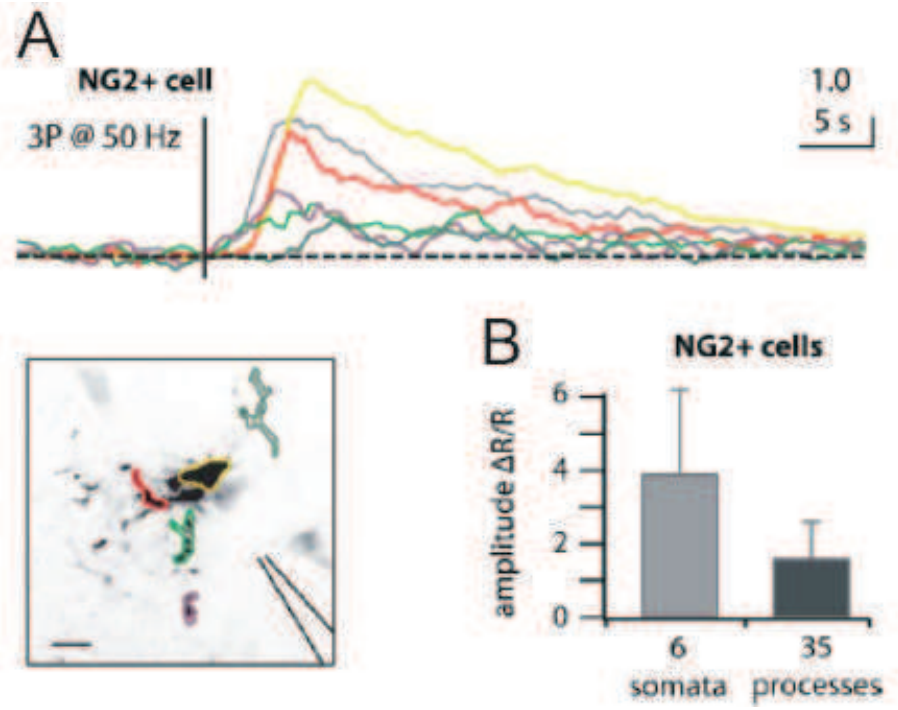

Figure 2.4: **Calcium signals in OPCs.**
A. Intracelullar calcium transients after three-pulse stimulations, the vertical line indicates the time of electrical stimulation. Note the decreases in the amplitude over time. The black box shows the recording area for imaging. Scale bar, 10 μm.
B. Histogram of fluorescence changes (ΔR/R), in arbitrary units, analyzed in regions of interest. From Honsek et al. (2012).

1956), respectively. Receptors located in the postsynaptic site respond to the neurotransmitters released into the synaptic cleft from the presynaptic terminal. This is the classical way to stimulate receptors in neurons; nevertheless it is not the only one. If the concentration of neurotransmitters increases enough during synaptic transmission, the neurotransmitter reaches receptors outside the postsynaptic densities by diffusion or spillover. On the other hand, presynaptic exocytosis is not limited to the active zone. Ectopic release of neurotransmitters can also contribute to the activation of extrasynaptic receptors in addition to the previously described synaptic release. In the absence of morphological specializations, vesicles fuse with the cell membrane in very close apposition to receptors, and it is therefore possible to record miniature postsynaptic currents in the absence of synapses. This has well described in Bergmann glia, where currents evoked by ectopic release are large and fast, similar to those recorded in true functional synapses (Matsui and Jahr, 2003, 2006). Along with these types of transmission, several other mechanisms also rely on neurotransmitter coming out of synaptic boundaries, as perisynaptic transmission, volume transmission and other forms of spillover (reviewed by Szapiro and Barbour, 2009). In particular, a local form of spillover transmission was recently described between climbing fiber-interneuron input in the cerebellum. It was characterized by small glutamatergic currents with slow and long-lasting kinetics compared to synaptic ones. These properties enable signaling over long temporal and spatial scales (Szapiro and Barbour, 2007).

2.2.1 Glutamate-mediated currents

Glutamate release from unmyelinated axons onto OPCs has been described in the *corpus callosum* (Ziskin et al., 2007; Kukley et al., 2007; Káradóttir et al., 2005; Etxeberria et al., 2010). However, it is not completely clear if this quantal release is synaptic or ectopic. Both Ziskin et al. (2007) and Kukley et al. (2007) described currents with fast rise and decay times in OPCs, similar to synaptic currents described in OPCs of grey matter regions. In addition, Ziskin et al. (2007) found parallel apposition of membranes and electron-dense material, supporting the presence of classical synaptic junctions. The presence of synaptic junctions between axons and putative OPCs were also observed in electron microscopy experiments in LPC-induced demyelinated lesions (Sahel et al., Annex). However, ultrastructural analyses in Kukley et al. (2007) failed to identify specialized synaptic junctions with electron-dense material, despite the presence of axonal varicosities, in close contact or not with OPC processes, which contained a variable number of putative presynaptic vesicles. In addition, the effect of AMPARs c-D-glutamylglycine (c-DGG) on glutamatergic currents was more pronounced in callosal OPCs than in CA1 pyramidal neurons (Kukley et al., 2007). Although this observation should be taken with caution because different cell types were compared, it may imply that a lower concentration of glutamate reaches OPC glutamate receptors similarly to that observed for ectopic release onto Bergman glia (Matsui and Jahr, 2003). Moreover, the number of glutamate vesicular transporter 1-positive (vGluT1$^+$) puncta

per callosal OPC at 14 days post-LPC injections, probably representing presynaptic axonal elements, is larger than in control conditions (Sahel et al., Annex). Together with the results obtained by Kukley et al. (2007), these data rise the possibility that both synaptic and non-synaptic junctions co-exist in *corpus callosum* in normal and demyelinating conditions and thus that either ectopic or another extrasynaptic mode of glutamatergic transmission onto white matter OPCs exists.

2.2.2 GABA-mediated currents

Similarly to glutamatergic transmission, initial reports described GABAergic signaling in OPCs at young and mature development stages (Lin and Bergles, 2004; Tanaka et al., 2009). However, a study from our team has questioned the presence of true functional GABAergic synaptic contacts in the adult. Whereas layer V OPCs of the barrel cortex exhibit fast $GABA_AR$-mediated synaptic currents upon low-frequency extracellular stimulation in the second postnatal week, they have slower currents of several milliseconds of rise time in the fourth postnatal week (Figure 2.5 A). In addition, this change in the kinetics of evoked currents is accompanied by a dramatic decrease in the frequency of spontaneous events (Figure 2.5 B).

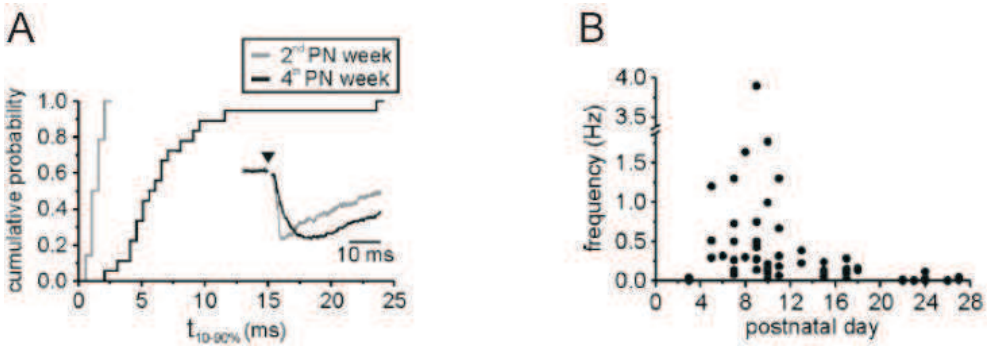

Figure 2.5: **Change in the mode of transmission from synaptic to extrasynaptic in cortical OPCs.**
A. Cumulative probabilities of rise times of evoked currents for OPCs in the second and fourth postnatal weeks. Note the slower rise time in the fourth postnatal week (black trace). The inset shows two examples of currents evoked in the two different developmental stages. The stimulation time is indicated by a black arrowhead.
B. Plot of the frequency of spontaneous synaptic current in OPCs against the PN days. Note the dramatic decrease in the frequency after PN10. From Vélez-Fort et al. (2010).

These features match with those described for local glutamatergic spillover at climbing fiber-interneuron input in the cerebellum (Szapiro and Barbour, 2007). Indeed, by the voltage jump technique, Vélez-Fort et al. (2010) excluded the possibility that the slow kinetics of evoked responses were the result of distortion or attenuation of the signal as consequence of inadequate space clamp. In addition, pharmacological approaches

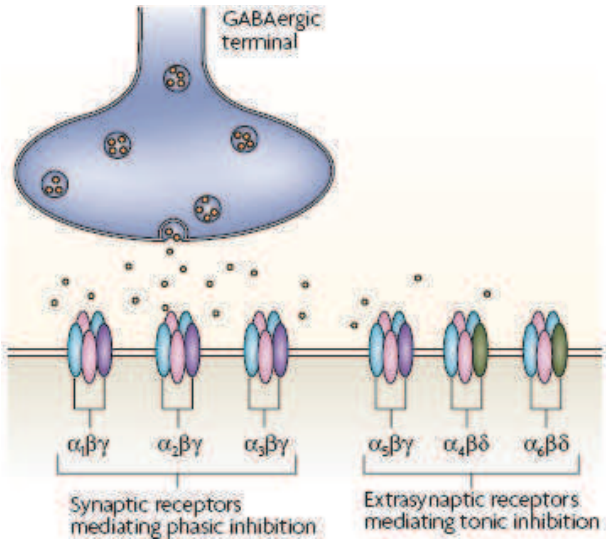

Figure 2.6: **Neuronal localization of GABA$_A$Rs.**
Schematic representation of clasical differences between cortical synaptic and extrasynaptic GABA$_A$Rs. Note that the association of the δ subunit gives a extrasynaptic localization. From Jacob et al. (2008).

also allow us to demonstrate that OPC-neuron signaling in older animals was mediated by GABA spillover and activation of extrasynaptic GABA$_A$Rs in the millisecond range. This change in the transmission is possibly the result of a rearrangement of the interneuron-OPC junction with age.

According to their subunit composition, GABA$_A$Rs are implicated in two different forms of neuronal inhibition: (1) phasic inhibition characterized by postsynaptic receptors exposed to a brief and high GABA concentrations and (2) tonic inhibition characterized by extrasynaptic receptors exposed to lower GABA concentration (Farrant and Nusser, 2005). Receptors composed of $\alpha_{1-3,6}\beta_{2-3}\gamma_2$ are benzodiazepine-sensitive and are synaptically located, whereas $\alpha_{4,6}\beta\delta$ and $\alpha_5\beta_3\gamma_2$ are benzodiazepine-insensitive and are mainly extrasynatically located (Figure 2.6) (Möhler et al., 2002; Farrant and Nusser, 2005; Jacob et al., 2008). Considering this evidence in neurons, hippocampal OPCs (PN9-PN12) show a small tonic current mediated by GABA$_A$Rs lacking the γ_2 subunit (Passlick 2013). Interestingly, Balia et al. (2013) shows that the γ_2 subunit, a crucial component for the clustering of GABA$_A$Rs at postsynaptic sites in neurons, is downregulated in cortical OPCs during development in concomitance with the change of transmission mode from synaptic to extrasynaptic. These are probably the two first studies addressing the subunit composition of GABA$_A$Rs in OPCs during development.

2.2.3 NMDA receptor-mediated currents

Properties

Brain region expression. In addition to AMPARs and $GABA_A$Rs, OPCs express several other receptors for neurotransmitters that are more probably located outside synapses. This is the case for NMDARs that have never been detected at OPC postsynaptic sites. The first clear demonstrations of NMDARs in cells of the oligodendroglia lineage were reported by Káradóttir et al. (2005) and Salter and Fern (2005). In the cerebellum, bath application of NMDA induces currents that are sensitive to D-AP5, blocked by increased magnesium concentration and reversed at 0 mV. In addition, the I-V relationships exhibit a region of negative slope in the presence of magnesium. All these results indicate that these induced currents are mediated by NMDARs (Figure 2.7 A). NMDARs are observed in OPCs of diverse brain regions and species including, the rat cerebellum (Káradóttir et al., 2005, 2008), the rat and mouse *corpus callosum* (Káradóttir et al., 2005; Ziskin et al., 2007; De Biase et al., 2010; De Biase et al., 2011) and the rat optic nerve (Salter and Fern, 2005), but most studies have been carry out in white matter.

Receptor subunit composition. NMDARs in neurons contain NR1, NR2A-D or NR3A subunits and 36% of them are extrasynaptic during postnatal development (PN14-PN21) (Harris and Pettit, 2007; Petralia, 2012, for review). They exhibit a voltage-dependent block by magnesium (Mayer et al., 1984) which acts on the M2 domain of the NR2 subunit. Receptors containing the NR2A/B are more sensitive to magnesium block compare to those having NR2C/D. In addition, the incorporation of NR3 subunit in heteromeric receptors decreases the sensitivity to this ion (reviewed by Paoletti et al., 2013). Since large NMDAR-mediated currents can be induced at physiological concentrations of magnesium in OPCs at negative potentials close to E_m, the subunit composition of NMDARs in these cells is probably NR1, NR2(A/B) and NR3. Transcripts analyses and immunostainings against different NMDAR subunits in cells of the oligodendrocyte lineage show the presence of NR1, NR2A, NR2B, NR2C, NR2D and NR3A clustered in cell processes (Salter and Fern, 2005). By immunostaining, the NR2A and NR2C subunits have also been shown to co-localize in optic nerve OPCs (Hamilton et al., 2010). In addition, a recent study from Li et al. (2013) has shown, the presence of NR1 and NR2A/B subunits by immunoinstaining and western blot analyses. However, in these both studies the NR3 subunit was not tested.

Characteristics during differentiation. Káradóttir et al. (2005) showed that NMDA receptor-mediated currents are smaller in OPCs than in mature oligodendrocytes, both cell types identified by their morphology and antibody labeling against the myelin basic protein (MBP). However, De Biase et al. (2010) reported that OPC NMDA receptor-

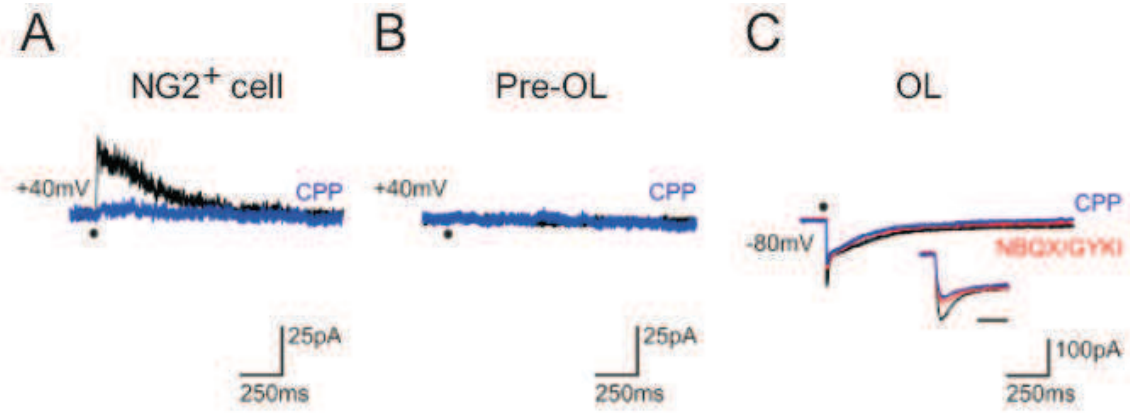

Figure 2.7: **NMDAR-mediated currents of callosal OPCs.**
A. Response of a NG2$^+$ cell to glutamate uncaging (black dot) recorded at +40 mV in the presence of NBQX/GYKI53655. The current was bloked in the presence of the NMDAR antagonist CPP.
B. Response of a pre-oligodendrocyte (pre-OL) to glutamate uncaging (black dot) under the same conditions than in A. Note that CPP-sensitive currents were observed only in 3/15 cells.
C. Response of an oligodendrocyte (OL) to glutamate uncaging (black dot) at -80 mV and in a perfusion solution containing 0 mM magnesium, 30 μM D-serine and NBQX and GYKI5365. The recordings were performed in these different conditions because the low oligodendrocyte input resistance prevent effective voltage-clamp at +40 mV. Note that CPP only slightly reduced the NMDAR-mediated currents. Adapted from De Biase et al. (2010).

mediated currents were decreased compared to those of differentiated oligodendrocytes (Figure 2.7). Furthermore, the mRNA expression of these receptor subunits also dropped to low levels when OPCs became oligodendrocytes (Cahoy et al., 2008; De Biase et al., 2010). These last results suggest that NMDARs are restricted to the OPC stage, but they are in contradiction to the observations reported by Káradóttir et al. (2005); Salter and Fern (2005). This discrepancy may be explained by differences on postnatal stages and regions studied by different authors. Also, we cannot exclude that the low input resistance of oligodendrocytes (for values see figure 6C Kukley et al., 2010), causes in some conditions an inadequate space clamp of recorded cells that avoid the detection of NMDAR-mediated currents at distal processes of the soma. Indeed, Salter and Fern (2005) reported that NMDARs receptors in oligodendrocyte lineage cells are preferentially located at the processes.

Function

A first role suggested for NMDARs in OPCs was in damage caused by elevated glutamate such as that observed during stroke. To evaluate this, Káradóttir et al. (2005) simulated a stroke condition by using an ischemia solution based in energy deprivation in brain slices. The currents induced by NMDARs in these conditions were 50% larger than those mediated by AMPA/kainate receptors. According to their results, this sensitivity to ischemia would not be exclusive to OPCs since oligodendrocytes also express NMDARs. Injury evoked by chemical ischemia affects both axons and myelin. Consistently, myelin damage is prevented by blocking NMDARs (Micu et al., 2006).

It has been shown that myelination is a process dependent on neuronal activity (reviewed by Zalc and Fields, 2000). The effect of electrical neuronal activity on myelin formation was primarily demonstrated by either blocking or increasing neuronal firing with TTX and α-scorpion toxin, respectively (Demerens et al., 1996). However, the cascades of events that link neuronal activity and myelination are not completely understood yet. One suitable mechanism to control activity-dependent myelin production could be through the NMDAR activation in OPCs. Although the role of these receptors is not well understood yet, evidences suggest that these receptors might play a role in myelination and remyelination. In co-cultures of OPCs and DRG neurons, the vesicular glutamate release from electrically stimulated axons initiates myelin production from OPCs, probably through a NMDAR-mediated process (Wake et al., 2011). This is supported by unpublished results from Karadottir's group showing that neuregulin-dependent myelination requires action potential and NMDAR activation (Luzhynskaya et al., 2009). Moreover, in a cuprizone model of demyelination, the block of the NMDARs also generates retardation in the remyelination process (Li et al., 2013).

In order to clarify the role of NMDARs in OPCs, the NMDAR subunit NR1 was specifically deleted in cells of the oligodendrocyte lineage (De Biase et al., 2011; Guo et al.,

2012). This subunit is required for the functional assembly of the receptor (Forrest et al., 1994). Surprisingly, no myelin defects is observed in conditional NR1 deleted mice (De Biase et al., 2011). Similarly, in experimental autoimmune encephalomyelitis, a multiple sclerosis model, the specific ablation of the NR1 subunit does not change the pathology of this illness (Guo et al., 2012). In the normal brain, OPCs lacking NMDAR-mediated currents in the knockout exhibits normal rates of proliferation, achieves normal densities in gray and white matters and differentiate into oligodendrocytes. They also continue to receive glutamatergic synaptic inputs and the expression of AMPARs seems to be the same (De Biase et al., 2011). There is, however, a change in the AMPAR subunit composition, since currents mediated by caAMPARs are increased in mice lacking the OPC NR1 subunit. The authors concluded that OPC NMDARs are not required for OPC development and myelination, but regulate the AMPAR signaling (De Biase et al., 2011). Nevertheless, they do not consider the possibility that the up-regulation of caAMPAR-mediated currents could result from the loss of NR1 in these mice to compensate the lack of functional NMDARs, since both caAMPARs and NMDARs are highly permeable to calcium. In addition, transient effects on myelination could occur before their observation time-window, *i.e.* before 26 days after NR1 ablation. Considering the controversy in this field further studies are needed to clarify whether NMDARs play a role or not in myelination and remyelination.

2.2.4 Other neurotransmitter receptors

OPCs express receptors for neurotransmitters, other than AMPARs, $GABA_A$Rs and NMDARS, but their activation mode and physiological roles have not been studied so far. Considering that synaptic release from neurons results only in the activation of AMPARs and $GABA_A$Rs, the most likely mechanism activating other receptors is extrasynaptic. Here, it will be summarized some findings concerning these receptors in OPCs.

Bath application of kainate in the presence of the AMPARs and NMDARs antagonists AP5/MK801 and GYKI53655 induces a small and persistent depolarizing current in hippocampal OPCs, demonstrating the presence of functional kainate receptors in these cells (Kukley and Dietrich, 2009). Kainate receptors subunits are GluR5-7 and KA1-2 (Fernandes et al., 2009). According to their pharmacology, kainate receptors in OPCs lack the GluR5 subunit, but the precise composition of these receptors is for the moment unknown. Since these receptors are probably located at extrasynaptic sites, they are problably activated by ambient glutamate from neuronal and non-neuronal sources such as astrocytes (Le Meur et al., 2007). Others ionotropic receptors might also be activated at locations distant from synapses such as purinergic (P2X7) and nicotinic acetylcholine receptors, as discussed in section 1.6.4. In addition, glycine (Belachew et al., 1998b) and serotonin 5-HT3 receptors (Belachew et al., 1998a) have been described in O2A cells, but evidence of these receptors in OPCs *in vivo* is still

lacking. If expressed in OPCs, these receptors also represent good candidates to be extrasynaptic.

In contrast to ionotropic receptors mediating fast signaling, metabotropic receptors activate a cascade of intracellular reactions that indirectly link them to ion channels, resulting in slower and long-lasting responses (Kandel et al., 2000). Very few information exists on metabotropic receptors acting through secondary messengers in OPCs, but the presence of these receptors in cultured O2A cells suggests their expression *in vivo*. Initial observations indicate that O2A cells express the mRNA (by RT-PCR analyses) and protein (by immunoblot analyses) of metabotropic glutamate receptor (mGluR) subtypes mGluR5 and mGluR3 (Luyt et al., 2003). These receptors are functional since mGluR5 activation after bath applications of DHPG (agonist of mGluR1/5) induces calcium oscillations and mGluR3 activation after bath applications of DCG-IV (agonist of mGluR2/3) reduces the levels of cAMP (Luyt et al., 2003). A further study demonstrate that mGluR5 is downregulated (mRNA and protein levels) when cultured O2A cells differentiated into oligodendrocytes while mGluR3 remains stable (Luyt et al., 2006). Neither the activation nor the inhibition of mGluR5 or mGluR3 affects O2A cell migration, but mGluR5 activation protects these cells from induced apoptosis (Luyt et al., 2006). Concerning the expression of metabotropic receptors in OPCs, bath focal application of DHPG, a specific agonist of group I mGluRs (mGluR1 and mGluR5) does not generate currents in OPCs of acute hippocampal slices, but instead, causes increases in $[Ca^{+2}]i$ (Haberlandt et al., 2011). In addition, it have been described co-localization between mGluR5 and O4 or $O1^+$ cells from rat *corpus callosum* (PN4 and PN7)(Luyt et al., 2003). Immunostaining against mGluR3 can not be performed due to the high background induced by the antibody for this receptor (Luyt et al., 2003).

The expression of metabrotropic $GABA_B$ receptors ($GABA_BR$) have been addressed in O2A cells by semiquantitative PCR analysis, founding that the $GABA_B1abcdf$ isoform is elevated in O2A cells compared to that in oligodendrocytes, whereas $GABA_B2$ remains similar. Activation of these receptors by baclofen induces currents showing that they promotes O2A cell migration and proliferation (Luyt et al., 2007). In addition, $GABA_BR$ co-localized with $O4^+$ cells in the SVZ (PN4) (Luyt et al., 2007). Other metabotropic receptors, such as muscarinic acetylcholine receptors (Ragheb et al., 2001) have also been described in cultured O2A cells.

Finally, OPC α1A and α1B adrenaline receptors have been found in the cortex (Papay et al., 2006, 2004). The *in vivo* identification of these receptors was done by using transgenic mice where these receptor were endogenously overexpressed, thus it was possible to determine their cellular localization in the brain at the protein level by immunostainings analyses (Papay et al., 2006, 2004).

The described above evidence clearly shows a lack of investigation addressing the *in vivo* function of the metabotropic receptors in OPCs. This is likely due to a in general

lack of characterization of these receptors, comparing to ionotropic receptors, and in the tools that allows for their unambiguously characterization.

General conclusion

If glutamatergic and GABAergic synaptic activity into OPCs is the main manner to control directly or indirectly the fate and function of OPCs, the understanding of these synapses might be essential for the comprehension of OPC physiology. It is thus important to determine how these cells are integrated in neuronal networks to sense their environment and which is the identity of their presynaptic inputs, with the aim to better understand OPC physiology and new potential functions. However, synapses are not the only mechanism underlying neuron-OPC communication, since extrasynaptic mechanisms also exists. If synaptic activity into OPCs is not the only way with which OPCs interact with neurons, we could expect to find other unknown mechanisms conferring undescribed roles for these cells. Up to now, the general believe is that the primary function of OPCs is the generation of oligodendrocytes, which implies that they are mainly progenitor cells.

Part II

Methodology

During this thesis, neuron-OPC interactions in the somatosensory cortex were mainly assessed with electrophysiological techniques: patch-clamp, extracellular stimulation and paired recordings. In addition, electrophysiology was combined with immunostainings, single-cell RT-PCR and holographic photolysis. The protocols used for each experiment are described in the articles (Part III and Annex). However, two unconventional techniques merit to be addressed in more detail: single-cell RT-PCR and holographic photolysis.

Chapter 1

Single-cell RT-PCR for Kir4.1 channels

During my thesis, I needed to identify molecularly and pharmacologically a potassium channel upregulated in cortical OPCs during development. Electrophysiological and pharmacological analyses strongly suggested Kir4.1 potassium channels as a good candidate (see article I). However, the lack of a specific pharmacology for this channel did not allow me to provide a complete identification of the channel and immunostainings revealed a high level of protein expression that made it difficult to distinguish and count individual cell bodies expressing Kir4.1, as previously observed (Poopalasundaram et al., 2000). To have a molecular confirmation and to overcome these limitations, I performed single-cell RT-PCR analyses to study the molecular expression of Kir4.1 channels in OPCs (Figure 1.1). This technique consists of harvesting the cytoplasm of an identified cell during patch-clamp recordings. Then, it relies in a reverse transcription, followed by a polymerase chain reaction (PCR) which allows biochemical analyses of messenger RNAs (mRNAs) expressed by single cells. This technique was originally developed to study the AMPAR subunit composition of cerebellar Purkinje cells in culture. In this particular case, only one primer was used to amplify the four cADNs, coding for the AMPAR subunits (GluR1 to 4 subunits). With a restriction enzyme reaction, it was possible to determine the relative proportion of each subunit expressed by one single cell (Lambolez et al., 1992).

Figure 1.1 details the protocol used to determine the presence of Kir4.1 potassium channel in OPCs of the somatosensory cortex.

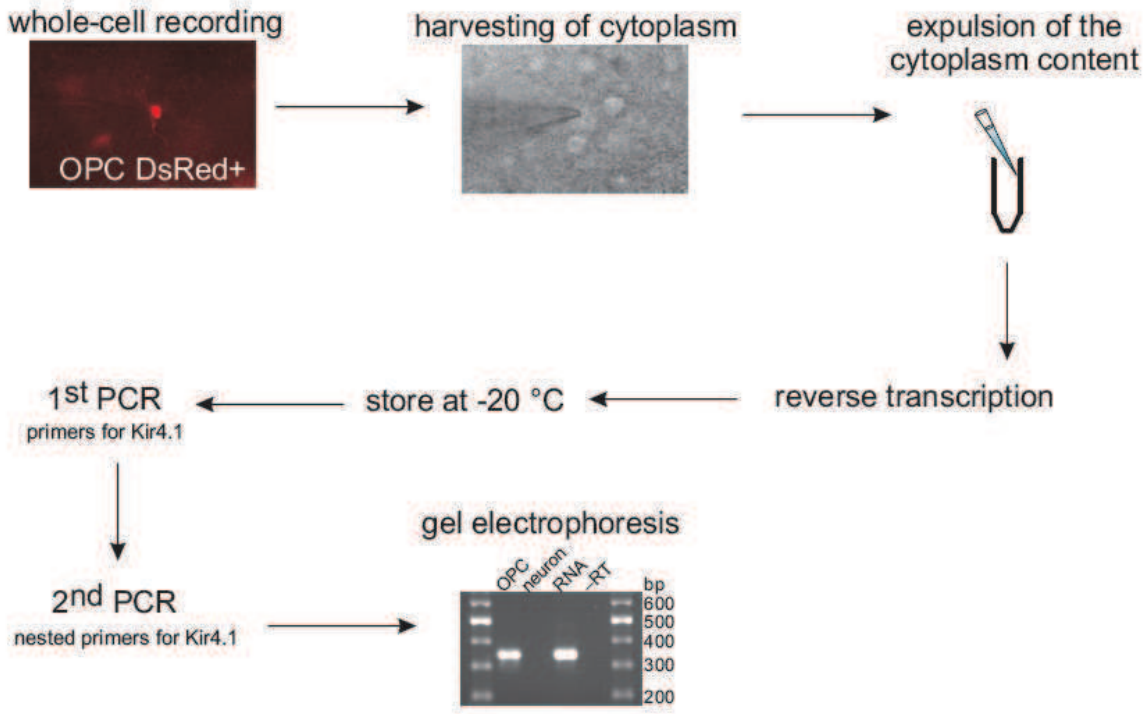

Figure 1.1: **Single-cell RT-PCR for Kir4.1 channels.**
A DsRed$^+$ OPC is first recorded with a patch pipette in acute somatosensory slices of a NG2-DsRed transgenic mouse. Then, the cytoplasm containing the mRNAs are haversted into the pippette and expelled into a test tube containing radom primers, dNTPs, DTT and the enzime RNAseOut (see Part III, Article I). A reverse transcription is performed immediately after haversting for 2h. After incubation, the tubes are stored at -20°C. RT products are then amplified with specific primers for Kir4.1 channels using a two-round nested PCR. Positive controls consist in running in paralel total mRNAs from mouse hippocampus and negative controls either omitting the reverse transcriptase enzime or harvesting neurons from cortical layer I-III. For details of reagents see Material and Methods of Article I.

.

Chapter 2

Holographic photolysis

Electrophysiology has provided an enormous amount of information about the physiological properties of OPCs, *e.g.* channel composition, cellular excitability, and synaptic inputs, among others. However, our understanding of these cells and their functions is still incomplete. Moreover, we are restricted by our inability to manipulate specifically different players in neuron-OPC interactions and to examine how their dynamic is related to cellular functions. Our limited knowledge about OPC function is also due to the lack of information on these cells *in vivo*. Tools that give us information about the properties and performance of these cells and their relationship with the whole system are necessary. One strategy to achieve these requirements is to combine electrophysiology with complementary optical methods and transgenic mice.

During my thesis, I used a technique to manipulate neuronal activity with light, with the aim to study the synaptic connectivity between interneurons and OPCs. We used a recently developed optical method that delivers light into the sample, called Digital Holography (DH). I performed holographic photolysis (HP) to uncage MNI-glutamate to stimulate interneurons of the developing mouse somatosensory cortex in order to elicit action potentials in these neurons with single cell resolution. The bases supporting the uncaging and HP techniques are described below.

2.1 Uncaging of neurotransmitters

Caged neurotransmitters are compounds derivates of amino acids or nucleotides, synthetically modified, in which a photochemical protecting (organic chromophore) group has been attached by a covalent bond to the acid or the amino group. Light breaks the bond and the caged compound is released, rendering active the molecule of interest (Figure 2.1)(Ellis-Davies, 2007; Yuste, 2011). The first caged molecule was adenosin

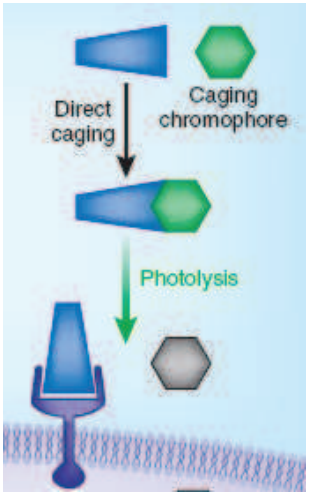

Figure 2.1: **Caged neurotransmitters.**
The caging chromophore prevents receptor binding until the bond is broken by light. Adapted from Ellis-Davies (2007).

.

triphosphate (ATP)(Kaplan and Forbush B 3rd, 1978) that had an ortho-nitrobenzyl protecting group attached. This caging chromophore has been extensively used because it is the only one that photo-cleaves all organic functionalities (ether, thioether, phosphate, amide, amine, among others), doing so *via* a nitroaromatic intramolecular photo-redox reaction.

The first truly successful protecting group for caged neurotransmitters was the α-carboxy-ortho-nitrobenzyl (CNB). CNB-caged glutamate has proven useful in research of neuronal function as its photochemical properties allow for activation of glutamate receptors on a timescale in the order of microseconds (Wieboldt et al., 1994). Unfortunately, this compound is not sensitive to two-photon uncaging. Therefore 4-methoxy-7-nitroindolinyl(MNI)-caged glutamate was developed (Figure 2.2)(Matsuzaki et al., 2001). Although, it was not sufficiently sensitive to two-photon excitation, this cage has many advantages: (1) very fast release of glutamate by light; (2) it is inert toward AMPARs and (3) it is very stable at a physiological pH and at 4°C.

2.1.1 Practical considerations

Many cages perform very well in organic chemistry laboratories, but in biological samples, several constraints limit their use. Just few cages are suitable for biological research purposes: the probes should be chemically stable at physiological pH and soluble in aqueous solution. This second requirement gives rise to difficulty in generating these compounds. Adding a chromophore (with one or more aromatic rings) to nat-

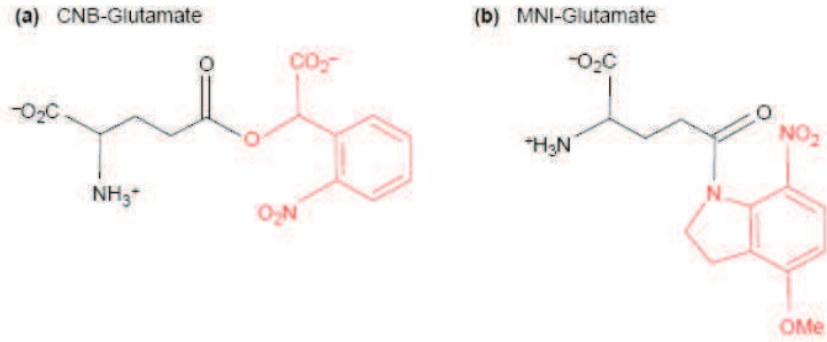

Figure 2.2: **Two different glutamate cages.**
Chemical structures of CNB- and MNI-caged glutamate. Caging groups are represented in red and glutamate in black. Adapted from Callaway and Yuste (2002)

.

ural products reduces their aqueous solubility (which necessitates addition of charged moieties), complicating considerably their synthesis. Additionally, the photochemical reaction should proceed at wavelengths longer than 300 nm, in order to avoid cellular damage. Moreover, if we want to mimic biological responses, then it is necessary that the neurotransmitter is released as quickly and efficiently as possible. Therefore, the efficiency per incident photon, the extinction coefficient (e) times the quantum yield (ϕ) should be high, in order to use less light (Ellis-Davies, 2007; Lester and Nerbonne, 1982; Yuste, 2011).

Finally, it is important that neither the caged compound nor the cage by itself affects the sample and leave the system unperturbed. In spite of the impressive performance of MNI-glutamate as a caged compound, this cage blocks $GABA_A$Rs. In fact, this is a common feature of many others, even those that are supposed to activate $GABA_A$Rs (Molnár and Nadler, 2000; Trigo et al., 2009). To overcome this problem, Rafael Yuste and collaborating chemists developed a new cage based in a ruthenium-bipyridine complex (RuBi), and subsequently generated both RuBi-Glutamate and RuBi-GABA (Salierno et al., 2010). RuBi-Glutamate exhibits a reduced block of inhibitory responses in comparison to other cages (Figure 2.3). The only inconvenience is that the photoreaction occurs in the UV-visible portion of the spectra and thus ambient light trigger the breaking, complicating the implementation of the experiments (Salierno et al., 2010).

2.1.2 Mapping brain circuitry with one-photon uncaging

One of the most common applications of neurotransmitter uncaging is the mapping of brain neuronal circuits. Uncaged glutamate can be used to generate action potentials in a potential presynaptic neuron and, by recording a postsynaptic neuron with a

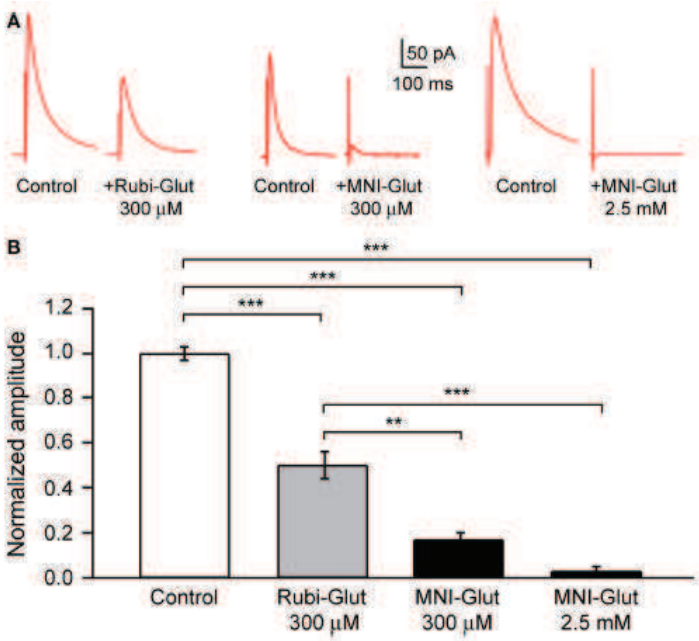

Figure 2.3: **Effects of glutamate cages on GABA$_A$R synaptic activity.**
A. IPSCs evoked in cortical pyramidal cells by extracellular stimulation in control conditions and after adding either MNI-glutamate or RuBi-Glutamate in the bath.
B. Histogram showing the block of GABA$_A$R-mediated synaptic responses by two different glutamate cages at different concentrations. $^{**}p<0.01$, $^{***}p<0.001$. From Fino et al. (2009).

.

patch pipette, it is possible to determine if a synaptic connection exists. Several brain regions have been investigated using this approach, *e.g.* cortex, superior culliculus, suprachiasmatic nucleus, and hippocampus, among others (reviewed by Callaway and Yuste, 2002). Initially, flash lamps were used, coupled to an alignment laser to indicate the position of the photostimulation (Callaway and Katz, 1993). Shortly afterwards, scanning-laser photostimulation was implemented, achieved by the use of a motorized square XY stage (Katz and Dalva, 1994) or with galvanometric mirrors to control the beam position (Shepherd et al., 2003). However, none of these configurations reaches single cell resolution, and could report only the connections between different areas of the brain, for example, studies of intracortical connectivity (Dantzker and Callaway, 2000; Shepherd et al., 2003; Yoshimura et al., 2005).

2.2 Digital Holography (DH)

Recently, the development of patterned light methods provides a spatial shaping of the light allowing for selective access to confined regions of interest (ROI). ROIs can be simultaneously excited by using of spatial light modulators (SLMs) that allow the intensity profile of the beam to be changed, either by modulating the amplitude or the phase of the beam. To modulate the phase, two approaches have been described: one based on the principle of digital holography (DH) and other based on the generalized phase contrast (GPC) (Papagiakoumou, 2013).

In DH, the phase of the wavefront beam is modulated by using a liquid crystal on silicon (LCOS) SLM. This is device that consist of a matrix of reconfigurable pixelated liquid crystals that can modulate the phase of a wavefront in a range from 0 to 2π. Modulating the wavefront is possible because each liquid crystal can be reoriented by applying an electric field, with a consequent change in the crystals refractive index. Thus, when the laser beam is addressed to the SLM, the diffracted wavefront is changed according to the phase profile configured at the SLM. The SLM plane is conjugated with the back aperture of the objective, which is related to its focal plane by a Fourier transform. In this way, the desired intensity is achieved at the focal plane of the objective (Papagiakoumou, 2013; Oron et al., 2012). For the calculation of the phase profile generated at the SLM, a computed iterative algorithm is used: Gerchberg and Saxton algorithm (Gerchberg and Saxton, 1972) or an improved version, Gerchberg-Saxton weighted algorithm (di Leonardo et al., 2007).

This technology was first used to generate multiple optical traps with optical tweezers (Curtis et al., 2002). By modulating the phase of the wavefront, it is possible not only to direct the beam to any desired point on the field, but also to shape the beam in any possible way. This allows the light to be delivered to fine structures such as dendritic spines or bigger areas such as axons or cell somata (Figure 2.4 A).

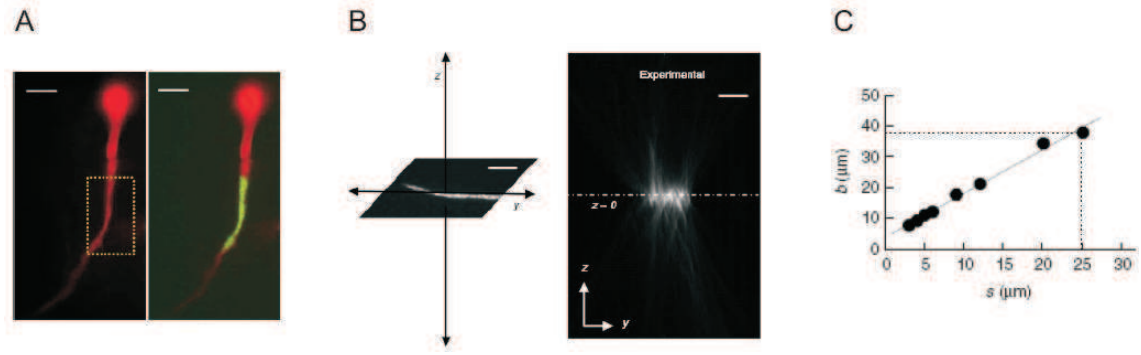

Figure 2.4: **Digital holography.**
A. Shaping of an exitation spot (yellow) to match a dendrite of a CA1 hippocampal pyramidal neuron. Scale bar, 10 μm.
B. Experimental y-z cross-section of the holographic beam used in A. According to the axial profile of the intensity distribution, this shaped holographic beam has a range of focus, b, of 9 μm. Scale bar, 10 μm.
C. Plot that shows the linear dependence between the range of focus, b, and the spot size, s. Note that if in A it would be used a circular spot to cover the same region, a holographic spot of $\sim$25 μm of diameter would be needed; such spot gives rise to a larger focus of $\sim$37 μm. Values indicated by the dashed line. Adapted from Lutz et al. (2008).

The neuronal applications of this method did not take too much time to come. Lutz et al. (2008) and Nikolenko et al. (2008) used one-photon or two-photon excitation and showed reliable neuronal responses upon MNI-glutamate uncaging, demonstrating that this technique can be used to control neuronal activity. After these pioneering studies, there have been some further improvements. In particular for one-photon DH, it has been achieved 3D holographic excitation (Yang et al., 2011), 3D excitation and imaging (Anselmi et al., 2011) and DH excitation combined with two-photon imaging (Dal Maschio et al., 2010). However, only few groups have used this technology to study neuronal physiology. Santos et al. (2012) have used it to study the cellular mechanisms of short-term information storage and retrieval in pyramidal cells of the hippocampal CA1 region. Notably, a recent work has used one-photon DH to stimulate ChR2 expressing retinal ganglion cells as a strategy to artificially stimulate neurons disrupted by, for example, outer-retinal degenerative diseases (Reutsky-Gefen et al., 2013). Finally, DH was used to stimulate inspiratory neurons and determine the minimal quantity of neurons required to trigger a respiratory-related rhythm (Kam et al., 2013).

There are numerous advantages of this technique: (1) the possibility of shaping the beam without any rearrangement of the optical pathway, facilitating the experiments, (2) a better axial confinement of extended spots in comparison to a Gaussian beam (this is achieved by overfilling the back aperture of the objective lens and, consequently, using the numerical aperture to its maximum capacity), (3) the illumination of a prede-

fined region by shaping the area rather than by making a circular spot, which permits an increased axial confinement and accelerated photo-evoked response kinetics (figure 2.4 B and C), and (4) since DH is a scanless method, the temporal resolution of photoactivation depends primarily on the kinetics of the excitable molecule employed (Papagiakoumou, 2013; Oron et al., 2012).

The main limitations are: the loss of incident light intensity due to diffraction at the SLM, the existence of intensity inhomogeneities or speckles in the generated light-pattern and the size of the excitation field that depends on the SLM pixel array size. Concerning this latter, a typical value for a DH setup is around 160 X 160 μm^2, much smaller than scanning systems (600 X 600 μm^2), limiting its use for imaging in large biological samples (Papagiakoumou, 2013; Oron et al., 2012).

Part III

Results

Chapter 1

Article I

Many evidences show that OPCs exhibit different electrophysiological, morphological and cellular properties depending on both the brain region and the particular stage of development (see Introduction, sections 1.1 and 1.6.1). Therefore, we decided to characterize the electrophysiological properties of these cells in the mouse somatosensory (barrel) cortex during the first postnatal month which corresponds to the period of active cortical myelination.

1.1 Rodent somatosensory barrel cortex

The barrel cortex processes the information from the whiskers of rodents and is therefore an important region for the detection, location and discrimination of textures and objects. Classically described by Woolsey and Van der Loos (1970), this structure is characterized by the presence of barrels in layer IV, a topographic representation of whiskers. The barrels are formed by a cell-dense wall surrounding a cell sparse hollow containing thalamic inputs and separated by each other by a region called septa. These cylindrical aggregates replicate the pattern array of whiskers on the contralateral snout and can be visualized by different methods such as the labeling of thalamocortical afferent terminals with the vesicular transport of glutamate vGlut2. Briefly, the synaptic pathway starts with a mechanical deflection of the whisker that evokes an action potential in the sensory neurons of the trigeminal nerve. These neurons release glutamate onto second order neurons located in barrelets in the brainstem, which in turn project to neurons located in barreloids in the thalamus. Finally, thalamic neurons send mainly their axons to the barrels in the cortex (Li and Crair, 2011; Petersen, 2007). Figure 1.1 shows the time course of the patterned formation in the different brain regions involved in the whisker-barrel pathway.

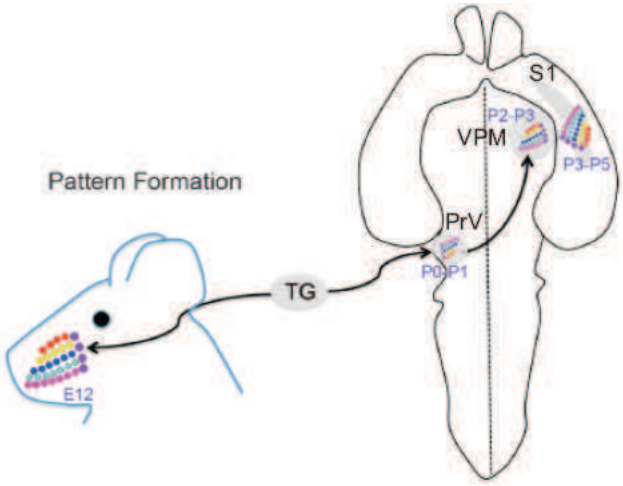

Figure 1.1: **Barrel cortex formation.**
Schematic representation that ilustrates of the timing of arrival of the neuronal afferents from whiskers to different brain structures and the emergence of axonal and cellular partterns (colored structures). TG, trigeminal ganglion; PrV, principal sensory nucleus of the trigeminal nerve; VPM, ventroposteromedial nucleus of the thalamus; S1, primary somatosensory cortex. From Erzurumlu and Gaspar (2012).

Two main reasons motivated our research in the barrel cortex region: the fact that it is one important and well-studied grey matter region in rodents and the high degree of myelination, mainly due to the presence of myelinated thalamic fibers. Myelination in the cortex starts during the first three postnatal weeks from *corpus callosum* to the pial surface (Trapp et al., 1997). The peak of OPC differentiation is reached around the second postnatal weak (Kang et al., 2010) and myelination is advanced at the end of the first postnatal month (Salami et al., 2003). However, the population of NG2 cells, although decreased, remains abundant in the cortex when myelin production is less required late in postnatal development. Also, they continue to proliferate in the adult, but at very slow rates (see Introduction, section 1.5). The abundance and widespread distribution of OPCs in the adult suggest that these cells might reside in the mature brain to perform other functions, different from that of progenitor. This hypothesis is supported by morphological and physiological data showing OPCs in the mature brain as cells with complex stellate morphology and low proliferation rate (Horner et al., 2002; Lytle et al., 2009). In addition, as discussed in section 1.6.2 (inward currents), there is an increase in potassium conductances during development that could account for a cellular function that is not needed at early stages of development when these cells actively proliferate and differentiate. Noteworthy, this apparent change in the electrophysiological profile seems to be related with grey matter regions, since white matter OPCs express less potassium currents at later stages (Lytle et al., 2009; Chittajallu et al., 2004).

Main results

In this first article we have recorded OPCs in the developing layer V of the mouse somatosensory cortex and by biophysical, pharmacological and single-cell RT-PCR approaches, we demonstrated that:

1. There is an up-regulation of Kir4.1 potassium channels of OPCs during the first postnatal month.
2. This conductance mediates a slow potassium current in OPCs upon extracellular stimulation of layer V axons, in the 4-5th postnatal weeks.
3. Action potential discharges of a single neuron can induce an inward current in a nearby adult OPC, indicating that OPCs are strategically located to detect local changes in extracellular potassium concentration during physiological neuronal activity.

In animals with advanced cortical myelination, adult OPCs acquire the machinery, through the postnatal upregulation of Kir4.1 potassium channels, to sense fine extracellular potassium increases generated by neuronal activity. OPCs gain physiological properties during postnatal development, conferring to these cells the capacity to communicate with neurons through a non-synaptic potassium-mediated mechanism. Beyond their abundance in the mature brain, the postnatal emergence of a physiological response of OPCs to neuronal network activity supports the view that in the adult these cells are not progenitors only (see Discussion).

Cellular/Molecular

Oligodendrocyte Precursor Cells Are Accurate Sensors of Local K^+ in Mature Gray Matter

Paloma P. Maldonado,[1,2,3] Mateo Vélez-Fort,[1,2,3] Françoise Levavasseur,[1,2,3] and María Cecilia Angulo[1,2,3]

[1]INSERM U603, 75006 Paris, France, [2]CNRS UMR 8154, 75006 Paris, France, and [3]Université Paris Descartes, Sorbonne Paris Cité, 75006 Paris, France

Oligodendrocyte precursor cells (OPCs) are the major source of myelinating oligodendrocytes during development. These progenitors are highly abundant at birth and persist in the adult where they are distributed throughout the brain. The large abundance of OPCs after completion of myelination challenges their unique role as progenitors in the healthy adult brain. Here we show that adult OPCs of the barrel cortex sense fine extracellular K^+ increases generated by neuronal activity, a property commonly assigned to differentiated astrocytes rather than to progenitors. Biophysical, pharmacological, and single-cell RT-PCR analyses demonstrate that this ability of OPCs establishes itself progressively through the postnatal upregulation of Kir4.1 K^+ channels. In animals with advanced cortical myelination, extracellular stimulation of layer V axons induces slow K^+ currents in OPCs, which amplitude correlates with presynaptic action potential rate. Moreover, using paired recordings, we demonstrate that the discharge of a single neuron can be detected by nearby adult OPCs, indicating that these cells are strategically located to detect local changes in extracellular K^+ concentration during physiological neuronal activity. These results identify a novel unitary neuron–OPC connection, which transmission does not rely on neurotransmitter release and appears late in development. Beyond their abundance in the mature brain, the postnatal emergence of a physiological response of OPCs to neuronal network activity supports the view that in the adult these cells are not progenitors only.

Introduction

Oligodendrocyte precursor cells (OPCs) are a class of progenitors that generate myelinating oligodendrocytes in the CNS during development and after demyelinating injury through a myelin repair process (Richardson et al., 2011). Recent Cre-Lox fate-mapping studies have also suggested that the fate of OPCs is relatively flexible, producing astrocytes and neurons in specific brain regions, although the multipotent capacity of OPCs is still a matter of intense debate (Richardson et al., 2011). In any case, OPCs have always been regarded as progenitors, even in the healthy adult brain where they constitute 2–3% of total cells in gray matter and 5–8% in white matter (Dawson et al., 2003). Nevertheless, their large abundance and widespread distribution have suggested that, in addition to their role as progenitors, OPCs reside in the mature brain to play other functions. In support of this view, a few scattered reports have shown that OPCs undergo important physiological modifications during postnatal development. In the hippocampus, the biophysical phenotype of OPCs, characterized by an outward rectifying *I–V* relationship during the two first postnatal weeks, progressively changes toward a linear shape (Kressin et al., 1995; Zhou et al., 2006). Developmental alterations in membrane receptor expression also occur in these cells. This is the case for the subunit composition of AMPA receptors (Ziskin et al., 2007; Mangin et al., 2008; Maldonado et al., 2011) and for the postnatal downregulation of nicotinic receptors (Vélez-Fort et al., 2009). Finally, complex changes have been reported concerning the mechanisms governing neuron-to-OPC communication in the brain. Glutamatergic synaptic responses of OPCs (Bergles et al., 2000; Karadottir et al., 2005; Kukley et al., 2007; Ziskin et al., 2007) increase in amplitude during the first three postnatal weeks, probably indicating a maturation process of these synapses (Ziskin et al., 2007; Mangin et al., 2008; De Biase et al., 2010). In contrast, direct GABAergic synaptic inputs of OPCs in the barrel cortex are lost early in postnatal development and replaced in the adult by an extrasynaptic mode of transmission, mediated solely by GABA spillover (Vélez-Fort et al., 2010).

Despite all these recent indications of divergent properties between young and adult OPCs, more efforts are needed to decipher developmental physiological changes that govern so far unrecognized functions of these cells in the brain. In particular, little information exists on neuron-to-OPC signaling in mature gray matter. In this report, we investigated the properties of neuron-to-OPC communication when myelination is advanced in the barrel cortex. We found that, beyond neurotransmitter transmission, adult OPCs are able to efficiently detect local $[K^+]_o$ in-

Received April 23, 2012; revised Nov. 7, 2012; accepted Dec. 7, 2012.

Author contributions: P.P.M., F.L., and M.C.A. designed research; P.P.M., M.V.-F., and M.C.A. performed research; F.L. contributed unpublished reagents/analytic tools; P.P.M. analyzed data; P.P.M., M.V.-F., and M.C.A. wrote the paper.

This work was supported by Grant R11077KK from Agence Nationale de la Recherche and Grants R09206KK and R11077KK from Fondation pour l'aide à la recherche sur la Sclérose en Plaques. P.P.M. was supported by a fellowship from Ecole des Neurosciences de Paris. M.V-F. was supported by a fellowship from Ligue Française contre la Sclérose en Plaques. We thank D.E. Bergles and F. Lesage for the gift of NG2-DsRed and TWIK1 $^{-/-}$ transgenic mice, respectively; Isabel Llano and Troy W. Margrie for helpful comments on the manuscript; E. Audinat for advice in single-cell RT-PCR and discussions; and N. Cortés, J. Montanaro, Q. Bourgeois, and the SCM Imaging Platform of the Sts-Pères Biomedical Sciences site of Paris Descartes University for technical assistance.

The authors declare no competing financial interests.

Correspondence should be addressed to Dr. María Cecilia Angulo, Laboratoire de Neurophysiologie et Nouvelles Microscopies, INSERM U603, CNRS UMR 8154, Université Paris Descartes, Sorbonne Paris Cité, 45 rue des Saints-Pères, 75006 Paris, France. E-mail: maria-cecilia.angulo@parisdescartes.fr.

M. Vélez-Fort's present address is Division of Neurophysiology, National Institute for Medical Research, Mill Hill, London NW7 1AA, United Kingdom.

DOI:10.1523/JNEUROSCI.1961-12.2013

 0270-6474/13/332432-11$15.00/0

creases generated by action potential discharges of individual cortical neurons. We also show that this process is mediated by the progressive upregulation of Kir4.1 channels in OPCs during postnatal development. The emergence of Kir4.1 channels in adult OPCs makes these cells accurate sensors of K^+ efflux during neuronal physiological activity.

Materials and Methods

Slice preparation and electrophysiology. All experiments followed European Union and institutional guidelines for the care and use of laboratory animals. Acute parasagittal slices (300 μm) of the barrel cortex were mainly performed at the 2 postnatal (PN) week and 4–5 PN weeks as previously described (Vélez-Fort et al., 2010). OPCs were identified in NG2-DsRed BAC transgenic mice (560 nm excitation and 620 nm emission wavelengths; Green OptoLed, Cairn Research). Patch-clamp recordings were performed at 33°C using an extracellular solution containing the following (in mM): 126 NaCl, 2.5 KCl, 1.25 NaH_2PO_4, 26 $NaHCO_3$, 20 glucose, 5 pyruvate, 2 $CaCl_2$, and 1 $MgCl_2$ (95% O_2, 5% CO_2). The intracellular solution was either a CsCl-based intracellular solution containing the following (in mM): 130 CsCl, 10 4AP, 5 TEA-Cl, 5 EGTA, 0.5 $CaCl_2$, 2 $MgCl_2$, 10 HEPES, 2 Na_2ATP, 0.2 Na-GTP, 10 Na_2-phosphocreatine, or a KCl-based intracellular solution containing the following (in mM): 130 KCl, 5 EGTA, 0.5 $CaCl_2$, 2 $MgCl_2$, 10 HEPES, 2 Na_2ATP, 0.2 Na-GTP, 10 Na_2-phosphocreatine (pH ~ 7.3, 296 mOsm). When isoflurane was used in the perfusion, it was dissolved in the extracellular solution immediately before its bath application at room temperature and maintained in a sealed bottle in which bubbling was stopped, as previously described (Taverna et al., 2005). Changes in $[K^+]_o$ from 2.5 to 10 mM were obtained by isotonic replacement of Na^+.

Extracellular stimulations were obtained using a monopolar electrode (glass pipette) placed in layer V of the barrel cortex (100 μs stimulations; Iso-Stim 01D, npi electronic). Paired-pulse and trains of stimulation of neurons were performed at 40 V, unless otherwise indicated. Neurons were recorded in voltage-clamp and current-clamp modes with an intracellular solution containing the following (in mM): 130 K-gluconate, 5 EGTA, 0.5 $CaCl_2$, 2 $MgCl_2$, 10 HEPES, 2 Na_2ATP, 0.2 Na-GTP, and 10 Na_2-phosphocreatine. They were held at −70 or −90 mV after correction for a liquid junction potential (10 mV). In simultaneous recordings between a neuron and an OPC, depolarizing current pulses of 200 or 400 pA were applied during 400 ms to the neuron, each 3–5 s to elicit action potential discharges. In simultaneous neuron-neuron recordings, the duration of this pulse was also increased to 800 ms, and the postsynaptic neuron was held to −90 mV as OPCs. Recordings were made without series resistance (R_s) compensation; R_s was monitored during recordings, and cells showing a change of >30% in R_s were discarded. Whole-cell recordings were obtained using Multiclamp 700B, filtered at 2–4 kHz, and digitized at 20 kHz. Digitized data were analyzed off-line using pClamp 10.1 (Molecular Devices) and Igor Pro 6.0.

Because the decay of inward K^+ currents evoked by neuronal stimulation was not well described by a single exponential function, we estimated the time required to decay by measuring the half-decay time of the current evoked by paired-pulse stimulation. The paired-pulse ratio of these currents was obtained by dividing the current amplitude of the second pulse by that of the first pulse. In simultaneous patch-clamp recordings, currents evoked in OPCs by single neuron firing were considered as a response only if they were on average larger than 2 times the SD of noise and if their amplitude distribution was significantly different from that of the noise.

Steady-state *I–V* curves were obtained by applying voltage steps of 400 ms from +40 mV to −140 mV and by measuring current amplitudes at 390 ms from the beginning of the steps. It is noteworthy that we already showed that neither the capacitance nor the morphology of OPCs of the barrel cortex changes during development (Vélez-Fort et al., 2010). *I–V* curves of currents sensitive to different agents were obtained by subtracting currents in the presence of a drug from their controls and normalizing with respect to the current elicited at +40 mV in control. To determine the percentage of OPCs having a young phenotype in 4–5PN weeks, we plotted the distribution of current amplitudes elicited at a voltage step of +40 mV in all recorded cells of the 2PN week. In the distribution graph, 90% of OPCs had a current amplitude inferior to 420 pA, which corresponds to the mean current amplitude plus the SD (mean ± SD: 220 ± 198; $n = 26$). We thus considered as a young phenotype all cells having a current <420 pA and as an adult phenotype those having currents >420 pA at a voltage step of +40 mV. Only cells recorded in the CsCl-based intracellular solution with an adult phenotype were considered for analysis (70% of OPCs in 4–5PN weeks).

Immunohistochemistry. For MBP and vGluT2 immunostainings, mice were perfused intracardially with PBS alone followed by 0.15 M phosphate buffer, pH 7.4 (PB) containing 4% paraformaldehyde at PN7, PN13–14, and PN27–31 ($n = 3$ animals for each developmental stage). Brains were removed and placed in a 4% paraformaldehyde solution overnight. Then, brain slices (50 μm) were prepared in PBS ice-cold solution (4°C), permeabilized with 1% Triton X-100 and 2% BSA for 1 h, and incubated two nights with antibodies diluted in a 0.2% Triton X-100 solution. Double immunostainings were performed by combining guinea pig polyclonal vGluT2 (1:1000; Millipore) with mouse monoclonal anti-MBP (1:100; Millipore). Primary antibodies were washed three times in PBS and incubated in secondary antibodies coupled to Alexa Fluor 488 or Alexa Fluor 633 (1:500; Invitrogen) for 2 h at room temperature.

For simultaneous recordings between neurons and OPCs, recorded cells were injected with 5.4 mM biocytin (Sigma-Aldrich). The slices containing the injected cells were then fixed overnight in 4% paraformaldehyde at 4°C, rinsed three times in PBS for 10 min, and incubated with 1% Triton X-100 and 2% BSA during 1 h. The slices were incubated overnight with rabbit polyclonal anti-NG2 antibody (1:400; Millipore) diluted in a 0.2% Triton X-100 solution. Then, they were washed three times in PBS and incubated in the secondary antibody coupled to Alexa Fluor 633 and streptavidin–Alexa Fluor 488 (Invitrogen) for 2 h.

Immunofluorescence was visualized with a confocal microscope (LSM 510, Carl Zeiss). Optical sections of confocal images were sequentially acquired using a 10× or 63× oil objectives (NA = 0.3 and 1.4, respectively) with the LSM-510 software. Images were processed and analyzed using ImageJ 1.44c (Wayne Rasband, National Institutes of Health). Because cortical layer I were poorly myelinated, we eliminated the background noise of MBP immunostainings by subtracting the fluorescence intensity of this layer to the whole image.

Single-cell RT-PCR and genotyping of NG2-DsRed::TWIK1 $^{-/-}$ transgenic mice. The analysis of single-cell transcripts for Kir4.1 channels was performed as previously described with modifications (Angulo et al., 1997; Seifert et al., 2009). Briefly, we harvested the cytoplasm of recorded cells with a patch pipette filled with 6 μl of an autoclaved DEPC-treated internal solution containing the following (in mM): 130 CsCl, 5 4-AP, 10 TEA-Cl, 2 $MgCl_2$, 0.2 EGTA, and 10 HEPES, pH 7.4, 290 mOsm. The content of the pipette was expelled into a test tube, and the reverse transcription (RT) was performed for 2 h at 50°C in a 10 μl reaction volume by adding the following components at final concentrations as indicated: 10 ng/μl hexamer random primers, 0.5 mM each dNTP, 5 mM DTT, 20 U of RNaseOut (Invitrogen), 100 U of Superscript III Reverse Transcriptase (Invitrogen), and 1× buffer supplied with the enzyme. After incubation, the tubes were kept at −20°C. The RT products were then amplified with primers for a two-round nested PCR (Seifert et al., 2009). The first PCR was done for 35 cycles (94°C, 30 s; 54°C, 30 s; 72°C, 45 s) after adding Taq polymerase (2.5 U; QIAGEN), 1× buffer supplied by the manufacturer, 100 μM dNTP, and the following primers (0.3 μM each): 5′ TATCAGAGCAGCCACTTCACCTTC 3′ and 5′ GGATCGTCTCGGCCCTCTTCTTAG 3′ (final volume, 100 μl). An aliquot of 1.5 μl of the PCR product was then used as a template for the second PCR (35 cycles; 94°C, 30 s; 58°C, 30 s; 72°C, 30 s) performed with the following nested primers: 5′ TTCACCTTCGAGCCAAGATGACG 3′ and 5′ AGGCGTGTGGTTGGCAGGAG 3′ (final volume, 25 μl). The positive control consisted of running in parallel RT-PCR for single cells and for total RNA (50 pg) from mouse hippocampus. Two negative controls were obtained by running RT-PCR either after omitting RT or for harvested cortical layer I-III neurons.

NG2-DsRed::TWIK1 $^{+/-}$ animals were generated by crossing heterozygous NG2-DsRed mice with homozygous TWIK1 knock-out

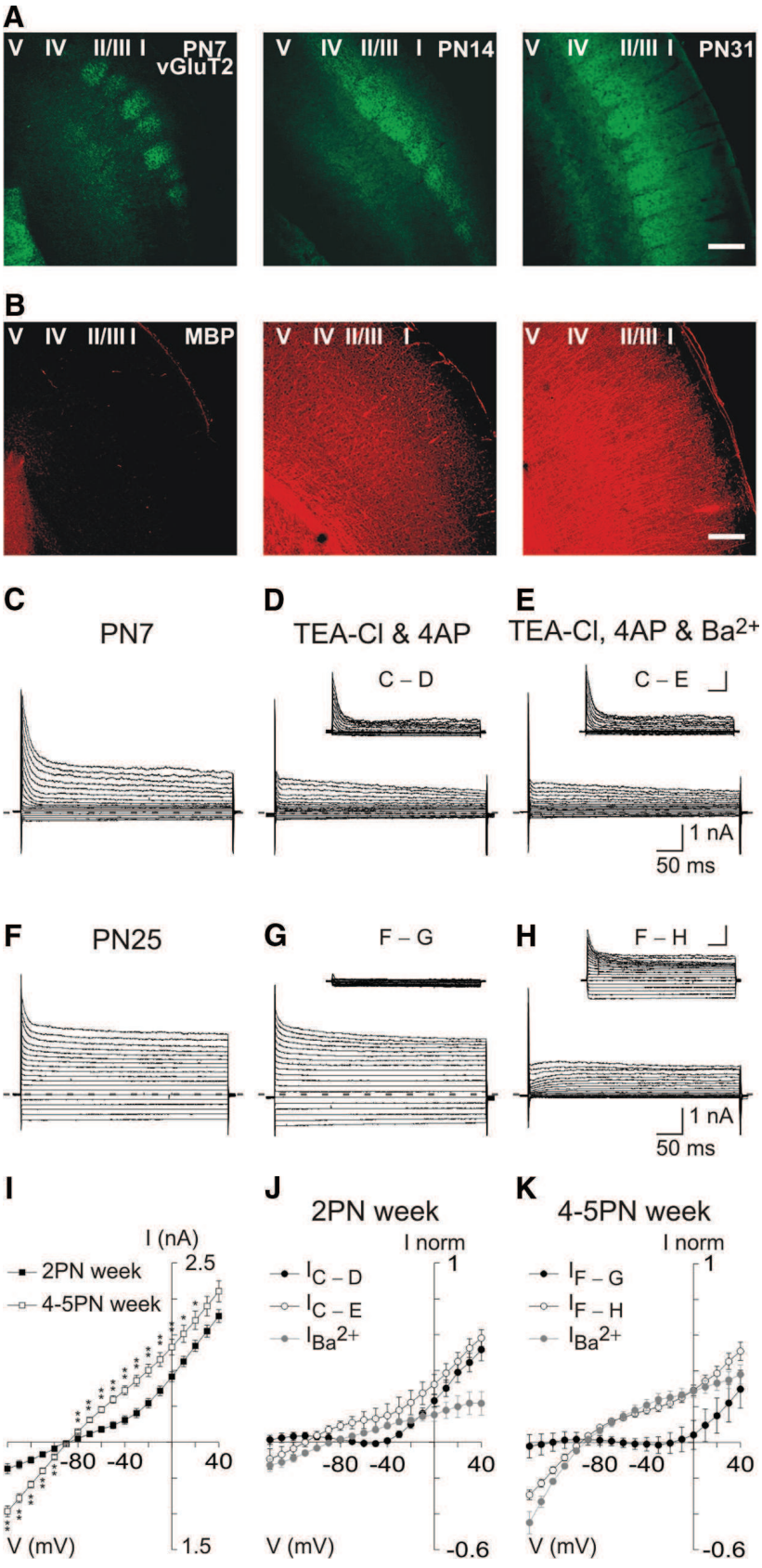

Figure 1. Cortical OPCs acquire a linear electrophysiological phenotype during postnatal myelination of the barrel cortex. ***A***, ***B***, Confocal images of a double immunostaining against the vesicular transporter for glutamate vGluT2 and the MBP at PN7, PN13–14, and PN27–31 (objective 10×; 1 optical section of 12.5 μm). vGluT2 immunoreactivity is enriched in barrel structures of layer IV (***A***). Note that cortical myelination starts in the 2PN week and is already advanced at 4–5PN weeks (***B***). Scale bar, 200 μm. ***C–H***, Currents induced in two OPCs held at −90 mV at PN7 (***C–E***) and PN25 (***F–H***) by voltage steps from +40 mV to −140 mV, using a KCl-based intracellular solution, in control conditions (***C***, ***F***), after adding in the bath 10 mM TEA and 4 mM 4AP (***D***, ***G***), and 10 mM TEA, 4 mM 4AP, and 100 μM Ba^{2+} (***E***, ***H***). Hyphenated gray lines correspond to zero current for all cases. Insets show subtracted currents with respect to controls. Calibration: 1 nA, 50 ms. ***I***, Comparison of steady-state *I–V* curves in control conditions between the 2PN and 4–5PN weeks ($n = 16$ and $n = 42$, respectively). Note that the outward rectification in the 2PN week changes to a linear shape in 4–5PN weeks. *$p < 0.05$. **$p < 0.01$. ***J***, ***K***, Comparison of steady-state *I–V* curves of currents sensitive to the large-spectrum K^+ channel blockers TEA, 4AP, and Ba^{2+} in the 2PN (***J***) and 4–5PN (***K***) weeks. Note that, in the 2PN week (***J***), a large outward TEA, 4AP-sensitive component (●, $n = 7$, $p < 0.05$ from −20 to +40 mV) does not significantly change after adding Ba^{2+} in the bath (○, $n = 7$, $p > 0.05$ for all potentials), and is larger than that obtained when Ba^{2+} is applied alone (gray circles, $n = 6$, $p < 0.05$ from 0 to +40 mV). In contrast, in 4–5PN weeks (***K***), a smaller TEA, 4AP-sensitive component exists (●, $n = 10$, $p < 0.05$ only for +40 mV), compared with a large Ba^{2+}-sensitive component present after adding Ba^{2+} in the bath (○, $n = 12$; $p < 0.001$ for all potentials except for −90 mV and −100 mV) or when Ba^{2+} is applied alone (gray circles, $n = 6$; $p < 0.05$ for all potentials except for −90 mV). Note that the Ba^{2+}-sensitive component is characterized by a weak inward rectification.

mice. Heterozygous double-transgenic mice were then crossed with TWIK1 $^{-/-}$ mice to obtain TWIK1 $^{-/-}$ mice expressing DsRed in littermates. This last generation was genotyped by PCR with primers designed to amplify a 434 bp and a 600 bp fragment for wild-type and knock-out sequences, respectively. PCR was done for 40 cycles (94°C, 30 s; 55.4°C, 30 s; 72°C, 1 min 30 s) with the following primers: 5′ TCCTTCCTACCGACAGCGAGAGA 3′ and 5′ GGGATGCCGATGACAGAGTAGAT 3′ for wild-type; 5′ TGCCTTTACGGTGTCTGT TC 3′ and 5′ GAGAAGGCAGAAATGGAAAC TG 3′ for knock-out. After patch-clamp experiments, we confirmed that killed animals were TWIK1 $^{-/-}$ by PCR.

Statistics. Data are expressed as mean ± SEM The nonparametric Mann–Whitney *U* test for independent samples was used to determine statistical differences between data obtained in different cells. Comparisons within single cells were performed with the Wilcoxon signed-rank test for related samples when $n \geq 6$; otherwise, we used a paired *t* test (GraphPad InStat software, Version 3.06). Amplitude distributions of induced currents in simultaneous recordings were compared using the Kolmogorov–Smirnov test (http://www.physics.csbsju.edu/stats).

Results

OPCs acquire a linear phenotype during postnatal development of the barrel cortex

The properties of OPCs of the barrel cortex during postnatal development were examined in layer V DsRed $^+$ cells recorded during 2PN and 4–5PN weeks in NG2-DsRed transgenic mice (Ziskin et al., 2007). These developmental stages were chosen to cover the critical period of

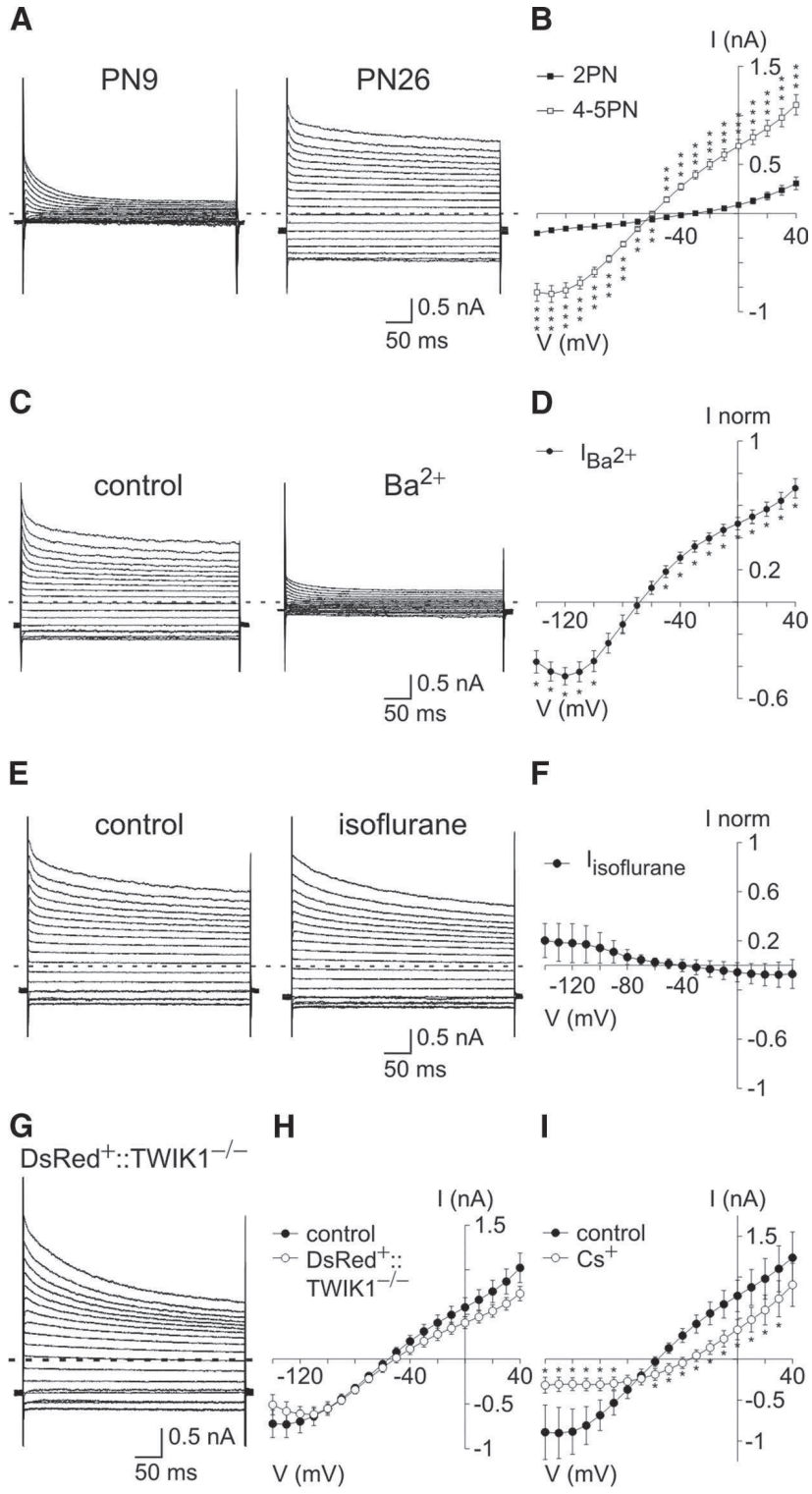

Figure 2. TWIK1 and TREK1 two-pore domain K^+ channels are not major conductances in adult OPCs. ***A***, Currents induced in OPCs held at −90 mV at PN9 and PN26 by voltage steps from +40 mV to −140 mV, using a CsCl-based intracellular solution containing TEA and 4AP. The same holding potential, voltage steps, and intracellular solution were used for the experiments below; hyphenated gray lines indicate zero current for all cases. ***B***, Steady-state mean *I–V* curves of OPCs between the 2PN ($n = 26$) and 4–5PN weeks ($n = 35$). Note the large component present only in OPCs of 4–5PN weeks. $^{**}p < 0.01$. $^{***}p < 0.001$. It is noteworthy that Na^+ currents were always observed in OPCs of 2PN week, but they are not visible with the time scale of 400 ms (see also Maldonado et al., 2011). ***C***, Currents induced in an OPC before (left) and after (right) bath application of 100 μM Ba^{2+}. ***D***, Mean steady-state *I–V* curves of currents sensitive to 100 μM Ba^{2+} ($n = 6$). $^*p < 0.05$. ***E***, Currents induced in an OPC before and after bath application of 10 mM isoflurane, a volatile anesthetic enhancing the opening of TREK1 channels (Patel et al., 1999). ***F***, Mean *I–V* curve of currents sensitive to 10 mM isoflurane. Note the lack of effect of this agent ($n = 8$). $p > 0.05$. It is also noteworthy that the acidification of intracellular medium known to increase TREK1-mediated currents (Lotshaw, 2007) instead reduced K^+ currents of OPCs (Fig. 3*B*,*D*). ***G***, Currents of OPCs in a double-transgenic NG2-DsRed::TWIK1 $^{-/-}$ mice. Because no specific pharmacological tools allowing for the unambiguous discrimination of TWIK1-mediated currents exist, these double-transgenic mice were generated to identify DsRed $^+$ OPCs in a context in which TWIK1 was inactivated (Materials and Methods). ***H***, Mean *I–V* curves of OPCs in control and NG2-DsRed::TWIK1 $^{-/-}$ mice. OPCs of NG2-DsRed::TWIK1 $^{-/-}$ mice had the same current amplitudes as those recorded in controls performed during the same period ($n = 10$ and $n = 13$, respectively). $p > 0.05$, for all potentials. ***I***, Mean *I–V* curves of OPCs in control and after bath application of 1 mM Cs^+. Note that extracellular Cs^+ abolishes most inward than outward currents ($n = 6$). $^*p < 0.05$.

myelination of deep layers of the barrel cortex (Fig. 1*A*,*B*). Indeed, cortical myelination starts in the 2PN week and is already advanced at PN30 (Fig. 1*B*), when the conduction velocity of action potentials of the thalamocortical pathway reaches a plateau (Salami et al., 2003) and intracortical circuits are relatively mature (Angulo et al., 1999; Morales et al., 2002).

OPCs were first recorded with a KCl-based intracellular solution and held at −90 mV. Application of voltage pulses from +40 mV to −140 mV revealed a dramatic developmental change in the *I–V* relationship. Comparison of steady-state *I–V* curves showed that the outward rectification observed in the 2PN week changes to a linear shape in 4–5PN weeks (Fig. 1*C*,*F*,*I*). This modification of the ion current profile was observed at least until PN54 ($n = 4$) and was accompanied by a more hyperpolarized resting membrane potential (−77.9 ± 2.7 mV in the 2 PN week vs −88.1 ± 2.5 mV in 4–5PN weeks, respectively; $p < 0.01$) and a decreased input resistance (281.8 ± 59.7 MΩ in the 2PN week against 70.9 ± 6.5 MΩ in the 4–5PN weeks, respectively; $p < 0.001$).

The sensitivity of currents evoked by voltage steps to the large-spectrum K^+ channel blockers TEA and 4AP was also different between both developmental stages. These antagonists blocked a large proportion of outward currents in the 2PN week (Fig. 1*D*,*J*) but affected to a smaller extent those in the 4–5PN weeks (Fig. 1*G*,*K*). In contrast, a subsequent application of Ba^{2+} inhibited modestly additional currents in young mice (Fig. 1*E*,*J*) but suppressed substantial currents in older mice (Fig. 1*H*,*K*). This is consistent with the effect of Ba^{2+} applied alone. Small Ba^{2+}-sensitive currents were revealed in the 2PN week (Fig. 1*J*), whereas large currents had similar amplitudes than those recorded in the presence of TEA, 4AP, and Ba^{2+} in 4–5PN weeks (Fig. 1*K*).

These results indicate that a Ba^{2+}-sensitive, TEA-insensitive, and 4AP-

insensitive conductance, the identity of which is unknown, is upregulated in OPCs during postnatal development of the barrel cortex. The weakly inward rectification of this conductance counteracts the outward rectification observed in the 2PN week, conferring a linear phenotype on OPCs in the adult (Fig. 1*I*,*K*).

Identification of Kir4.1 channels as a major postnatal upregulated conductance in OPCs

The emergence of a linear *I–V* curve has been previously described in hippocampal OPCs (Kressin et al., 1995; Zhou et al., 2006), but the conductance conferring a linear phenotype in the adult has not been identified yet. To isolate the Ba^{2+}-sensitive current upregulated in OPCs, we tested a CsCl-based intracellular solution containing TEA and 4AP, known to suppress from the inside most currents mediated by voltage-gated K^+ channels. This solution almost completely abolished intrinsic currents in young mice, whereas significant currents still remained in 70% of OPCs of 4–5PN weeks (considered as OPCs with an adult phenotype; see Materials and Methods; Fig. 2*A*,*B*). Furthermore, bath application of 100 μM Ba^{2+} almost completely blocked currents of intrinsic *I–V* curves in adult OPCs (Fig. 2*C*,*D*), indicating that this intracellular solution is convenient to block voltage-gated K^+ channels and isolate the currents of our interest.

To identify the K^+ conductance postnatally upregulated in OPCs, we examined the effect of different blockers for K^+ channels insensitive to TEA and 4AP and sensitive to Ba^{2+} (i.e., small-conductance Ca^{2+}-activated potassium [SK] channels) (Sah and Faber, 2002), the two-pore domain K^+ channels TREK1 and TWIK1 (Lesage et al., 1996; Lotshaw, 2007), and inwardly rectifying (Kir) channels (Hibino et al., 2010). First, we excluded the contribution of SK channels in OPCs of 4–5PN weeks by applying their selective antagonist apamin and detecting no effects on the recorded currents (200 nM; $p > 0.05$; $n = 5$) (Sah and Faber, 2002). Then, we examined whether TWIK1 and TREK1 were functionally expressed. According to a transcriptome database, the mRNAs of the two-pore domain K^+ channels TWIK1 and TREK1 are preferentially enriched in acutely isolated purified OPCs (Cahoy et al., 2008). However, the lack of effect of isoflurane in these currents, an anesthetic activating TREK1 (Fig. 2*E*,*F*), and the unchanged electrophysiological phenotype of OPCs in a transgenic mouse expressing inactivated TWIK1 (Fig. 2*G*,*H*) (Nie et al., 2005) show that, contrary to astrocytes (Seifert et al., 2009; Zhou et al., 2009), two-pore domain K^+ channels are poorly expressed in adult OPCs.

It is well known that Cs^+ blocks Kir channels from the outside in a voltage-dependent manner (Hibino et al., 2010; Tang et al., 2010). In a CsCl-based intracellular solution, bath applications of 1 mM Cs^+ blocked currents of the *I–V* curve from the outside as expected for Kir channels (i.e., abolishing most inward currents and only weakly outward currents; Fig. 2*I*) (Hibino et al., 2010; Tang et al., 2010). Although the effect of intracellular Cs^+ is poorly characterized for Kir channels, some effect was evident because currents, particularly inward currents, appeared reduced compared with those recorded in KCl-based intracellular solution (Fig. 2*B* for CsCl vs Fig. 1*I* for KCl) and E_{rev} was shifted from -88.14 ± 2.46 mV to -59.30 ± 1.30 mV ($p < 0.001$). These data strongly suggest a major expression of a Kir conductance in adult OPCs. In support of this and as mentioned above, 100 μM Ba^{2+}, a well-known Kir blocker at this concentration (Hibino et al., 2010), abolished currents of intrinsic *I–V* curves in adult OPCs (Fig. 2*C*,*D*).

Among Kir channels, Kir4.1 channels are found almost exclusively in glial cells (Poopalasundaram et al., 2000; Higashi et al., 2001; Seifert et al., 2009; Tang et al., 2009). Because the deletion of Kir4.1 channels in transgenic mice is lethal around the end of the third PN week (Kofuji et al., 2000; Djukic et al., 2007), we used pharmacological tools to examine its functional expression in OPCs of the 4–5PN weeks. First, we assessed the effect of the tricyclic antidepressant desipramine, an inhibitor of Kir4.1 currents that affects only slightly other Kir currents in heterologous expression systems (Su et al., 2007). In adult OPCs recorded in CsCl-based intracellular solution, this agent almost completely abolished K^+ currents (Fig. 3*A*,*C*). Previous works also demonstrated a partial sensitivity of Kir4.1 channels to an intracellular pH of 6.5 (Tucker et al., 2000; Pessia et al., 2001). To test for the effect of acidic pH, we performed two consecutive whole-cell patch-clamp recordings on the same cell with intracellular solutions at pH of 7.4 and 6.3, respectively (Fig. 3*B*,*D*). We observed a decrease of current amplitudes to voltage steps during the second whole-cell recording, an effect compatible to the acidic pH sensitivity reported for homomeric Kir4.1 channels (reduction of $51.0 \pm 5.9\%$ at +40 mV; Fig. 3*D*) (Tucker et al., 2000; Pessia et al., 2001). To verify that this effect was not caused by degradation of the cell by removing the first patch pipette, we performed the same experiments without changing the pH during the second whole-cell recording. In that case, no changes on the *I–V* relationship were observed, confirming the effect of acidic pH (Fig. 3*D*, black circles). Finally, we performed single-cell nested RT-PCR experiments to detect transcripts for Kir4.1 channels in OPCs of the barrel cortex (Fig. 3*E*; see Materials and Methods). Kir4.1 transcripts were found in 7 of 9 recorded adult OPCs (78%), whereas they were amplified in only 1 of 10 cortical neurons (10%). Biophysical, pharmacological, and molecular analyses indicate that Kir4.1 channels are by far the major K^+ conductance developmentally upregulated in OPCs of the mature barrel cortex and that this conductance contribute to the linear phenotype of *I–V* relationships in the adult.

Adult OPCs detect local K^+ increases through upregulated Kir4.1 channels

Astrocytes are accurate detectors of neuronal activity through a Kir4.1 conductance (De Saint Jan and Westbrook, 2005; Djukic et al., 2007). Because Kir4.1 channels are postnatally upregulated in OPCs, we tested whether, similarly to astrocytes, these cells are able to sense extracellular $[K^+]_o$ increases through these channels in the mature neuronal network. For this, an extracellular electrode placed in layer V was used to stimulate neuronal fibers while $NG2^+$/$DsRed^+$ OPCs were recorded at -70 mV with the CsCl-based intracellular solution to accurately isolate Kir4.1-mediated currents (Fig. 4*A*,*B*). Experiments in older mice were performed in OPCs having an adult phenotype. Paired-pulse stimulation easily elicited currents in OPCs of the 2PN and 4–5PN weeks (mean amplitude of first pulse: -136.8 ± 41.5 pA and -159.5 ± 45.0 pA; $n = 8$ and $n = 13$, respectively; Fig. 4*C*,*D*, gray traces) (Vélez-Fort et al., 2010). However, whereas the ionotropic glutamatergic and GABAergic receptor antagonists in young mice abolished these currents, a persistent current remained in older mice ($1.7 \pm 0.6\%$ and $17.7 \pm 4.4\%$ in 2PN and 4–5PN weeks, respectively; $p < 0.001$; Fig. 4*C*,*D*, black traces). This persistent current in older mice was characterized by long-lasting kinetics with a half-decay time of 0.45 ± 0.03 s and a much weaker paired-pulse depression compared with control conditions (paired-pulse ratio of 0.93 ± 0.03 in antagonists against 0.22 ± 0.03 in controls, $n = 13$; $p < 0.001$; see Materials and Methods). Moreover, its amplitude increased an average when the stimulation intensity varied from 20 to 40 V (increment of 70.1%; $n = 13$ and $n = 23$, respectively; $p < 0.01$) or when trains

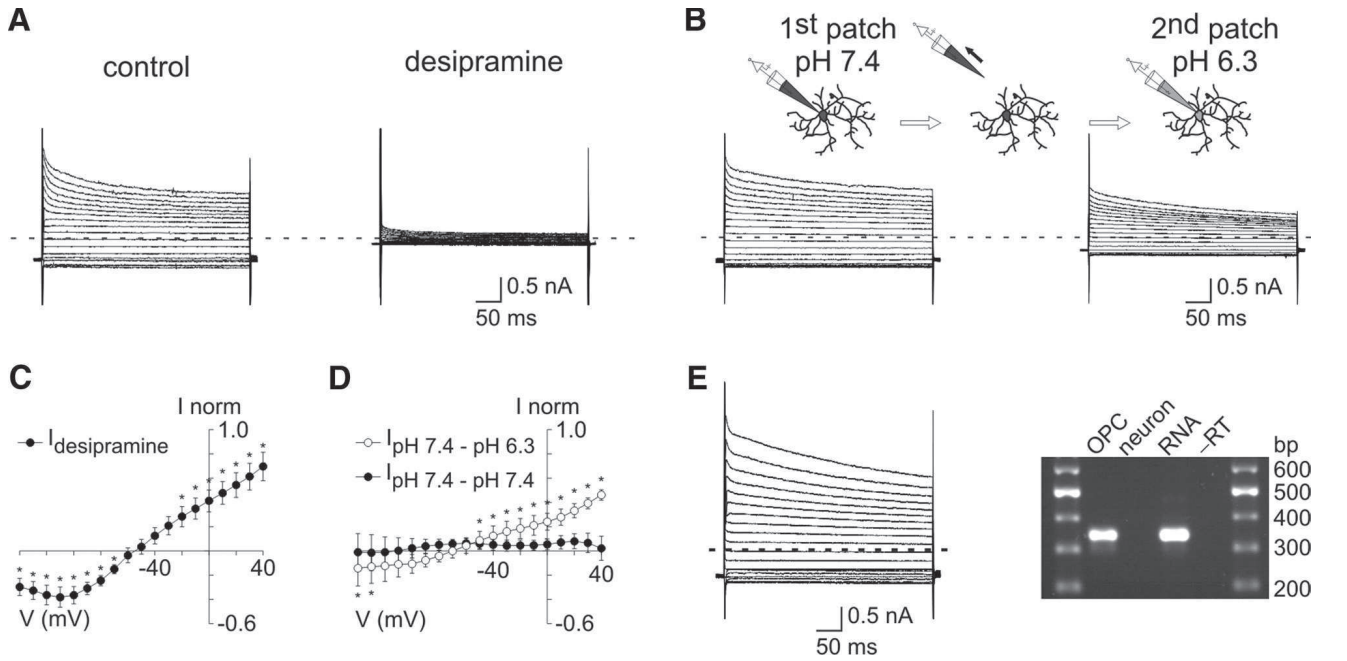

Figure 3. Kir4.1 channels are upregulated in OPCs of the mature barrel cortex. ***A***, ***C***, Effect of 100 μM desipramine on currents induced in an OPC using a CsCl-based intracellular solution containing TEA and 4AP and held at −90 mV by voltage steps from +40 mV to −140 mV in 4–5PN weeks. The mean steady-state *I–V* curve shows currents sensitive to desipramine (***C***) ($n = 6$). *$p < 0.05$. The same holding potential and voltage steps were used for the experiments below; and hyphenated gray lines indicate zero current for all cases. ***B***, ***D***, Effect of intracellular acidification on currents induced in OPCs in 4–5PN weeks. As shown in the diagram (top), two consecutive patches were performed in the same cell with CsCl-based intracellular solutions at a pH of 7.4 and of 6.3. Mean steady-state *I–V* curves were obtained by subtracting current traces of the second patch from those of the first patch (***D***) (○; $n = 7$). *$p < 0.05$. As a control, the same experiment was performed without changing the pH during the second whole-cell recording (***D***) (●; $n = 4$). $p > 0.05$ for all potentials. ***E***, Currents induced in OPCs at PN23 (left) and analyzed by single-cell RT-PCR (right). After recording, the cytoplasm was harvested and nested RT-PCR for the Kir4.1 channel was performed. Kir4.1 was expressed in this OPC as shown in the agarose gel (338 bp; right). Note that the control of total RNA (RNA; 50 pg) was positive, whereas either a neuron or the negative control without RT (−RT) was not.

of stimuli were applied (50 Hz; peak amplitude: −207.61 ± 59.7 pA; $n = 5$; Fig. 4*F*). In contrast, even at high rates of stimulation, the persistent current was negligible in OPCs of the 2PN week (50 Hz; peak amplitude: −10.1 ± 4.5 pA; $n = 8$; Fig. 4*E*). In older animals, the supplement in the antagonist solution of metabotropic glutamatergic and GABAergic receptor blockers LY341495 (50 μM) and CPG55845 (5 μM) and of the purinergic receptor blocker PPADS (30 μM) were without effect, indicating that the persistent current in 4–5PN weeks is not mediated by common ionotropic and metabotropic receptors ($n = 4$; $p > 0.05$, Fig. 4*G*). Yet, it was completely abolished by the Na^+ channel blocker TTX, showing that it is induced by neuronal activity (88.6 ± 11.7% of block; $n = 4$; Fig. 4*H*). Because this current is not mediated by common neurotransmitter receptors, it probably reflects a K^+ efflux from neurons during action potential discharges as it has been described previously for astrocytes (De Saint Jan and Westbrook, 2005). Because the amplitude and kinetics of persistent currents in OPCs vary with the intensity and frequency of neuronal stimulation, the response of OPCs is able to follow different regimens of neuronal activity.

The emergence of a resistant current during development was concomitant with the upregulation of Kir4.1 channels. To analyze whether Kir4.1 channels mediated this current, we used the same pharmacological tools as described previously (Fig. 3). First, neuronal-evoked inward currents were reduced by the Kir channel blocker Ba^{2+} (71.0 ± 8.2% reduction; $n = 6$; $p < 0.05$; Fig. 5*A*). A similar effect of Ba^{2+} was seen when recording OPCs with a KCl-based intracellular solution, confirming that these Ba^{2+}-sensitive currents are evoked in physiological K^+ concentrations (91.0 ± 7.0% reduction; $n = 6$; $p < 0.05$; Fig. 5*B*). Because desipramine reduced the amplitude of synaptic currents in postsynaptic recorded neurons (reduction of 51.4 ± 14.1%; $n = 9$; $p < 0.05$), we could not use this drug. Instead, we attempted to decrease the inward K^+ current evoked by neuronal stimulation from the inside with the acidic intracellular solution. As expected for Kir4.1 channels and in agreement with our results on intrinsic *I–V* curves (Fig. 3), we obtained that the persistent inward current was significantly reduced in adult OPCs recorded at a pH of 6.3 compared with controls performed at a physiological pH, in the same slices and with the same stimulation electrodes (reduction of 50.5%, $n = 13$ and $n = 11$, respectively; $p < 0.01$; Fig. 5*C*).

If persistent inward currents reflect a transient $[K^+]_o$ rise caused by action potential discharges, their *I–V* curve should be shifted toward more positive potentials. To assess the *I–V* curve of neuronal-evoked inward currents resistant to antagonists, we performed 100 ms ramps from +40 mV to −140 mV before the stimulation and at the peak of the second response (Fig. 6*A*). As expected for a K^+ conductance, E_{rev} shifted to a more depolarized potential in all tested cells during stimulation (shift of 4.3 ± 1.2 mV; $n = 5$; $p < 0.05$; Fig. 6*B*), a value below that obtained in intrinsic *I–V* curves when $[K^+]_o$ was artificially raised to 10 mM (shift of 8.7 ± 2.3 mV; $n = 6$; $p < 0.05$; Fig. 6*C*,*D*). Therefore, neuronal stimulation induces a K^+ current in OPCs that reflects a K^+ efflux from neurons comprised between 2.5 and 10 mM as expected for physiological rates of action potential discharges (Heinemann and Lux, 1977; Kofuji and Newman, 2004).

Our data reveal that, in addition to respond to neurotransmitter release, OPCs acquire the ability during postnatal development to detect transient $[K^+]_o$ increases caused by neuronal activity via the postnatal upregulation of Kir4.1 channels. These results add a further complexity to the mechanisms governing neuron–OPC communication in the mature brain.

OPCs are accurate sensors of K^+ increases generated by single nearby neurons

To test whether adult OPCs are able to sense fine $[K^+]_o$ increases of single nearby neurons when they discharge action potentials, we performed simultaneous patch-clamp recordings between a neuron and an OPC, which somata were separated by <18 μm (range, 0–18 μm). Figure 7*A* illustrates a labeled neuron and NG2$^+$/DsRed$^+$ OPCs recorded with intracellular solutions containing biocytin. Depolarizing current pulses of 400 ms were elicited in the recorded neuron to induce action potential firing while recording the nearby OPC with a KCl-based intracellular solution (in physiological K^+ concentrations) (Fig. 7*A*, right, and 7*B*). For 21 of 26 simultaneous recordings, a train of action potentials in the neuron elicited a current in the OPC that had a mean peak amplitude of −3.1 ± 0.5 pA and showed always an amplitude distribution significantly different to that of the noise (Fig. 7*B*,*E*). Neurons eliciting a response in OPCs showed variable discharge frequencies ranging from 27.5 to 121.8 Hz, which includes pyramidal cells and interneurons, indicating that the OPC current is not induced by a specific neuronal cell type (mean frequency, 70.3 ± 15.9 Hz). It is noteworthy that neither the frequency nor the distance between cell somata where correlated to the amplitude of the current ($p > 0.05$). In addition, despite the presence of a large repertoire of K^+ channels in neurons, such current was never observed in simultaneous recordings between two neurons which somata were separated by <13 μm (range, 1–13 μm), even when the depolarizing pulse duration was increased to 800 ms (mean amplitude: −0.35 ± 0.35 pA; $n = 7$; Fig. 7*G*).

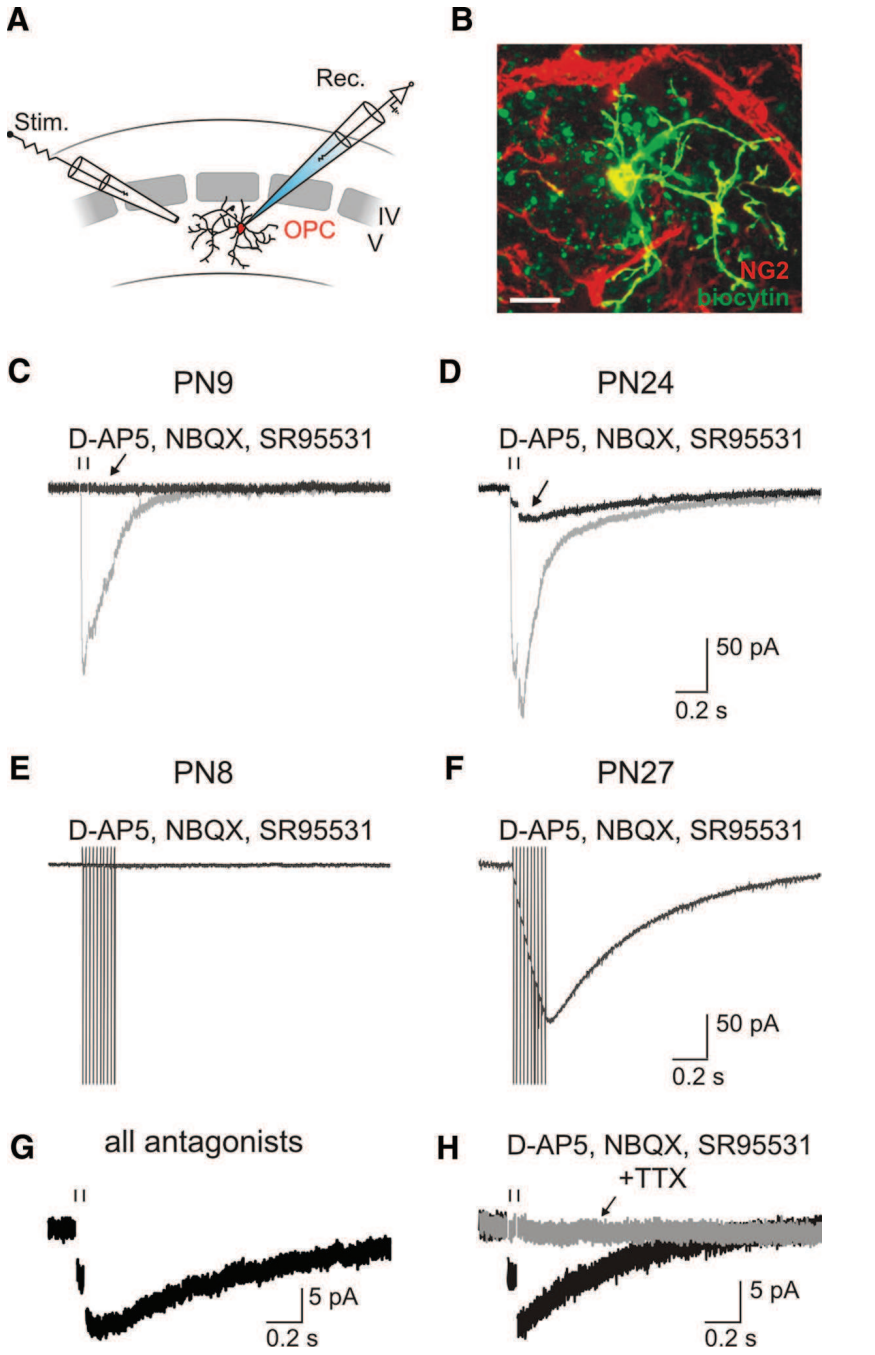

Figure 4. OPCs sense local increases of $[K^+]_o$ during neuronal activity in the mature barrel cortex. ***A***, Schematic representation of extracellular stimulation of layer V neuronal fibers during patch-clamp recordings of OPCs of the barrel cortex. ***B***, Confocal image of an NG2$^+$/DsRed$^+$ OPC recorded with an intracellular solution containing biocytin at PN24 (objective 63×; stack of 18 *z* section, each 1 μm, see Materials and Methods). Scale bar, 15 μm. ***C***,***D***, Paired-pulse stimulation of neuronal fibers elicited inward currents in two OPCs held at −70 mV at PN9 (***C***) and PN24 (***D***) (gray traces; pulses separated by 50 ms; 100 μs, 40 V). Although the evoked current was completely abolished by 10 μM NBQX, 50 μM D-AP5, and 5 μM SR95531 in ***C***, a persistent current remained in ***D*** (black traces). Stimulus artifacts were blanked for visibility; the time of stimulation is indicated with a vertical line. ***E***,***F***, Inward currents elicited by γ frequency train stimulation (50 Hz) of neuronal fibers in two OPCs held at −70 mV at PN8 (***E***) and PN27 (***F***), in the presence of antagonists. Stimulus artifacts were truncated for visibility. ***G***, Inward current evoked in an OPC by neuronal stimulation, resistant to a mixture of antagonists consisting of 10 μM NBQX, 50 μM D-AP5, 5 μM SR95531, 50 μM LY341495, 5 μM CPG55845, and 30 μM PPADS (all antagonists). ***H***, Effect of 0.5 μM TTX on currents induced by paired-pulse stimulation of neuronal fibers in an OPC held at −70 mV and recorded in the presence of 10 μM NBQX, 50 μM D-AP5, and 5 μM SR95531. Note the block of the current by TTX.

It is known that OPCs detect neuronal activity through synaptic and extrasynaptic signaling mechanisms dependent on neurotransmitter release (Maldonado et al., 2011). However, the current elicited in OPCs by single neuron stimulation was insensitive to metabotropic and ionotropic glutamate, GABA, and purinergic receptor antagonists; thus, it did not result from either classical synaptic transmission or spillover of neurotransmitters (−3.2 ± 1.0 pA and −3.4 ± 1.0 pA in control and all antagonists, respectively; $p > 0.05$; $n = 5$; Fig. 7*C*,*F*). This current developed progressively during neuronal firing without evidence of postsynaptic events, suggesting a nonsynaptic nature of the response (Fig. 7*B*,*C*). Nevertheless, considering that OPCs have a relatively low input resistance in KCl-based intracellular solution (~70 MΩ), we cannot completely exclude that the current recorded in the OPC results from an artifactual detection through the patch pipette of the depolarizing current injected to the neuron. To discard this possibility, we hyperpolarized the neuron to prevent action potential dis-

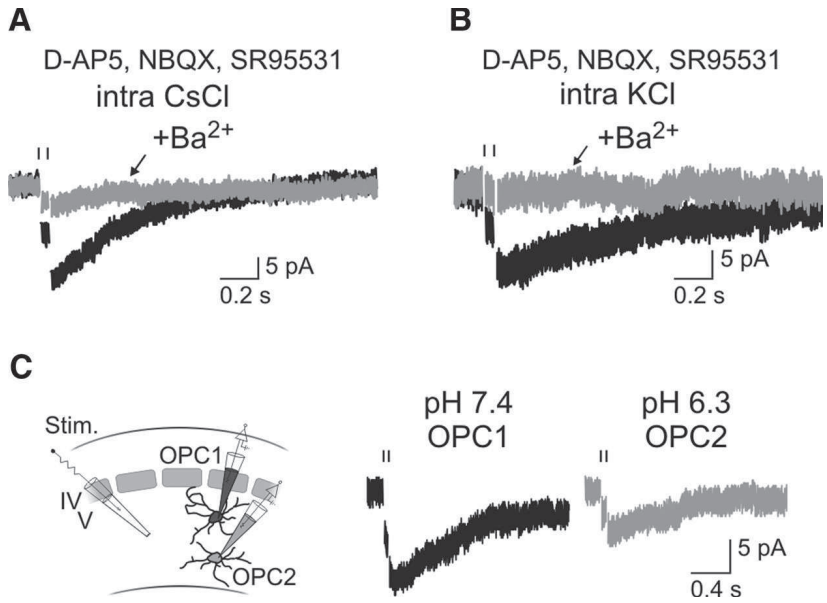

Figure 5. K^+ currents induced by neuronal activity in OPCs of 4–5PN weeks are mediated by Kir4.1 channels. ***A***, ***B***, Effect of 100 μM Ba^{2+} on inward currents resistant to antagonists and evoked by paired-pulse stimulation of neuronal fibers in OPCs held at −70 mV and recorded in CsCl-based intracellular solution (***A***) and KCl-based intracellular solution (***B***). Stimulus artifacts were blanked for visibility. A vertical line indicates the time of stimulation. Pulses were separated by 50 ms in all cases (100 μs, 40 V). ***C***, Inward currents evoked in two OPCs recorded with an intracellular solution at a pH of 7.4 (left) and of 6.3 (right) in the same slice and with the same stimulation electrode as shown in the diagram (left).

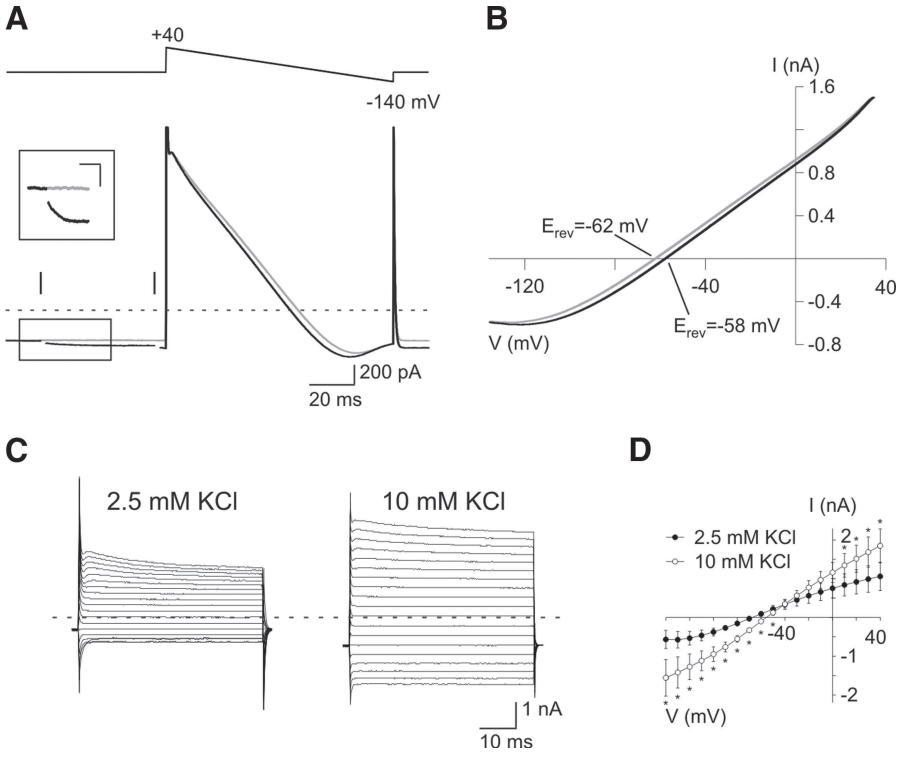

Figure 6. *I–V* curve of the persistent K^+ current evoked by neuronal stimulation. ***A***, Inward currents induced in an OPC by 100 ms ramps from +40 mV to −140 mV before the extracellular stimulation (gray trace) and at the peak of the second evoked response in the presence of 10 μM NBQX, 50 μM D-AP5, and 5 μM SR95531 (black trace; pulses separated by 50 ms; 100 μs, 40 V). The inset illustrates the persistent current evoked by paired-pulse stimulation at the first pulse. Calibration: 25 ms; 25 pA. Stimulus artifacts were blanked for visibility. A vertical line indicates the time of stimulation; a hyphenated gray line indicates zero current. ***B***, Mean *I–V* curves obtained with ramps before the stimulation (gray trace) and at the peak of the second evoked response (black trace; $n = 5$). ***C***, Effect of bath application of an increase in $[K^+]_o$ from 2.5 to 10 mM on an adult OPC held at −90 mV and recorded with the CsCl-based intracellular solution. ***D***, Comparison of mean steady-state *I–V* curves in control and after application of high $[K^+]_o$ shows an increase of induced currents and a shift in E_{rev} of −8.7 ± 2.3 mV ($p < 0.05$; $n = 6$). *$p < 0.05$.

charges while applying the same depolarizing current pulse (Fig. 7*H*,*I*). In four simultaneous recordings, the evoked current observed in the OPCs during action potential discharges was completely abolished when the neuron did not fire during current injection, confirming that neuronal action potentials are necessary to elicit a response in the OPC (−2.3 ± 1.1 pA vs 0.1 ± 0.1 pA). In addition, this current was inhibited by 100 μM Ba^{2+}, indicating that stimulation of a single neuron induces K^+ currents in OPCs through Kir4.1 channels that reflects neuronal K^+ efflux during action potential discharges (86.3 ± 8.4% of block, $n = 6$; $p < 0.05$; Fig. 7*D*,*F*). It is noteworthy that the frequency of discharge of recorded neurons remained unchanged in the presence of 100 μM Ba^{2+} (28.1 ± 6.4 Hz and 30.0 ± 6.9 Hz in control and Ba^{2+}, respectively; $p > 0.05$; $n = 6$; Fig. 7*B*,*D*, upper traces).

Altogether, our results show a novel form of unitary neuron–OPC connections that allows adult OPCs to sense finely and reliably $[K^+]_o$ increases through Kir4.1 channels during physiological activity of a single nearby neuron.

Discussion

In this report, we demonstrated that Kir4.1 channels are upregulated in cortical OPCs after the 2PN week (i.e., during their massive differentiation into oligodendrocytes) (Baracskay et al., 2002). The emergence of this conductance allows the majority of OPCs to sense local K^+ increases induced by neuronal activity, conferring to these cells a new functional property in the mature neuronal network. This novel neuron-to-OPC signaling mechanism does not rely on neurotransmitter release and is robust at a single-cell level as demonstrated by unitary neuron–OPC connections mediated by Kir4.1 channels. Astrocytes are also known to detect neuronal-induced K^+ increases through Kir4.1 channels (De Saint Jan and Westbrook, 2005; Djukic et al., 2007), but it is unknown whether they detect $[K^+]_o$ changes as locally as OPCs (i.e., upon a single neuron stimulation).

Kir channels are known to be upregulated in OPCs during postnatal development, but their expression is thought to remain low and reach high levels only in differentiated oligodendrocytes (Sontheimer et al., 1989; Berger et al., 1991; Neusch et al., 2001). However, most functional work on Kir channels of OPCs has been done either in culture or in acute slices of animals younger than four postnatal weeks (i.e., in conditions where these channels

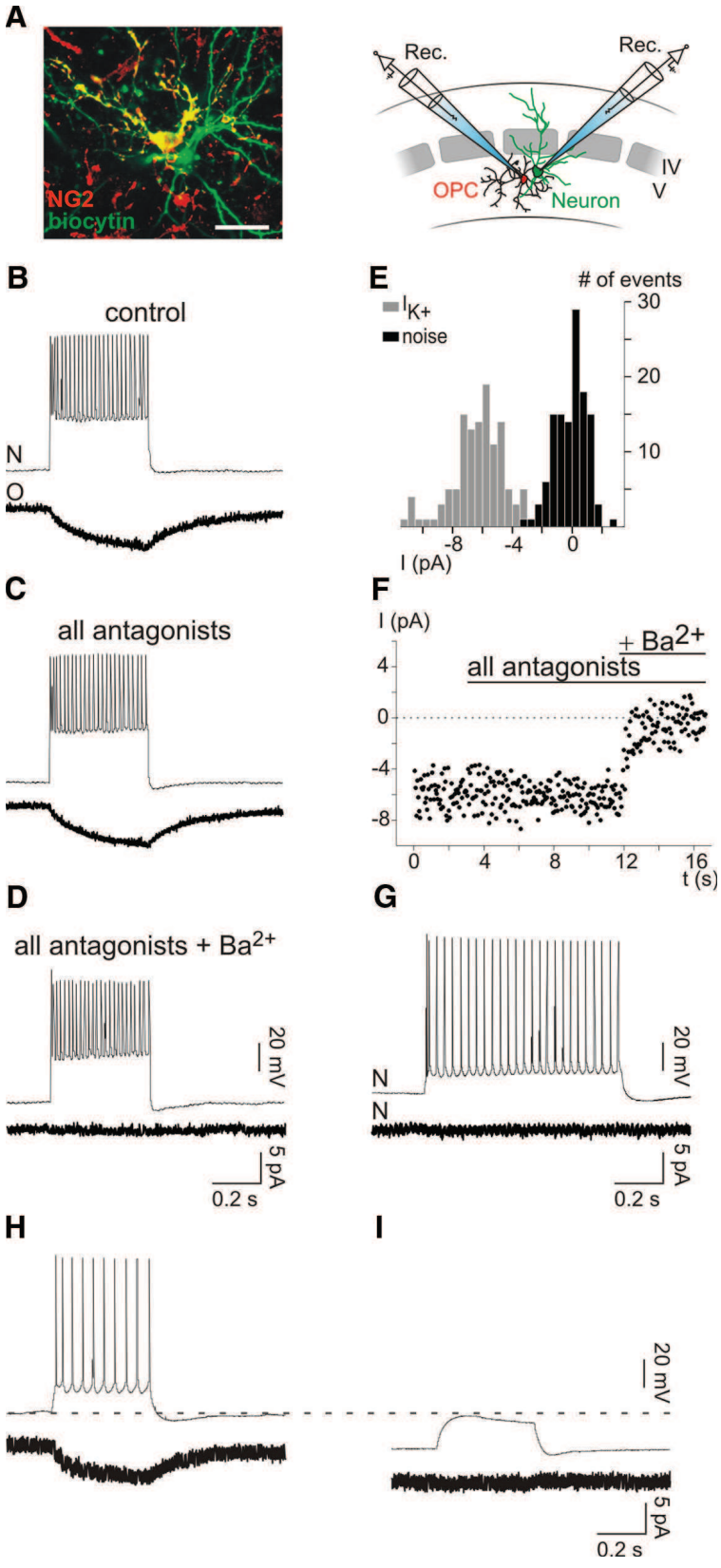

Figure 7. Single neuron stimulation induces Kir4.1-mediated K^+ currents in individual OPCs. ***A***, Confocal image of a neuron (green) and an $NG2^+$ OPC (yellow) simultaneously recorded in whole-cell configuration with intracellular solutions containing biocytin (left; stack of 17 *z* sections, each 1 μm; see Materials and Methods). The amplitude of the current elicited in this OPC by single neuron stimulation was −2.93 pA. Scale bar, 20 μm. A schematic representation of simultaneous neuron–OPC recordings is also shown (right). ***B–D***, Simultaneous recording of a neuron held at −70 mV in current clamp and an OPC held at −90 mV in voltage clamp in control (***B***), in the presence of a mixture of ionotropic and metabotropic receptor antagonists (***C***), and after bath application of 100 μM Ba^{2+} (***D***). The mixture of antagonists consists of 10 μM NBQX, 50 μM D-AP5, 5 μM SR95531, 50 μM LY341495, 5 μM CPG55845, and 30 μM PPADS. Note the lack of effect of the antagonists and the complete block of the induced current by Ba^{2+}. The train of action potentials in the recorded neuron was obtained by applying a 400 ms pulse of 400 pA, each 3 s. Only a single representative train of discharge is illustrated in each condition. Current traces of OPCs are averages of 122, 117, and 68 responses. ***E***, Amplitude distributions of the noise of the trace (black) and of the K^+ current (gray) of the recorded OPC in control conditions ($p < 0.001$). ***F***, Time course of the experiment of the same neuron–OPC simultaneous recording. ***G***, Simultaneous recording of a neuron held at −70 mV in current clamp and another neuron held at −90 mV in voltage clamp. The train of action potentials in the neuron (top) is obtained by applying 800 ms pulse of 200 pA. Note the lack of induced current in the other neuron (bottom). The current trace is an average of 37 sweeps. ***H***, ***I***, Simultaneous recording of a neuron held at −65 mV (***H***) and −90 mV (***I***) in current clamp and an OPC held at −90 mV in voltage clamp. Note that the hyperpolarization of the neuron abolishes both action potential discharges upon the same current injection and the evoked current in the OPC. The current traces are an average 51 (***H***) and 49 (***I***) sweeps.

probably do not attain their maximal expression). Although Kir4.1 channels have already been demonstrated in OPCs, only a weak expression was reported in these cells (Schroder et al., 2002; Tang et al., 2009). We showed here that expression levels of Kir4.1 channels progressively increase in most OPCs during postnatal development of the barrel cortex, conferring a linear *I–V* relationship on adult cells (Fig. 1*F*,*I*). This linear phenotype results from the weak rectification displayed by native Kir4.1 channels in physiological K^+ concentrations (Kucheryavykh et al., 2007; Seifert et al., 2009; Hibino et al., 2010). Interestingly, most of the linear *I–V* curve of astrocytes also depends on the expression of Kir4.1 channels (Djukic et al., 2007; Seifert et al., 2009). However, OPCs and astrocytes differ in that the later express functional two-pore domain K^+ channels TREK1 and probably TWIK1 (Seifert et al., 2009; Zhou et al., 2009).

Whereas voltage-gated K^+ channels expressed by OPCs play a key role during cell proliferation (Sontheimer et al., 1989; Gallo et al., 1996; Chittajallu et al., 2002), the function of Kir channels in these cells has not been well defined. Recent studies on knock-out Kir4.1 channels demonstrated that the deletion of these channels in glial cells was associated to an early lethality caused by a severe hypomyelinating phenotype (Neusch et al., 2001; Djukic et al., 2007). This has suggested that Kir4.1 channels play a role in OPC differentiation. However, the percentage of complex glia (presumably OPCs) decreases 11-fold in PN5–10 knock-out mice (Djukic et al., 2007) when functional Kir channels are poorly expressed in these cells (Fig. 1*C*) (Kressin et al., 1995). Con-

sequently, the precocious loss of progenitors probably results from an indirect effect of Kir4.1 channel deletion in other cell types, such as astrocytes, rather than from a direct effect on OPC maturation. A reduced pool of OPCs in early development is probably a major cause of hypomyelination in Kir4.1 channel knock-out mice, although a default in linear progression from preoligodendrocytes to myelinating oligodendrocytes in a successive postnatal stage may also play a role.

Interestingly, Kir4.1 channels are found almost exclusively in glial cells (Poopalasundaram et al., 2000; Higashi et al., 2001; Tang et al., 2009). The two predominant functions of these channels described so far are as follows: (1) to set the resting membrane potential and (2) to regulate $[K^+]_o$ during neuronal activity (Kofuji et al., 2000; Higashi et al., 2001; Neusch et al., 2006). Kir4.1 channels contribute to set the resting membrane potential of adult OPCs because we observed that their expression is accompanied by a more hyperpolarized resting membrane potential, and its block by different agents depolarizes the cells. Our observations showing that Kir4.1-mediated K^+ currents in adult OPCs occur upon the stimulation of neuronal fibers also suggests that neuronal activity control transient changes in the membrane potential of OPCs. Indeed, we found that γ frequency train stimulations, in the presence of AMPA, NMDA, and GABA receptor antagonists, evoked a Kir4.1-mediated current of 208 pA in adult OPCs (Fig. 4*F*). Considering that these cells have an input resistance of 70 MΩ, the current evoked by γ frequency neuronal activity should lead to a depolarization of 15 mV. It is known that whisker activation in rodents elicits the synchronization of neural ensembles at the γ frequency in the barrel cortex (Ahissar and Vaadia, 1990; Jones and Barth, 1997). Our results raises the possibility that $[K^+]_o$ increases, resulting from neuronal network oscillations, depolarize adult OPCs in the barrel cortex. The depolarizing effect of K^+ probably accumulates with that induced by activation of ligand-gated receptors during neurotransmitter release.

As a weakly inwardly rectifying conductance allowing the flow of inward and outward currents, Kir4.1 channels are suited to regulate local $[K^+]_o$ increases resulting from neuronal activity. Indeed, these channels can mediate both K^+ entry at sites of maximal accumulation and K^+ exit at sites of lower concentration. This mechanism of K^+ removal requires that cells in charge of K^+ redistribution have a high permeability for this ion and a resting membrane potential close to E_{rev} for K^+. Astrocytes are considered major players of K^+ buffering because K^+ can enter the astrocytic syncytium formed by gap junctions in a region of high neuronal activity and leave it in a remote region, the so-called spatial K^+ buffering (Orkand et al., 1966). However, this form of K^+ buffering is not sufficient to maintain $[K^+]_o$ at low levels, and it works most probably in concert with other auxiliary mechanisms (Newman et al., 1984; Ballanyi et al., 1987; Kofuji and Newman, 2004; Wallraff et al., 2006). This is particularly true for adult animals where volumes of extracellular space decrease with age in correlation with the myelination process and generate more considerable changes in $[K^+]_o$ (Chvatal et al., 1997). The presence of Kir4.1 channels in adult OPCs raises the possibility that these cells contribute to take up the K^+ released by nearby active neurons at sites that are not reached by astrocytic processes. Consistent with this, OPCs sense $[K^+]_o$ rises generated by a single neuronal firing, suggesting that astrocytes do not intervene between the neuron and the OPC to absorb K^+. Indeed, it is known that OPCs in the mature brain are closely associated with neurons by forming intimate contacts with neuronal somata, dendritic trees, and nodes of Ranvier (Butt et al., 2005). They are thus ideally located to sense K^+ increases and possibly remove the excess of K^+ caused by neuronal K^+ efflux at specific sites devoid of astrocytes. Because cortical OPCs are not connected by gap junctions (Vélez-Fort et al., 2010), one possibility is that this ion is temporarily sequestered at specific sites and then released back either to another site of the extracellular space reached by the cell or to blood vessels. Indeed, single OPCs project their processes to distinct cell layers and to blood vessels (Butt et al., 2005). This role could not be accomplished by young OPCs because they do not respond to neuronal activity through Kir4.1 channels.

In conclusion, our data reconcile a developmental upregulation of a K^+ channel with the capacity of adult OPCs to sense fine changes of local $[K^+]_o$ increases induced by physiological neuronal activity. They thus add a further complexity, previously unsuspected, to the mechanisms used by OPCs to detect neuronal activity in mature gray matter. This new functional property of adult OPCs in the neuronal network suggests that these cells might play a role in K^+ uptake in the mature healthy brain and, beyond their large abundance, the postnatal gain of physiological properties in neuronal networks support the view that these cells are not progenitors only.

References

Ahissar E, Vaadia E (1990) Oscillatory activity of single units in a somatosensory cortex of an awake monkey and their possible role in texture analysis. Proc Natl Acad Sci U S A 87:8935–8939. CrossRef Medline

Angulo MC, Lambolez B, Audinat E, Hestrin S, Rossier J (1997) Subunit composition, kinetic, and permeation properties of AMPA receptors in single neocortical nonpyramidal cells. J Neurosci 17:6685–6696. Medline

Angulo MC, Staiger JF, Rossier J, Audinat E (1999) Developmental synaptic changes increase the range of integrative capabilities of an identified excitatory neocortical connection. J Neurosci 19:1566–1576. Medline

Ballanyi K, Grafe P, ten Bruggencate G (1987) Ion activities and potassium uptake mechanisms of glial cells in guinea-pig olfactory cortex slices. J Physiol 382:159–174. Medline

Baracskay KL, Duchala CS, Miller RH, Macklin WB, Trapp BD (2002) Oligodendrogenesis is differentially regulated in gray and white matter of jimpy mice. J Neurosci Res 70:645–654. CrossRef Medline

Berger T, Schnitzer J, Kettenmann H (1991) Developmental changes in the membrane current pattern, K+ buffer capacity, and morphology of glial cells in the corpus callosum slice. J Neurosci 11:3008–3024. Medline

Bergles DE, Roberts JD, Somogyi P, Jahr CE (2000) Glutamatergic synapses on oligodendrocyte precursor cells in the hippocampus. Nature 405:187–191. CrossRef Medline

Butt AM, Hamilton N, Hubbard P, Pugh M, Ibrahim M (2005) Synantocytes: the fifth element. J Anat 207:695–706. CrossRef Medline

Cahoy JD, Emery B, Kaushal A, Foo LC, Zamanian JL, Christopherson KS, Xing Y, Lubischer JL, Krieg PA, Krupenko SA, Thompson WJ, Barres BA (2008) A transcriptome database for astrocytes, neurons, and oligodendrocytes: a new resource for understanding brain development and function. J Neurosci 28:264–278. CrossRef Medline

Chittajallu R, Chen Y, Wang H, Yuan X, Ghiani CA, Heckman T, McBain CJ, Gallo V (2002) Regulation of Kv1 subunit expression in oligodendrocyte progenitor cells and their role in G_1/S phase progression of the cell cycle. Proc Natl Acad Sci U S A 99:2350–2355. CrossRef Medline

Chvátal A, Berger T, Vorísek I, Orkand RK, Kettenmann H, Syková E (1997) Changes in glial K+ currents with decreased extracellular volume in developing rat white matter. J Neurosci Res 49:98–106. CrossRef Medline

Dawson MR, Polito A, Levine JM, Reynolds R (2003) NG2-expressing glial progenitor cells: an abundant and widespread population of cycling cells in the adult rat CNS. Mol Cell Neurosci 24:476–488. CrossRef Medline

De Saint Jan D, Westbrook GL (2005) Detecting activity in olfactory bulb glomeruli with astrocyte recording. J Neurosci 25:2917–2924. CrossRef Medline

De Biase LM, Nishiyama A, Bergles DE (2010) Excitability and synaptic communication within the oligodendrocyte lineage. J Neurosci 30:3600–3611. CrossRef Medline

Djukic B, Casper KB, Philpot BD, Chin LS, McCarthy KD (2007) Condi-

tional knock-out of Kir4.1 leads to glial membrane depolarization, inhibition of potassium and glutamate uptake, and enhanced short-term synaptic potentiation. J Neurosci 27:11354–11365. CrossRef Medline

Gallo V, Zhou JM, McBain CJ, Wright P, Knutson PL, Armstrong RC (1996) Oligodendrocyte progenitor cell proliferation and lineage progression are regulated by glutamate receptor-mediated K+ channel block. J Neurosci 16:2659–2670. Medline

Heinemann U, Lux HD (1977) Ceiling of stimulus induced rises in extracellular potassium concentration in the cerebral cortex of cat. Brain Res 120:231–249. CrossRef Medline

Hibino H, Inanobe A, Furutani K, Murakami S, Findlay I, Kurachi Y (2010) Inwardly rectifying potassium channels: their structure, function, and physiological roles. Physiol Rev 90:291–366. CrossRef Medline

Higashi K, Fujita A, Inanobe A, Tanemoto M, Doi K, Kubo T, Kurachi Y (2001) An inwardly rectifying K(+) channel, Kir4.1, expressed in astrocytes surrounds synapses and blood vessels in brain. Am J Physiol Cell Physiol 281:C922–C931. Medline

Jones MS, Barth DS (1997) Sensory-evoked high-frequency (γ-band) oscillating potentials in somatosensory cortex of the unanesthetized rat. Brain Res 768:167–176. CrossRef Medline

Káradóttir R, Cavelier P, Bergersen LH, Attwell D (2005) NMDA receptors are expressed in oligodendrocytes and activated in ischaemia. Nature 438:1162–1166. CrossRef Medline

Kofuji P, Newman EA (2004) Potassium buffering in the central nervous system. Neuroscience 129:1045–1056. CrossRef Medline

Kofuji P, Ceelen P, Zahs KR, Surbeck LW, Lester HA, Newman EA (2000) Genetic inactivation of an inwardly rectifying potassium channel (Kir4.1 subunit) in mice: phenotypic impact in retina. J Neurosci 20:5733–5740. Medline

Kressin K, Kuprijanova E, Jabs R, Seifert G, Steinhäuser C (1995) Developmental regulation of Na+ and K+ conductances in glial cells of mouse hippocampal brain slices. Glia 15:173–187. CrossRef Medline

Kucheryavykh YV, Pearson WL, Kurata HT, Eaton MJ, Skatchkov SN, Nichols CG (2007) Polyamine permeation and rectification of Kir4.1 channels. Channels (Austin) 1:172–178. Medline

Kukley M, Capetillo-Zarate E, Dietrich D (2007) Vesicular glutamate release from axons in white matter. Nat Neurosci 10:311–320. CrossRef Medline

Lesage F, Guillemare E, Fink M, Duprat F, Lazdunski M, Romey G, Barhanin J (1996) TWIK-1, a ubiquitous human weakly inward rectifying K+ channel with a novel structure. EMBO J 15:1004–1011. Medline

Lotshaw DP (2007) Biophysical, pharmacological, and functional characteristics of cloned and native mammalian two-pore domain K+ channels. Cell Biochem Biophys 47:209–256. CrossRef Medline

Maldonado PP, Vélez-Fort M, Angulo MC (2011) Is neuronal communication with NG2 cells synaptic or extrasynaptic? J Anat 219:8–17. CrossRef Medline

Mangin JM, Kunze A, Chittajallu R, Gallo V (2008) Satellite NG2 progenitor cells share common glutamatergic inputs with associated interneurons in the mouse dentate gyrus. J Neurosci 28:7610–7623. CrossRef Medline

Morales B, Choi SY, Kirkwood A (2002) Dark rearing alters the development of GABAergic transmission in visual cortex. J Neurosci 22:8084–8090. Medline

Neusch C, Rozengurt N, Jacobs RE, Lester HA, Kofuji P (2001) Kir4.1 potassium channel subunit is crucial for oligodendrocyte development and in vivo myelination. J Neurosci 21:5429–5438. Medline

Neusch C, Papadopoulos N, Müller M, Maletzki I, Winter SM, Hirrlinger J, Handschuh M, Bähr M, Richter DW, Kirchhoff F, Hülsmann S (2006) Lack of the Kir4.1 channel subunit abolishes K+ buffering properties of astrocytes in the ventral respiratory group: impact on extracellular K+ regulation. J Neurophysiol 95:1843–1852. CrossRef Medline

Newman EA, Frambach DA, Odette LL (1984) Control of extracellular potassium levels by retinal glial cell K^+ siphoning. Science 225:1174–1175. CrossRef Medline

Nie X, Arrighi I, Kaissling B, Pfaff I, Mann J, Barhanin J, Vallon V (2005) Expression and insights on function of potassium channel TWIK-1 in mouse kidney. Pflugers Arch 451:479–488. CrossRef Medline

Orkand RK, Nicholls JG, Kuffler SW (1966) Effect of nerve impulses on the membrane potential of glial cells in the central nervous system of amphibia. J Neurophysiol 29:788–806. Medline

Patel AJ, Honoré E, Lesage F, Fink M, Romey G, Lazdunski M (1999) Inhalational anesthetics activate two-pore-domain background K^+ channels. Nat Neurosci 2:422–426. CrossRef Medline

Pessia M, Imbrici P, D'Adamo MC, Salvatore L, Tucker SJ (2001) Differential pH sensitivity of Kir4.1 and Kir4.2 potassium channels and their modulation by heteropolymerisation with Kir5.1. J Physiol 532:359–367. CrossRef Medline

Poopalasundaram S, Knott C, Shamotienko OG, Foran PG, Dolly JO, Ghiani CA, Gallo V, Wilkin GP (2000) Glial heterogeneity in expression of the inwardly rectifying K(+) channel, Kir4.1, in adult rat CNS. Glia 30:362–372. CrossRef Medline

Richardson WD, Young KM, Tripathi RB, McKenzie I (2011) NG2-glia as multipotent neural stem cells: fact or fantasy? Neuron 70:661–673. CrossRef Medline

Sah P, Faber ES (2002) Channels underlying neuronal calcium-activated potassium currents. Prog Neurobiol 66:345–353. CrossRef Medline

Salami M, Itami C, Tsumoto T, Kimura F (2003) Change of conduction velocity by regional myelination yields constant latency irrespective of distance between thalamus and cortex. Proc Natl Acad Sci U S A 100:6174–6179. CrossRef Medline

Schröder W, Seifert G, Hüttmann K, Hinterkeuser S, Steinhäuser C (2002) AMPA receptor-mediated modulation of inward rectifier K+ channels in astrocytes of mouse hippocampus. Mol Cell Neurosci 19:447–458. CrossRef Medline

Seifert G, Hüttmann K, Binder DK, Hartmann C, Wyczynski A, Neusch C, Steinhäuser C (2009) Analysis of astroglial K+ channel expression in the developing hippocampus reveals a predominant role of the Kir4.1 subunit. J Neurosci 29:7474–7488. CrossRef Medline

Sontheimer H, Trotter J, Schachner M, Kettenmann H (1989) Channel expression correlates with differentiation stage during the development of oligodendrocytes from their precursor cells in culture. Neuron 2:1135–1145. CrossRef Medline

Su S, Ohno Y, Lossin C, Hibino H, Inanobe A, Kurachi Y (2007) Inhibition of astroglial inwardly rectifying Kir4.1 channels by a tricyclic antidepressant, nortriptyline. J Pharmacol Exp Ther 320:573–580. CrossRef Medline

Tang X, Taniguchi K, Kofuji P (2009) Heterogeneity of Kir4.1 channel expression in glia revealed by mouse transgenesis. Glia 57:1706–1715. CrossRef Medline

Tang X, Schmidt TM, Perez-Leighton CE, Kofuji P (2010) Inwardly rectifying potassium channel Kir4.1 is responsible for the native inward potassium conductance of satellite glial cells in sensory ganglia. Neuroscience 166:397–407. CrossRef Medline

Taverna S, Tkatch T, Metz AE, Martina M (2005) Differential expression of TASK channels between horizontal interneurons and pyramidal cells of rat hippocampus. J Neurosci 25:9162–9170. CrossRef Medline

Tucker SJ, Imbrici P, Salvatore L, D'Adamo MC, Pessia M (2000) pH dependence of the inwardly rectifying potassium channel, Kir5.1, and localization in renal tubular epithelia. J Biol Chem 275:16404–16407. CrossRef Medline

Vélez-Fort M, Audinat E, Angulo MC (2009) Functional α 7-containing nicotinic receptors of NG2-expressing cells in the hippocampus. Glia 57:1104–1114. CrossRef Medline

Vélez-Fort M, Maldonado PP, Butt AM, Audinat E, Angulo MC (2010) Postnatal switch from synaptic to extrasynaptic transmission between interneurons and NG2 cells. J Neurosci 30:6921–6929. CrossRef Medline

Wallraff A, Köhling R, Heinemann U, Theis M, Willecke K, Steinhäuser C (2006) The impact of astrocytic gap junctional coupling on potassium buffering in the hippocampus. J Neurosci 26:5438–5447. CrossRef Medline

Zhou M, Schools GP, Kimelberg HK (2006) Development of GLAST(+) astrocytes and NG2(+) glia in hippocampus CA1: mature astrocytes are electrophysiologically passive. J Neurophysiol 95:134–143. CrossRef Medline

Zhou M, Xu G, Xie M, Zhang X, Schools GP, Ma L, Kimelberg HK, Chen H (2009) TWIK-1 and TREK-1 are potassium channels contributing significantly to astrocyte passive conductance in rat hippocampal slices. J Neurosci 29:8551–8564. CrossRef Medline

Ziskin JL, Nishiyama A, Rubio M, Fukaya M, Bergles DE (2007) Vesicular release of glutamate from unmyelinated axons in white matter. Nat Neurosci 10:321–330. CrossRef Medline

Chapter 2

Article II

Vélez-Fort et al. (2010) demonstrated that neocortical OPCs receive a major intracortical synaptic input from GABAergic interneurons that disappears after the second postnatal week. Cortical GABAergic synapses of OPCs are thus transient during development and prevailed during the active phase of proliferation and differentiation of these cells, *i. e.* the second postnatal week (Kang et al., 2010). This correlation between high GABAergic synaptic activity and proliferation/differentiation suggests a role of these synapses in OPC development. However, the investigation of the role of GABAergic transmission in OPCs has been difficult by the lack of knowledge about the $GABA_A$Rs expressed by these cells, the identity of presynaptic inputs and the connectivity patterns that underlie interneuron-OPC microcircuits. Our team recently demonstrated that the loss of synaptic activity in OPCs is accompanied by a down-regulation of the $\gamma 2$ subunit of $GABA_A$R as well as by other changes in $GABA_A$R subunit expression (Balia et al., 2013). However, nothing is known about the presynaptic interneurons that synaptically contact OPCs and the properties of individual synapses. We thus studied these two aspects in this article (Orduz*, Maldonado* et al. to be submitted in Nat. Neurosci. as a Brief Communication).

2.1 General anatomical structure of the neocortex

The neocortex is the largest and newest part of the cerebral cortex and is considered to be the key that enables higher cognitive functions (Lui et al., 2011). This structure is organized in layers, typically I to VI, defined by the absence or presence of cell soma containing different densities and types of neurons. This arrangement in layers is the substrate to organize the inputs, mainly from thalamus and other regions, and the outputs to the contralateral side, basal ganglia, thalamus, pontine nuclei and spinal cord (Kandel et al., 2000). Nevertheless, neurons in the cortex are not only distributed

in layers; they also exhibit a vertical or columnar organization (de Nó, 1949; Hubel et al., 1977; Mountcastle, 1997, review). Defined by Krieger et al. (2007): "the fundamental unit of cortical organization is a group of interconnected neurons that share a certain set of properties and extend vertically through the cortical layers to form a column". There are mini-columns (diameter around 50 μm) and macro-columns (diameter around 300-500 μm) (reviewed by Rockland, 2010). The latter can be defined by metabolic zones, connectional columns and functional or activity columns (reviewed by Rockland, 2010). These columns or modules as basic units are supposed to perform similar computational tasks in the form of local repeated neuronal circuits (Mountcastle, 1997).

The stereotyped distribution and organization of neurons has enabled the characterization of different cell types. In general, they can be defined as projecting neurons, typically pyramidal cells, located mainly in layer III, IV and V, releasing glutamate as principal neurotransmitter and constituting 70-80% of the total neurons. On the other hand, local interneurons are located in all layers, release GABA and constitute 20-30% of neurons (Kandel et al., 2000). Although probably an over-simplification, a general belief supposes that pyramidal cells have more homogeneous anatomical, physiological and molecular properties than interneurons. Conversely, interneurons exhibit a huge diversity in all these parameters, making difficult to study them systematically (Markram et al., 2004).

2.1.1 Interneurons

The diversity of interneurons has been a matter of intense investigation in the last twenty years and, although a consensual classification of interneurons has been difficult to achieve, an effort to define a unified nomenclature has been done by the scientific community (The Petilla Interneuron Nomenclature Group, 2008). The most common subtypes of neocortical interneurons can be divided in seven distinct groups according to electrophysiological, morphological and biochemical characteristics: parvalbumin (PV)-positive fast-spiking cells, showing either chandelier or basket cell morphology, somatostatin (SOM)-positive low-threshold-spiking Martinotti cells, SOM-positive regular-spiking cells, vasoactive intestinal protein (VIP)-positive bursting or regular-spiking cells and neuroglialform cells (Cauli et al., 1997; The Petilla Interneuron Nomenclature Group, 2008; Fishell and Rudy, 2011).

Despite the mentioned diversity, one important common feature of cortical interneurons is their ability to mediate inhibition because of the hyperpolarizing effect of GABA in mature neurons. Possible functions have been recently reviewed by Fino et al. (2013) such as their participation in pyramidal cells networks with repeated (motifs) patterns, control of pyramidal cell function by adjusting their gain and generation or termination of particular neuronal network states.

Figure 2.1: **Inhibition of inhibition in the visual neocortex.**
Schematic representation of connectivy pattern between three types of interneurons and pyramidal cells. Arrows indicate the preference of connectivity. Vip, vasoactive intestinal peptide; Sst, somatostatin; Pvalb, paravalbumin; Pyr, pyramidal cell. From Pfeffer et al. (2013).

Even if different interneurons target specific subcellular compartments and thus perform a selective task (Somogyi et al., 1998), two recent works showed that SOM (Fino and Yuste, 2011) and PV (Packer and Yuste, 2011) interneurons carve out unspecific and dense connections with pyramidal cells of the frontal and somatosensory cortex. This was done mainly, by performing two-photon RuBi-Glutamate uncaging in acute brain slices. Taking advantage of the restricted and tiny excitation volume of two-photon microscopy and by multiplexing the laser beam to stimulate sequentially several neurons, this technique allowed for finding large number of unitary synaptic connections, with a single-cell resolution, providing the map of connectivity for each neuron (Nikolenko et al., 2007). The apparent promiscuity in the SOM and PV connectivity with pyramidal cells was addressed by Packer et al. (2012). They found that the lack of specificity of these interneurons relies in a mere spatial overlapping of axonal and dendrite arborizations and their laminar projection patterns. Morphological reconstructions of SOM axons showed that they project to layer I, which lacks pyramidal cell somata, whereas PV axons projected to other layers rich in pyramidal cell somata, avoiding layer I (Packer et al., 2012). In spite of this lack of specificity of connections between interneurons and pyramidal cells, interneurons behave in a different manner when they are connected among them, *i.e.* the inhibition of inhibition. In the visual cortex, between PN18 and PN30, PV, SOM and VIP interneurons exhibit particular connectivity patterns (Figure 2.1)(Pfeffer et al., 2013). This evidence indicates that the connectivity of these cells cannot be generalized and categorized in a simple way.

Whether interneuron-OPC synaptic connectivity is governed by specific rules is completely unknown. In the adult CNS, OPCs are distributed in a grid-like fashion, with non-overlapping domains (Hughes et al., 2013). This is also probably the case in young animals. In addition, at least until PN15, OPCs exhibit a layer-specific distribution. Low fluorescence of NG2 immunoinstaining is observed in layer IV compared to layer II/III, V and VI, and high fluorescence in layer V. From these evidences we could infer that probably OPCs and interneurons overlap spaces as pyramidal cells do. If

we take in consideration Packer et al. (2012) statement: "interneurons connect with whomever they encounter", we should expect a high and unspecific connectivity between interneurons and OPCs. However, this is probably not the case. Indeed, the frequency and amplitude of synaptic events of OPCs is small compare with those reported for neurons, suggesting that the connectivity between interneurons and OPCs does not rely in a mere overlap. To resolve this issue we must first know how, when and which interneurons innervate OPCs.

Main results

In this second article, my major role was to implement the Holographic Photolysis (HP) in the team and compare the spatial organization of GABAergic connectivity of OPCs and pyramidal cells. We decided to map the connectivity between layer V interneurons and OPCs during the second postnatal week of the mouse somatosensory cortex, the period where synaptic contacts are still present. For this purpose, we used HP of MNI-glutamate to establish local GABAergic connectivity maps in vGAT-venus;NG2-DsRed mice. In addition, we investigate the pre- and postsynaptic properties of unitary connections by performing paired recordings. Paired recordings were performed by David Orduz.

We found that:

1. HP is an interesting alternative tool to map local unitary connections in acute brain slices.
2. OPCs display more local connectivity maps than pyramidal cells.
3. Interneurons contact transiently OPCs through single or double release sites.
4. OPCs are synaptically connected by fast-spiking and non-fast-spiking interneurons.
5. Fast-spiking interneurons predominantly innervate OPCs compare to non-fast-spiking interneurons, targeting specifically postsynaptic sites containing $GABA_A$Rs with $\gamma 2$ subunits.

Altogether, these results indicate that the establishment of local microcircuits during development is not only confined to neurons, but also includes a non-neuronal cell. In addition, they suggest that fast-spiking interneurons play a major role in controlling OPC activity during a specific stage of postnatal development.

Specific rules of synaptic connectivity between cortical GABAergic interneurons and NG2 cells

David Orduz[1,2,3,6], Paloma P. Maldonado[1,2,3,6], Mateo Vélez-Fort[1,2,3,5], Vincent de Sars[1,2,3], Yuchio Yanagawa[4], Valentina Emiliani[1,2,3], María Cecilia Angulo[1,2,3]

[1] INSERM U603, Paris, France.
[2] CNRS UMR 8154, Paris, France.
[3] Université Paris Descartes, Sorbonne Paris Cité, France.
[4] Department of Genetic and Behavioral Neuroscience, Gunma University Graduate School of Medicine, Maebashi, Japan.
[5] Present address: Division of Neurophysiology, The National Institute for Medical Research, Mill Hill NW7 1AA, UK.
[6] These authors contributed equally to this work.

Corresponding author
María Cecilia Angulo, Laboratoire de Neurophysiologie et Nouvelles Microscopies; INSERM U603, CNRS UMR 8154; Université Paris Descartes, Sorbonne Paris Cité; 45, rue des Saints-Pères; 75006 Paris; FRANCE. Tel: 33-1-70649935; FAX: 33-1-42864151. e-mail address: maria-cecilia.angulo@parisdescartes.fr

Acknowledgments
We thank all physicists of the department that helped us with the holographic system, in particular E. Papagiakoumou, and the SCM Imaging Platform of the Sts-Pères Biomedical Sciences site of Paris Descartes University for confocal images. Venus was developed by Dr. Atsushi Miyawaki at RIKEN, Wako, Japan. This work was supported by grants from Agence Nationale de la Recherche (ANR), Fondation pour la Recherche sur le Cerveau (FRC) and Fondation pour l'aide à la recherche sur la Sclérose en Plaques (ARSEP). D.O. and P.P.M. were supported by fellowships from Nerf-île-nce and from Ecole des Neurosciences de Paris (ENP), respectively.

Abstract

We adapted holographic photolysis and paired recordings to analyze unitary synaptic connections between cortical GABAergic interneurons and oligodendrocyte precursors called NG2 cells. These progenitors display more local connectivity maps than pyramidal cells and are transiently innervated by interneurons during development through single or double release sites. Fast-spiking interneurons provide a predominant input onto NG2 cells and form highly specific connections by targeting postsynaptic sites containing $GABA_A$ receptors with $\gamma 2$ subunits.

Oligodendrocyte precursors expressing the proteoglycan NG2 (NG2 cells) are contacted by functional synapses from neurons in the brain (Bergles et al., 2000). Neocortical NG2 cells receive a major synaptic input from GABAergic interneurons that disappears after the second postnatal week (Vélez-Fort et al., 2010; Balia et al., 2013). They are thus transiently embedded in local microcircuits. While the connectivity patterns underlying neocortical GABAergic neuronal networks begin to be elucidated (Pfeffer et al., 2013), the rules governing the GABAergic connectivity of NG2 cells are elusive.

The flexibility and high spatial precision of holographic photolysis (Lutz et al., 2008; Zahid et al., 2010) were exploited to establish local GABAergic connectivity maps of NG2 cells in acute somatosensory cortical slices of two week-old vGAT-venus;NG2-DsRed mice (Supplementary Fig. 1). NG2 cells were recorded with a Cs-Methanosulfonate (CsMeS)-based intracellular solution at 0 mV, while interneurons were photostimulated with single-cell resolution in a volume of 1.05 x 106 μm^3, using 50 μM of MNI-glutamate (Fig. 1a-h; Supplementaries Fig. 2 and 4). Photo-induced outward postsynaptic currents (PSCs) in NG2 cells were sensitive to the $GABA_A$ receptor antagonist SR95531 (5 μM) and, compared to those in pyramidal neurons, displayed very small amplitudes and failures of response (Fig. 1a-b, d-e; Supplementary Fig. 4). Their connection probability was around half less than that of pyramidal cells and their connectivity maps involved more local microcircuits, never exceeding 70 μm of interneuron-NG2 cell intersomatic distances (Fig. 1c-g, f-h; Supplementary Fig. 4g).

We next performed paired recordings to define presynaptic and postsynaptic properties of unitary connections. Action potentials elicited in presynaptic interneurons induced unitary inward PSCs in NG2 cells recorded in CsCl-based intracellular solution at -70 mV. PSCs were sensitive to SR95531 (5 μM), showed small amplitudes, fast rise times, short latencies, high failure rates and relatively small coefficients of variation (Fig. 2a, c; Supplementary Fig. 5). The connectivity probability reached a peak at PN10 and then decreased, confirming the transient GABAergic innevation (Vélez-Fort et al., 2010; Balia et al., 2013) (Supplementary Fig. 5g). To determine the number of release sites contacting NG2 cells, we manipulated the release probabilities by using paired-pulse stimulation of presynaptic interneurons. All connections showed paired-pulse depression and no recovery from depression within 250 ms (Fig. 2a, c; Supplementary Fig. 5a, h). In 44% of connections, we observed no statistical differences between the cumulative distributions of PSC1 and PSC2 amplitudes without failures, although their probabilities of response differed (Fig. 2a-b, e-f). This implies that PSC amplitudes without failures corresponded to postsynaptic responses to one quantum of transmitter and that interneurons innervated NG2 cells with a single functional release site (Stevens and Wang, 1995) (apparent quantal size: -7.71$\pm$0.71 pA; n=8). The other 56% of connections had amplitudes and probabilities of response that were around twice for PSC1 and equal for PSC2 when compared to those of PSC1 of single site connections, thereby exhibiting double release sites (Fig. 2c-d, e-f). Hence, GABAergic interneurons transiently contact NG2 cells through a single or double functional release sites.

A key unresolved question is the identity of the interneurons contacting NG2 cells. By analysing the firing properties of interneurons, we distinguished fast-spiking (FSIs)

from non-fast-spiking interneurons (NFSIs) by their rapid action potentials with profound after hyperpolarization (AHP), a small change in both spike duration increase and spike amplitude reduction as well as parvalbumin expression (Daw et al., 2007) (PV; Fig. 3a-d; Supplementaries Fig. 6a, 7 and Table 1). Both FSIs and NFSIs established synaptic connections with NG2 cells (Fig. 3d, f). However, FSIs, a relatively homogeneous class of interneurons, were highly connected to NG2 cells (43% from tested FSI) compared to the notoriously heterogeneous population of NFSIs (21% from tested NSFI) that encompasses many different types of interneurons (Pfeffer et al., 2013) (Fig. 3d-f; Supplementaries 6b and Table 1). Moreover, by using bath application of the positive modulator diazepam (DZP), a benzodiazepine acting mainly at the interface between α and $\gamma 2$ subunits, FSIs preferentially targeted postsynaptic sites of NG2 cells containing $GABA_A$ receptors with $\gamma 2$ subunits, whereas NFSIs favored postsynaptic sites lacking this subunit (Fig. 3g-i). In conclusion, FSIs provide a predominant presynaptic input onto NG2 cells targeting specific postsynaptic sites. In addition to the role played by FSIs in controlling neocortical networks, these interneurons might control cortical NG2 cell development and myelination, a potential novel role for these interneurons that could have major implications in development and myelin diseases.

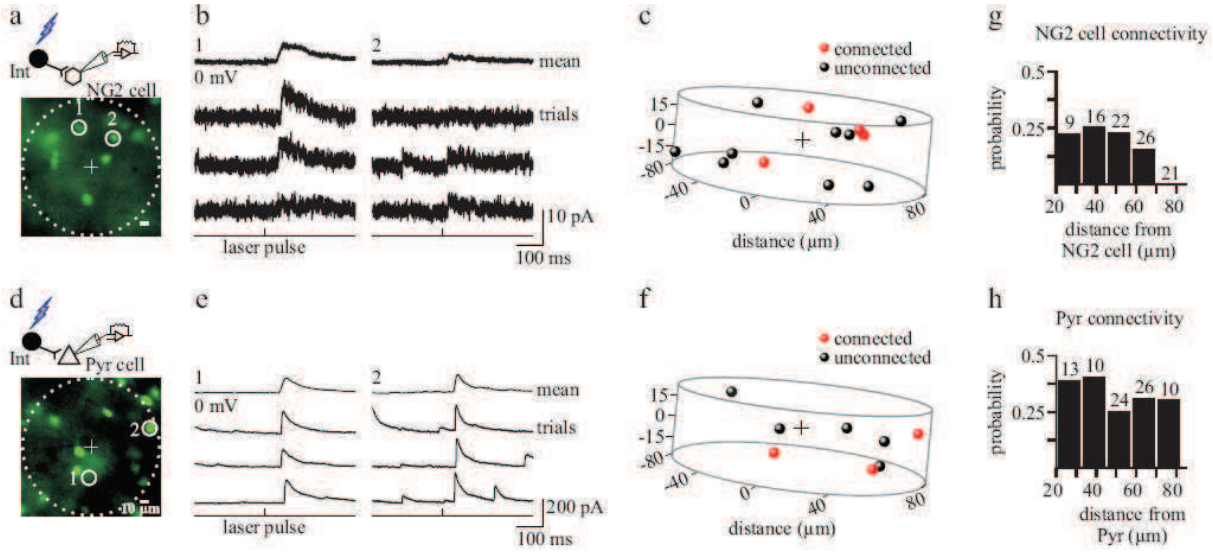

Figure 1: **GABAergic connectivity maps of NG2 cells and pyramidal neurons.**
(a, d) Diagram of optically-detected unitary connection (top). Excitation fields (dashed circles) in epifluorescent images of venus^{+} interneurons (bottom). Recorded NG2 cell **(a)** and pyramidal neuron **(d)** are in the center (+, non visible). **(b, e)** Photostimulation of interneurons (1 and 2) in a and d induces unitary PSCs in a recorded NG2 cell **(b)** and pyramidal neuron **(e)**. **(c, f)** Local GABAergic connectivity maps of the same recorded cells showing connected (red) and unconnected (black) interneurons. **(g, h)** Distribution of connection probabilities for different intersomatic distances between interneurons and either NG2 cells **(g)** or pyramdial neurons **(h)**. Number of tested cells per distance on top of bars.

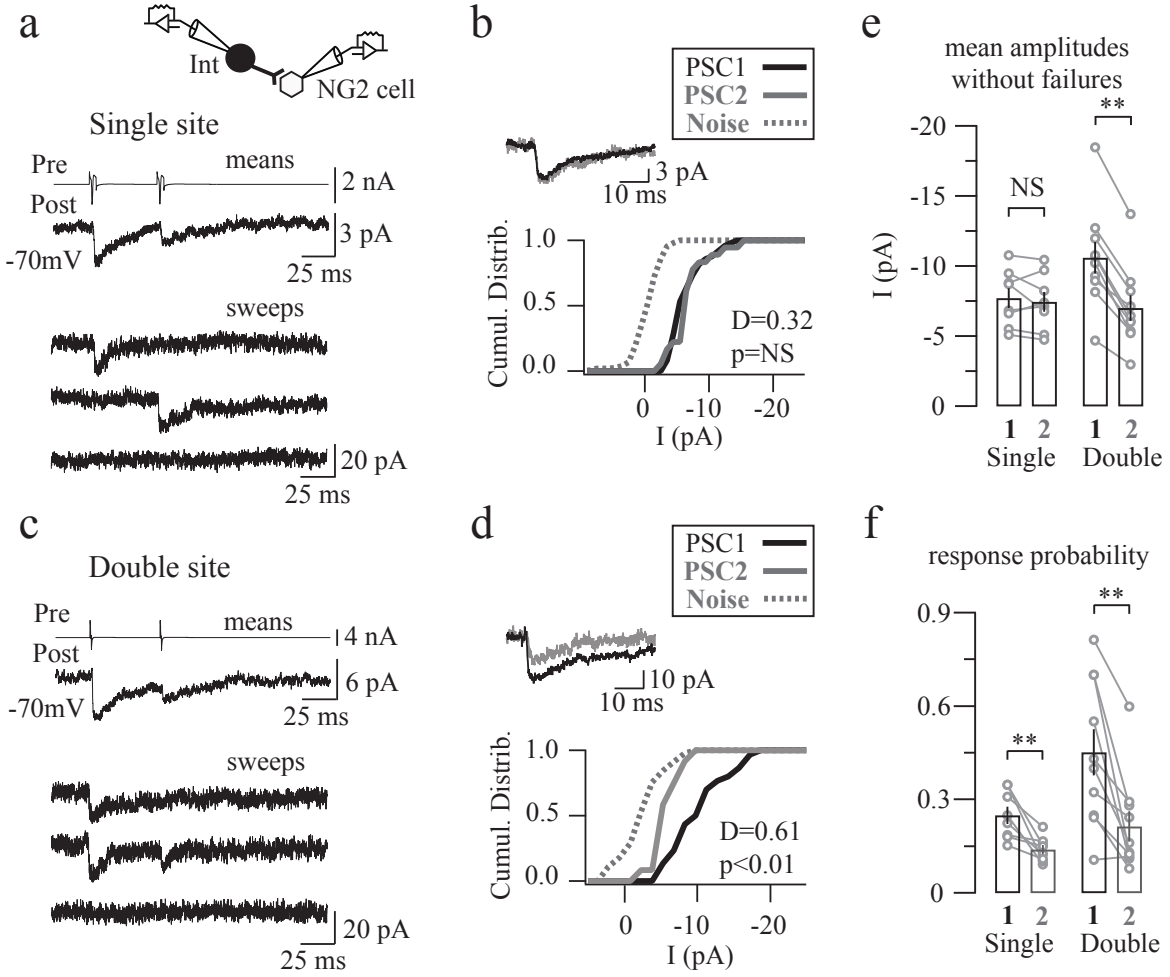

Figure 2: **NG2 cells are innervated by single or double release sites.**
(a, c) Unitary connections with single **(a)** and double **(c)** release sites. Diagram of paired recordings (top). Mean (middle traces) and individual (bottom traces) PSCs recorded in NG2 cells in response to two action currents evoked in presynaptic interneurons (top traces). **(b, d)** Cumulative distributions of PSC1 and PSC2 without failures for connections shown in a and c. Mean currents are shown in insets (top traces). **(e, f)** Histograms of amplitudes without failures **(e)** and response probabilities (**f**) of PSC1 and PSC2 for single and double site connections (n=8 and n=10, respectively; NS: not significant; $^*p<0.05$; $^{**}p<0.01$).

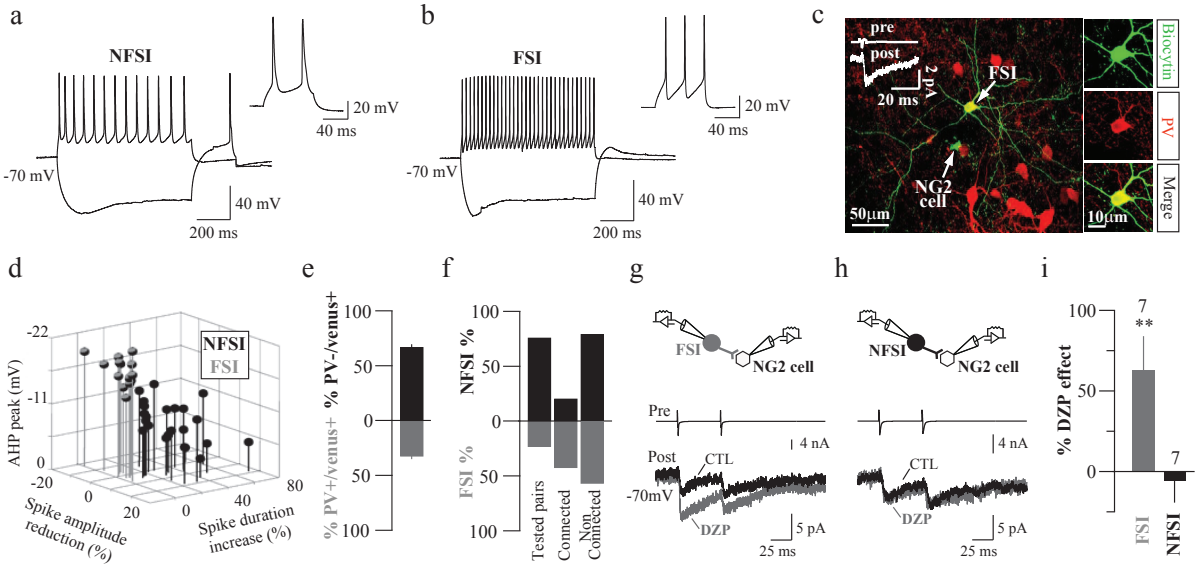

Figure 3: **FSIs provide a predominant and specific input onto NG2 cells.** **(a, b)** (Current-clamp recordings of a NFSI **(a)** and a FSI **(b)** connected to NG2 cells during injections of -200 and 200 pA (left). Note the differences on spike morphology between the two cells (insets, right). **(c)** A connected FSI labeled with biocytin and immunoreactive for PV. **(d)** 3D plot of major electrophysiological parameters distinguishing connected NFSIs (black; n=23) from FSIs (gray; n=15). **(e)** Histograms showing the fraction of PV^+ cells with respect to $venus^+$ interneurons (e, n=6 animals). **(f)** Percentages of tested and connected FSIs and NFSIs. **(g, h)** Diagram of paired recordings (top). DZP effect on PSCs induced in two NG2 cells by paired-pulse stimulations of a FSI (**g**) and a NFSI **(h)**. **(i)** Histogram comparing DZP effect on PSCs evoked in FSIs and NFSIs (**$p<0.01$).

Methods

Acute slice preparation and electrophysiology. Acute parasagittal slices (300 μm) of the barrel cortex with an angle of 10° to the sagittal plane were obtained from a double vGAT-venus;NG2-DsRed transgenic mouse (Wang et al., 2009; Ziskin et al., 2007), as previously described (Vélez-Fort et al., 2010). Excitation light to visualize venus and DsRed fluorescent proteins was provided by Optoled Light Sources (Blue and Green Optoleds; Cairn Research, UK) and images were collected with an iXon+ 14-bit digital camera (Andor Technology, UK) through an Olympus BX51 microscope equipped with a 40x fluorescent water-immersion objective. Excitation and emission wavelengths were obtained by using respectively 470 nm and 525 nm filters for venus and 560 nm and 620 nm filters for DsRed. The Imaging Workbench 6.0 software (Indec Biosystems, USA) was utilized to acquire and store images for off-line analysis. Patch-clamp recordings were performed at RT or 33°C using an extracellular solution containing (in mM): 126 NaCl, 2.5 KCl, 1.25 NaH2PO4, 26 NaHCO3, 20 glucose, 5 pyruvate, 3 CaCl2 and 1 MgCl2 (95% O2, 5% CO2). NG2 cells were recorded with different intracellular solutions according to the experiment and containing (in mM): either 125 CsCH3SO3H (CsMeS), or 130 CsCl, 5 4-aminopyridine, 10 tetraethylammonium chloride, 0.2 EGTA, 0.5 CaCl2, 2 MgCl2, 10 HEPES, 2 Na2-ATP, 0.2 Na-GTP and 10 Na2-phosphocreatine (pH $\approx$ 7.3). Presynaptic interneurons were recorded with an intracellular solution containing (in mM): 130 K-Gluconate (KGlu), 10 GABA, 0.1 EGTA, 0.5 CaCl2, 2 MgCl2, 10 HEPES, 2 Na2-ATP, 0.2 Na-GTP and 10 Na2-phosphocreatine (pH $\approx$ 7.3). Potentials were corrected for a junction potential of -10 mV when using CsMeS and KGlu-based intracellular solutions. Whole-cell recordings were obtained using Multiclamp 700B, filtered at 4 kHz and digitized at 20 kHz. Digitized data were analyzed off-line using pClamp10.1 software (Molecular Devices), Neuromatic package (http://www.neuromatic.thinkrandom.com/) and custom routines withing IGOR Pro 6.0 environment (Wavemetrics, USA).

Holographic photolysis. The holographic setup was adapted to the Olympus microscope as previously described (Lutz et al., 2008; Zahid et al., 2010) (Supplementary Fig. 2c). Briefly, a 405 nm diode CW-laser (CUBE 405-100, Coherent) was used for uncaging experiments. The output beam was expanded (6X) to match the input window of a LCOS-SLM (X10468-01, Hamamatsu), which operates in reflection mode. The device was controlled by a custom-designed software that calculated the corresponding phase-hologram and addressed the pattern to the LCOS-SLM, given a target intensity distribution at the focal plane of the microscope objective (Lutz et al., 2008; Zahid et al., 2010). The SLM plane was imaged at the back aperture of the microscope objective through a telescope (L1, f1 = 350 mm; L2, f2 = 180 mm). The undiffracted component (zero-order spot) was masked at the focal plane of L1 using a coverslip with a black dot.

Acute slices transferred into the recording chamber were perfused with the extracellular solution at 2-3 mL/min using a recycling bubbled system (10 mL) that allows for the continuous perfusion of the caged MNI-glutamate (50 μM). Selective photostimula-

tion of interneurons during patch-clamp recordings of NG2 cells and pyramidal neurons was obtained with 5 m illumination spots during 3-8 ms and a laser power of ∼12 mW under the objective (Supplementary Fig. 3 and 4). The protocol consisted in using an initial photostimulation of 3 ms that photo-evoked single or few action potentials in most targeted interneurons (Supplementary Fig. 3d). The spatial selectivity of the stimulation was tested by changing the laser time pulse and by moving the illumination spot outside the target soma of the interneuron (Supplementary Fig. 4a-d). We considered as photo-induced unitary PSCs those that: (1) showed an increased occurrence probability of individual PSCs whithin 100 ms after photostimulation when visualized in raster plots; and (2) were detected in averaged traces with a threshold of 2 times the standard deviation of the noise (Supplementary Fig. 4a, c).

Paired recordings. Paired recordings allowed us to gain access to both presynaptic and postsynaptic compartments with high level of detail. Those recordings were performed between a venus$^+$ interneuron and a DsRed$^+$ NG2 cell both held at 70 mV with two patch pipettes. To test for a functional connection, a paired-pulse stimulation was applied to the interneuron in voltage-clamp mode to elicit action currents at 12 s intervals (1 ms, 80 mV pulse; 50 ms paired-pulse interval). This protocol allows for a precise timing of action potential generation in interneurons. We considered as a unitary connection those pairs showing averaged PSCs in NG2 cells larger than 2 times the standard deviation of the noise. To evaluate the recovery from depression, we applied two test pulses using interstimulus intervals ranging from 10 ms to 250 ms. Paired-pulse ratios were calculated as PSC2/PSC1.

Immunostainings. Interneurons and NG2 cells were recorded with intracellular solutions containing 5.4 mM biocytin. Slices containing the injected cells were fixed overnight in 4% paraformaldehyde at 4°C and immunostained with rabbit polyclonal anti-parvalbumin antibody (1:2000; Swant, Switzerland) following standard procedures. Biocytin was revealed with Cy-5 conjugated streptavidin during incubation with the secondary antibody. Optical sections of confocal images were sequentially acquired using a 10X or 63X oil objectives (NA=1.4) with the LSM-710 software (Zeiss, Germany). Images were processed and analysed using ImageJ software. For counting layer V PV$^+$ interneurons, we analysed 225 x 225 m of 55 Z-sections (each 0.5 μm) from PV immunostainings of barrel cortex of venus$^+$ mice (Wayne Rasband, National Institutes of Health, USA).

Statistics. Data are expressed as mean±SEM. The statistical significance was determined using the nonparametric Mann-Whitney or Wilconxon tests. Cumulative distributions were compared using Kolmogorov-Smirnov test.

Supplementary Material

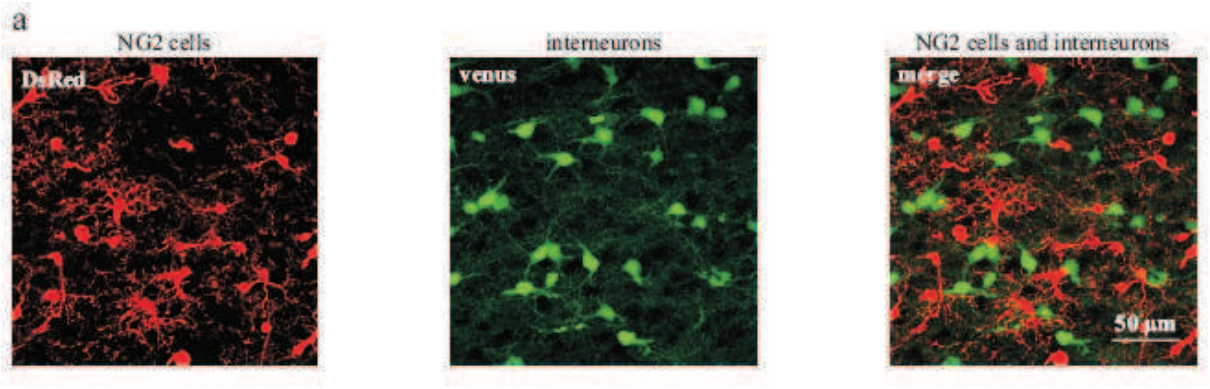

Figure 1: **Double vGAT-venus;NG2-DsRed transgenic mouse.**
(a) Confocal images of the vGAT-venus;NG2-DsRed transgenic mouse in which interneurons and NG2 cells were identified by the expression of the fluorescent proteins venus (green) and DsRed (red), respectively (Z-stacks of 15 sections; each 0.5 μm).

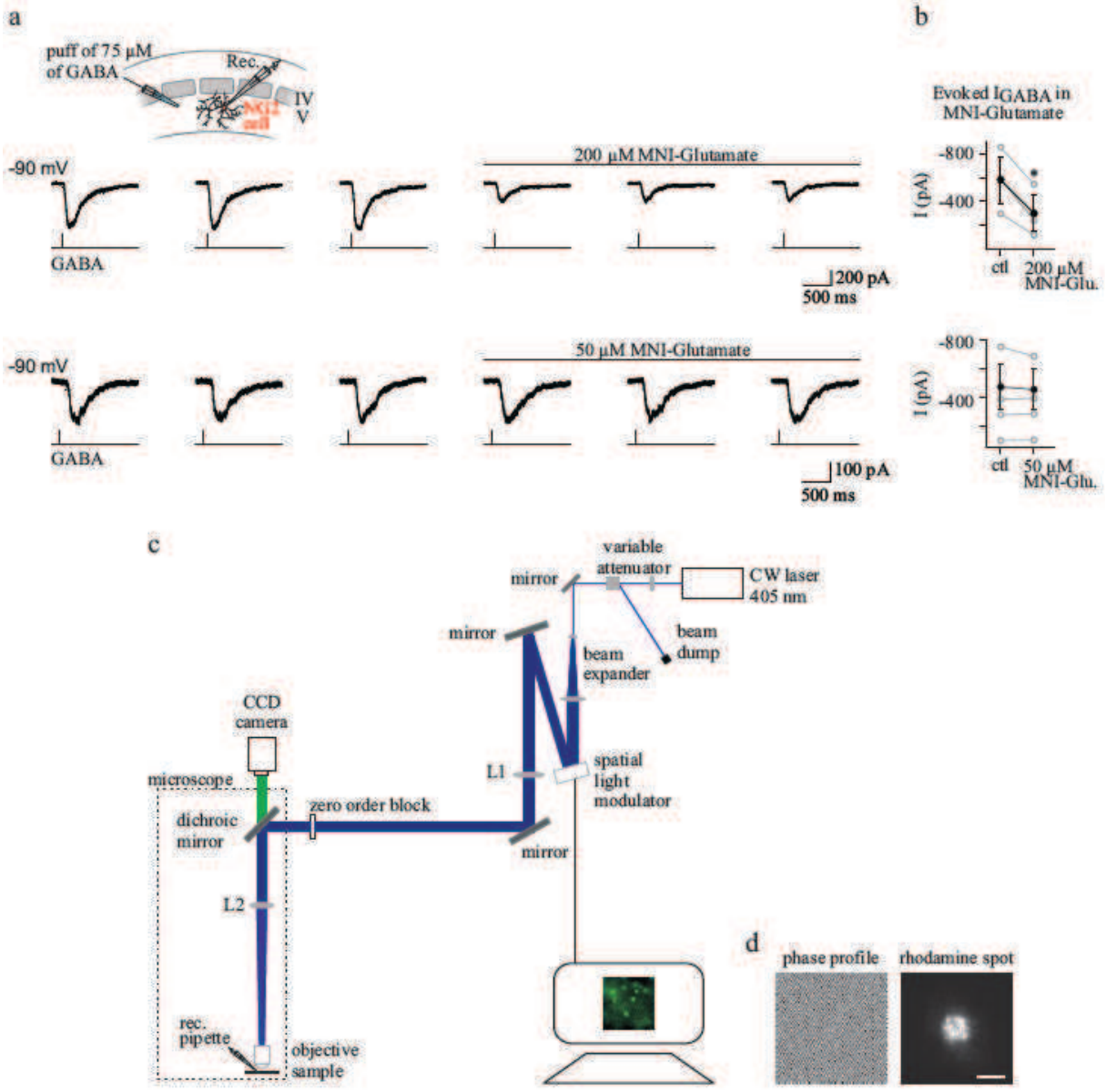

Figure 2: **Effect of MNI-glutamate on $GABA_A$ receptor-mediated currents in OPCs and optical set-up.**
(a) Diagram of local application of 75 μM GABA on recorded layer V NG2 cells (top). GABA was prepared in the extracellular solution and applied by pressure from a patch pipette (250 ms, each 10-15 s; 0.52 bars). The application pipette was positioned at 50-100 μm from cells recorded in CsCl-based intracellular solution. Inward currents were elicited by local applications of GABA at a holding potential of -90 mV in control conditions and in the presence of MNI-glutamate (traces). Note the amplitude reduction of elicited currents in 200 μM, but not in 50 μM of MNI-glutamate. **(b)** Plots of current amplitudes elicited in different NG2 cells in control conditions (ctrl) and in the presence of MNI-glutamate (MNI-Glu). Mean amplitudes are shown in black (*p<0.05). **(c)** Optical set-up for holographic photolysis (left). The focal length of the lenses are f1=350 mm (L1) and f2=180 mm (L2; see Materials and Methods for details). **(d)** Phase hologram (left) used to create a 5 μm spot (right). This illumination spot used in the present study was visualized by exciting a thin layer of rhodamine (right). Scale bar: 50 μm.

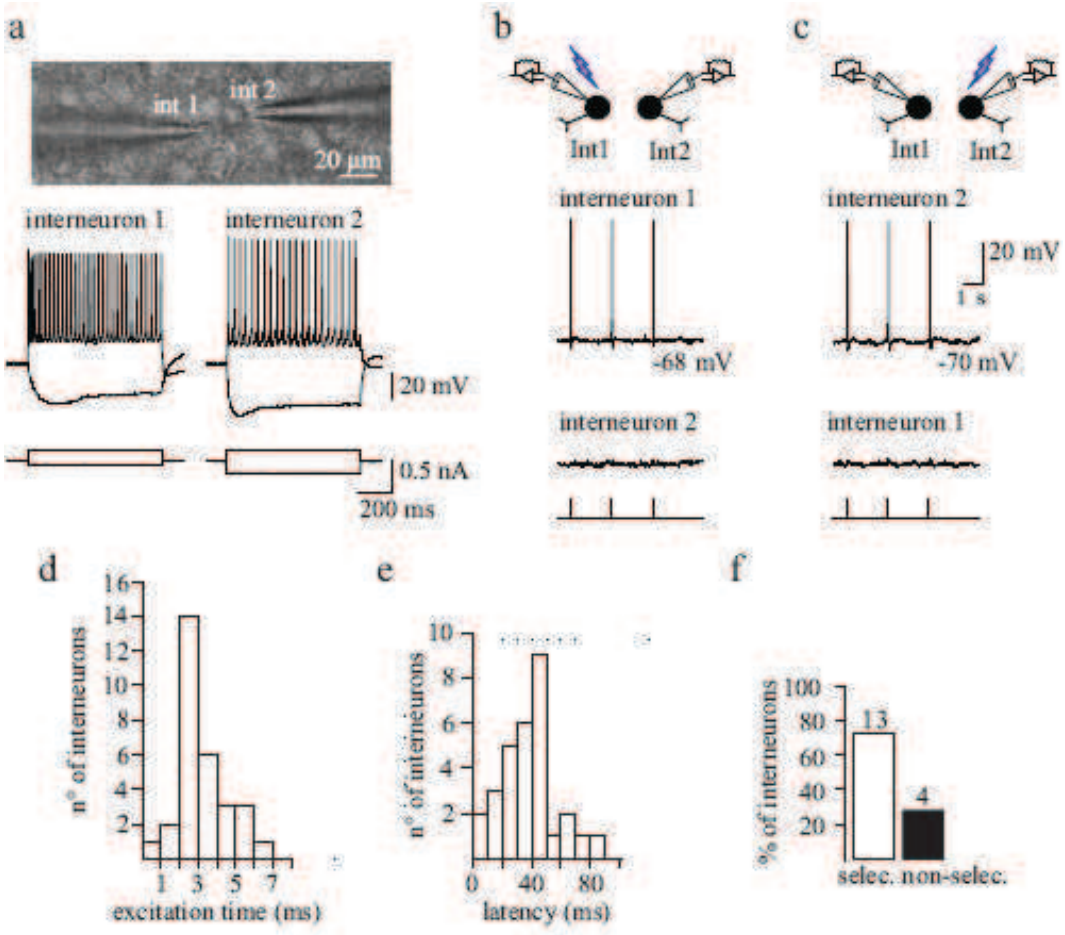

Figure 3: **Spatial selectivity of holographic photostimulation of targeted venus$^+$ interneurons.**
(a) DIC image of a simultaneous patch-clamp recording of two photostimulated venus$^+$ interneurons (top; fluorescence not shown). Note the close proximity of the two cell somata. Current-clamp recordings obtained for each recorded interneuron in response to current injections (bottom). **(b, c)** Diagram of holographic photostimulation during simultaneous patch-clamp recordings of two closeby interneurons (top). Simultaneous current-clamp recordings in response to single-cell photostimulation of either interneuron 1 **(b)** or interneuron 2 **(c)**. Note that the laser pulse elicits a reproducible action potential in the target interneuron (top traces), but not in the nearby interneuron (bottom traces). **(d)** Histogram of minimal excitation time needed to photo-evoke a single action potential in different venus$^+$ interneurons. Most interneurons are photo-activated by less than 3 ms pulses. **(e)** Histogram of latency between the beginning of the laser pulse and the peak of the photo-evoked action potential for the same interneurons. Note that although most interneurons spike within 50 ms after the photostimulation, this latency can reach 100 ms. **(f)** Histogram of the percentage of interneurons for which the photostimulation was selective when the illumination spot was moved onto the soma of the other interneuron. Note that the selectivity is attained for most interneurons, close to that reported for two-photon uncaging microscopy (Fino and Yuste, 2011). It is noteworthy that simultaneous recordings were performed between interneurons located at different planes and at very short intersomatic distances (mean intersomatic distance measured between the center of somata: 21.8±2.0 μm, n=17 simultaneous recordings). In addition, the time pulse used to test the spatial selectivity to generate action potentials in simultaneous recordings of two interneurons was always the minimal time needed to elicit an action potential in the nearby non-photostimulated interneuron).

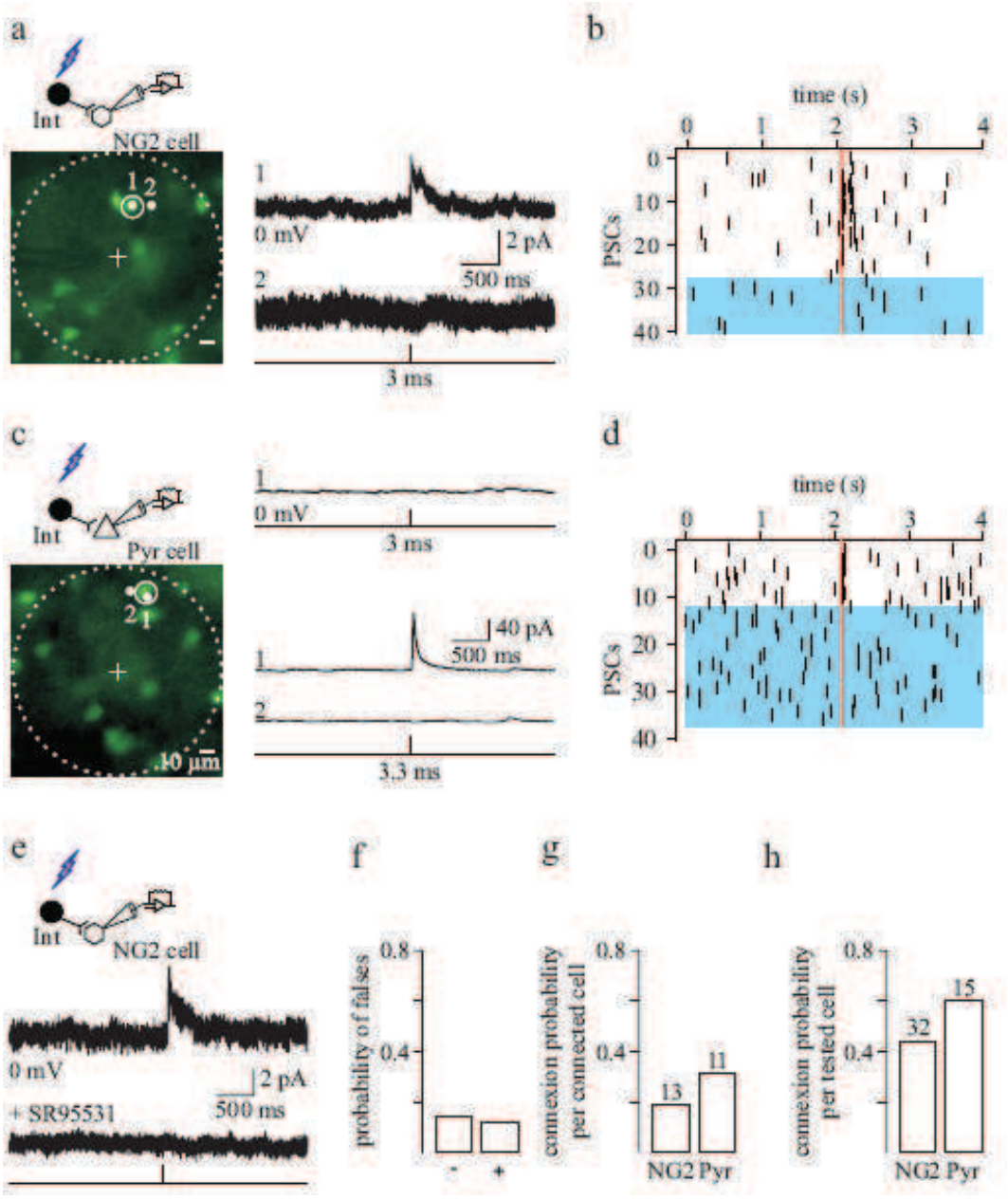

Figure 4: **Spatial selectivity of holographic photostimulation to detect unitary synaptic connections**.

(a,c) Diagram of optically-detected unitary connection (top). Excitation fields (dashed circles) in epifluorescent images of venus$^+$ interneurons (bottom). Recorded NG2 cell **(a)** and pyramidal neuron **(c)** are in the center (+, non visible). A 3 ms photostimulation of an interneuron (a; spot 1) induces unitary PSCs in a NG2 cell held at 0 mV and recorded with a CsMeS-based intracellular solution (top trace; average of 28 traces). This holding potential is selected to minimize a potential activation of glutamate receptors expressed by recorded NG2 cells in the excitation field. The spatial selectivity of this interneuron-NG2 cell connection is confirmed by displacing the illumination spot 5 μm apart (spot 2; bottom trace; average of 12 traces). **(b)** Raster plot of GABAergic synaptic events from the recorded NG2 cell illustrated in a. Note that random and sparse spontaneous synaptic currents are observed 2 s before and after interneuron photostimulation (red dashed vertical line), whereas synaptic events reproducibly occur within 100 ms after the photostimulation. These events disappear when the 5 μm spot is moved to spot 2 (blue box). **(c)** A 3 ms photostimulation of an interneuron (c; spot 1) does not induce unitary synaptic currents in a pyramidal neuron held at 0 mV and recorded with a CsMeS-based intracellular solution (top trace; average of 6 traces). Nevertheless, an increase in the excitation time of the interneuron to 3.3 ms induces unitary PSCs in the pyramidal neuron (spot 1; middle trace; average of 11 traces) that disappear when the spot is displaced 5 μm apart, confirming the photostimulation selectivity (spot 2; bottom trace; average of 26 traces). **(d)** Raster plot of GABAergic synaptic events from the recorded pyramidal neuron illustrated in c. Note that random spontaneous synaptic currents are observed 2 s before and after interneuron photostimulation (3.3 ms; dashed vertical line), whereas synaptic events reproducibly occur within 100 ms after photostimulation. These events disappear when the 5 μm spot is moved to position 2 (blue box). Failures of response were rarely observed in pyramidal neurons. **(e)** Diagram of optically-detected unitary connection (top). Averaged unitary PSC photo-induced in a recorded NG2 cell (middle trace; average of 9 traces) and completely abolished by 5 μM SR95531 (bottom trace; average of 13 traces). **(f)** Probability of encountering false negative and false positive connections. Unspecific connections were discriminated by changing the pulse duration of the laser and the position of the spot. In rare cases, the unambiguous discrimination of connected interneurons was not possible and thus these targeted interneurons were not considered in cell maps (2.8% of all tested interneurons and 13.7% of connected interneurons). **(g,h)** Connection probabilities for connected **(g)** and tested **(h)** NG2 cells and pyramidal neurons. By its flexibility and high axial and lateral resolution, holographic photolysis constitutes a suitable optical method to elicit easily action potentials in multiple venus$^+$ interneurons with single-cell resolution and find unitary connections in different recorded cell types.

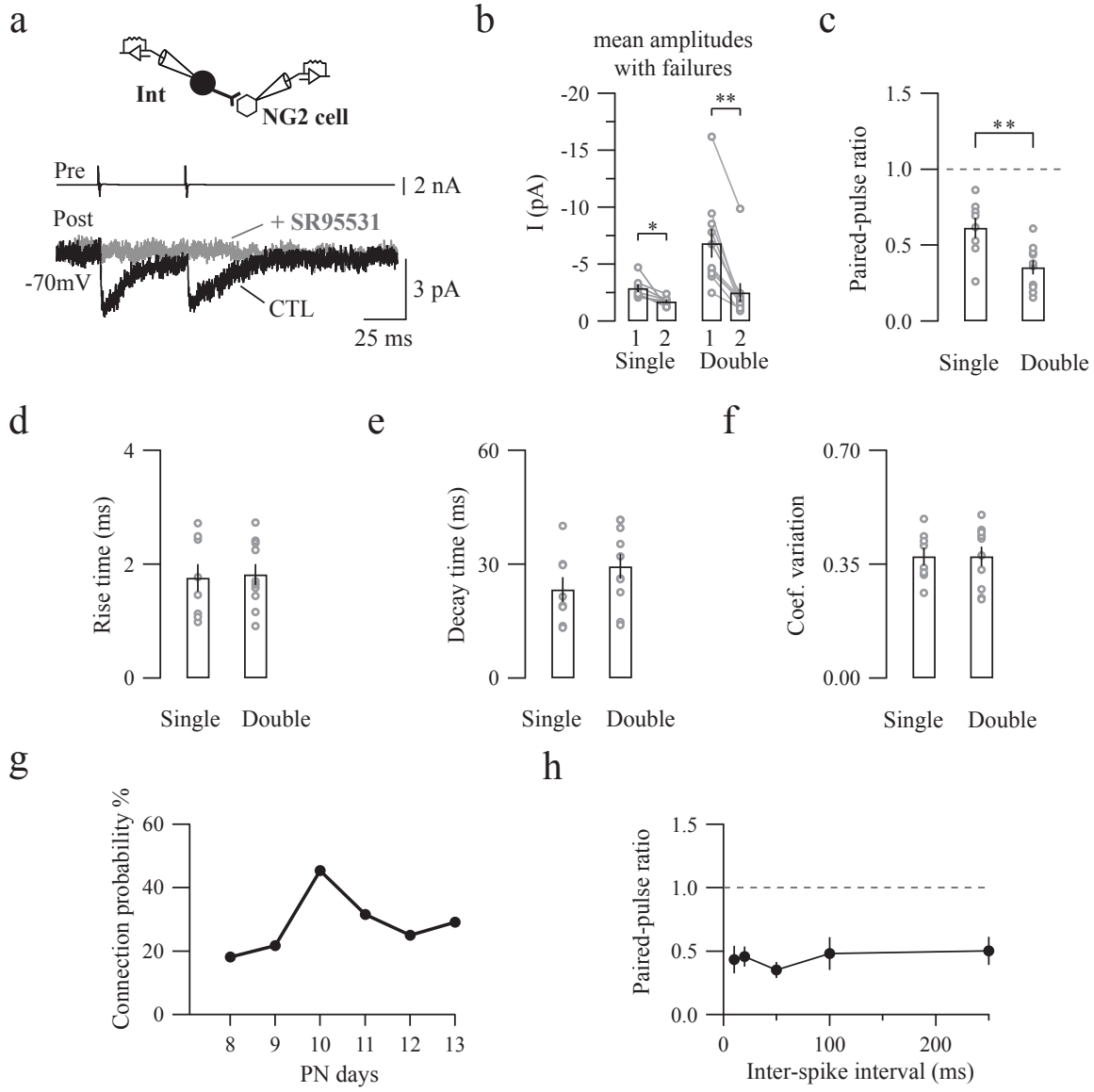

Figure 5: **Properties of unitary synaptic connections recorded by paired recordings between interneurons and NG2 cells**.
(a) Diagram of a paired recording between an interneuron and a NG2 cell (top). Two action currents evoked in presynaptic interneurons elicited PSCs recorded in NG2 cells (black trace; average of 100 traces) that are completely abolished by 5 μM SR95531 (gray trace; average of 100 traces). It is noteworthy that no differences were observed on PSCs of NG2 cells when connected interneurons were stimulated in current-clamp mode (n=3 connections). **(b-f)** Comparison of synaptic properties between connections showing single and double release sites. Note that the mean amplitudes with failures (**(b)** of PSC1 (1) and PSC2 (2) and the paired-pulse ratio **(c)** were different between these two types of connections, whereas rise **(d)** and decay **(e)** times and the coefficient of variation **(f)** were similar. $^*p<0.05$, $^{**}p<0.001$. These analyses were performed on 17 out of 38 connections for which 100 or more traces were recorded and individual PSCs in single traces could be differentiated from the noise using a detection threshold of 2 times the standard deviation. **(g)** Connection probability as a function of postnatal days. Note the peak of connection probability at PN10 (19-25 pairs tested per day). **(h)** Interneuron-NG2 cell connections did not show any recovery from depression within 250 ms interstimulus interval (n=5-10).

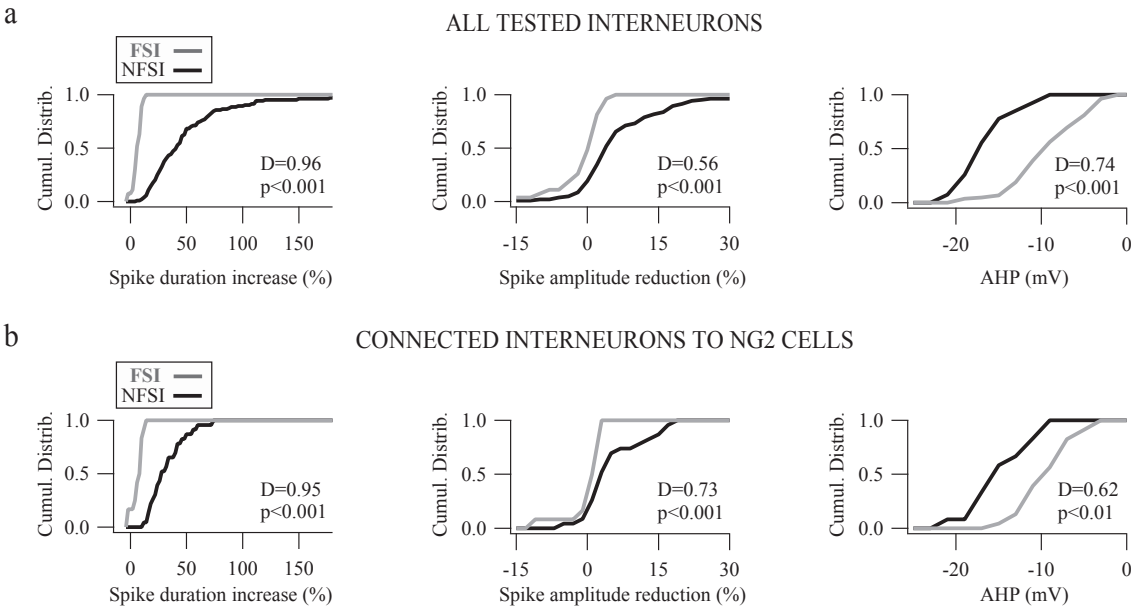

Figure 6: **Cumulative distributions for the three main electrophysiological parameters used to differentiate FSI from NFSI.**
(a, b) Comparison of cumulative distributions for spike duration increase (left), spike amplitude reduction (middle) and AHP (right) between FSI (gray traces) and NFSI (black traces) for all tested interneurons (a, n=132) and for connected interneurons to NG2 cells (b, n=38). Note the restricted distributions of these parameters for FSIs compared to NFSIs for both all and connected neurons. No significant differences were observed between all tested and connected FSIs as well as between all tested and connected NFSIs ($p>0.05$). Altogether, these results support the idea that FSIs constitute a homogeneous population, whereas NFSIs, connected or not to NG2 cells, form a heterogeneous group of interneurons.

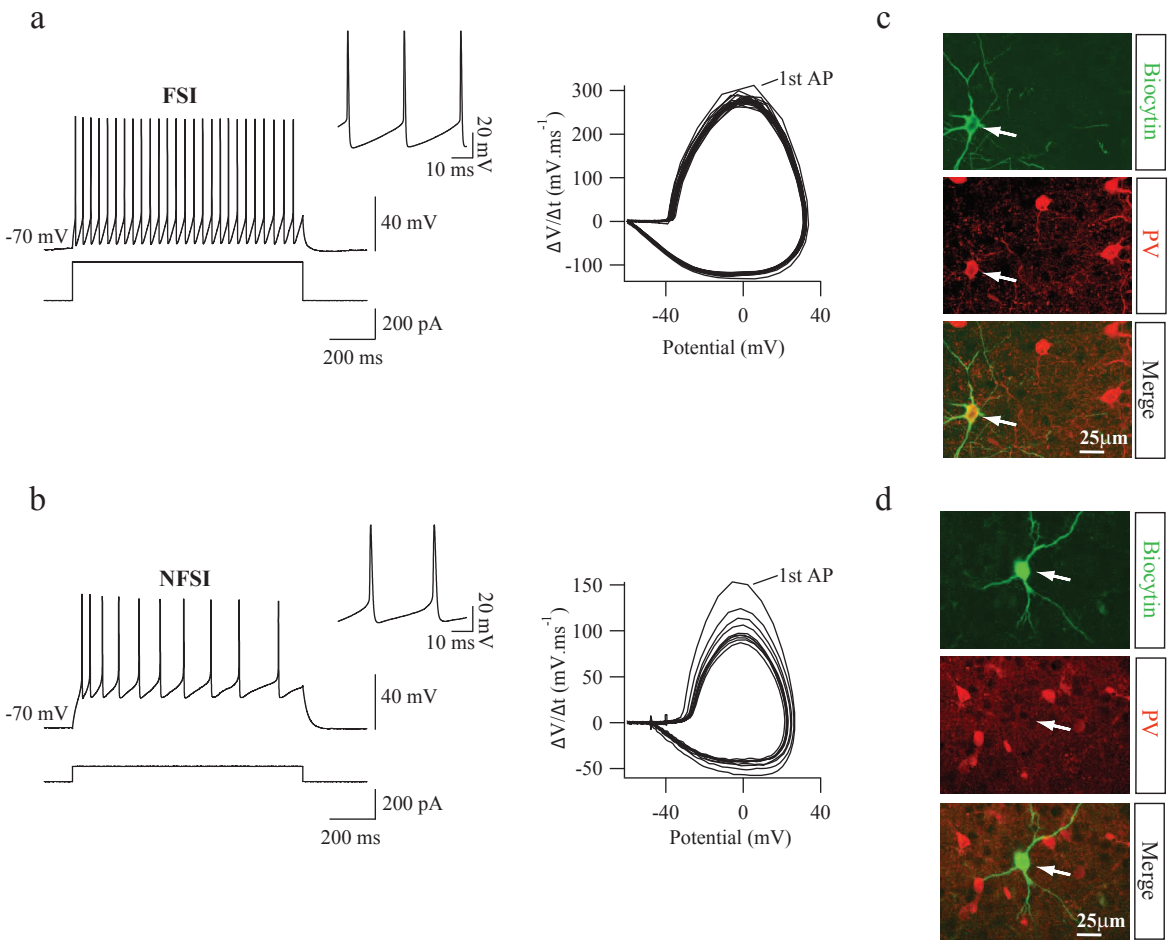

Figure 7: **PV marker is expressed in FSIs, but not in NFSIs.**
(a, b) Current-clamp recordings of a FSI **(a)** and a NFSI **(b)** connected to NG2 cells during current injections (left). Note the differences on spike morphology between the two cells (insets, right). Phase plots ($\Delta V/\Delta t$ versus potential; right) illustrate differences on spiking pattern for the same discharge (Daw et al., 2007). During a train discharge, action potentials are relatively homogeneous for FSIs, but they change drastically for NFSIs as revealed by the variance of successive loops in the phase plot. **(c, d)** PV immunostaining of biocytin-loaded FSI (c; n=5) and NFSI (d; n=3). Note the lack of PV labeling for NFSI (objective 63X; stacks of 27 and 17 Z sections, respectively, each 0.5 μm).

Parameter	FSI (n=27)	NFSI (n=105)	*p*	Comparison
F_{total} (Hz)	28.32 ± 2.73	24.18 ± 0.93	NS	-
F_{init} (Hz)	37.12 ± 3.89	45.29 ± 2.3	NS	-
F_{200} (Hz)	29.55 ± 2.73	24.48 ± 0.89	NS	-
F_{final} (Hz)	26.36 ± 2.72	21.11 ± 0.83	NS	-
Early accomodation	14.14 ± 3.61	39.33 ± 1.85	<0.0001	FSI < NFSI
Late accomodation	11.43 ± 3.01	8.87 ± 0.68	NS	-
Threshold (mV)	-35.68 ± 0.64	-36.31 ± 0.47	NS	-
First spike amplitude (mV)	70.73 ± 2.33	70.61 ± 1.09	NS	-
Second spike amplitude (mV)	70.55 ± 2.08	65.51 ± 1.3	NS	-
Spike amplitude reduction	**-0.24 ± 0.94**	**7.59 ± 1.14**	**<0.0001**	**FSI < NFSI**
First spike duration (ms)	1.37 ± 0.1	2.41 ± 0.1	<0.0001	FSI < NFSI
Second spike duration (ms)	1.46 ± 0.11	3.83 ± 0.22	<0.0001	FSI < NFSI
Spike duration increase	**6.79 ± 0.75**	**55.06 ± 5.92**	**<0.0001**	**FSI < NFSI**
AHP (mV)	**-15.89 ± 0.61**	**-8.43 ± 0.4**	**<0.0001**	**FSI > NFSI**
AHP width (ms)	25.57 ± 1.61	21.53 ± 1.05	NS	-
Peak to AHP trough (ms)	7.18 ± 0.92	13.85 ± 0.88	<0.0001	FSI < NFSI
AP-depolarizing slope (mV/ms)	207.34 ± 12.86	140.45 ± 5.63	<0.0001	FSI > NFSI
AP-hyperpolarizing slope (mV/ms)	-67.38 ± 4.35	-32.81 ± 1.36	<0.0001	FSI > NFSI
R_{in} (MΩ)	208.22 ± 17.97	399.96 ± 19.75	<0.0001	FSI < NFSI

Figure 8: **Table 1. Electrophysiological properties of venus$^+$ FSI and NFSI.** For the identification of FSI and NFSI by firing properties, we first analyzed spike-frequencies in Venus$^+$-interneurons during suprathreshold pulses in current clamp configuration from -60 mV (200 pA, 800-1000 ms). Firing frequency was calculated for the entire pulse as the number of spikes divided by the pulse duration (F_{total}). Three instantaneous discharge frequencies were also calculated: (1) between the first pair of spikes ($F_{initial}$); (2) at 200 ms from the beginning (F200); and (3) at the end of the pulse (F_{final}). These values were used to quantify both early and late accommodations in accordance with the following formulas: ($F_{initial}$-F_{200}/$F_{initial}$) and (F_{200}-F_{final}/$F_{initial}$), respectively. We also dissected the spike morphology from action potentials elicited by 80 ms suprathreshold pulses from -70 mV (150-200 pA). From these recordings, the spike threshold corresponded to the voltage at which the derivative of the AP (dV/dt) experienced a two-fold increase. The amplitudes the 1^{st} and the 2^{nd} AP (A_1 and A_2) were calculated from the threshold to peak. Their duration (D_1 and D_2) corresponded to the full-width at half maximum (FWHM) from a Gaussian fit of the depolarized face of the AP immediately after the threshold. Both amplitude reduction and duration increase were calculated by the formulas A_1-A_2/A_1 and D_2-D_1/D_1, respectively. The amplitude of the afterhyperpolarization (AHP) was calculated as the difference between the threshold and the peak of the fast hyperpolarization. We also estimated the AHP width as the FWHM and the latency of AP peak to AHP trough. We extracted the positive and negative peaks from the derivative of the AP waveform to quantify the maximal speed excursion of the membrane voltage during both depolarizing and hyperpolarizing faces of the AP. Finally, the input resistance (Rin) was measured in current clamp by applying hyperpolarizing pulses from -60 mV (-200 pA). The three major parameters to differentiate FSI from NFSI appeared in bold. Note that seven other parameters also easily differentiate these interneurons. NS: no significant difference.

Bibliography

Balia, M., Vélez-Fort, M., Stefan, P., Scäfer, C., Audinat, E., Steinhäuser, C., Seifert, G., and Angulo, M. C. (2013). Regulation of oligodendrocyte development in the vertebrate CNS. *Cerebral Cortex*, In Press.

Bergles, D. E., Roberts, J. D., Somogy, P., and Jahr, C. E. (2000). Glutamatergic synapses on oligodendrocyte precursor cells in the hippocampus. *Nature*, 6783(405):187–191.

Daw, M. I., Ashby, M. C., and Isaac, J. T. R. (2007). Coordinated developmental recruitment of latent fast spiking interneurons in layer IV barrel cortex. *Nature Neuroscience*, 10(4):453–61.

Fino, E. and Yuste, R. (2011). Dense inhibitory connectivity in neocortex. *Neuron*, 69(6):1188–203.

Lutz, C., Otis, T. S., Desars, V., Charpak, S., Digregorio, D. A., and Emiliani, V. (2008). Holographic photolysis of caged neurotransmitters. *Nature Methods*, 5(9):821–827.

Pfeffer, C. K., Xue, M., He, M., Huang, Z. J., and Scanziani, M. (2013). Inhibition of inhibition in visual cortex: the logic of connections between molecularly distinct interneurons. *Nature Neuroscience*, 16(8):1068–1076.

Stevens, C. F. and Wang, Y. (1995). Facilitation and Depression at Single Central Synapses. *Neuron*, 14(4):795–802.

Vélez-Fort, M., Maldonado, P. P., Butt, A. M., Audinat, E., and Angulo, M. C. (2010). Postnatal switch from synaptic to extrasynaptic transmission between interneurons and NG2 cells. *The Journal of Neuroscience*, 30(20):6921–9.

Wang, Y., Kakizaki, T., Sakagami, H., Saito, K., Ebihara, S., Kato, M., Hirabayashi, M., Saito, Y., Furuya, N., and Yanagawa, Y. (2009). Fluorescent labeling of both GABAergic and glycinergic neurons in vesicular GABA transporter (VGAT)-venus transgenic mouse. *Neuroscience*, 164(3):1031–1043.

Zahid, M., Vélez-Fort, M., Papagiakoumou, E., Ventalon, C., Angulo, M. C., and Emiliani, V. (2010). Holographic photolysis for multiple cell stimulation in mouse hippocampal slices. *PloS One*, 5(2):e9431.

Ziskin, J. L., Nishiyama, A., Rubio, M., Fukaya, M., and Bergles, D. E. (2007). Vesicular release of glutamate from unmyelinated axons in white matter. *Nature Neuroscience*, 10(3):321–30.

Part IV

Discussion

In article I, we showed that adult OPCs of the barrel cortex sense fine extracellular potassium increases generated by neuronal activity, a property commonly assigned to differentiated astrocytes rather than to progenitors. This ability of OPCs establishes itself progressively through the postnatal upregulation of Kir4.1 potassium channels. In animals with advanced cortical myelination, extracellular stimulation of layer V axons induces slow potassium currents in OPCs, which amplitude correlates with presynaptic action potential rate. Moreover, we demonstrated that the discharge of a single neuron can be detected by nearby adult OPCs, indicating that these cells are strategically located to detect local changes in extracellular potassium concentration during physiological neuronal activity.

In article II, reliable and complete mapping of local GABAergic connectivity of layer V OPCs and pyramidal cells (pyr) have been obtained by holographic photolysis of glutamate. The connectivity probability of OPCs was around half less than that of pyr cells and involved more local microcircuits. In addition, by performing paired-recordings, OPCs showed to be transiently contacted by fast-spiking (FSI) and non-fast-spiking (NFSI) interneurons, trough single or double release sites. Finally, FSIs constituted a predominant input on OPCs and targeted postsynaptic sites containing $GABA_A$Rs composed by the $\gamma 2$ subunit.

Chapter 1

Article I

1.1 Kir4.1 expression and function in OPCs

Since the discovery of $NG2^+$ cells as progenitors showing an electrophysiological phenotype intermediate between neurons and glia (Stallcup and Cohn, 1976), many groups have studied their membrane conductances. Among these conductances, voltage-gated potassium channels have attracted more attention because of their important role in OPC proliferation (Gallo et al., 1996; Knutson et al., 1997). However, the expression and function of voltage-independent potassium channels have been poorly characterized. In acute slices, Kressin et al. (1995) and Chittajallu et al. (2004) described a potassium inward current in OPCs without identifying the corresponding channel and, Schröder et al. (2002) and Tang et al. (2009) suggested the expression of Kir channels, but did not identify OPCs with accurate criteria, *i.e.* electrophysiological profile and presence of a biomarker at the same time. In this context, article I provides a first complete identification of Kir4.1 potassium channels in OPCs of the mouse barrel cortex. Its expression was determined during development, founding that these channels are upregulated after the second postnatal week, and opening the possibility of new roles in the adult for these cells, related to their biophysical properties.

In the presence of voltage-gated potassium channel blockers inside the patch pipette, the I-V curve of OPCs is shifted *ca* 25 mV towards more depolarized potentials when we added 1 mM of extracellular cesium,a non-specific Kir channel antagonist, in the $4\text{-}5^{th}$ postnatal week (Article I, Figure 2I). In agreement with this finding, Djukic et al. (2007), observed that hippocampal complex glia, presumably OPCs, exhibited a depolarized E_m in a Kir4.1 channel conditional knockout (cKO) mouse and after 100 μm barium bath applications in wild-type animals. This indicates that Kir4.1 is probably the main conductance that determines the OPC E_m. It is noteworthy, however, that two-pore domain potassium channels suspected to be responsible, at least in part, for

the ohmic I-V relationship of astrocytes (Zhou et al., 2009), could also be expressed in OPCs and contribute to the linear IV curve observed in the 4-5th PN week.

A second predominant and extensively characterized function of these channels is their participation in potassium clearance from the extracellular space by astrocytes. In principle, the only requirement ensuring a high permeability for potassium through a cell is to have a membrane highly permeable to this ion that sets E_m close to the potassium equilibrium potential (Figure 1.1). In this condition, modifications in the extracellular potassium concentration confer a driven force that "transports" potassium through the cell membrane, more efficiently than by simple diffusion through a large extracellular space (Gardner-Medwin, 1983). Kir4.1 channels not only let the entrance of potassium to the cell, but they also have the additional property of inward rectification, facilitating the passage of ions towards the inside rather than the outside of the cell (Ransom and Sontheimer, 1995). A sustained potassium uptake, however, could generate a permanent increase in the intracellular potassium concentration, followed by water influx and swelling. Nevertheless, this phenomenon is not observed in astrocytes, electrically coupled cells forming a large network or syncytium. Indeed, potassium flows from a region of high concentration to regions of low concentration, driven by the difference between the E_m of the astrocytic syncytium and of the local potential generated by jigh extracellular potassium.

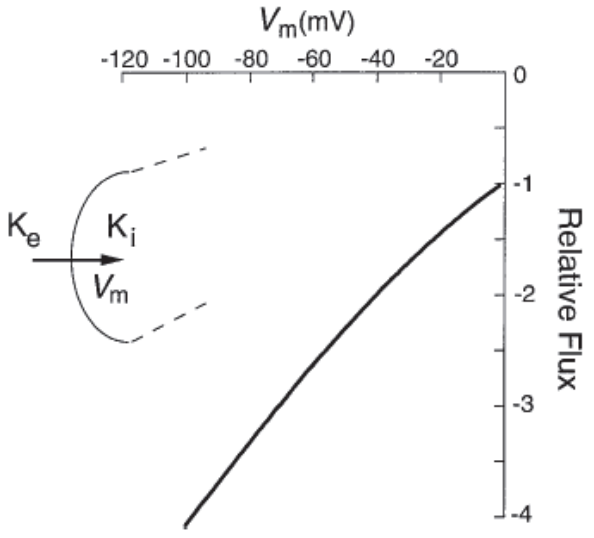

Figure 1.1: **Membrane potential and flux of potassium.**
High membrane potential permeability contributes to potassium uptake from extracellular space by spatial buffering. Note that as V_m becomes more negative, inward current is increased. K_e, extracellular potassium; K_i, intracellular potassium; V_m, membrane potential. From Amédée et al. (1997).

OPCs also express Kir4.1 channels but do not establish a cell network among them. Do they play a function in potassium clearance? If true, how are they able to generate the

required driven force? One explanation could be that OPCs detect changes in extracellular potassium concentration that occur in small restricted areas surrounding their processes. Otherwise, the cell would only suffer a depolarization and no net current will flux through the cell as a consequence of the new potassium reversal potential. This is unlikely to occur, since OPCs are characterized by the presence of very thin processes, occupying in average a volume of 100 μm^3 (Wigley and Butt, 2009; Vélez-Fort et al., 2010) and the potassium released from one single neuron is probably not enough to cover homogeneously the whole OPC surface (Article I, Figure 7).

It is fair to ask: if astrocytes are more abundant and already efficient in clearing potassium, what do OPCs more? At advanced stages of myelination, the extracellular space is reduced compared to young animals and the extracellular potassium concentration can increase highly in restricted areas (Chvátal et al., 1997). Astrocytes could have a limited access to some areas occupied by OPCs. Indeed, these progenitors are located in close apposition with neurons, contacting their soma, dendrites and nodes of Ranvier (Butt et al., 2005). They thus could have a privileged access to reduced domains in the adult. In addition, even if astrocytes and OPCs form intimate contacts with the same neurons and exhibit overlapping domains, their interaction with neurons is different (Wigley and Butt, 2009). Astrocytes ensheath pre- and postsynaptic terminals and Kir4.1 are found in processes surrounding synapses (Hibino et al., 2004). We could hypothesize that Kir4.1 located in OPC processes, could also be close to neuronal synapses. In addition since OPCs also exhibit *bona fide* synapses with neurons (Bergles et al., 2000), they could have an easier access to potassium at their own synaptic contacts.

Even if there is a large consensus on the role of Kir4.1 channels in potassium buffering, there is evidence showing that this is not the only mechanism responsible for potassium clearance. Alternative pathways have been proposed: glial and neuronal Na^+/K^+-ATPase activity and Na^+/K^+2Cl^- co-transporters (reviewed by Kofuji and Newman, 2004). Chever et al. (2010) addressed the *in vivo* implication of Kir4.1 in potassium buffering and suggested that, even though Kir4.1 channels have a predominant role in the clearance of potassium, they are not essential for potassium buffering. A Kir4.1 cKO mouse under the GFAP promoter did not show evidence of sustained extracellular accumulation of potassium or epileptic seizures (Chever et al., 2010). Nevertheless, these seizures have been related with impairment in glial potassium buffering in the past (Bordey and Sontheimer, 1998).

Besides a potential role of Kir4.1 channels of OPCs in setting E_m and participating in potassium clearance, a recent work by Chan et al. (2013) described a background barium- and bupivacaine-sensitive current responsible for the low OPC input resistance (averaged membrane resistance 4.1 $K\Omega\ cm^2$) that mediates an attenuation in both the excitatory postsynaptic potential (EPSP) along the processes and the amplitude and sharpeness of the EPSP. Chan et al. (2013) propose that this current is mediated by Kir4.1 channels, but does not exclude the participation of other channels.

1.2 Developmental changes in OPC electrophysiological properties are region-dependent

In our study, we demonstrated a developmental upregulation of Kir4.1 in OPCs (Article I, Figure 2 and 4). Previous studies did not describe this phenomenon in detail for several reasons: they did not identify the type of Kir channel (Kressin et al., 1995), the identification of OPC was not clear (Kressin et al., 1995), the study was performed in culture (Sontheimer et al., 1989) or, the animals were younger than 4-5th postnatal weeks (Berger et al., 1991; Neusch et al., 2001).

In addition to the upregulation of Kir4.1 in the somatosensory cortex, our unpublished data show that this change depends on the brain region. Indeed, adult OPCs in *corpus callosum* presented small currents compared to those in the barrel cortex and similar to those of cortical OPCs in the second postanatal week, suggesting that Kir4.1 channels are not upregulated in white matter (Figure 1.2)(see also Sahel et al. in demyelinated lesions, Annex). In agreement with this idea, it has been hypothesized by Chittajallu et al. (2004) that the region where OPCs resides determines their electrophysiological profile. Several other changes have been described in membrane properties (Introduction, section 1.3), other potassium conductances (Introduction, section 1.6.2) and morphology (Introduction, section 1.1).

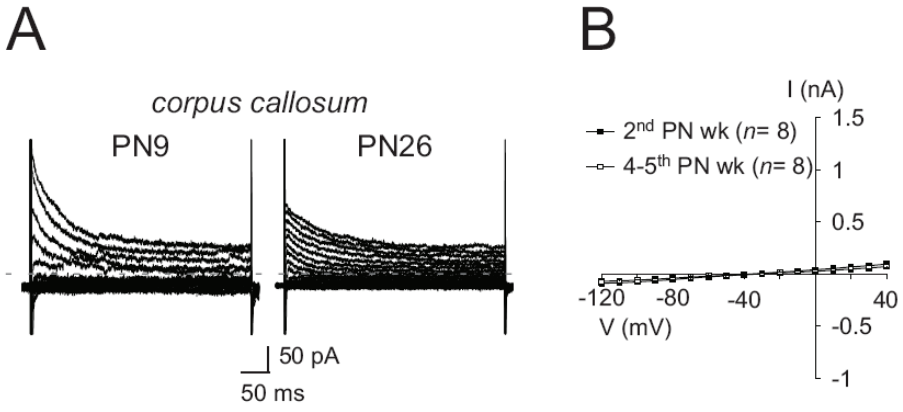

Figure 1.2: **OPC potassium currents in the *corpus callosum* during development.**
A. Currents induced in two OPCs held at -90 mV at PN9 (left) and PN26 (right) by voltage steps from +40 to -120 mV, by using a CsCl-based intracellular solution, containing 4AP and TEA-Cl.
B. Comparison of mean strady-state IV curves at both developmental stages. Note that these I-V curves do not change with age compared to cortical OPCs (Article I, Figure 2a and b). $p>0.05$. (Unpublished data).

Differences between OPCs of grey and white matter regions are not restricted to electrophysiological and anatomical properties. It was recently demonstrated that the

"niche" from where OPCs belong determines their fate (Viganò et al., 2013). OPCs derived from white matter differentiate into oligodendrocytes, independently if they are transplanted to white or grey matter, whereas OPCs derived from grey matter did not. The location of OPCs seems therefore to confer special factors and intrinsic differences. However, it could also be possible that, before the environment inflicts particular features to OPCs, a different program makes them to interact with their environment in a special manner. This program could vary according to the embryonic origin. Although Kessaris et al. (2006) did not find any evidence of heterogeneity among OPCs from different origins in the forebrain, the functionality was only evaluated in terms of their capability to differentiate. Other features of OPCs were not addressed in the study.

1.3 Future directions in determination of Kir4.1 role

One important aspect that remains to be resolved is whether Kir4.1 channel activation in OPCs affects neuronal activity. Probably, the best approach to study this problem would be to use an inducible Kir4.1 KO mouse, specifically in OPCs. These would allow for deleting Kir4.1 at different developmental stages and analyzing the consequences of this deletion in both OPCs and neurons. However, it is important to be aware that some aspects of the effect of glial Kir4.1 deletion on neuronal activity have been addressed before with a limited success (Djukic et al., 2007). Indeed, intrinsic membrane properties, firing pattern profile, evoked responses after electrical stimulation or paired-pulse facilitation of CA1 pyr cells do not show any difference compared to those of wild-type animals. Solely the frequency and amplitude of spontaneous activity and the intial phase of the LTP were increased in Kir4.1 cKO animals (Djukic et al., 2007), suggesting a role of Kir4.1-mediated potassium buffering in controling LTP induction (Djukic et al., 2007).

Although the implication of OPC Kir4.1 channels on potassium buffering remains a hypothesis, Article I shows that OPCs are able to sense and follow neuronal action potential discharges through an inward potassium current mediated by these channels (Figure 4 and 7). The amplitude of Kir4.1-mediated currents induced by a single neuron discharge is small (average -3 pA). However, it reaches tens or hundreds of pA when several neurons are stimulated with single pulses or γ-frequency trains, respectively. A similar mode of sensing has also been described in astrocytes of the olfactory bulb, where it allows for the detection of synchronized activity from both axons of olfactory sensory neurons and mitral/tufted cells that converge to the same glomerulus (De Saint Jan and Westbrook, 2005). The relevance in OPC physiology of this non-synaptic-mediated manner to detect neuronal activity remains to be investigated.

1.4 OPCs: the fourth glia cell type of the CNS

The primary function demonstrated for OPCs is their capacity to generate oligodendrocytes (at least). This implies that these cells are mainly progenitor cells. However, some inconsistencies regarding a unique role of OPCs as progenitors are intriguing. OPCs persist in the adult brain even after the myelination peak (Nishiyama, 2007), they are distributed throughout the brain even in non-myelinated regions (Introduction, section 1.4) and their abundance is not correlated with the degree of myelination or oligodendrocyte density (Nishiyama, 2007). Furthermore, OPC processes contact mainly the soma and dendrites of neurons which are non-myelinated compartments (Wigley and Butt, 2009).

The gain of new properties of OPCs during development strongly supports the view that OPCs are not only progenitor cells. Although no evidence of a different role for these cells in the brain, they have been considered as a fourth glia cell type of the CNS by several other groups (Nishiyama et al., 1999; Chang et al., 2000; Butt et al., 2002, 2005; Dawson et al., 2003; Peters, 2004; Mangin and Gallo, 2011). The possibility that OPCs do not behave necessarily as progenitors is not in contradiction with their ability to generate oligodendrocytes, but it adds a further complexity on the functioning of these cells that merits to be investigated in the future.

Chapter 2

Article II

2.1 Unitary GABAergic synaptic connections between interneurons and OPCs

The presence of functional synapses between neurons and OPCs is one major physiological feature of these cells. Most information on synaptic physiology of OPCs has been obtained from the description of spontaneous or evoked synaptic currents resulting from neurotransmitter release by unknown presynaptic cells. In Article II, we combined holographic photolysis and paired recordings, two very sensitive techniques (Lutz et al., 2008; Debanne et al., 2008), to have access to the presynaptic and postsynaptic compartment of unitary synaptic connections (USCs) between cortical GABAergic interneurons and OPCs. Up to now, nobody has reported USCs between a neuron and a glia cell type. This is not due to a lack of attempt. Mangin et al. (2008) reported that they looked for USCs between hilar interneurons of the dentate gyrus and OPCs in the hippocampus without success. Probably, they were not in the optimal conditions to detect them. Indeed, Mangin et al. (2008) used a CNP-EGFP mouse not only to identify OPCs, but also GFP^+ interneurons which were in close proximity to OPCs. This subpopulation of interneurons, however, is restricted to some SOM^+ and PV^+ cells which synaptic target could not be OPCs. Secondly, the large time window of their study (PN3-PN21) could also influence their results. Without a systematic evaluation regarding the GABAergic connectivity during development, it is difficult to know the optimal period to look for connections.

A key point in the finding of USCs between interneurons and OPCs of the somatosensory cortex was the use of a double vGAT-venus;NG2-DsRed transgenic mouse in which all types of interneurons express the fluorescent protein venus and OPCs, the DsRed (Article II, Supplementary Figure 1). We also concentrated our analysis on the second

postnatal week that corresponds to the period of GABAergic synapses are present in OPCs of the somatosensory cortex (Vélez-Fort et al., 2010; Balia et al., 2013). By using this double transgenic mouse there was an increase in the number of connected pairs compare to those from the NG2-DsRed transgenic mouse (3 out of 57 v/s 35 out of 144, in the double transgenic mouse). In addition, the used of the holographic photolysis to test several interneurons per OPC decreased the time employed to find a connected pair and allowed for an accurate analyses of the spatial distribution of the connections.

2.2 HP, a suitable technique to map USCs

The use of an optical method based in the phase modulation of the beam, such as digital holography (DH), allows us to change quickly the intensity profile that targets single cells and, therefore, to photostimulate easily several neurons per field in a brain slice. The time to compute the hologram and reconfigure the spatial light modulator (SLM) per neuron is around 600 ms in our system. Recently, Nikolenko et al. (2007) reported that they are able to stimulate 500 neurons in 10 minutes using two-photon uncaging of MNI-glutamate with a beam multiplexing system. In the case of DH, 500 neurons could be stimulated, in theory, in around 5 min. However, the number of excited cells is also determined by the field of view, *i.e.* by the objective magnification and the pixel array of the SLM for DH. To get large-scale connectivity maps with DH, our system could be improved using a 20X objective, with a numerical aperture equivalent at least to that of the 40X objective that we used (0.8-1.0).

Several parameters determine the effectiveness to stimulate only one neuron by performing HP. These parameters are, among others, the light confinement, which will be greater in two-photon excitation compare to one-photon excitation (Denk et al., 1990), the length of the pulse duration and the power intensity, which will influence the number of uncaged molecules, and the area of excitation, which will determine both the number of uncaged molecules and the axial resolution for a holographic beam (Lutz et al., 2008). In addition, the variability in the action potential threshold of different types of cortical interneurons makes difficult to apply the same protocol for every tested cell. Previous experiments aiming at studying neuronal connectivity maps with single cell resolution in two-photon microscopy targeted subpopulations of interneurons with relatively homogenous intrinsic properties (Fino and Yuste, 2011; Packer and Yuste, 2011). Probably, this facilitates the standarization of the photostimulation protocol to elicit action potentials in presynaptic neurons in terms of duration and intensity of the laser pulse. In our case, we developed a more complex protocol in which we systematically increased or decreased the time of the laser pulse per interneuron in order to take into account different action potential thresholds and reveal false positive or negative connections (Article II, Supplementary Figure 4c y d). Nevertheless,

large time pulses could worsen the selectivity of the photostimulation by increasing the number of uncaged molecules that can reach untargeted cells by diffusion. Therefore a limited time of 8 ms was stipulated. With this procedure and by displacing the spot away from the soma, the selectivity of the system was evaluated "online", given reliable maps of connectivity (Article II, Supplementary Figure 4a-d). It is noteworthy that if $GABA_A$Rs were not so susceptible to caged-compounds, the selectivity of the method could be increased by increasing the concentration of MNI-Glutamate and decreasing the pulse duration and power intensity.

An alternative method to photostimulate selectively interneurons in brain slices would be the use of photosensitive proteins such as channelrhopsin-2 (ChR2) expressed in these cells. This photochemical tool has the advantage to provide an additional level of selectivity compared to uncaging since molecules do not diffuse in the tissue. ChR2 has been expressed in subpopulation of interneurons using transgenic mice and viral injections (Zhao et al., 2011; Cardin et al., 2009). However, although this method can be easily applied in the adult, it had limitations in developmental studies. Indeed, a good expression of ChR2 in neurons needs often several weeks to be effective, but our connectivity peak is around PN10. A possibility could be to do in utero electroporation to deliver the ChR2 to interneurons, but the set-up of this operation is likely to be very time consuming. Therefore, holographic photolysis was the good alternative.

2.3 Connectivity maps

By performing holographic photolysis of MNI-glutamate on venus$^+$ interneurons and recording layer V GABAergic USCs in OPCs and pyr cells of the developing somatosensory cortex, we compare the local connectivity maps of OPCs and pyr cells (Article II, Figure 1). By comparing the maps of connectivity between pyr cells and OPCs from the same region, we found that the somata of interneurons synaptically connected to OPCs are closer than those connected to pyr cells (Article II, Figure 1g and h). The connectivity map of pyr cells is relatively homogeneous within 100 μm (article II, figure 1h). In agreement with this, it has been shown that SOM$^+$ interneurons located in the same column (<100 μm) of pyr cells in layer II/III are more likely to be connected than those out of the column (>200 μm) (Fino and Yuste, 2011). It seems that more local circuits involve interneuron-OPC connections. This close proximity could be established from embryonic stages. The embryonic origin of cortical interneurons derives from the ganglionic eminence, a region located in the telencephalon ventral area, around embryonic day 13.5, and in particular from the caudal (CME) and medial ganglionic eminence (MGE) (Kelsom and Lu, 2013). The CME give rise to 5HT3a receptor-expressing interneurons and the MGE to most PV$^+$ and SOM$^+$ interneurons (Kelsom and Lu, 2013). Interestingly, OPCs arise from the MGE in a first wave (Kessaris et al., 2006) and from the lateral and caudal eminences in a second wave (Kessaris et al., 2006).

This suggests that interneurons and OPCs sharing embryonic origins could migrate together until finding their final position in the cortex. Supporting this idea, Mangin et al. (2008) found that OPCs from the hippocampus establish a preferential and close (average distance of 15 μm) association with interneurons, which is not random. This direct opposition of OPCs to interneurons let to call them satellite OPCs.

The probability of connection between layer V interneurons and pyr cells in the second postnatal week was smaller (0.3 at 80 μm, Article II, Figure 1) than that reported for pyr cells from layer II/III by Fino and Yuste (2011, 0.5 at 80 μm). The smaller number of tested interneurons per pyr cell in our study; the fact that we tested a entire population of interneurons whereas they targeted only SOM^+ cells and that we were more focused on an early developmental stage, where the maximal connectivity is not reached yet (Pangratz-Fuehrer and Hestrin, 2011), can account for this difference. Nevertheless, we observed a 2-fold higher probability of connections for pyr cells than for OPCs. The more local connectivity maps and the lower connection probability suggest a higher specificity in the connections between interneurons and OPCs than between interneurons and pyr cells. Indeed, it has been reported that no specificity exists between the spatial profile of interneuron-pyr cell connectivity maps in the neocortex (Packer et al., 2012). It is noteworthy that contrary to inhibition, pyr cells of the rat visual cortex layer II/III exhibit subnetworks of excitatory connections: they share common inputs from layer II/III and IV when they are connected and very little when they are not (Yoshimura et al., 2005).

2.4 Targeted connections

If there is a sort of selectivity in the connectivity between interneurons and OPCs, which could be the mechanisms that underly it? It is well known that interneurons target specific subcellular compartments of their postsynaptic counterpart (see section 2.1.1). Such compartmentalization allows an effective regulation of synaptic integration, plasticity and spiking, probably derived from specific distribution of channels, receptors and signaling mechanisms (Huang et al., 2007). Although OPCs receive inputs from fast-spiking (FSI) and non-fast-spiking (NFSI) interneurons (Article II, Figure 3), FSI is a preferential input of these cells that targets $GABA_A$Rs containing the γ2 subunit (Article II, Figure 3g). It has been shown that pyr cell USCs mediated by fast-spiking basket cells are more sensitive to zolpidem, an agonist of α1-containing $GABA_A$Rs, than non-fast-spiking basket cells (Thomson et al., 2000). Moreover, PV^- basket cells than PV^+ basket cells, both innervating the same pyr cell domain, contact postsynaptic sites with α2-containing $GABA_A$Rs (Nyíri et al., 2001). Our results suggest that postsynaptic receptors with a particular subunit composition in OPCs are the target of specific subtypes of interneurons.

Regarding the subpopulation of interneurons, FSIs are a homogeneous population compare to NFSIs (article II, supplementary figure 6). Due to their narrow integration windows and high-frequency non-adapting firing, mature FSIs play a role in the temporal control of their targets (Okaty et al., 2009). However, immature FSIs possess different properties, *e.g.* high input resistance, relatively low membrane time constants and spike-frequency adaptation, and are thus unlikely to perform the same function (Okaty et al., 2009). A differential role of FSIs and NFSIs in OPC physiology is still elusive.

2.5 Function of GABAergic synapses onto OPCs

One potential role of GABAergic synapses in OPCs is to control their differentiation, influencing in turn the myelination process. Nevertheless, interneurons are characterized by relatively short axons that do not project out of the cortex and are thought to lack myelin. Myelination increases the conduction velocity, affecting spike timing and oscillations in neurons (Fields et al., 2013). Our results raise the possibility that interneurons, in particular FS interneurons, are indeed myelinated. This phenomenon is likely to occur since myelin is important for the organization of Kv1 channels (Rasband et al., 1998) that are expressed in interneurons (Toledo-Rodriguez et al., 2004). These channels have been proposed to mediate the variability in FSI firing pattern, *i.e.* these cells can discharge action potentials after the onset of depolarizing current steps or after a prolonged delay (Golomb et al., 2007). In any manner, MBP (myelin basic protein) immunostaining for PV^+ interneurons or another interneuron subtype is an easy mean to test for this hypothesis.

Finally, the connectivity between interneurons and OPCs exhibited a peak at PN10 (Article II, Supplementary Figure 5g), if GABAergic synapses have any relevance in OPC physiology, why the USCs are transient? Conversely, the connection probability between FSIs and pyr cells reaches a *plateau* at PN15 (around 50%) without any indication of transient innervation (Pangratz-Fuehrer and Hestrin, 2011). After PN10, the decrease in synaptic innervation is accompanied by other relevant changes. There is a decrease in the amplitude of the GABA-mediated miniature events (Balia et al., 2013); Kir channels start to be dramatically upregulated after PN10 (Kressin et al., 1995); the first wave of oligodendrocytes arising from MGE and the anterior entopeduncular area from Nkx2.1-expressing precursors is eliminated and the myelination process starts (not shown). This could suggest that, after PN10, OPCs become a different population of cells with another physiological function or that transient synaptic connections are only needed to transmit a signal that will trigger a cellular process such as differentiation, for instance; then this signal is off because it is no longer required.

Concluding remarks

Throughout this manuscript different features and properties of OPCs have been described, highlighting the dynamism and plasticity of these cells to respond to their environment. Even if for many aspects there are controversial findings, some common agreement strengthen their positioning as a glia cell type in the adult, opposite to passive or quiescent cells. The understanding and discovery of new features of these cells will provide the tools to answer many open questions: which is the role of these cells in the network and how are they connected with neurons or other glial cell types? Does synaptic activity controls proliferation, differentiation and myelination or remyelination? Conversely, if OPCs possess a fine machinery to sense neuronal activity, are they able to release any molecule that in turn can affect neuronal activity? All of these questions will need to be addressed in order to get close to the real relevance of these cells in the CNS.

Bibliography

Aguirre, A. and Gallo, V. (2004). Postnatal neurogenesis and gliogenesis in the olfactory bulb from NG2-expressing progenitors of the subventricular zone. *The Journal of Neuroscience*, 24(46):10530–41.

Aguirre, A. a., Chittajallu, R., Belachew, S., and Gallo, V. (2004). NG2-expressing cells in the subventricular zone are type C-like cells and contribute to interneuron generation in the postnatal hippocampus. *The Journal of Cell Biology*, 165(4):575–89.

Akopian, G., Kressin, K., Derouiche, A., and Steinhäuser, C. (1996). Identified glial cells in the early postnatal mouse hippocampus display different types of Ca^{2+} currents. *Glia*, 17:181–194.

Amédée, T., Robert, A., and Coles, J. A. (1997). Potassium homeostasis and glial energy metabolism. *Glia*, 21:46–55.

Anselmi, F., Ventalon, C., Bègue, A., Ogden, D., and Emiliani, V. (2011). Three-dimensional imaging and photostimulation by remote-focusing and holographic light patterning. *Proceedings of the National Academy of Sciences of the United States of America*, 108(49):19504–9.

Attali, B., Wang, N., Kolot, A., Sobko, A., Cherepanov, V., and Soliven, B. (1997). Characterization of Delayed Rectifier Kv Channels in Oligodendrocytes and Progenitor Cells. *The Journal of Neuroscience*, 17(21):8234–8245.

Balia, M., Vélez-Fort, M., Passlick, S., Scäfer, C., Audinat, E., Steinhäuser, C., Seifert, G., and Angulo, M. C. (2013). Regulation of oligodendrocyte development in the vertebrate CNS. *Cerebral Cortex*, doi: 10.1093/cerco/bht309.

Barres, B. (1991). Five electrophysiological properties of glial cells. *Annals of the New York Academy of Sciences*, 633:248–254.

Barres, B. and Raff, M. (1993). Proliferation of oligodendrocyte precursor cells depends on electrical activity in axons. *Nature*, 361:258–260.

Barres, B. a., Chun, L. L., and Corey, D. P. (1989). Glial and neuronal forms of the voltage-dependent sodium channel: characteristics and cell-type distribution. *Neuron*, 2(4):1375–88.

Barres, B. A., Chun, L. L. Y., and Corei, D. P. (1990a). Ion channels in vertebrate glia. *Annu Rev Neurosci*, 13:441–471.

Barres, B. A., Koroshetz, W. J., Swartz, K. J., Chun, L. L., and Corey, D. P. (1990b). Ion channel expression by white matter glia: the O-2A glial progenitor cell. *Neuron*, 4(4):507–24.

Bean, B. P. (2007). The action potential in mammalian central neurons. *Nature Reviews. Neuroscience*, 8(6):451–65.

Belachew, S., Chittajallu, R., Aguirre, A. a., Yuan, X., Kirby, M., Anderson, S., and Gallo, V. (2003). Postnatal NG2 proteoglycan-expressing progenitor cells are intrinsically multipotent and generate functional neurons. *The Journal of Cell Biology*, 161(1):169–86.

Belachew, S., Malgrange, B., Rigo, J. M., Rogister, B., Coucke, P., Mazy-Servais, C., and Moonen, G. (1998a). Developmental regulation of neuroligand-induced responses in cultured oligodendroglia. *NeuroReport*, 9(6):973–80.

Belachew, S., Rogister, B., Rigo, J. M., Malgrange, B., Mazy-Servais, C., Xhauflaire, G., Coucke, P., and Moonen, G. (1998b). Cultured oligodendrocyte progenitors derived from cerebral cortex express a glycine receptor which is pharmacologically distinct from the neuronal isoform. *The European Journal of Neuroscience*, 10(11):3556–64.

Berger, T., Schnitzer, J., and Kettenmann, H. (1991). Developmental changes in the membrane current pattern, K^+ buffer capacity , and morphology of glial cells in the corpus callosum slice. *The Journal of Neuroscience*, 11:3008–3024.

Bergles, D. E., Roberts, J. D., Somogy, P., and Jahr, C. E. (2000). Glutamatergic synapses on oligodendrocyte precursor cells in the hippocampus. *Nature*, 405:187–191.

Berridge, M. J., Lipp, P., and Bootman, M. D. (2000). The versatility and signalling. *Nature Reviews. Molecular Cell Biology*, 1(1).

Bichet, D., Haass, F. a., and Jan, L. Y. (2003). Merging functional studies with structures of inward-rectifier K(+) channels. *Nature Reviews. Neuroscience*, 4(12):957–67.

Binamé, F., Sakry, D., Dimou, L., Jolivel, V., and Trotter, J. (2013). NG2 regulates directional migration of oligodendrocyte precursor cells via Rho GTPases and polarity complex proteins. *The Journal of Neuroscience*, 33(26):10858–74.

Bjelke, B. and Seiger, A. (1989). Morphological distribution of MBP-like immunoreactivity in the brain during development. *Internationl Journal of Developmental Neuroscience*, 7(2):145–164.

Blankenfeld, G., Verkhratsky, A. N., and Kettenmann, H. (1992). Ca^{2+} channel expression in the oligodendrocyte lineage. *European Journal of Neuroscience*, 4(11):1035–1048.

Bordey, A. and Sontheimer, H. (1998). Properties of human glial cells associated with epileptic seizure foci. *Epilepsy Research*, 32:286–303.

Butt, A., Kiff, J., Hubbard, P., and Berry, M. (2002). Synantocytes: new functions for novel NG2 expressing glia. *Journal of Neurocytology*, 31:551–565.

Butt, A. M., Hamilton, N., Hubbard, P., Pugh, M., and Ibrahim, M. (2005). Synantocytes: the fifth element. *Journal of Anatomy*, 207(6):695–706.

Cahoy, J. D., Emery, B., Kaushal, A., Foo, L. C., Zamanian, J. L., Christopherson, K. S., Xing, Y., Lubischer, J. L., Krieg, P. a., Krupenko, S. a., Thompson, W. J., and Barres, B. a. (2008). A transcriptome database for astrocytes, neurons, and oligodendrocytes: a new resource for understanding brain development and function. *The Journal of Neuroscience*, 28(1):264–78.

Callaway, E. M. and Katz, L. C. (1993). Photostimulation using caged glutamate reveals functional circuitry in living brain slices. *Proceedings of the National Academy of Sciences of the United States of America*, 90(16):7661–5.

Callaway, E. M. and Yuste, R. (2002). Stimulating neurons with light. *Current Opinion in Neurobiology*, 12(5):587–92.

Cardin, J. A., Carlén, M., Meletis, K., Knoblich, U., Zhang, F., Deisseroth, K., Tsai, L.-H., and Moore, C. I. (2009). Driving fast-spiking cells induces gamma rhythm and controls sensory responses. *Nature*, 459(7247):663–668.

Catterall, W. A. (2000a). From ionic currents to molecular mechanisms : the structure and function of voltage-Gated sodium channels. *Neuron*, 26:13–25.

Catterall, W. A. (2000b). Structure and regulation of voltage-gated ca^{2+} channels. *Annual Reviews Cell and Developmental Biology*, 16:521–555.

Cauli, B., Audinat, E., Lambolez, B., Angulo, M. C., Ropert, N., Tsuzuki, K., Hestrin, S., and Rossier, J. (1997). Molecular and Physiological Diversity of Cortical Nonpyramidal Cells Bruno. *The Journal of Neuroscience*, 17(10):3894–3906.

Chan, C.-F., Kuo, T.-W., Weng, J.-Y., Lin, Y.-C., Chen, T.-Y., Cheng, J.-K., and Lien, C.-C. (2013). Ba^{2+}- and bupivacaine-sensitive background K^+ conductances mediate rapid EPSP attenuation in oligodendrocyte precursor cells. *The Journal of Physiology*, 591(Pt 19):4843–58.

Chang, A., Nishiyama, A., Peterson, J., Prineas, J., and Trapp, B. D. (2000). NG2-positive oligodendrocyte progenitor cells in adult human brain and multiple sclerosis lesions. *The Journal of Neuroscience*, 20(17):6404–6412.

Chever, O., Djukic, B., McCarthy, K. D., and Amzica, F. (2010). Implication of Kir4.1 channel in excess potassium clearance: an in vivo study on anesthetized glial-conditional Kir4.1 knock-out mice. *The Journal of Neuroscience*, 30(47):15769–77.

Chittajallu, R., Aguirre, a., and Gallo, V. (2004). NG2-positive cells in the mouse white and grey matter display distinct physiological properties. *The Journal of Physiology*, 561(Pt 1):109–22.

Chittajallu, R., Aguirre, A. a., and Gallo, V. (2005). Downregulation of platelet-derived growth factor-alpha receptor-mediated tyrosine kinase activity as a cellular mechanism for K+-channel regulation during oligodendrocyte development in situ. *The Journal of Neuroscience*, 25(38):8601–10.

Chittajallu, R., Chen, Y., Wang, H., Yuan, X., Ghiani, C. A., Heckman, T., Mcbain, C. J., and Gallo, V. (2002). Regulation of Kv1 subunit expression in oligodendrocyte progenitor cells and their role in G 1 S phase progression of the cell cycle. *Proceedings of the National Academy of Sciences of the United States of America*, 99(4):2350–2355.

Choe, S. (2002). Potassium channel structures. *Nature Reviews. Neuroscience*, 3(2):115–21.

Chvátal, A., Berger, T., Vorisek, I., Orkand, R. K., Kettenmann, H., and Syková, E. (1997). Changes in glial K^+ currents with decreased extracellular volume in developing rat white matter. *Journal of Neuroscience Research*, 49:98–106.

Clapham, D. E. (2007). Calcium signaling. *Cell*, 131(6):1047–58.

Clarke, L. E., Young, K. M., Hamilton, N. B., Li, H., Richardson, W. D., and Attwell, D. (2012). Properties and fate of oligodendrocyte progenitor cells in the corpus callosum, motor cortex, and piriform cortex of the mouse. *The Journal of Neuroscience*, 32(24):8173–85.

Coetzee, W. a., Amarillo, Y., Chiu, J., Chow, a., Lau, D., McCormack, T., Moreno, H., Nadal, M. S., Ozaita, a., Pountney, D., Saganich, M., Vega-Saenz de Miera, E., and Rudy, B. (1999). Molecular diversity of K+ channels. *Annals of the New York Academy of Sciences*, 868:233–85.

Couteaux, R. and Pécot-Dechavassine, M. (1970). Synaptic vesicles and pouches at the level of "actives zones" of the neuromuscular junction. *Comptes Rendus Hebdomadaires des Séances de l'Académie des Sciences*, 271:2346–2349.

Curtis, J. E., Koss, B. A., and Grier, D. G. (2002). Dynamic Holographic Optical Tweezers. *Optics Communications*, 207:169–175.

Dal Maschio, M., Difato, F., Beltramo, R., Blau, A., Benfenati, F., and Fellin, T. (2010). Simultaneous two-photon imaging and photo-stimulation with structured light illumination. *Optics Express*, 18(18):18720–31.

Dantzker, J. L. and Callaway, E. M. (2000). Laminar sources of synaptic input to cortical inhibitory interneurons and pyramidal neurons. *Nature Neuroscience*, 3(7):701–7.

Dawson, M. R., Polito, A., Levine, J. M., and Reynolds, R. (2003). NG2-expressing glial progenitor cells: an abundant and widespread population of cycling cells in the adult rat CNS. *Molecular and Cellular Neuroscience*, 24(2):476–488.

De Biase, L. M., Kang, S. H., Baxi, E. G., Fukaya, M., Pucak, M. L., Mishina, M., Calabresi, P. A., and Bergles, D. E. (2011). NMDA receptor signaling in oligodendrocyte progenitors is not required for oligodendrogenesis and myelination. *The Journal of Neuroscience*, 31(35):12650–12662.

De Biase, L. M., Nishiyama, A., and Bergles, D. E. (2010). Excitability and synaptic communication within the oligodendrocyte lineage. *The Journal of Neuroscience*, 30(10):3600–11.

de Nó, L. (1949). *Cerebral cortex: architecture, intracortical connections, motor projections, in Physiology of the Nervous System, 3rd edition*. Oxford.

De Saint Jan, D. and Westbrook, G. L. (2005). Detecting activity in olfactory bulb glomeruli with astrocyte recording. *The Journal of Neuroscience*, 25(11):2917–2924.

Debanne, D., Boudkkazi, S., Campanac, E., Cudmore, R. H., Giraud, P., Fronzaroli-Molinieres, L., Carlier, E., and Caillard, O. (2008). Paired-recordings from synaptically coupled cortical and hippocampal neurons in acute and cultured brain slices. *Nature Protocols*, 3(10):1559–68.

Demerens, C., Stankoff, B., Logak, M., Anglade, P., Allinquant, B., Couraud, F., Zalc, B., and Lubetzki, C. (1996). Induction of myelination in the central nervous system by electrical activity. *Proceedings of the National Academy of Sciences of the United States of America*, 93(18):9887–92.

Denk, W., Strickler, J. H., and Webb, W. W. (1990). Two-photon laser scanning fluorescence microscopy. *Science*, 248:73–76.

di Leonardo, R., La, R., Moro, P. A., Ianni, F., Ruocco, G., Fisica, D., and La, R. (2007). Computer generation of optimal holograms for optical trap arrays. *Optical Express*, 15(4):1913–1922.

Dimou, L., Simon, C., Kirchhoff, F., Takebayashi, H., and Götz, M. (2008). Progeny of Olig2-expressing progenitors in the gray and white matter of the adult mouse cerebral cortex. *The Journal of Neuroscience*, 28(41):10434–42.

Djukic, B., Casper, K. B., Philpot, B. D., Chin, L.-S., and McCarthy, K. D. (2007). Conditional knockout of Kir4.1 leads to glial membrane depolarization, inhibition of potassium and glutamate uptake, and enhanced short-term synaptic potentiation. *The Journal of Neuroscience*, 27(42):11354–65.

Ellis-Davies, G. (2007). Caged compounds: photorelease technology for control of cellular chemistry and physiology. *Nature Methods*, 4(8):619–628.

Erzurumlu, R. S. and Gaspar, P. (2012). Development and critical period plasticity of the barrel cortex. *The European Journal of Neuroscience*, 35(10):1540–53.

Etxeberria, A., Mangin, J.-M., Aguirre, A., and Gallo, V. (2010). Adult-born SVZ progenitors receive transient synapses during remyelination in corpus callosum. *Nature Neuroscience*, 13(3):287–9.

Fang, X., Burg, M. a., Barritt, D., Dahlin-Huppe, K., Nishiyama, A., and Stallcup, W. B. (1999). Cytoskeletal reorganization induced by engagement of the NG2 proteoglycan leads to cell spreading and migration. *Molecular Biology of the Cell*, 10(10):3373–87.

Farrant, M. and Nusser, Z. (2005). Variations on an inhibitory theme: phasic and tonic activation of GABA(A) receptors. *Nature reviews. Neuroscience*, 6(3):215–29.

Fatt, B. and Katz, B. (1953). The electrical properties of crustacean muscle fibres. *Journal of Physiology*, 120:171–204.

Fernandes, H. B., Catches, J. S., Petralia, R. S., Copits, B. a., Xu, J., Russell, T. a., Swanson, G. T., and Contractor, A. (2009). High-affinity kainate receptor subunits are necessary for ionotropic but not metabotropic signaling. *Neuron*, 63(6):818–29.

Fields, R. D., Araque, A., Johansen-Berg, H., Lim, S.-S., Lynch, G., Nave, K.-A., Nedergaard, M., Perez, R., Sejnowski, T., and Wake, H. (2013). Glial Biology in Learning and Cognition. *The Neuroscientist*, doi:10.1177/1073858413504465.

Fino, E., Araya, R., Peterka, D. S., Salierno, M., Etchenique, R., and Yuste, R. (2009). RuBi-Glutamate: Two-Photon and Visible-Light Photoactivation of Neurons and Dendritic spines. *Frontiers in Neural Circuits*, 3(2):1–9.

Fino, E., Packer, A. M., and Yuste, R. (2013). The Logic of Inhibitory Connectivity in the Neocortex. *The Neuroscientist*, 19(3):228–237.

Fino, E. and Yuste, R. (2011). Dense inhibitory connectivity in neocortex. *Neuron*, 69(6):1188–203.

Fishell, G. and Rudy, B. (2011). Mechanism of inhibition within the telencephalon: "where the wild things are". *Annual Reviews of Neuroscience*, pages 535–567.

Forrest, D., Yuzaki, M., Soares, H. D., Ng, L., Luk, D. C., Sheng, M., Stewart, C. L., Morgan, J. I., Connor, J. a., and Curran, T. (1994). Targeted disruption of NMDA receptor 1 gene abolishes NMDA response and results in neonatal death. *Neuron*, 13(2):325–38.

Franklin, R. J. M. and Ffrench-Constant, C. (2008). Remyelination in the CNS: from biology to therapy. *Nature Reviews. Neuroscience*, 9(11):839–55.

Fulton, D., Paez, P. M., Fisher, R., Handley, V., Colwell, C. S., and Campagnoni, A. T. (2010). Regulation of L-type Ca^{++} currents and process morphology in white matter oligodendrocyte precursor cells by golli-myelin proteins. *Glia*, 58(11):1292–303.

Gallo, V., Zhou, J. M., McBain, C. J., Wright, P., Knutson, P. L., and Armstrong, R. C. (1996). Oligodendrocyte progenitor cell proliferation and lineage progression are regulated by glutamate receptor-mediated K^+ channel block. *The Journal of Neuroscience*, 16(8):2659–70.

Gardner-Medwin, A. (1983). A study of the mechanism by which potassium moves through brain tissue in the rat. *Journal of Physiology*, 335:353–374.

Ge, W.-P., Yang, X.-J., Zhang, Z., Wang, H.-K., Shen, W., Deng, Q.-D., and Duan, S. (2006). Long-term potentiation of neuron-glia synapses mediated by Ca^{2+}-permeable AMPA receptors. *Science*, 312(5779):1533–7.

Ge, W.-P., Zhou, W., Luo, Q., Jan, L. Y., and Jan, Y. N. (2009). Dividing glial cells maintain differentiated properties including complex morphology and functional synapses. *Proceedings of the National Academy of Sciences of the United States of America*, 106(1):328–33.

Gerchberg, R. W. and Saxton, W. O. (1972). A practical algorithm for the determination of the phase from image and diffraction pictures. *Optik*, 35:237–246.

Ghiani, C. a., Eisen, a. M., Yuan, X., DePinho, R. a., McBain, C. J., and Gallo, V. (1999a). Neurotransmitter receptor activation triggers p27^{Kip1} and p21^{CIP1} accumulation and G1 cell cycle arrest in oligodendrocyte progenitors. *Development*, 126(5):1077–90.

Ghiani, C. A., Yuan, X., Eisen, A. M., Knutson, P. L., Depinho, R. A., Mcbain, C. J., and Gallo, V. (1999b). Voltage-activated K^+ channels and membrane depolarization regulate accumulation of the cyclin-dependent kinase inhibitors p27^{Kip1} and p21^{CIP1} in glial progenitor cells. *The Journal of Neuroscience*, 19(13):5380–5392.

Giaume, C. and Naus, C. C. (2013). Connexins, gap junctions, and glia. *Wiley Interdisciplinary Reviews: Membrane Transport and Signaling*, 2(4):133–142.

Golomb, D., Donner, K., Shacham, L., Shlosberg, D., Amitai, Y., and Hansel, D. (2007). Mechanisms of firing patterns in fast-spiking cortical interneurons. *PLoS Computational Biology*, 3(8):e156.

Goretzki, L., Burg, M. A., Grako, K. A., and Stallcup, W. B. (1999). High-affinity binding of basic fibroblast growth factor and platelet-derived growth factor-AA to the core protein of the NG2 proteoglycan. *Journal of Biological Chemistry*, 274(24):16831–16837.

Grienberger, C. and Konnerth, A. (2012). Imaging calcium in neurons. *Neuron*, 73(5):862–85.

Gudz, T. I., Komuro, H., and Macklin, W. B. (2006). Glutamate stimulates oligodendrocyte progenitor migration mediated via an alphav integrin/myelin proteolipid protein complex. *The Journal of Neuroscience*, 26(9):2458–66.

Guo, F., Ma, J., McCauley, E., Bannerman, P., and Pleasure, D. (2009). Early postnatal proteolipid promoter-expressing progenitors produce multilineage cells in vivo. *The Journal of Neuroscience*, 29(22):7256–70.

Guo, F., Maeda, Y., Ko, E. M., Delgado, M., Horiuchi, M., Soulika, A., Miers, L., Burns, T., Itoh, T., Shen, H., Lee, E., Sohn, J., and Pleasure, D. (2012). Disruption of NMDA receptors in oligodendroglial lineage cells does not alter their susceptibility to experimental autoimmune encephalomyelitis or their normal development. *The Journal of Neuroscience*, 32(2):639–45.

Haberlandt, C., Derouiche, A., Wyczynski, A., Haseleu, J., Pohle, J., Karram, K., Trotter, J., Seifert, G., Frotscher, M., Steinhäuser, C., and Jabs, R. (2011). Gray matter NG2 cells display multiple Ca^{2+}-signaling pathways and highly motile processes. *PloS One*, 6(3):e17575.

Hamilton, N., Vayro, S., Kirchhoff, F., Verkhratsky, A., Robbins, J., Gorecki, D. C., and Butt, A. M. (2008). Mechanisms of ATP- and glutamate-mediated calcium signaling in white matter astrocytes. *Glia*, 56(7):734–49.

Hamilton, N., Vayro, S., Wigley, R., and Butt, A. M. (2010). Axons and astrocytes release ATP and glutamate to evoke calcium signals in NG2-glia. *Glia*, 58(1):66–79.

Harris, A. Z. and Pettit, D. L. (2007). Extrasynaptic and synaptic NMDA receptors form stable and uniform pools in rat hippocampal slices. *Journal of Physiology*, 2(2007):509–519.

Hibino, H., Fujita, A., Iwai, K., Yamada, M., and Kurachi, Y. (2004). Differential assembly of inwardly rectifying K^+ channel subunits, Kir4.1 and Kir5.1, in brain astrocytes. *The Journal of Biological Chemistry*, 279(42):44065–73.

Hibino, H., Inanobe, A., Furutani, K., Murakami, S., and Findlay, I. A. N. (2010). Inwardly Rectifying Potassium Channels: Their Structure, Function, and Physiological Roles. *Physiological Reviews*, 90(1):291–366.

Hille, B., editor (2001). *Ion channels of excitable membrane, third edition*. Sinahuer Associates Inc.

Honsek, S. D., Walz, C., Kafitz, K. W., and Rose, C. R. (2012). Astrocyte calcium signals at Schaffer collateral to CA1 pyramidal cell synapses correlate with the number of activated synapses but not with synaptic strength. *Hippocampus*, 22(1):29–42.

Horner, P. J., Thallmair, M., and Gage, F. H. (2002). Defining the NG2-expressing cell of the adult CNS. *Journal of Neurocytology*, 480(2002):469–480.

Hsiao, C.-F., Kaur, G., Vong, A., Bawa, H., and Chandler, S. H. (2009). Participation of Kv1 channels in control of membrane excitability and burst generation in mesencephalic V neurons. *Journal of Neurophysiology*, 101(3):1407–18.

Huang, Z. J., Di Cristo, G., and Ango, F. (2007). Development of GABA innervation in the cerebral and cerebellar cortices. *Nature Reviews. Neuroscience*, 8(9):673–86.

Hubel, D. H., Wiesel, T. N., and Stryker, M. P. (1977). Orientation columns in macaque monkey visual cortex demostrated by the 2-deoxyglucose autoradiographic technique. *Nature*, 269:328–330.

Hughes, E. G., Kang, S. H., Fukaya, M., and Bergles, D. E. (2013). Oligodendrocyte progenitors balance growth with self-repulsion to achieve homeostasis in the adult brain. *Nature Neuroscience*, 16(6):668–76.

Itoh, T., Beesley, J., Itoh, A., Cohen, A. S., Kavanaugh, B., Coulter, D. A., Grinspan, J. B., and Pleasure, D. (2002). AMPA glutamate receptor-mediated calcium signaling is transiently enhanced during development of oligodendrocytes. *Journal of Neurochemistry*, 81:390–402.

Jabs, R., Pivneva, T., Hüttmann, K., Wyczynski, A., Nolte, C., Kettenmann, H., and Steinhäuser, C. (2005). Synaptic transmission onto hippocampal glial cells with hGFAP promoter activity. *Journal of Cell Science*, 118(Pt 16):3791–803.

Jacob, T. C., Moss, S. J., and Jurd, R. (2008). GABA(A) receptor trafficking and its role in the dynamic modulation of neuronal inhibition. *Nature Reviews. Neuroscience*, 9(5):331–43.

Kam, K., Worrell, J. W., Ventalon, C., Emiliani, V., and Feldman, J. L. (2013). Emergence of Population Bursts from Simultaneous Activation of Small Subsets of preBo tzinger Complex Inspiratory Neurons. *The Journal of Neuroscience*, 33(8):3332–3338.

Kandel, E. C., Schwartz, J. H., and Jessel, T. M., editors (2000). *Principles of neuronal science, fourth edition*. MacGraw-Hill.

Kang, S., Fukaya, M., Yang, J., Rothstein, J., and Bergles, D. (2010). NG2+ CNS glial progenitors remain committed to the oligodendrocyte lineage in postnatal life and following neurodegeneration. *Neuron*, 68(4):668–681.

Kaplan, J. and Forbush B 3rd, Hoffman, J. (1978). Rapid photolytic release of adenosine 5'-triphosphate from a protected analogue: utilization by the Na:K pump of human red blood cell ghosts. *Biochemistry*, 17:1929–1935.

Káradóttir, R., Cavelier, P., Bergersen, L. H., and Attwell, D. (2005). NMDA receptors are expressed in oligodendrocytes and activated in ischaemia. *Nature*, 438(7071):1162–6.

Káradóttir, R., Hamilton, N. B., Bakiri, Y., and Attwell, D. (2008). Spiking and nonspiking classes of oligodendrocyte precursor glia in CNS white matter. *Nature Neuroscience*, 11(4):450–6.

Karwoski, C. J., Lu, H.-k., , and Newman, E. A. (1989). Increases by retinal Müller (glial) cells. *Science*, 244(12):578–580.

Katz, L. C. and Dalva, M. B. (1994). Scanning laser photostimulation: a new approach for analyzing brain circuits. *Journal of Neuroscience Methods*, 54(2):205–18.

Keilhauer, G., Meier, D., Kuhlmann-Krieg, S., Nieke, J., and Schachner, M. (1985). Astrocyte ssupportin complete differentiation of an oligodendrocyte precursor cell. *The EMBO Journal*, 4(10):2499–2504.

Kelsom, C. and Lu, W. (2013). Development and specification of GABAergic cortical interneurons. *Cell and Bioscience*, 3(1):19.

Kessaris, N., Fogarty, M., Iannarelli, P., Grist, M., Wegner, M., and Richardson, W. D. (2006). Competing waves of oligodendrocytes in the forebrain and postnatal elimination of an embryonic lineage. *Nature Neuroscience*, 9(2):173–9.

Kettenmann, H., Hanisch, U.-k., Noda, M., and Verkhratsky, A. (2011). Physiology of Microglia. *Physiol Rev*, 91:461–553.

Kettenmann, H. and Verkhratsky, A. (2008). Neuroglia: the 150 years after. *Trends in Neurosciences*, 31(12):653–9.

Kirchhoff, F. and Kettenmann, H. (1992). GABA triggers a $[Ca^{2+}]$i increase in murine precursor cells of the oligodendrocyte lineage. *European Journal of Neuroscience*, 4:1049–1058.

Knutson, P., Ghiani, C. a., Zhou, J. M., Gallo, V., and McBain, C. J. (1997). K^+ channel expression and cell proliferation are regulated by intracellular sodium and membrane depolarization in oligodendrocyte progenitor cells. *The Journal of Neuroscience*, 17(8):2669–82.

Kofuji, P. and Newman, E. A. (2004). Potassium buffering in the central nervous system. *Neuroscience*, 129(4):1045–56.

Kondo, T. and Raff, M. (2000). Oligodendrocyte precursor cells reprogrammed to become multipotential CNS stem cells. *Science*, 289:1754–1757.

Kressin, K., Kuprijanova, E., Jabs, R., Seifert, G., and Steinhäuser, C. (1995). Developmental regulation of Na^+ and K^+ conductances in glial cells of mouse hippocampal brain slices. *Glia*, 15(2):173–87.

Krieger, P., Kuner, T., and Sakmann, B. (2007). Synaptic connections between layer 5B pyramidal neurons in mouse somatosensory cortex are independent of apical dendrite bundling. *The Journal of Neuroscience*, 27(43):11473–11482.

Kukley, M., Capetillo-Zarate, E., and Dietrich, D. (2007). Vesicular glutamate release from axons in white matter. *Nature Neuroscience*, 10(3):311–20.

Kukley, M. and Dietrich, D. (2009). Kainate receptors and signal integration by NG2 glial cells. *Neuron Glia Biology*, 5(1-2):13–20.

Kukley, M., Kiladze, M., Tognatta, R., Hans, M., Swandulla, D., Schramm, J., and Dietrich, D. (2008). Glial cells are born with synapses. *The FASEB Journal*, 22(8):2957–69.

Kukley, M., Nishiyama, A., and Dietrich, D. (2010). The fate of synaptic input to NG2 glial cells: neurons specifically downregulate transmitter release onto differentiating oligodendroglial cells. *The Journal of Neuroscience*, 30(24):8320–31.

Lambolez, B., Audinat, E., Bochet, P., Crépel, F., and Rossier, J. (1992). AMPA receptor subunits expressed by single Purkinje cells. *Neuron*, 9(2):247–58.

Le Meur, K., Galante, M., Angulo, M. C., and Audinat, E. (2007). Tonic activation of NMDA receptors by ambient glutamate of non-synaptic origin in the rat hippocampus. *The Journal of Physiology*, 580(Pt. 2):373–83.

Lester, H. and Nerbonne, J. (1982). Physiological and pharmacological manipulations with light flashes. *Annual Review of Biophysics and Bioengineering*, 11:151–178.

Levine, J. M. and Card, J. P. (1987). Light and electron microscopic localization of a cell surface antigen (NG2) in the rat cerebellum: association with smooth protoplasmic astrocytes. *Journal of Neuroscience*, 7:2711–2720.

Levine, J. M. and Stallcup, W. B. (1987). Plasticity of developing cerebellar cells in vitro studied with antibodies against the NG2 antigen. *Journal of Neuroscience*, 7:2721–2731.

Li, C., Xiao, L., Liu, X., Yang, W., Shen, W., Hu, C., Yang, G., and He, C. (2013). A functional role of NMDA receptor in regulating the differentiation of oligodendrocyte precursor cells and remyelination. *Glia*, 61(5):732–49.

Li, H. and Crair, M. C. (2011). How do barrels form in somatosensory cortex? *Annals of the New York Academy of Sciences*, 1225:119–29.

Lin, S.-C. and Bergles, D. E. (2002). Physiological characteristics of NG2-expressing glial cells. *Journal of Neurocytology*, 549(2002):537–549.

Lin, S.-c. and Bergles, D. E. (2004). Synaptic signaling between GABAergic interneurons and oligodendrocyte precursor cells in the hippocampus. *Nature Neuroscience*, 7(1):24–32.

Lin, S.-c., Huck, J. H. J., Roberts, J. D. B., Macklin, W. B., Somogyi, P., and Bergles, D. E. (2005). Climbing fiber innervation of NG2-expressing glia in the mammalian cerebellum. *Neuron*, 46:773–785.

Lisman, J. (1989). A mechanism for the Hebb and the anti-Hebb processes underlying learning and memory. *Proceedings of the National Academy of Sciences of the United States of America*, 86(23):9574–9578.

Lui, J. H., Hansen, D. V., and Kriegstein, A. R. (2011). Development and evolution of the human neocortex. *Cell*, 146(1):18–36.

Lutz, C., Otis, T. S., Desars, V., Charpak, S., Digregorio, D. A., and Emiliani, V. (2008). Holographic photolysis of caged neurotransmitters. *Nature Methods*, 5(9):821–827.

Luyt, K., Slade, T. P., Dorward, J. J., Durant, C. F., Wu, Y., Shigemoto, R., Mundell, S. J., Váradi, A., and Molnár, E. (2007). Developing oligodendrocytes express functional GABA(B) receptors that stimulate cell proliferation and migration. *Journal of Neurochemistry*, 100(3):822–40.

Luyt, K., Váradi, A., Durant, C. F., and Molnár, E. (2006). Oligodendroglial metabotropic glutamate receptors are developmentally regulated and involved in the prevention of apoptosis. *Journal of Neurochemistry*, 99(2):641–56.

Luyt, K., Varadi, A., and Molnar, E. (2003). Functional metabotropic glutamate receptors are expressed in oligodendrocyte progenitor cells. *Journal of Neurochemistry*, 84(6):1452–1464.

Luzhynskaya, A., Lundgaard, I., Wang, Z., ffrench Constant, C., Attwell, D., and Káradóttir, R. (2009). Neurogulin induces NMDA receptor dependent myelination by oligodendrocytes [abstract]. *Glia*, 57:S43.

Lytle, J. M., Chittajallu, R., Wrathall, J. R., and Gallo, V. (2009). NG2 cell response in the CNP-EGFP mouse after contusive spinal cord injury. *Glia*, 57(3):270–85.

Maldonado, P. P., Vélez-Fort, M., and Angulo, M. C. (2011). Is neuronal communication with NG2 cells synaptic or extrasynaptic? *Journal of Anatomy*, 219(1):8–17.

Mangin, J.-M. and Gallo, V. (2011). The curious case of NG2 cells: transient trend or game changer? *ASN Neuro*, 3(1):37–49.

Mangin, J.-M., Kunze, A., Chittajallu, R., and Gallo, V. (2008). Satellite NG2 progenitor cells share common glutamatergic inputs with associated interneurons in the mouse dentate gyrus. *The Journal of Neuroscience*, 28(30):7610–23.

Mangin, J.-M., Li, P., Scafidi, J., and Gallo, V. (2012). Experience-dependent regulation of NG2 progenitors in the developing barrel cortex. *Nature Neuroscience*, 15(9):1192–4.

Markram, H., Toledo-Rodriguez, M., Wang, Y., Gupta, A., Silberberg, G., and Wu, C. (2004). Interneurons of the neocortical inhibitory system. *Nature Reviews. Neuroscience*, 5(10):793–807.

Matsui, K. and Jahr, C. E. (2003). Ectopic release of synaptic vesicles. *Neuron*, 40(6):1173–83.

Matsui, K. and Jahr, C. E. (2006). Exocytosis unbound. *Current Opinion in Neurobiology*, 16(3):305–11.

Matsuzaki, M., Ellis-Davies, G. C., Nemoto, T., Miyashita, Y., Iino, M., and Kasai, H. (2001). Dendritic spine geometry is critical for AMPA receptor expression in hippocampal CA1 pyramidal neurons. *Nature Neuroscience*, 4(11):1086–92.

Mayer, M. L., Westbrook, G. L., and Guthrie, P. B. (1984). Voltage-dependent block by Mg^{2+} of NMDA responses in spinal cord neurons. *Nature*, 309:261–263.

Menn, B., Garcia-Verdugo, J. M., Yaschine, C., Gonzalez-Perez, O., Rowitch, D., and Alvarez-Buylla, A. (2006). Origin of oligodendrocytes in the subventricular zone of the adult brain. *The Journal of Neuroscience*, 26(30):7907–18.

Micu, I., Jiang, Q., Coderre, E., Ridsdale, a., Zhang, L., Woulfe, J., Yin, X., Trapp, B. D., McRory, J. E., Rehak, R., Zamponi, G. W., Wang, W., and Stys, P. K. (2006). NMDA receptors mediate calcium accumulation in myelin during chemical ischaemia. *Nature*, 439(7079):988–92.

Möhler, H., Fritschy, J. M., and Rudolph, U. (2002). A new benzodiazepinepharmacology. *Perspectives in Pharmacology*, 300(1):2–8.

Molnár, P. and Nadler, J. V. (2000). gamma-Aminobutyrate, alpha-carboxy-2-nitrobenzyl ester selectively blocks inhibitory synaptic transmission in rat dentate gyrus. *European Journal of Pharmacology*, 391(3):255–62.

Mountcastle, V. B. (1997). The columnar organization of the neocortex. *Brain*, 120:701–722.

Müller, J., Reyes-Haro, D., Pivneva, T., Nolte, C., Schaette, R., Lübke, J., and Kettenmann, H. (2009). The principal neurons of the medial nucleus of the trapezoid body and NG2$^+$ glial cells receive coordinated excitatory synaptic input. *The Journal of General Physiology*, 134(2):115–27.

Neusch, C., Rozengurt, N., Jacobs, R. E., Lester, H. a., and Kofuji, P. (2001). Kir4.1 potassium channel subunit is crucial for oligodendrocyte development and in vivo myelination. *The Journal of Neuroscience*, 21(15):5429–38.

Nikolenko, V., Poskanzer, K. E., and Yuste, R. (2007). Two-photon photostimulation and imaging of neural circuits. *Nature Methods*, 4(11):943–950.

Nikolenko, V., Watson, B. O., Araya, R., Woodruff, A., Peterka, D. S., and Yuste, R. (2008). SLM Microscopy: Scanless Two-Photon Imaging and Photostimulation with Spatial Light Modulators. *Frontiers in Neural Circuits*, 2:1–14.

Nishiyama, A. (2007). Polydendrocytes: NG2 cells with many roles in development and repair of the CNS. *The Neuroscientist*, 13(1):62–76.

Nishiyama, A., Chang, A., and Trapp, B. (1999). NG2$^+$ glial cells: a novel glial cell population in the adult brain. *Journal of Neuropathology and Experimental Neurology*, 58:1113–1124.

Nishiyama, A., J.Dahlin, K., Prince, J. T., Johnstone, S. R., and Stallcup, W. B. (1991). The primary structure of NG2, a novel membrane-spanning proteoglycan. *The Journal of Cell Biology*, 114(2):1819–1832.

Nishiyama, A., Komitova, M., Suzuki, R., and Zhu, X. (2009). Polydendrocytes (NG2 cells): multifunctional cells with lineage plasticity. *Nature Reviews. Neuroscience*, 10(1):9–22.

Nishiyama, A., Lin, X.-H., Giese, N., Heldin, C.-H., and Stallcup, W. (1996). Co-localization of NG2 proteoglycan and PDGF alpha-receptor on O2A progenitor cells in the developing rat brain. *Journal of Neuroscience Research*, 43:299–314.

Noble, M. and Murray, K. (1984). Purified astrocytes promote the in vitro division of a bipotential glial progenitor cell. *The EMBO Journal*, 3(10):2243–2247.

Nyíri, G., Freund, T. F., and Somogyi, P. (2001). Input-dependent synaptic targeting of a 2 -subunit-containing GABA A receptors in synapses of hippocampal pyramidal cells of the rat. *European Journal of Neuroscience*, 13:428–442.

Okaty, B. W., Miller, M. N., Sugino, K., Hempel, C. M., and Nelson, S. B. (2009). Transcriptional and electrophysiological maturation of neocortical fast-spiking GABAergic interneurons. *The Journal of Neuroscience*, 29(21):7040–52.

Orkand, R. K., Nicholls, J. G., and W, K. S. (1966). Effect of nerve impulses on the membrane potential of glial cells in the central nervous system. *Journal of Neurophysiology*, 4:788–806.

Oron, D., Papagiakoumou, E., Anselmi, F., and Emiliani, V. (2012). *Two-photon optogenetics.*, volume 196. Elsevier B.V., 1 edition.

Packer, A. M., McConnell, D. J., Fino, E., and Yuste, R. (2012). Axo-dendritic overlap and laminar projection can explain interneuron Connectivity to Pyramidal Cells. *Cerebral Cortex*, doi :10.1093/cercor/bhs210.

Packer, A. M. and Yuste, R. (2011). Dense, unspecific connectivity of neocortical parvalbumin-positive interneurons: a canonical microcircuit for inhibition? *The Journal of Neuroscience*, 31(37):13260–71.

Paez, P. M., Fulton, D., Spreuer, V., Handley, V., and Campagnoni, A. T. (2011). Modulation of canonical transient receptor potential channel 1 in the proliferation of oligodendrocyte precursor cells by the golli products of the myelin basic protein gene. *The Journal of Neuroscience*, 31(10):3625–37.

Paez, P. M., Fulton, D. J., Spreuer, V., Handley, V., Campagnoni, C. W., Macklin, W. B., Colwell, C., and Campagnoni, A. T. (2009). Golli myelin basic proteins regulate oligodendroglial progenitor cell migration through voltage-gated Ca^{2+} influx. *The Journal of Neuroscience*, 29(20):6663–76.

Palay, S. L. (1956). Synapses in the central nervous system. *The Journal of Biophysical and Biochemical Cytology*, 2(4):193–202.

Pangratz-Fuehrer, S. and Hestrin, S. (2011). Synaptogenesis of electrical and GABAergic synapses of fast-spiking inhibitory neurons in the neocortex. *The Journal of Neuroscience*, 31(30):10767–75.

Paoletti, P., Bellone, C., and Zhou, Q. (2013). NMDA receptor subunit diversity: impact on receptor properties, synaptic plasticity and disease. *Nature Reviews. Neuroscience*, 14(6):383–400.

Papagiakoumou, E. (2013). Optical developments for optogenetics. *Biology of the Cell*, 105:1–22.

Papay, R., Gaivin, R., Jha, A., Mccune, D. A. N. F., Mcgrath, J. C., Rodrigo, M. C., Simpson, P. C., and Doze, V. A. N. A. (2006). Localization of the mouse α_{1A}-adrenergic receptor (AR) in the brain: α_{1A}AR is expressed in neurons, GABAergic interneurons , and NG2 Oligodendrocyte Progenitors. *The Journal of Comparative Neurology*, 497:209–222.

Papay, R., Gaivin, R., McCune, D. F., Rorabaugh, B. R., Macklin, W. B., McGrath, J. C., and Perez, D. M. (2004). Mouse α_{1B}-adrenergic receptor is expressed in neurons and NG2 oligodendrocytes. *The Journal of Comparative Neurology*, 478(1):1–10.

Passlick, S., Grauer, M., Schäfer, C., Jabs, R., Seifert, G., and Steinhäuser, C. (2013). Expression of the γ2-Subunit Distinguishes Synaptic and Extrasynaptic GABAA Receptors in NG2 Cells of the Hippocampus. *The Journal of Neuroscience*, 33(29):12030–40.

Perea, G. and Araque, A. (2005). Glial calcium signaling and neuron-glia communication. *Cell Calcium*, 38(3-4):375–82.

Peters, A. (2004). A fourth type of neuroglial cell in the central nervous system. *Journal of Neurocytology*, 33:345–357.

Petersen, C. C. H. (2007). The functional organization of the barrel cortex. *Neuron*, 56(2):339–55.

Petralia, R. S. (2012). Distribution of extrasynaptic NMDA receptors on neurons. *The Scientific World Journal*, 2012:267120.

Pfeffer, C. K., Xue, M., He, M., Huang, Z. J., and Scanziani, M. (2013). Inhibition of inhibition in visual cortex: the logic of connections between molecularly distinct interneurons. *Nature Neuroscience*, 16(8):1068–1076.

Polito, A. and Reynolds, R. (2005). NG2-expressing cells as oligodendrocyte progenitors in the normal and demyelinated adult central nervous system. *Journal of Anatomy*, 207(6):707–16.

Poopalasundaram, S., Knott, C., Shamotienko, O. G., Foran, P. G., Dolly, J. O., Ghiani, C. a., Gallo, V., and Wilkin, G. P. (2000). Glial heterogeneity in expression of the inwardly rectifying K^+ channel, Kir4.1, in adult rat CNS. *Glia*, 30(4):362–72.

Psachoulia, K., Jamen, F., Young, K. M., and Richardson, W. D. (2009). Cell cycle dynamics of NG2 cells in the postnatal and ageing brain. *Neuron Glia Biology*, 5(3-4):57–67.

Raff, M. C. and Miller, R. H. (1983). A glial progenitor cell that develops in vitro into an astrocyte or an oligodendrocyte depending on culture medium. *Nature*, 303(2):390–396.

Ragheb, F., Molina-Holgado, E., Cui, Q. L., Khorchid, a., Liu, H. N., Larocca, J. N., and Almazan, G. (2001). Pharmacological and functional characterization of muscarinic receptor subtypes in developing oligodendrocytes. *Journal of Neurochemistry*, 77(5):1396–406.

Ransom, C. B. and Sontheimer, H. (1995). Biophysical and pharmacological characterization of inwardly rectifying K^+ currents in rat spinal cord astrocytes. *Journal of Neurophysiology*, 73(1):333–346.

Rasband, M. N., Trimmer, J. S., Schwarz, T. L., Levinson, S. R., Ellisman, M. H., Schachner, M., and Shrager, P. (1998). Potassium channel distribution, clustering, and function in remyelinating rat axons. *The Journal of Neuroscience*, 18(1):36–47.

Reutsky-Gefen, I., Golan, L., Farah, N., Schejter, A., Tsur, L., Brosh, I., and Shoham, S. (2013). Holographic optogenetic stimulation of patterned neuronal activity for vision restoration. *Nature Communications*, 4:1509.

Reynolds, R., Dawson, M., Papadopoulos, D., Polito, A., Di Bello, I. C., Pham-Dinh, D., and Levine, J. (2002). The response of NG2-expressing oligodendrocyte progenitors to demyelination in MOG-EAE and MS. *Journal of Neurocytology*, 31(6-7):523–36.

Richardson, W. D., Pringle, N., Mosley, M. J., and Westermark, B. (1988). A Role for Platelet-Derived Growth Factor in Normal Gliogenesis in the Central Nervous System. *Cell*, 53:309–319.

Rivers, L. E., Young, K. M., Rizzi, M., Jamen, F., Psachoulia, K., Wade, A., Kessaris, N., and Richardson, W. D. (2008). PDGFRA/NG2 glia generate myelinating oligodendrocytes and piriform projection neurons in adult mice. *Nature Neuroscience*, 11(12):1392–401.

Robins, S. C., Villemain, A., Liu, X., Djogo, T., Kryzskaya, D., Storch, K.-F., and Kokoeva, M. V. (2013). Extensive regenerative plasticity among adult NG2-glia populations is exclusively based on self-renewal. *Glia*, 61(10):1735–47.

Rockland, K. S. (2010). Five points on columns. *Frontiers in Neuroanatomy*, 4(June):22.

Salami, M., Itami, C., Tsumoto, T., and Kimura, F. (2003). Change of conduction velocity by regional myelination yields constant latency irrespective of distance between thalamus and cortex. *Proceedings of the National Academy of Sciences of the United States of America*, 100(10):6174–6179.

Salierno, M., Marceca, E., Peterka, D. S., Yuste, R., and Etchenique, R. (2010). A fast ruthenium polypyridine cage complex photoreleases glutamate with visible or IR light in one and two photon regimes. *Journal of Inorganic Biochemistry*, 104(4):418–22.

Salter, M. G. and Fern, R. (2005). NMDA receptors are expressed in developing oligodendrocyte processes and mediate injury. *Nature*, 438(7071):1167–71.

Santos, M. D., Mohammadi, M. H., Yang, S., Liang, C. W., Kao, J. P. Y., Alger, B. E., Thompson, S. M., and Tang, C.-M. (2012). Dendritic hold and read: a gated mechanism for short term information storage and retrieval. *PloS One*, 7(5):e37542.

Schmidt, K. and Eulitz, D. (1999). Heterogeneous expression of voltage-gated potassium channels of the shaker family (Kv1) in oligodendrocyte progenitors. *Brain Research*, 843:145–160.

Schröder, W., Seifert, G., Hüttmann, K., Hinterkeuser, S., and Steinhäuser, C. (2002). AMPA receptor-mediated modulation of inward rectifier K^+ channels in astrocytes of mouse hippocampus. *Molecular and Cellular Neurosciences*, 19(3):447–58.

Seifert, G., Hüttmann, K., Binder, D. K., Hartmann, C., Wyczynski, A., Neusch, C., and Steinhäuser, C. (2009). Analysis of astroglial K+ channel expression in the developing hippocampus reveals a predominant role of the Kir4.1 subunit. *The Journal of Neuroscience*, 29(23):7474–88.

Shepherd, G. M. G., Pologruto, T. a., and Svoboda, K. (2003). Circuit analysis of experience-dependent plasticity in the developing rat barrel cortex. *Neuron*, 38(2):277–89.

Simon, C., Götz, M., and Dimou, L. (2011). Progenitors in the adult cerebral cortex: cell cycle properties and regulation by physiological stimuli and injury. *Glia*, 59(6):869–81.

Somogyi, P., Lujan, R., and Buhl, E. H. (1998). Salient features of synaptic organisation in the cerebral cortex. *Brain Research Reviews*, 26(2-3):113–135.

Song, J., Zhong, C., Bonaguidi, M. a., Sun, G. J., Hsu, D., Gu, Y., Meletis, K., Huang, Z. J., Ge, S., Enikolopov, G., Deisseroth, K., Luscher, B., Christian, K. M., Ming, G.-l., and Song, H. (2012). Neuronal circuitry mechanism regulating adult quiescent neural stem-cell fate decision. *Nature*, 489(7414):150–4.

Sontheimer, H., Trotter, J., Schachner, M., and Kettenmann, H. (1989). Channel expression correlates with differentiation stage during the development of oligodendrocytes from their precursor cells in culture. *Neuron*, 2(2):1135–45.

Stallcup, W., Beasley, L., and Levine, J. (1983). Cell-surface molecules that characterize different stages in the development of cerebellar interneurons. *Cold Spring Harbor Symposia on Quantitative Biology*, 48:761–774.

Stallcup, W. B. (2002). The NG2 proteoglycan : Past insights and future prospects. *Journal of Neurocytology*, 435(6-7):423–435.

Stallcup, W. B. and Beasley, L. (1987). Bipotential glial precursor cells of the optic nerve express the NG2 proteoglycan. *The Journal of Neuroscience*, 7(9):2737–44.

Stallcup, W. B. and Cohn, M. (1976). Correlation of surface antigens central nervous and cell type in cloned cell lines from the rat system. *Experimental Cell Research*, 98:285–297.

Stegmüller, J., Werner, H., Nave, K.-A., and Trotter, J. (2003). The proteoglycan NG2 is complexed with alpha-amino-3-hydroxy-5-methyl-4-isoxazolepropionic acid (AMPA) receptors by the PDZ glutamate receptor interaction protein (GRIP) in glial progenitor cells. Implications for glial-neuronal signaling. *The Journal of Biological Chemistry*, 278(6):3590–8.

Steinhäuser, C., Berger, T., Frotscher, M., and Kettenmann, H. (1992). Heterogeneity in the Membrane Current Pattern of Identified Glial Cells in the Hippocampal Slice. *The European Journal of Neuroscience*, 4(6):472–484.

Steinhäuser, C., Jabs, R., and Kettenmann, H. (1994). Properties of GABA and glutamate responses in identified glial cells of the mouse hippocampal slice. *Hippocampus*, 4(1):19–35.

Szapiro, G. and Barbour, B. (2007). Multiple climbing fibers signal to molecular layer interneurons exclusively via glutamate spillover. *Nature Neuroscience*, 10(6):735–742.

Szapiro, G. and Barbour, B. (2009). Review parasynaptic signalling by fast neurotransmitters : the cerebellar cortex. *Neuroscience*, 162(3):644–655.

Takumi, T., Ishii, T., Horio, Y., Morishige, K., Takahashi, N., Yamada, M., Yamashita, T., Kiyama, H., Sohmiya, K., Nakanishi, S., and Kurachi, Y. (1995). A novel ATP-dependent inward rectifier potassium channel expressed predominantly in glial cells. *The Journal of Biological Chemistry*, 270(27):16339–16346.

Tanaka, Y., Tozuka, Y., Takata, T., Shimazu, N., Matsumura, N., Ohta, A., and Hisatsune, T. (2009). Excitatory GABAergic activation of cortical dividing glial cells. *Cerebral Cortex*, 19(9):2181–95.

Tang, X., Taniguchi, K., and Kofuji, P. (2009). Heterogeneity of Kir4.1 channel expression in glia revealed by mouse transgenesis. *Glia*, 57(16):1706–15.

The Petilla Interneuron Nomenclature Group (2008). Petilla terminology: nomenclature of features of GABAergic interneurons of the cerebral cortex. *Nature Reviews. Neuroscience*, 9(7):557–568.

Thomson, A. M., Bannister, A. P., Hughes, D. I., and Pawelzik, H. (2000). Differential sensitivity to Zolpidem of IPSPs activated by morphologically identified CA1 interneurons in slices of rat hippocampus. *European Journal of Neuroscience*, 12(2):425–436.

Toledo-Rodriguez, M., Blumenfeld, B., and Wu, C. (2004). Correlation Maps Allow Neuronal Electrical Properties to be Predicted from Single-cell Gene Expression Profiles in Rat Neocortex. *Cerebral Cortex*, 14:1310–1327.

Tong, X.-p., Li, X.-y., Zhou, B., Shen, W., Zhang, Z.-j., Xu, T.-l., and Duan, S. (2009). Ca^{2+} signaling evoked by activation of Na^{+} channels and Na^{+}/Ca^{2+} exchangers is required for GABA-induced NG2 cell migration. *The Journal of Cell Biology*, 186(1):113–28.

Trapp, B. D., Nishiyama, A., Cheng, D., and Macklin, W. (1997). Differentiation and Death of Premyelinating Oligodendrocytes in Developing Rodent Brain. *The Journal of Cell Biology*, 137(2):459–468.

Trigo, F. F., Corrie, J. E. T., and Ogden, D. (2009). Laser photolysis of caged compounds at 405 nm: photochemical advantages, localisation, phototoxicity and methods for calibration. *Journal of Neuroscience Methods*, 180(1):9–21.

Tripathi, R. B., Rivers, L. E., Young, K. M., Jamen, F., and Richardson, W. D. (2010). NG2 glia generate new oligodendrocytes but few astrocytes in a murine experimental autoimmune encephalomyelitis model of demyelinating disease. *The Journal of Neuroscience*, 30(48):16383–90.

Trotter, J., Karram, K., and Nishiyama, A. (2010). NG2 cells : Properties , progeny and origin Cell lineage. *Brain Research Reviews*, 63(1-2):72–82.

Vélez-Fort, M., Audinat, E., and Angulo, M. C. (2009). Functional α7-containing nicotinic receptors of NG2-expressing cells in the hippocampus. *Glia*, 57(10):1104–1114.

Vélez-Fort, M., Maldonado, P. P., Butt, A. M., Audinat, E., and Angulo, M. C. (2010). Postnatal switch from synaptic to extrasynaptic transmission between interneurons and NG2 cells. *The Journal of Neuroscience*, 30(20):6921–9.

Verkhratsky, A. and Steinhäuser, C. (2000). Ion channels in glial cells. *Brain Research Reviews*, 32(2–3):380–412.

Viganò, F., Möbius, W., Götz, M., and Dimou, L. (2013). Transplantation reveals regional differences in oligodendrocyte differentiation in the adult brain. *Nature Neuroscience*, 16(10):1370–2.

Volterra, A. and Meldolesi, J. (2005). Astrocytes, from brain glue to communication elements: the revolution continues. *Nature Reviews. Neuroscience*, 6(8):626–640.

Wake, H., Lee, P. R., and Fields, R. D. (2011). Control of local protein synthesis and initial events in myelination by action potentials. *Science*, 333(6049):1647–51.

Watanabe, M., Toyama, Y., and Nishiyama, A. (2002). Differentiation of proliferated NG2-positive glial progenitor cells in a remyelinating lesion. *Journal of Neuroscience Research*, 69(6):826–36.

Wieboldt, R., Gee, K. R., Niu, L., Ramesh, D., Carpenter, B. K., and Hess, G. P. (1994). Photolabile precursors of glutamate: synthesis, photochemical properties, and activation of glutamate receptors on a microsecond time scale. *Proceedings of the National Academy of Sciences of the United States of America*, 91(19):8752–6.

Wigley, R. and Butt, A. M. (2009). Integration of NG2-glia (synantocytes) into the neuroglial network. *Neuron Glia Biology*, 5(1-2):21–8.

Wilson, S. S., Baetge, E. E., and Stallcup, W. B. (1981). Antisera specific for cell lines with mixed neuronal and glial properties. *Developmental Biology*, 83(1):146–53.

Woolsey, T. A. and Van der Loos, H. (1970). The structural organization of layer iv in the somatosensory region (si) of mouse cerebral cortex.the description of a cortical field composed of discrete cytoarchitectonic units. *Brain Research*, 17:205–242.

Xie, M., Lynch, D. T., Schools, G. P., Feustel, P. J., Kimelberg, H. K., and Zhou, M. (2007). Sodium channel currents in rat hippocampal NG2 glia: characterization and contribution to resting membrane potential. *Neuroscience*, 150(4):853–62.

Yang, S., Papagiakoumou, E., Guillon, M., de Sars, V., Tang, C.-M., and Emiliani, V. (2011). Three-dimensional holographic photostimulation of the dendritic arbor. *Journal of neural engineering*, 8(4):046002.

Yoshimura, Y., Dantzker, J., and Callaway, E. (2005). Excitatory cortical neurons form fine-scale functional networks. *Nature*, 433:868–873.

Young, K. M., Psachoulia, K., Tripathi, R. B., Dunn, S.-J., Cossell, L., Attwell, D., Tohyama, K., and Richardson, W. D. (2013). Oligodendrocyte dynamics in the healthy adult CNS: evidence for myelin remodeling. *Neuron*, 77(5):873–85.

Yuan, X., Eisen, a. M., McBain, C. J., and Gallo, V. (1998). A role for glutamate and its receptors in the regulation of oligodendrocyte development in cerebellar tissue slices. *Development*, 125(15):2901–14.

Yuste, R., editor (2011). *Imaging: A laboratory manual*. Cold Spring Harbor Laboratory Press.

Zalc, B. and Fields, R. D. (2000). Do Action Potentials Regulate Myelination? *Neuroscientist*, 6(1):5–13.

Zhao, S., Ting, J. T., Atallah, H. E., Qiu, L., Tan, J., Gloss, B., Augustine, G. J., Deisseroth, K., Luo, M., Graybiel, A. M., and Feng, G. (2011). Cell typespecific channelrhodopsin-2 transgenic mice for optogenetic dissection of neural circuitry function. *Nature Methods*, 8(9):745–752.

Zhou, M., Xu, G., Xie, M., Zhang, X., Schools, G. P., Ma, L., Kimelberg, H. K., and Chen, H. (2009). TWIK-1 and TREK-1 Are Potassium Channels Contributing Significantly to Astrocyte Passive Conductance in Rat Hippocampal Slices. *The Journal of Neuroscience*, 29(26):8551–8564.

Zhu, X., Bergles, D. E., and Nishiyama, A. (2008a). NG2 cells generate both oligodendrocytes and gray matter astrocytes. *Development*, 135:145–157.

Zhu, X., Hill, R. a., Dietrich, D., Komitova, M., Suzuki, R., and Nishiyama, A. (2011). Age-dependent fate and lineage restriction of single NG2 cells. *Development*, 138(4):745–53.

Zhu, X., Hill, R. A., and Nishiyama, A. (2008b). NG2 cells generate oligodendrocytes and gray matter astrocytes in the spinal cord. *Neuron Glia Biology*, 4(1):19–26.

Ziskin, J. L., Nishiyama, A., Rubio, M., Fukaya, M., and Bergles, D. E. (2007). Vesicular release of glutamate from unmyelinated axons in white matter. *Nature Neuroscience*, 10(3):321–30.

Zonouzi, M., Renzi, M., Farrant, M., and Cull-Candy, S. G. (2011). Bidirectional plasticity of calcium-permeable AMPA receptors in oligodendrocyte lineage cells. *Nature Neuroscience*, 14(11):1430–8.

Annex

Cellular/Molecular

Postnatal Switch from Synaptic to Extrasynaptic Transmission between Interneurons and NG2 Cells

Mateo Vélez-Fort,[1,2,3] Paloma P. Maldonado,[1,2,3] Arthur M. Butt,[4] Etienne Audinat,[1,2,3] and María Cecilia Angulo[1,2,3]

[1]Institut National de la Santé et de la Recherche Médicale Unité 603, [2]Centre National de la Recherche Scientifique Unité Mixte de Recherche 8154, [3]Université Paris Descartes, 75006 Paris, France, and [4]Institute for Biomedical and Biomolecular Sciences, School of Pharmacy and Biomedical Sciences, University of Portsmouth, Portsmouth 2O1 UP, United Kingdom

NG2 cells, oligodendrocyte precursors, play a critical role in myelination during postnatal brain maturation, but a pool of these precursors is maintained in the adult and recruited to lesions in demyelinating diseases. NG2 cells in immature animals have recently been shown to receive synaptic inputs from neurons, and these have been assumed to persist in the adult. Here, we investigated the GABAergic synaptic activity of NG2 cells in acute slices of the barrel cortex of NG2-DsRed transgenic mice during the first postnatal month, which corresponds to the period of active myelination in the neocortex. Our data demonstrated that the frequency of spontaneous and miniature GABAergic synaptic activity of cortical NG2 cells dramatically decreases after the second postnatal week, indicating a decrease in the number of synaptic inputs onto NG2 cells during development. However, NG2 cells still receive GABAergic inputs from interneurons in the adult cortex. These inputs do not rely on the presence of functional synapses but involve a form of GABA spillover. This GABA volume transmission allows interneurons to induce phasic responses in target NG2 cells through the activation of extrasynaptic $GABA_A$ receptors. Hence, after development is complete, volume transmission allows NG2 cells to integrate neuronal activity patterns at frequencies occurring during *in vivo* sensory stimulation.

Introduction

Oligodendrocyte precursors expressing the proteoglycan NG2 (NG2 cells) constitute a main type of glial cell in the postnatal (PN) brain (Nishiyama et al., 2009). These cells represent an important endogenous pool of progenitors for oligodendrocytes in the adult, although they are also regarded as multipotent cells endowed with the ability to generate presumably astrocytes and neurons (Guo et al., 2009; Nishiyama et al., 2009). In pathological conditions, NG2 cells serve as a major source of remyelinating oligodendrocytes in demyelinated lesions (Chang et al., 2000). Anatomical and physiological data support the idea that CNS myelination is dependent on neuronal activity (Zalc and Fields, 2000). Reports have demonstrated the existence of glutamatergic and GABAergic synapses formed between neurons and NG2 cells (Bergles et al., 2000; Lin and Bergles, 2004). Synaptic transmission of NG2 cells is an attractive candidate for controlling proliferation and differentiation of these cells in an activity-dependent manner and thus for influencing CNS myelination, although direct evidence is lacking. Indeed, proliferating NG2 cells keep their synapses and transfer them to their progeny during cell division (Kukley et al., 2008; Ge et al., 2009). In addition, there is an increasing axonal glutamatergic "synaptic-like" activity in NG2 cells of the corpus callosum that evolves in parallel with the maturation of the white matter tract (Ziskin et al., 2007). In the hippocampus, glutamatergic synaptic activity also increases during the first three postnatal weeks (Mangin et al., 2008). However, although GABAergic synapses have been reported in NG2 cells (Lin and Bergles, 2004; Jabs et al., 2005; Karadottir et al., 2008; Tanaka et al., 2009), GABAergic transmission during postnatal development has not been studied to date. Yet, GABA is one of the most predominant neurotransmitters during brain development and controls cell cycle kinetics of neocortical precursor cells by acting on $GABA_A$ receptors (LoTurco et al., 1995; Nguyen et al., 2001).

Here we examined the synaptic properties of NG2 cells in the barrel cortex during the first postnatal month, i.e., the period of active myelination in the neocortex (Bjelke and Seiger, 1989; Salami et al., 2003). We found that synaptic activity of cortical NG2 cells is predominantly GABAergic in the second PN week and dramatically decreases thereafter. However, the developmental loss of direct GABAergic synaptic transmission of cortical NG2 cells is replaced by an extrasynaptic mode of communication mediating phasic responses in which $GABA_A$ receptors are activated by pure GABA spillover. This mode of spillover or volume transmission mediates sustained GABAergic responses in NG2 cells during repetitive neuronal stimulation in the range of gamma oscillations that occur naturally *in vivo*, suggesting that interneurons signal to NG2 cells during sensory processing.

Received Jan. 14, 2010; revised March 19, 2010; accepted April 3, 2010.

This work was supported by young investigator grants from Agence Nationale de la Recherche and Fédération pour la Recherche sur le Cerveau. M.V.-F. was supported by fellowships from Région Ile-de-France and Ligue Française contre la Sclérose en Plaques (LFSEP). A.M.B. was supported by the Biotech and Biological Sciences Research Council. We thank Boris Barbour and Serge Charpak for helpful discussions and comments on the manuscript. We also thank Dwight E. Bergles for the gift of NG2-DsRed transgenic mice.

Correspondence should be addressed to María Cecilia Angulo, Laboratoire de Neurophysiologie et Nouvelles Microscopies, Institut National de la Santé et de la Recherche Médicale, Unité 603, Centre National de la Recherche Scientifique, Unité Mixte de Recherche 8154, Université Paris Descartes, 45 Rue des Saints-Pères, 75006 Paris, France. E-mail: maria-cecilia.angulo@parisdescartes.fr.

DOI:10.1523/JNEUROSCI.0238-10.2010

 0270-6474/10/306921-09$15.00/0

Materials and Methods

Slice preparation. All experiments followed European Union and institutional guidelines for the care and use of laboratory animals. Acute parasagittal slices (300 μm) of the barrel cortex with an angle of 10° to the sagittal plane were obtained from NG2-DsRed BAC transgenic mice (Ziskin et al., 2007) at postnatal day 3 (PN3) to PN28. Slices were prepared in an ice-cold solution containing the following (in mM): 215 sucrose, 2.5 KCl, 1.25 NaH_2PO_4, 26 $NaHCO_3$, 20 glucose, 5 pyruvate, 1 $CaCl_2$, and 7 $MgCl_2$ (95% O_2, 5% CO_2); the slices then were incubated for 20 min at 33°C in a solution containing 126 mM NaCl instead of sucrose and 1 mM $MgCl_2$ and 2 mM $CaCl_2$. Finally, the slices were transferred to a recording chamber perfused with the same solution at 2–3 ml/min and at 30–32°C.

Electrophysiology. NG2 cells were identified by detecting DsRed fluorescence using 560 nm excitation and 620 nm emission wavelengths and visualized using IR-DIC video microscopy. Excitation and emission wavelengths for DsRed were obtained by using 560 and 620 nm filters, respectively. Patch pipettes were filled with an intracellular solution containing the following (in mM): 130 CsCl, 10 4-AP, 5 tetraethylammonium chloride (TEA-Cl), 5 EGTA, 0.5 $CaCl_2$, 2 $MgCl_2$, 10 HEPES, 2 Na_2ATP, 0.2 Na-GTP, 10 Na_2-phosphocreatine, pH $\approx$ 7.3). In some experiments, 1 mM extracellular Ba^{2+} was added in the perfusate to increase the membrane resistance of recorded cells (Velez-Fort et al., 2009). Recordings were made without series resistance (R_s) compensation [$R_s = 10.1 \pm 0.6$ MΩ ($n = 25$) and $R_s = 11.6 \pm 0.9$ MΩ ($n = 22$) in the second and fourth PN weeks, respectively; $p > 0.05$]. Series resistances were monitored during recordings, and cells showing a change of >30% were discarded. Extracellular stimulations were obtained using a monopolar electrode placed in layer V of the barrel cortex in a position that evoked stable responses (100 μs; 2–40 V at a rate of 0.025–0.1 Hz; Iso-Stim 01D, NPI Electronic).

Analysis. Whole-cell recordings of NG2 cells were obtained using MultiClamp 700B (Molecular Devices), filtered at 2–4 kHz, and digitized at 10–20 kHz. Digitized data were analyzed off-line using pClamp 10.1 software (Molecular Devices). Spontaneous and miniature synaptic currents were recorded at a holding potential of −90 mV, detected with a detection threshold of 4 times SD, and rise times ($t_{10-90\%}$) <3 ms. For detection of spontaneous GABAergic slow currents, we analyzed cells recorded between 6 and 18 min. For extracellular stimulations, cells were recorded at a holding potential of −70 mV, and traces not showing evoked responses larger than 2 times the SD were considered as failures. It is noteworthy that we clamped the cells at −90 mV when studying spontaneous synaptic events to increase the driving force of synaptic currents and, thus, the chance of detecting spontaneous events. Instead, we used −70 mV to study evoked currents because these experiments required a longer recording time, sometimes 1 h, and cells were healthier at this potential. The paired-pulse ratio was estimated by averaging 20–75 sweeps; the current amplitude at the second pulse was estimated after subtracting the decay of the current elicited at the first pulse. The mean rise times of evoked currents were calculated by averaging the synaptic responses excluding failures. The voltage-jump technique was adapted from Szapiro and Barbour (2007). The averaged evoked currents at each potential and at the jump was estimated by averaging 14–50 sweeps. The frequency of evoked miniature events obtained by replacing Ca^{2+} by Sr^{2+} was calculated during 3 s after stimulation. No or very few events were observed before the stimulation in Sr^{2+}. In experiments with NNC711 (10 μM), currents elicited by trains of stimuli (10 pulses at 100 Hz) were low-pass filtered at 100 Hz to eliminate the stimulation artifacts. Then, the charge of the averaged traces in control conditions and in NNC711 was measured over 500 ms from the current onset.

Morphology. Recorded NG2 cells were injected for 15–20 min with 5.4 mM biocytin contained in the intracellular solution. Slices were then fixed overnight in 4% paraformaldehyde at 4°C and biocytin was revealed with Alexa-488-conjugated streptavidin for 4 h at room temperature. Images were acquired on a LSM 510 metaconfocal microscope (Zeiss) using a ×40 oil-immersion lens with high numerical aperture (1.3). Fluorescence was visualized at 488 nm (green) using an argon laser. A pinhole of one airy unit or less was used, with an average of four scans per image, and the number of *z*-sections and resolution were optimized using the Zeiss acquisition software. Image visualization and analysis was performed using Volocity4 software (Improvision, PerkinElmer). Reiterative restoration (deconvolution) was performed to reduce background and improve the signal:noise ratio. Measurements of cell volume were made of voxels in three dimensions using Volocity4.

Calcium imaging. Slices of the barrel cortex were loaded with the cell-permeant Ca^{2+} indicator Oregon Green BAPTA-1AM (11 μM) for 1 h at 33°C. Changes in intracellular Ca^{2+} concentrations upon muscimol (50 μM) applications in the presence of a mixture of antagonists were assessed using an Olympus BX51 microscope equipped with 40× fluorescent water-immersion objective. Excitation light was provided by an OptoLED light source (Blue OptoLED; Cairn Research), and images were collected with an iXon cooled (−80°C) 14-bit digital camera (Andor Technology). Excitation and emission wavelengths were obtained by using 470 and 525 nm filters, respectively. The Imaging Workbench 6.0 software (Indec Biosystems) was used to acquire and store images for off-line analysis. Exposure times were 20–50 ms and images were collected at 2–4 Hz. The background fluorescence was subtracted, and Ca^{2+} responses were expressed as relative changes in fluorescence ($\Delta F/F$).

Statistics. Data are expressed as mean ± SEM. The nonparametric Mann–Whitney *U* test for independent samples was used to determine statistical differences between data obtained in the second and fourth postnatal weeks. When comparisons within single cells were required, the Wilcoxon signed-rank test for related samples was used (GraphPad InStat software, version 3.06). The correlation between cell membrane resistance and synaptic current frequency was tested with the Pearson *r* test. Cumulative distributions of rise times were compared using the Kolmogorov–Smirnov test.

Results

Spontaneous GABAergic synaptic activity of cortical NG2 cells decreases during postnatal development

Whole-cell recordings of $DsRed^+$ NG2 cells were performed with a CsCl-based intracellular solution containing 4-AP and TEA-Cl in layer V of the barrel cortex of NG2-DsRed transgenic mice (Ziskin et al., 2007) during the first postnatal month. As shown in Figure 1, *a* and *b*, spontaneous inward synaptic currents, recognized by their fast rise time, were detected after PN3 in NG2 cells held at −90 mV (see Materials and Methods). The frequency of these synaptic currents, however, dramatically decreased after the second PN week (Fig. 1*a–c*). The NG2 cell membrane resistance also decreased during development [from 638.8 ± 121.2 MΩ ($n = 25$) to 137.8 ± 42.5 MΩ ($n = 22$) in the second and fourth PN weeks, respectively; $p < 0.001$]. Although the membrane resistance remained relatively high in our recording conditions, the apparent reduction in synaptic activity might be caused by a decrease of the membrane space constant and thus by a filtering of postsynaptic currents at later developmental stages. However, no correlation was observed between synaptic current frequency and membrane resistance of cortical NG2 cells (Fig. 1*d*). Additionally, no significant developmental changes in morphology were observed between the second and fourth PN weeks (supplemental Fig. 1, available at www.jneurosci.org as supplemental material) ($p > 0.05$).

NG2 cells receive direct glutamatergic and GABAergic synaptic inputs from neurons in the hippocampus (Bergles et al., 2000; Lin and Bergles, 2004; Jabs et al., 2005), and thus pharmacological experiments were performed to discriminate synaptic currents mediated by glutamate and GABA in the barrel cortex. The $GABA_A$ receptor antagonist SR95531 (5 μM) blocked >90% of spontaneous synaptic activity in the second postnatal week, indicating that most of this activity was GABAergic early in postnatal life (Fig. 1*e*). At the later developmental stage, SR95531 did not change significantly the frequency of the few remaining fast spon-

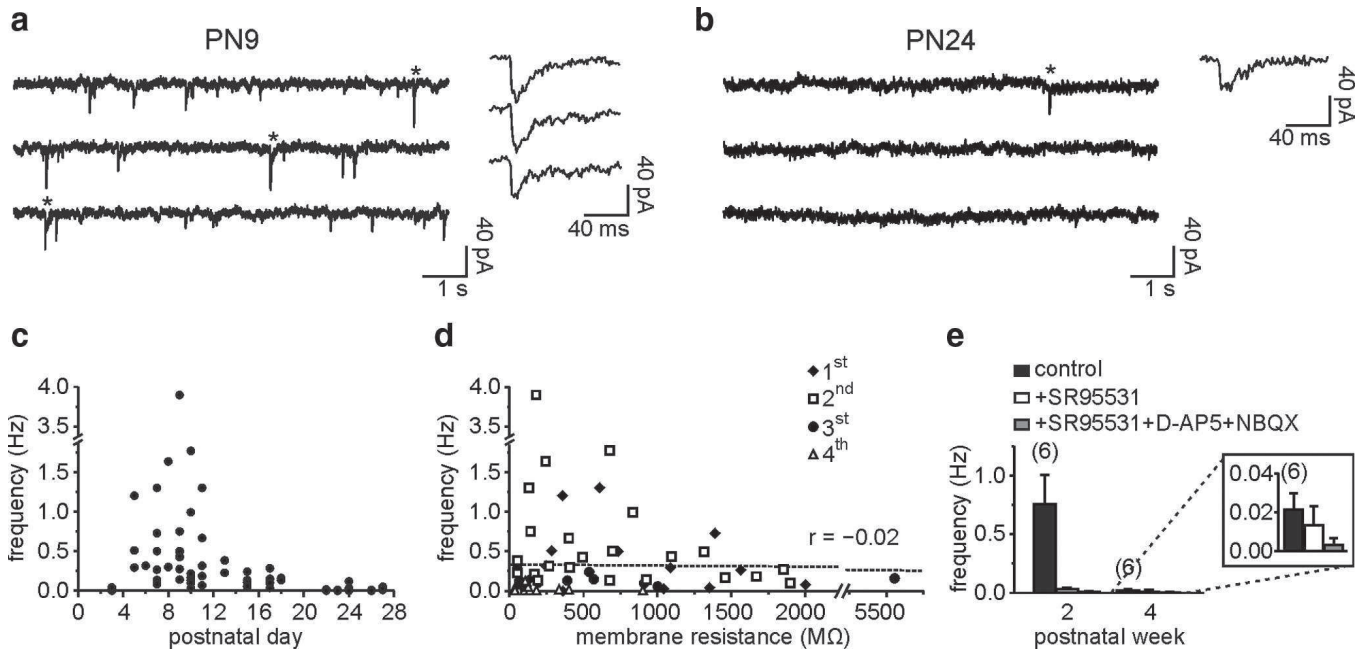

Figure 1. Decrease of spontaneous synaptic activity of NG2 cells during postnatal development. ***a*** and ***b***, Spontaneous synaptic currents of two NG2 cells held at −90 mV at PN9 (***a***) and PN24 (***b***). Note the fast rise times of individual currents at both ages (<2.1 ms). ***c***, Plot of spontaneous synaptic current frequency against PN day. ***d***, Plot of synaptic current frequency against cell membrane resistance. There was not a significant correlation between these two parameters ($r = -0.02$; $p > 0.05$). Each cell is marked with a different symbol according to its PN week. ***e***, Histogram of spontaneous synaptic current frequency in control, after bath application of 5 μM SR95531, and after a further addition of 50 μM D-AP-5 and 10 μM NBQX for the second and fourth PN weeks. Note the absence of block by 5 μM SR95531 in the fourth PN week (inset).

taneous events (Fig. 1*e*, inset); the large decrease of this spontaneous activity is thus probably caused by a loss of GABAergic synaptic currents during development. Consistent with data already reported in the neocortex (Chittajallu et al., 2004), the estimated frequency of glutamatergic synaptic currents was very low during the first postnatal month (<0.033 Hz) (Fig. 1*e*).

To test whether the decrease in GABAergic synaptic activity of cortical NG2 cells during development was accompanied by a loss of $GABA_A$ receptors, we applied in the bath a saturating concentration of the $GABA_A$ receptor agonist muscimol (50 μM) in the presence of a mixture of antagonists for other ionotropic and metabotropic receptors (supplemental Fig. 2*a*, available at www.jneurosci.org as supplemental material). Similar current densities were observed in the presence of this agonist in the second and fourth PN weeks (supplemental Fig. 2b, available at www.jneurosci.org as supplemental material) ($p > 0.05$). The activation of $GABA_A$ receptors has been reported to produce a depolarizing effect on NG2 cells during different PN stages that increases intracellular Ca^{2+} concentration (Lin and Bergles, 2004; Tanaka et al., 2009; Tong et al., 2009). Calcium imaging experiments in slices loaded with the Ca^{2+} indicator Oregon Green BAPTA-1AM showed that muscimol, but not extracellular stimulation, induced Ca^{2+} signals at both developmental periods (supplemental Fig. 2*c–e*, available at www.jneurosci.org as supplemental material). The results demonstrate that NG2 cells still express functional $GABA_A$ receptors at the end of the first PN month.

Finally, we analyzed the frequency of miniature GABAergic synaptic currents of NG2 cells in the presence of the Na^+ channel blocker tetrodotoxin (TTX), the AMPA/kainate antagonist 2,3-dioxo-6-nitro-1,2,3,4-tetrahydro-benzo[f]quinoxline-7-sulfonamide (NBQX), and the NMDA antagonist D-AP-5. Miniature synaptic events were detected in the second PN week (0.027 ± 0.005 Hz; $n = 4$). Averaged miniature GABAergic synaptic currents had a peak amplitude of −12.8 ± 3.3 pA, a rise time ($t_{10-90\%}$) of 1.0 ± 0.1 ms, and a decay time fitted with a single exponential function of 15.3 ± 2.9 ms. In contrast, only one miniature current was observed in four cells of the fourth PN week. Together, these results showed a strong reduction of GABAergic synaptic activity after the second PN week.

Properties of evoked GABAergic currents in NG2 cells change during postnatal development

The presence of functional $GABA_A$ receptors and the dramatic decrease of spontaneous GABAergic synaptic activity during development prompted us to study the mechanisms of activation of these receptors by evoked neuronal activity in the second and fourth PN weeks. Low-frequency stimulations (0.025–0.1 Hz) were applied with an extracellular electrode placed in layer V of cortical slices, while NG2 cells were recorded in voltage clamp at −70 mV in the presence of NBQX and D-AP-5 to block glutamatergic activity. Similar extracellular stimulations in neurons induced current densities 9.3 ± 2.4 larger than those in NG2 cells ($n = 10$; comparison between the second and fourth PN weeks in supplemental Fig. 3, available at www.jneurosci.org as supplemental material). $GABA_A$ receptor-mediated currents, sensitive to SR95531 and reversing near 0 mV, were easily elicited at both postnatal periods (Fig. 2*a*,*b*). However, the properties of the evoked currents were different between the second and fourth PN weeks. Although a paired-pulse depression was observed at both developmental stages, stimulation elicited currents in NG2 cells of older mice with fewer failures of transmission and less current amplitude variability, as quantified by the coefficient of variation (supplemental Table 1, available at www.jneurosci.org as supplemental material). Moreover, evoked GABAergic currents had unusually very slow rise times at later stages (Fig. 2*c*) [$t_{10-90\%}$ = 1.5 ± 0.1 ms ($n = 28$) and $t_{10-90\%}$ = 7.2 ± 1.1 ms ($n = 18$) in the second and fourth PN weeks, respectively; $p < 0.001$]. Similar

slow transient $GABA_A$ receptor currents occurred spontaneously in cells of the fourth PN week, i.e., in the absence of electrical stimulation (Fig. 2*d*). In six of twelve NG2 cells recorded in the presence of NBQX and D-AP-5, we detected spontaneous slow rising currents that had a mean rise time of 5.1 ± 0.7 ms, a peak amplitude of 18.1 ± 5 pA, and a decay time of 18.8 ± 2.5 ms (Fig. 2*d*). The frequency of these slow transient events was, however, very low (0.005 ± 0.003 Hz); only one slow transient current was observed in the presence of SR95531 (5 μM; $n = 5$; duration of the recordings: from 6 to 18 min).

The observed prolonged responses could result from considerable distortion and attenuation of signals occurring as a consequence of an inadequate space clamp (Pearce, 1993; Szapiro and Barbour, 2007). The slow kinetics of evoked responses during development may thus be a consequence of the displacement of synaptic contacts to distant electrotonic sites during development. First, we tested whether the rise times of the responses were accelerated by increasing the membrane resistance in older mice with 1 mM extracellular Ba^{2+} in the perfusate [137.8 ± 42.5 MΩ in control ($n = 22$) vs 938.2 ± 166.2 MΩ in presence of Ba^{2+} ($n = 15$)] (Velez-Fort et al., 2009). Even in conditions with high membrane resistances, evoked currents at the fourth PN week maintained slow rise times, similar to those recorded without Ba^{2+} [$t_{10-90\%} = 9.5 \pm 1.8$ ms in Ba^{2+} ($n = 15$); $p > 0.05$]. It is also noteworthy that evoked currents obtained in this optimal clamp condition showed slower weighted decay times than those recorded in similar clamp conditions in younger mice [$\tau = 52.3 \pm 12.0$ ms in Ba^{2+} in the fourth PN week mice ($n = 13$) vs $\tau = 32.2 \pm 1.9$ ms without Ba^{2+} in the second PN week mice ($n = 20$); $p < 0.05$]. Second, we used the voltage-jump technique to examine whether slow evoked currents in older mice were caused by a genuinely long-lasting conductance or a brief conductance subjected to considerable filtering (Pearce, 1993; Szapiro and Barbour, 2007). As shown in Figure 3, *a* and *b*, the voltage jump method consisted of applying a voltage step of −30 mV during the evoked responses of cells held at −40 mV to increase the driving force (see Materials and Methods). The averaged current obtained after subtracting the capacity transients was then compared with those elicited at constant holding potentials of −40 and −70 mV (Fig. 3*a*,*b*). The voltage jump rapidly changed the evoked currents, indicating that little distortion of the time course occurred and, therefore, that the GABAergic conductance was still active at the time of the step (Fig. 3*b*). The time required by the current (10–90%) during the voltage jump to reach the response at a steady-state holding potential of −70 mV (t_{jump}) was 1.2 ± 0.4 ms, always inferior to the rise time ($t_{10-90\%}$) of evoked currents (Fig. 3*c*). Hence, the slow rise times of evoked GABAergic responses in the fourth PN week were genuine and did not result from a strong filtering.

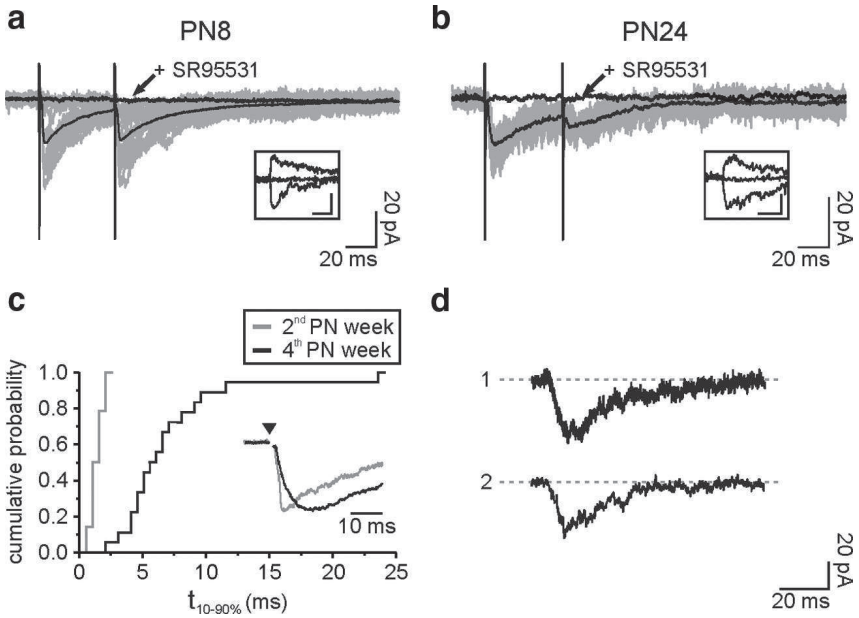

Figure 2. Evoked and spontaneous slow rising GABAergic currents for NG2 cells in the fourth PN week. ***a*** and ***b***, Paired-pulse stimulation of neuronal fibers elicited inward currents in two NG2 cells held at −70 mV at PN8 (***a***) and PN24 (***b***), in the presence of 10 μM NBQX and 50 μM D-AP-5. Individual sweeps (gray) and averaged currents (black) are shown. Note the lack of failures of transmission in ***b***. Evoked currents were sensitive to SR95531 (arrows) and reversed near 0 mV at both developmental stages (insets: single traces at −70 mV, 0 mV, and +35 mV; scale bars: 20 pA; 20 ms). ***c***, Different cumulative probabilities of rise times for cells in the second (gray) and fourth (black) PN weeks ($p < 0.001$). The inset shows superimposed normalized averaged currents of two NG2 cells held at −70 mV at PN24 (black) and PN11 (gray) obtained with a single pulse stimulation in the presence of 10 μM NBQX and 50 μM D-AP-5. Stimulus artifacts were blanked for visibility; the time of stimulation is indicated with an arrowhead. ***d***, Spontaneous slow rising currents of two NG2 cells held at −90 mV at PN21 (1) and PN22 (2) in the presence of 10 μM NBQX and 50 μM D-AP-5.

GABAergic miniature currents are detectable for NG2 cells in the second but not in the fourth PN week

To test whether evoked currents come from GABA release at interneuron-NG2 cell synaptic contacts at both stages of development, we used Sr^{2+} to desynchronize vesicular release and isolate GABAergic miniature currents (Goda and Stevens, 1994). When replacing extracellular Ca^{2+} with 5 mM Sr^{2+}, a large decrease in the amplitude of evoked responses was observed, indicating that evoked currents resulted from the exocytotic release of GABA in the second and fourth PN weeks [82 ± 10% ($n = 6$) and 80 ± 9% ($n = 7$) of reduction, respectively] (Fig. 4*a*,*b*). As expected for a synapse, asynchronous miniature events were apparent in all NG2 cells recorded in the second PN week ($n = 6$) (Fig. 4*c*,*e*). Evoked miniature currents had a rise time of 1.4 ± 0.4 ms, a peak amplitude of −15.7 ± 1.3 pA, and a decay time described with a single exponential of 14.7 ± 4.2 ms, similar to those reported above for spontaneous miniature events (Fig. 4*e*, inset) ($p > 0.05$). However, a different behavior was observed in older mice, where almost no miniature events were observed (Fig. 4*d*,*e*) ($p < 0.01$).

To strengthen our observation showing that GABAergic miniature currents did not persist in the fourth PN week, we performed experiments in the presence of the potent secretagogue ruthenium red and of TTX, D-AP-5, and NBQX. As described for miniature GABAergic currents in NG2 cells of the hippocampus (Lin and Bergles, 2004), ruthenium red largely increased the postsynaptic current frequency in the second PN week. However, miniature events remained almost undetectable in the fourth PN week (Fig. 4*f*) ($p < 0.01$). The presence of extracellular Ba^{2+} in the perfusate, which increased the membrane resistance of recorded cells (Velez-Fort et al., 2009), did not further increase the

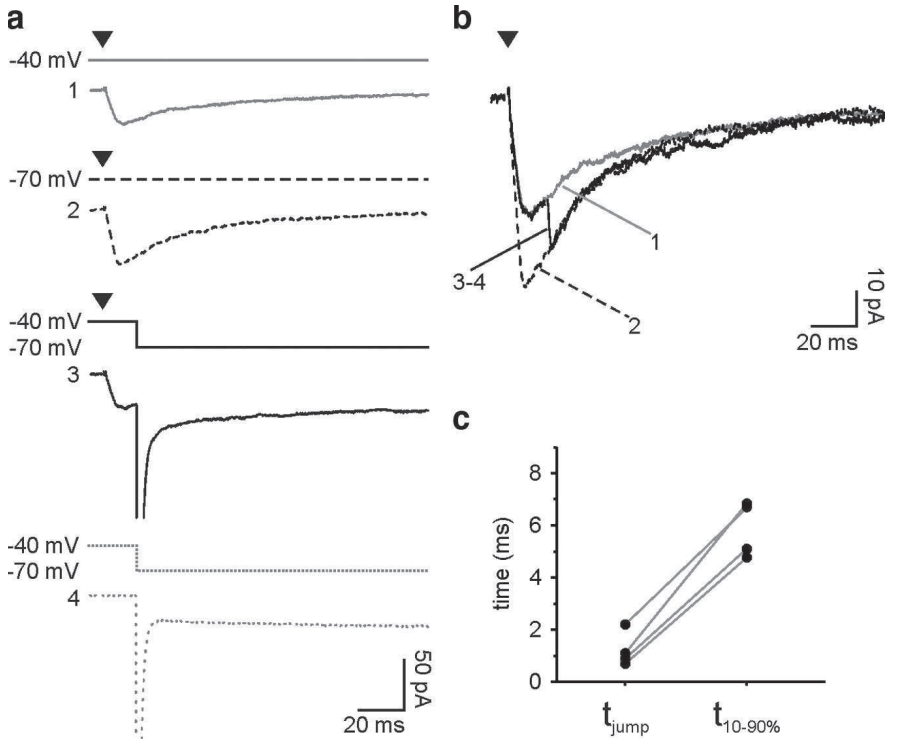

Figure 3. Slow kinetics of evoked GABAergic currents are not due to filtering. ***a***, Voltage jump protocol to test the speed of clamp of the synaptic conductance. Averaged currents evoked by extrasynaptic stimulation at a holding potential of −40 mV (solid gray) or −70 mV (dashed black) during voltage jumps from −40 mV to −70 mV (solid black) and averaged capacity transients recorded with a pulse of −30 mV from −40 mV (dashed gray). These experiments were done in the presence of 1 mM Ba^{2+}, 10 μM NBQX and 50 μM D-AP-5. ***b***, Superposition of the same averaged currents at a holding potential of −40 mV (solid gray) or −70 mV (dashed black) and after subtracting the capacity transients during voltage jumps from −40 mV to −70 mV (solid black). Note that the GABAergic conductance is still active during the voltage jump. Stimulus artifacts were blanked for visibility; the time of stimulation is indicated with an arrowhead. ***c***, Plot comparing the time required by the current (10–90%) to reach the response at −70 mV during the voltage jump (t_{jump}) with the rise time ($t_{10-90\%}$) of averaged evoked currents at −70 mV in individual experiments.

apparent frequency of miniature events, demonstrating that in optimal space-clamp conditions miniature GABAergic synaptic currents are rarely observed in older mice (Fig. 4*f*). In conclusion, functional GABAergic synaptic contacts are lost during postnatal development of NG2 cells.

A switch from synaptic to extrasynaptic transmission between interneurons and NG2 cells during development

Whereas fast $GABA_A$ receptor-mediated currents elicited in NG2 cells by low-frequency stimulation had all the features of direct synaptic transmission in the second PN week, the prolonged rise times of evoked responses as well as the rare number of miniature events observed in the fourth postnatal week strongly suggest that $GABA_A$ receptors in older mice were activated exclusively at extrasynaptic sites. Recently, an unusual mechanism of pure spillover transmission that induce phasic responses in the absence of classical synaptic activity has been described for neuronal connections in the cerebellum (Szapiro and Barbour, 2007) and the neocortex (Olah et al., 2009). By using pharmacological agents, we tested whether this mode of neuronal communication also controls GABAergic transmission from interneurons to NG2 cells in the barrel cortex after the second PN week.

Responses due to spillover are more sensitive to uptake blockers than synaptic ones. In the case of inhibitors of GABA transporters, two major effects have been described: a significant prolongation of the decay of $GABA_A$ receptor-mediated currents upon low-frequency stimulation (Rossi and Hamann, 1998; Szabadics et al., 2007; Gonzalez-Burgos et al., 2009), and a large increase in current amplitudes upon high-frequency stimulation (Alle and Geiger, 2007; Gonzalez-Burgos et al., 2009). We thus analyzed the effect of the GAT-1 blocker NNC711 on $GABA_A$ receptor-mediated responses elicited by either a single pulse or a train of stimuli in the presence of the $GABA_B$ receptor antagonist CGP55845 (5 μm) to exclude any effects of $GABA_B$ receptor activation. We considered that the comparison between young and older animals was valid since, although the expression of GAT-1 transporters increases during PN development of the neocortex, the protein levels in rodents are already 85% of the adult at PN10 (Conti et al., 2004). The decay of evoked currents upon low-frequency stimulation was not changed in the second PN week (Fig. 5*a*,*c*), but became markedly prolonged in the fourth PN week (Fig. 5*b*,*c*) ($p < 0.05$). A 3.5-fold increase of the decay time constant was observed in NNC711 in older mice. Additionally, trains of stimuli (100 Hz) resulted in a response that was potentiated by NNC711 in the fourth but not in the second PN week (Fig. 5*d–f*) ($p < 0.05$). Evoked responses in older mice are thus probably caused by GABA spillover rather than from direct synaptic terminals on NG2 cells.

If slowly evoked currents reflect the activation of extrasynaptic receptors by GABA diffusing a significant distance, the concentration reaching these receptors would be expected to be lower than that in the synaptic cleft. Therefore, the degree of inhibition of evoked responses by a low-affinity antagonist of $GABA_A$ receptors should be greater in the fourth than in the second PN week. Figure 6, *a* and *b*, illustrates the effect of the low-affinity competitive $GABA_A$ receptor antagonist (1,2,5,6-tetrahydropyridin-4-yl)methylphosphinic acid (TPMPA) (Jones et al., 2001) on responses elicited by single-pulse stimulations. The effect of TPMPA on the amplitude of averaged currents was significantly greater in the fourth PN week [amplitude decrease 81 ± 7 ($n = 6$) vs 52 ± 11 ($n = 6$) in the second and fourth PN week, respectively; $p < 0.05$]. Assuming that the subunit composition of $GABA_A$ receptors is similar between the second and fourth week, these results suggest that lower GABA concentrations reached the receptors in older mice. In keeping with this assumption, the high affinity competitive antagonist SR95531 at low concentration (100 nM), which shows a slower unbinding time constant than TPMPA (Jones et al., 2001), decreased the evoked responses at both developmental stages similarly [amplitude decrease 59 ± 11% ($n = 5$) and 40 ± 6% ($n = 5$) at the second and fourth PN week, respectively; $p > 0.05$]. Finally, we took advantage of the effect of TPMPA to test whether the slow transient currents reflect merely a loss of direct synaptic activation with age, instead of the appearance of a new mode of signaling in older animals. If slow transient currents are present in young mice, the kinetics of evoked responses should be faster when blocking the slow component with TPMPA. We observed

that this is not the case, since the rise times were 1.7 ± 0.3 and 1.6 ± 0.3 ms in control and TPMPA conditions, respectively ($n = 6$; $p > 0.05$). Therefore, there is probably a loss of direct synaptic activation and the appearance of a new transmission mode with age.

Together, our results demonstrate that, in contrast to classical synaptic transmission observed in NG2 cells of the second PN week, GABA released upon extracellular stimulation diffused to and exclusively activated distant $GABA_A$ receptors of these cells in the fourth PN week.

Differential effect of gamma-frequency stimulation on synaptic and spillover mediated NG2 cell currents

Whisker activation in rodents elicits gamma neuronal network activity in the barrel cortex (Jones and Barth, 1997), even as early as the first PN week (Yang et al., 2009). We thus compared the evoked currents mediated by synaptic and spillover transmission during repetitive gamma frequency neuronal stimulation (50 Hz, 200 ms), a frequency pattern that is likely to be relevant in the somatosensory cortex *in vivo* (Ahissar and Vaadia, 1990; Jones and Barth, 1997). As expected for synaptic but not spillover transmission, individual signals within the train were more easily resolved for NG2 cells in the second PN week (Fig. 7*a*). Although a paired-pulse depression was observed at both developmental stages (Fig. 2*a*,*b*; supplemental Table 1, available at www.jneurosci.org as supplemental material), the longer duration of spillover-mediated currents in older mice led to a greater temporal summation of responses during a stimulus train (Fig. 7*b*). Thus, the ratio of the current reached at the end of the train (I_{sum}) over the initial current response (I_1) was almost two times larger in the fourth than in the second PN week [I_{sum}/I_1 of 1,2 ± 0,3 ($n = 6$) and 2,2 ± 0,4 ($n = 6$) in the second and fourth PN week, respectively; $p < 0.05$]. In conclusion, GABA spillover allows a more efficient temporal summation in mature NG2 cells during neuronal bursts.

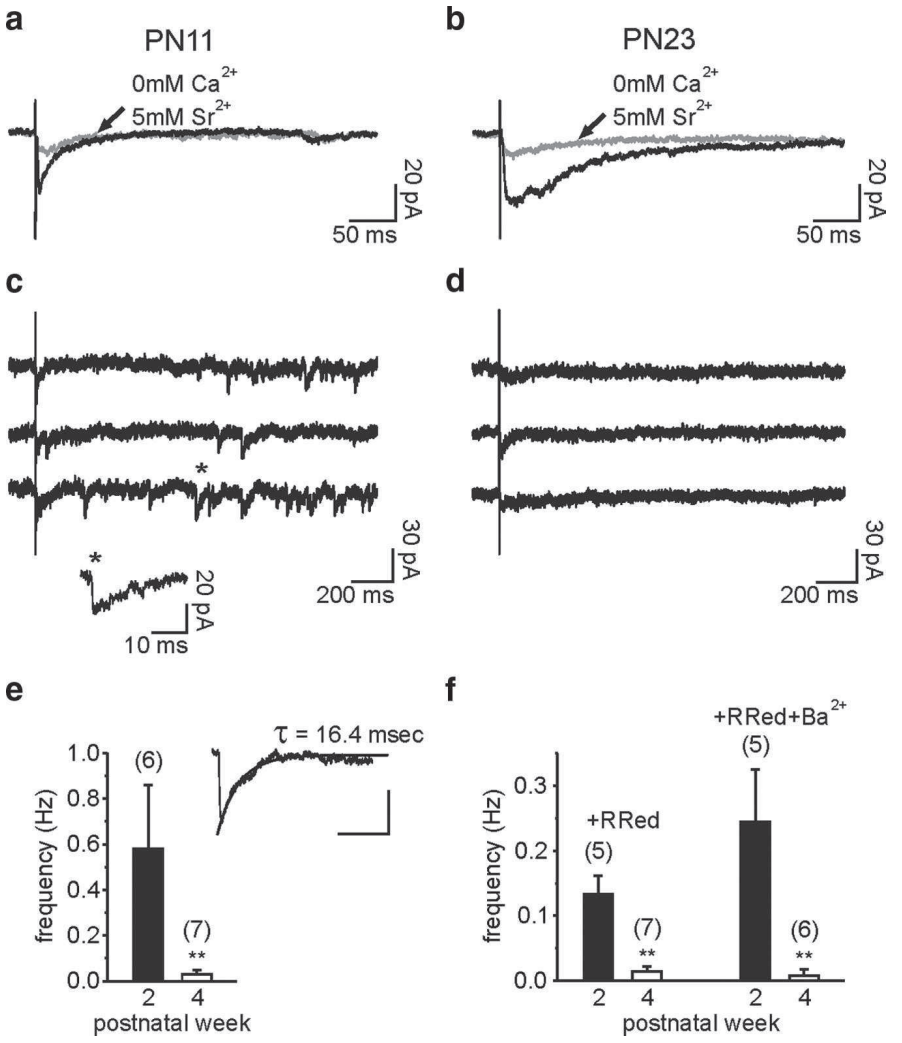

Figure 4. Miniature GABAergic synaptic currents of NG2 cells dramatically decrease during development. ***a*** and ***b***, Averaged traces of evoked currents of two NG2 cells held at −70 mV at PN11 (***a***) and PN23 (***b***) in control (black) and when 2 mM Ca^{2+} was replaced by 5 mM Sr^{2+} (gray). In these experiments, 10 μM NBQX and 50 μM D-AP-5 were added in the perfusate. Note that currents were strongly decreased in the presence of Sr^{2+} at both developmental stages. ***c*** and ***d***, Single traces of evoked currents of the same NG2 cells. Note the presence of miniature events with fast rise times at PN11 (***c***), but not at PN23 (***d***). ***e***, Histogram of the frequency of the evoked miniature events in Sr^{2+} for cells in the second and fourth PN weeks. The inset illustrates the average of 25 evoked miniature currents of a NG2 cell at PN11 fitted by a single exponential. Scale bars, 10 pA and 40 ms. ***f***, Histograms of the frequency of the miniature events in the presence of 75 μM ruthenium red (R Red) and 75 μM ruthenium red plus 1 mM Ba^{2+} for cells in the second and fourth PN weeks. In these experiments, 0.5 μM TTX, 10 μM NBQX, and 50 μM D-AP-5 were also added in the perfusate.

Discussion

We have reported here that the frequency of spontaneous and evoked miniature events in NG2 cells, which are predominantly GABAergic after the second postnatal week in the barrel cortex, dramatically decreases during development. However, this is not due to a developmental loss of functional $GABA_A$ receptors. Low-frequency extracellular stimulation revealed that $GABA_A$ receptor activation of NG2 cells at later developmental stages mediates transient responses with unusually slow kinetics. The absence of miniature events as well as the higher sensitivity of evoked responses to NNC711 and TPMPA in the fourth PN week with respect to the second PN week supports the notion that $GABA_A$ receptor-mediated responses in NG2 cells from older mice arise from an extrasynaptic mode of diffuse transmission mediated solely by GABA spillover from neuronal terminals.

The extrasynaptic signaling between interneurons and NG2 cells of the barrel cortex has specific characteristics that differ from those between other glial cell types, in particular astrocytes (Perea et al., 2009) and Bergmann glia (Matsui and Jahr, 2003), as follows: (1) spillover effect on NG2 cells is mediated by ionotropic $GABA_A$ receptors; (2) although slower than direct synaptic events, spontaneous and evoked transient currents in NG2 cells occurred with a time course of few milliseconds; and (3) diffuse transmission in NG2 cells emerges after a loss of synaptic transmission and thus probably results from a rearrangement of interneuron-NG2 cell junctions during cortical network maturation. Because of these unique properties, spillover transmission between interneurons and NG2 cells can be considered as a novel mode of neuron-glia communication.

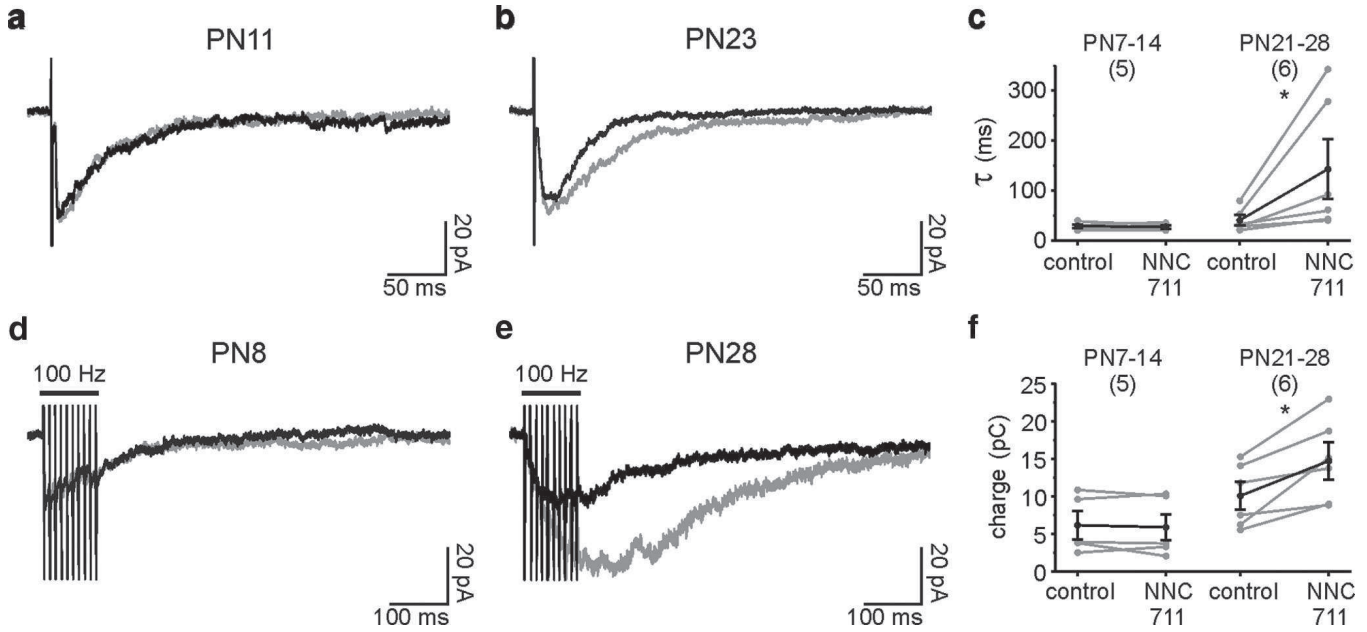

Figure 5. Interneuron-to-NG2 cell GABAergic transmission is sensitive to uptake blockers in the fourth PN week. ***a*** and ***b***, Averaged inward currents evoked by single stimuli in two NG2 cells held at −70 mV at PN11 (***a***) and PN23 (***b***) in control (black) and in the presence of 10 μM NNC711 (gray). In these experiments, 10 μM NBQX and 50 μM D-AP-5 were present in the perfusate. Note the increase in the decay time constant at PN23, but not at PN11. ***c***, Effect of 10 μM NNC711 on the decay time constant (τ) of individual experiments in the second and the fourth PN week. ***d*** and ***e***, Averaged inward currents evoked by trains of stimuli (10 pulses at 100 Hz) in two NG2 cells held at −70 mV at PN8 (***d***) and PN28 (***e***) in control (black) and in the presence of 10 μM NNC711 (gray). Note the large increase in the amplitude at PN28, but not at PN8. ***f***, Effect of 10 μM NNC711 on the charge integrated over 500 ms from the first stimulation in the second and the fourth postnatal weeks.

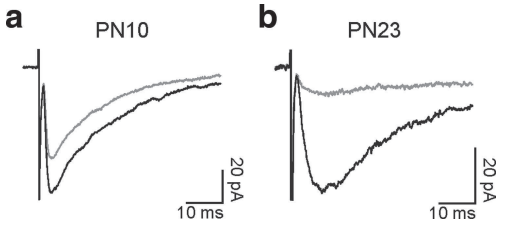

Figure 6. Effects of the low-affinity antagonist TPMPA on evoked $GABA_A$ receptor-mediated responses during development. ***a*** and ***b***, Average inward currents evoked by single stimuli in two NG2 cells held at −70 mV at PN10 (***a***) and PN23 (***b***) in control (black) and in the presence of 100 μM TPMPA (gray). In these experiments, 10 μM NBQX and 50 μM D-AP-5 were added in the perfusate. Note the stronger inhibition at PN23 with respect to PN10.

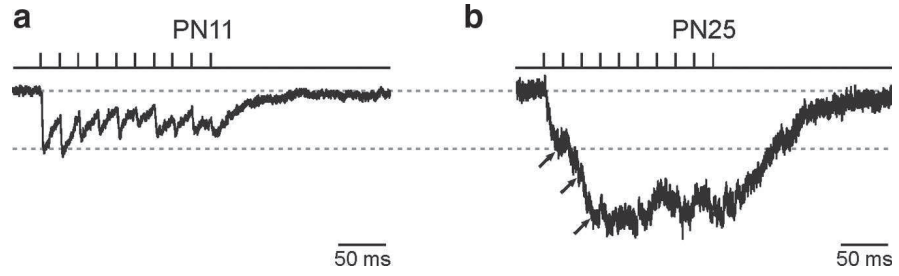

Figure 7. Effect of gamma frequency stimulation on evoked $GABA_A$ receptor-mediated currents during development. ***a*** and ***b***, Inward currents elicited by gamma frequency (50 Hz) train stimulation of neuronal fibers in two NG2 cells held at −70 mV at PN11 (***a***) and PN25 (***b***) in the presence of 10 μM NBQX and 50 μM D-AP-5. Both currents were normalized at the first stimulation pulse. Traces in SR95531 were subtracted to the trace control (average of five traces in each case); artifacts were blanked. The current peaks reached at the first three stimulation pulses for the cell at PN25 are indicated (arrows). Note the presence of single synaptic events within the train in the second PN week and the larger temporal summation of spillover-mediated currents in the fourth PN week.

Low-frequency spontaneous currents and electrically evoked responses mediated by $GABA_A$ receptors were recently described in cortical nestin$^+$/NG2$^+$ cells of 8-week-old mice (Tanaka et al., 2009). The authors assumed that the observed GABAergic currents in adult animals resulted from a direct synaptic innervation between interneurons and NG2 cells, without testing for a genuine synaptic response. They reported low-frequency spontaneous currents with prolonged rise times (4.7 ms) similar to those observed here (5.1 ms), which are not compatible with values expected for classical synaptic currents ($\leq$1 ms) (Farrant and Nusser, 2005). By using the voltage jump technique, we demonstrated that slow kinetics of GABAergic responses did not result from signal filtering. Our results also argue against slow kinetics caused by direct synaptic asynchronous release on NG2 cells, since asynchronous synaptic events were never resolved during the rising phase of evoked currents, and single miniature events were almost undetectable in the presence of strontium or ruthenium red. Nevertheless, we cannot entirely exclude that GABAergic activity of cortical NG2 cells arises from asynchronous release from remote neuronal synapses. Finally, we cannot totally exclude that changes in the subunit composition of $GABA_A$ receptors expressed in NG2 cells partially explain the slowdown kinetics of GABAergic responses during development.

The release of GABA from a synaptic terminal induces a rapid activation of receptors at adjacent postsynaptic densities (Farrant and Nusser, 2005), as observed in cortical NG2 cells of the second PN week. In fact, the presence of neuronal glutamatergic and GABAergic synaptic-like contacts on these cells has been found by electron microscopy in different structures of the CNS (Bergles et al., 2000; Lin and Bergles, 2004; Lin et al., 2005; Kukley et al., 2007; Ziskin et al., 2007). However, our results raise questions about the anatomical and functional junctions formed between interneurons and NG2

cells in the adult. The three-dimensional reconstruction and quantification of interneuron and NG2 cell membrane appositions at different developmental PN stages of the barrel cortex would be of particular interest to understand the morphological changes carrying out the switch from synaptic to extrasynaptic transmission mode. GABA spillover appears to be a reliable mechanism to activate $GABA_A$ receptors of NG2 cells in the millisecond scale and, therefore, GABA probably diffuses over relatively short distances from the neuronal synapses shown to be directly apposed to NG2 cell membranes (Farrant and Nusser, 2005). The lack of a tonic current accompanying spillover phasic responses [current amplitude blocked by 5 μM SR95531: 0.3 $\pm$ 6.1 pA ($n = 6$) and 2.5 $\pm$ 9.8 pA ($n = 4$) in the second and fourth PN weeks, respectively] also supports the view that a widespread diffusion of transmitter does not take place and that it occurs at local sites on NG2 cell membranes. Interestingly, a pure glutamate spillover transmission has been described in climbing fiber-interneuron connections (Szapiro and Barbour, 2007). Ultrastructural analyses of climbing fiber terminals and molecular layer interneurons have shown tight membrane appositions external to but in the region of active zones (Kollo et al., 2006), which provides an indirect morphological support for glutamate spillover transmission at these particular junctions. In addition, a recent report showed that cortical neurogliaform interneurons do not require direct synaptic junctions to induce unitary GABA-mediated responses in target neurons (Olah et al., 2009), corroborating our evidence that pure spillover connections may constitute a precise phasic mode of communication between interneurons and NG2 cells in the mature brain.

Recent reports have shown that, during cell division, NG2 cells maintain their glutamatergic and GABAergic synapses and transfer them to their progeny (Kukley et al., 2008; Ge et al., 2009). Although the function of NG2 cell synapses is not known, there is an emerging idea that direct synaptic activity may influence NG2 cell proliferation and differentiation (Nishiyama et al., 2009). Additionally, synaptic $GABA_A$ receptor activation may induce NG2 cell migration through activation of a Na^+ channel-Na^+/Ca^{2+} exchanger pathway (Tong et al., 2009). Our results in the barrel cortex support the hypothesis that direct synaptic activity has a developmental function in NG2 cells, since the frequency of spontaneous GABAergic synaptic activity dramatically decreases after the second postnatal week, which corresponds with the peak period of oligodendrocyte differentiation (Baracskay et al., 2002) and active myelination (Bjelke and Seiger, 1989; Salami et al., 2003). However, we show that as development in the neocortex nears completion, GABAergic signaling onto NG2 cells is not lost, but instead there is developmental switch from synaptic transmission to spillover transmission. Hence, if $GABA_A$ receptors are important in regulating NG2 cell differentiation, then the mode of transmission must be critical, and it will be worth examining whether there is a return to synaptic transmission in pathology such as demyelination. In addition, NG2 cells may have unresolved physiological functions, and spillover transmission would allow NG2 cells to integrate neuronal network activity patterns occurring during sensory processing. We found that gamma frequency neuronal activity evoked sustained extrasynaptic responses in NG2 cells. Although extracellular stimulation in brain slices does not necessarily mimic the spatial patterns of activity that occur *in vivo* and may favor spillover mechanisms with respect to more physiological conditions, our results are consistent with the possibility that interneurons signal to NG2 cells during sensory-evoked gamma oscillations *in vivo*. A pure GABA spillover transmission may constitute a signaling mechanism to maintain NG2 cells as differentiated cells but may also play an important role in pathological processes. Indeed, GABA promotes the production of BDNF in cortical NG2 cells after ischemic stroke, suggesting a neuroprotective role of these cells in injured areas (Tanaka et al., 2009). Although NG2 cells serve as precursors for oligodendrocytes during early postnatal development, our results suggest that these cells play additional roles in the adult.

References

Ahissar E, Vaadia E (1990) Oscillatory activity of single units in a somatosensory cortex of an awake monkey and their possible role in texture analysis. Proc Natl Acad Sci U S A 87:8935–8939.

Alle H, Geiger JR (2007) GABAergic spill-over transmission onto hippocampal mossy fiber boutons. J Neurosci 27:942–950.

Baracskay KL, Duchala CS, Miller RH, Macklin WB, Trapp BD (2002) Oligodendrogenesis is differentially regulated in gray and white matter of jimpy mice. J Neurosci Res 70:645–654.

Bergles DE, Roberts JD, Somogyi P, Jahr CE (2000) Glutamatergic synapses on oligodendrocyte precursor cells in the hippocampus. Nature 405:187–191.

Bjelke B, Seiger A (1989) Morphological distribution of MBP-like immunoreactivity in the brain during development. Int J Dev Neurosci 7:145–164.

Chang A, Nishiyama A, Peterson J, Prineas J, Trapp BD (2000) NG2-positive oligodendrocyte progenitor cells in adult human brain and multiple sclerosis lesions. J Neurosci 20:6404–6412.

Chittajallu R, Aguirre A, Gallo V (2004) NG2-positive cells in the mouse white and grey matter display distinct physiological properties. J Physiol 561:109–122.

Conti F, Minelli A, Melone M (2004) GABA transporters in the mammalian cerebral cortex: localization, development and pathological implications. Brain Res Brain Res Rev 45:196–212.

Farrant M, Nusser Z (2005) Variations on an inhibitory theme: phasic and tonic activation of GABA(A) receptors. Nat Rev Neurosci 6:215–229.

Ge WP, Zhou W, Luo Q, Jan LY, Jan YN (2009) Dividing glial cells maintain differentiated properties including complex morphology and functional synapses. Proc Natl Acad Sci U S A 106:328–333.

Goda Y, Stevens CF (1994) Two components of transmitter release at a central synapse. Proc Natl Acad Sci U S A 91:12942–12946.

Gonzalez-Burgos G, Rotaru DC, Zaitsev AV, Povysheva NV, Lewis DA (2009) GABA transporter GAT1 prevents spillover at proximal and distal GABA synapses onto primate prefrontal cortex neurons. J Neurophysiol 101:533–547.

Guo F, Ma J, McCauley E, Bannerman P, Pleasure D (2009) Early postnatal proteolipid promoter-expressing progenitors produce multilineage cells in vivo. J Neurosci 29:7256–7270.

Jabs R, Pivneva T, Huttmann K, Wyczynski A, Nolte C, Kettenmann H, Steinhauser C (2005) Synaptic transmission onto hippocampal glial cells with hGFAP promoter activity. J Cell Sci 118:3791–3803.

Jones MS, Barth DS (1997) Sensory-evoked high-frequency (gamma-band) oscillating potentials in somatosensory cortex of the unanesthetized rat. Brain Res 768:167–176.

Jones MV, Jonas P, Sahara Y, Westbrook GL (2001) Microscopic kinetics and energetics distinguish GABA(A) receptor agonists from antagonists. Biophys J 81:2660–2670.

Karadottir R, Hamilton NB, Bakiri Y, Attwell D (2008) Spiking and nonspiking classes of oligodendrocyte precursor glia in CNS white matter. Nat Neurosci 11:450–456.

Kollo M, Holderith NB, Nusser Z (2006) Novel subcellular distribution pattern of A-type K^+ channels on neuronal surface. J Neurosci 26:2684–2691.

Kukley M, Capetillo-Zarate E, Dietrich D (2007) Vesicular glutamate release from axons in white matter. Nat Neurosci 10:311–320.

Kukley M, Kiladze M, Tognatta R, Hans M, Swandulla D, Schramm J, Dietrich D (2008) Glial cells are born with synapses. FASEB J 22:2957–2969.

Lin SC, Bergles DE (2004) Synaptic signaling between GABAergic interneurons and oligodendrocyte precursor cells in the hippocampus. Nat Neurosci 7:24–32.

Lin SC, Huck JH, Roberts JD, Macklin WB, Somogyi P, Bergles DE (2005)

Climbing fiber innervation of NG2-expressing glia in the mammalian cerebellum. Neuron 46:773–785.

LoTurco JJ, Owens DF, Heath MJ, Davis MB, Kriegstein AR (1995) GABA and glutamate depolarize cortical progenitor cells and inhibit DNA synthesis. Neuron 15:1287–1298.

Mangin JM, Kunze A, Chittajallu R, Gallo V (2008) Satellite NG2 progenitor cells share common glutamatergic inputs with associated interneurons in the mouse dentate gyrus. J Neurosci 28:7610–7623.

Matsui K, Jahr CE (2003) Ectopic release of synaptic vesicles. Neuron 40:1173–1183.

Nguyen L, Rigo JM, Rocher V, Belachew S, Malgrange B, Rogister B, Leprince P, Moonen G (2001) Neurotransmitters as early signals for central nervous system development. Cell Tissue Res 305:187–202.

Nishiyama A, Komitova M, Suzuki R, Zhu X (2009) Polydendrocytes (NG2 cells): multifunctional cells with lineage plasticity. Nat Rev Neurosci 10:9–22.

Olah S, Fule M, Komlosi G, Varga C, Baldi R, Barzo P, Tamas G (2009) Regulation of cortical microcircuits by unitary GABA-mediated volume transmission. Nature 461:1278–1281.

Pearce RA (1993) Physiological evidence for two distinct GABAA responses in rat hippocampus. Neuron 10:189–200.

Perea G, Navarrete M, Araque A (2009) Tripartite synapses: astrocytes process and control synaptic information. Trends Neurosci 32:421–431.

Rossi DJ, Hamann M (1998) Spillover-mediated transmission at inhibitory synapses promoted by high affinity alpha6 subunit GABA(A) receptors and glomerular geometry. Neuron 20:783–795.

Salami M, Itami C, Tsumoto T, Kimura F (2003) Change of conduction velocity by regional myelination yields constant latency irrespective of distance between thalamus and cortex. Proc Natl Acad Sci U S A 100:6174–6179.

Szabadics J, Tamas G, Soltesz I (2007) Different transmitter transients underlie presynaptic cell type specificity of GABAA, slow and GABAA, fast. Proc Natl Acad Sci U S A 104:14831–14836.

Szapiro G, Barbour B (2007) Multiple climbing fibers signal to molecular layer interneurons exclusively via glutamate spillover. Nat Neurosci 10:735–742.

Tanaka Y, Tozuka Y, Takata T, Shimazu N, Matsumura N, Ohta A, Hisatsune T (2009) Excitatory GABAergic activation of cortical dividing glial cells. Cereb Cortex 19:2181–2195.

Tong XP, Li XY, Zhou B, Shen W, Zhang ZJ, Xu TL, Duan S (2009) Ca(2+) signaling evoked by activation of Na(+) channels and Na(+)/Ca(2+) exchangers is required for GABA-induced NG2 cell migration. J Cell Biol 186:113–128.

Velez-Fort M, Audinat E, Angulo MC (2009) Functional alpha 7-containing nicotinic receptors of NG2-expressing cells in the hippocampus. Glia 57:1104–1114.

Yang JW, Hanganu-Opatz IL, Sun JJ, Luhmann HJ (2009) Three patterns of oscillatory activity differentially synchronize developing neocortical networks in vivo. J Neurosci 29:9011–9025.

Zalc B, Fields RD (2000) Do action potentials regulate myelination? Neuroscientist 6:5–13.

Ziskin JL, Nishiyama A, Rubio M, Fukaya M, Bergles DE (2007) Vesicular release of glutamate from unmyelinated axons in white matter. Nat Neurosci 10:321–330.

Journal of Anatomy

J. Anat. (2011) **219**, pp8–17 doi: 10.1111/j.1469-7580.2011.01350.x

REVIEW

Is neuronal communication with NG2 cells synaptic or extrasynaptic?

Paloma P. Maldonado,[1,2,3] Mateo Vélez-Fort[1,2,3] and María Cecilia Angulo[1,2,3]

[1]*Inserm U603*
[2]*CNRS UMR 8154*
[3]*Université Paris Descartes, Paris, France*

Abstract

NG2-expressing glial cells (NG2 cells) represent a major pool of progenitors able to generate myelinating oligodendrocytes, and perhaps astrocytes and neurones, in the postnatal brain. In the last decade, it has been demonstrated that NG2 cells receive functional glutamatergic and GABAergic synapses mediating fast synaptic transmission in different brain regions. However, several controversies exist in this field. While two classes of NG2 cells have been defined by the presence or absence of Na^+ channels, action potential firing and neuronal input, other studies suggest that all NG2 cells possess Na^+ conductances and are the target of quantal neuronal release, but are unable to trigger action potential firing. Here we bring new evidence supporting the idea that the level of expression of Na^+ conductances is not a criterion to discriminate NG2 cell subpopulations in the somatosensory cortex. Surprisingly, recent reports demonstrated that NG2 cells detect quantal glutamate release from unmyelinated axons in white matter regions. Yet, it is difficult from these studies to establish whether axonal vesicular release in white matter occurs at genuine synaptic junctions or at ectopic release sites. In addition, we recently reported a new mode of extrasynaptic communication between neurones and NG2 cells that relies on pure GABA spillover and does not require GABAergic synaptic input. This review discusses the properties of quantal neuronal release onto NG2 cells and gives an extended overview of potential extrasynaptic modes of transmission, from ectopic to diffuse volume transmission, between neurones and NG2 cells in the brain.

Key words: extrasynaptic transmission; GABA(A, slow); oligodendrocyte precursor cells (OPCs); synaptic transmission.

Introduction

Glial cells express a large set of metabotropic and ionotropic receptors for neurotransmitters that allow them to respond to neuronal activity. Neurotransmitter receptor activation, extensively studied in astrocytes, leads to complex information processing in the form of calcium signals (Pasti et al. 1997; Perea & Araque, 2005; Wang et al. 2006; Schummers et al. 2008). In the absence of evidence for anatomical synaptic contacts between neurones and astrocytes, the extrasynaptic action of neurotransmitters spilling out of synaptic cleft is likely the major neurone-to-astrocyte signalling mechanism. Another mode of extrasynaptic communication exists between climbing fibres and Bergmann glia in the cerebellum. Non-synaptic quantal events mediated by α-amino-3-hydroxy-5-methyl-4-isoxazolepropionic acid receptor (AMPA) receptors in Bergmann glia result from an ectopic release of glutamate from climbing fibres outside active zones (Matsui & Jahr, 2003; Matsui et al. 2005). Spillover and ectopic release are thus two modes of communication between neurones and glia implicating extrasynaptic receptors.

Although chemical synapses have long been regarded as a signalling mechanism exclusive to neurones in the brain, Bergles et al. (2000) demonstrated the presence of functional and morphological synaptic contacts between neurones and NG2-expressing glial cells (NG2 cells) in the postnatal hippocampus. Since this pioneer work, fast glutamatergic and/or GABAergic synaptic currents have

Correspondence
María Cecilia Angulo, Laboratoire de Neurophysiologie et Nouvelles Microscopies; INSERM U603, CNRS UMR 8154; Université Paris Descartes; 45, rue des Saints-Pères; 75006 Paris, France.
T: + 33 1 42864153; F: + 33 1 42864151; E: maria-cecilia.angulo@parisdescartes.fr

Accepted for publication *23 January 2011*
Article published online *24 February 2011*

been observed in different regions of grey matter, including neocortex (Chittajallu et al. 2004; Kukley et al. 2008; Ge et al. 2009; Velez-Fort et al. 2010), hippocampus (Lin & Bergles, 2004; Jabs et al. 2005; Ge et al. 2006), cerebellum (Lin et al. 2005) and medial nucleus of the trapezoid body (Muller et al. 2009). Surprisingly, it has also been established that NG2 cells detect quantal neurotransmitter release from unmyelinated axons in white matter regions such as corpus callosum (Kukley et al. 2007; Ziskin et al. 2007), optic nerve (Kukley et al. 2007) and white matter cerebellum (Karadottir et al. 2005, 2008). Whether vesicular release in white matter occurs at genuine synaptic junctions or at ectopic release sites is still controversial.

These cells constitute the main endogenous pool of progenitors in the postnatal brain, which serves as a major source of myelinating oligodendrocytes during postnatal development, and perhaps as progenitors endowed with the ability to generate astrocytes and neurones. In addition, they play a crucial role during remyelination which occurs as a repair process in demyelinating lesions (Nishiyama et al. 2009). A tempting hypothesis on the role of synaptic transmission in NG2 cells is that this point-to-point communication allows neurones to control NG2 cell activity precisely, influencing oligodendrogenesis and thus myelination of the brain. In support of this hypothesis, recent findings have shown that the transition of NG2 cells towards a premyelinating stage is accompanied by a rapid loss of glutamatergic synaptic inputs under normal conditions (De Biase et al. 2010; Kukley et al. 2010) and after demyelinating lesions (Etxeberria et al. 2010). In addition, the frequency of spontaneous GABAergic synaptic activity dramatically decreases in NG2 cells of the barrel cortex after the second postnatal week (Velez-Fort et al. 2010), when cortical oligodendrocyte differentiation reaches a peak (Baracskay et al. 2002). However, the millisecond time scale of fast synaptic signals and the low frequency of synaptic events in NG2 cells suggest that this synaptic communication is more suitable for other cellular functions requiring precise spatiotemporal signals. Among these functions, recognition of specific axonal partners, process motility and promotion of migration are good candidates.

Although AMPA and $GABA_A$ receptors of NG2 cells are believed to operate mainly through conventional synaptic transmission, these and other receptors expressed in the membrane of these cells may also be activated by extrasynaptic neurotransmitters. In tissue preparations, NG2 cells express different functional receptors such as NMDA, kainate, nicotinic and purinergic receptors that are probably activated extrasynaptically and may be powerful transducers of neuronal signals (Karadottir et al. 2005; Kukley & Dietrich, 2009; Velez-Fort et al. 2009; Hamilton et al. 2010). Also, we recently demonstrated that direct quantal release of GABA on NG2 cells is lost early in postnatal cortical development and replaced by an unusual extrasynaptic mode of communication, mediated solely by GABA spillover (Velez-Fort et al. 2010). In this review we discuss the evidence for synaptic neurone-to-NG2 cell signalling and evaluate the possible existence of multiple modes of extrasynaptic communication from ectopic to diffuse volume transmission between neurones and NG2 cells.

Synaptic transmission in grey matter NG2 cells

Evidence for direct synaptic contacts on NG2 cells has been the subject of recent reviews and we will thus succinctly describe the physiological and morphological properties of these synapses in this section (see Gallo et al. 2008; Nishiyama et al. 2009; Bergles et al. 2010). Patch-clamp recordings in NG2 cells of the hippocampus revealed the presence of spontaneous rapid AMPA and $GABA_A$ receptor-mediated currents (Bergles et al. 2000; Lin & Bergles, 2004; Jabs et al. 2005). In grey matter regions, these currents exhibit the typical characteristics of neuronal synaptic events, i.e. submillisecond rise times and decays with time constants of few milliseconds (Bergles et al. 2000). We should take into account, however, that spontaneous synaptic events occur at frequencies 30–97% lower than those recorded in neurones of the same region (Mangin et al. 2008; Muller et al. 2009). In the presence of the Na^+ channel blocker tetrodotoxin (TTX), miniature glutamatergic and GABAergic events are also detected at very low frequencies of between < 0.01 and 0.03 Hz (Bergles et al. 2000; Velez-Fort et al. 2010). These frequencies can be enhanced when potent secretagogues such as α-latrotoxin and ruthenium red are added in the bath, demonstrating that miniature currents result from the spontaneous fusion of transmitter-filled vesicles (Bergles et al. 2000; Lin & Bergles, 2004). In addition, neuronal fibre stimulation evoked glutamatergic responses characterized by short onset latencies, variable amplitudes and fast kinetics, as expected for a synchronized vesicular release. It is noteworthy, however, that evoked GABAergic currents do not always have kinetics compatible with a synaptic release, as discussed below (Tanaka et al. 2009; Velez-Fort et al. 2010).

Physiological data have been corroborated by ultrastructural analyses revealing the presence of morphological specialized junctions between presynaptic neuronal terminals and NG2 cells (Fig. 1A; Bergles et al. 2000; Lin & Bergles, 2004; Lin et al. 2005; Jabs et al. 2005; Muller et al. 2009; Kukley et al. 2008). Indeed, vesicle-containing terminals are apposed to NG2 cell processes and, although not always detectable in biocytin-stained cells, postsynaptic densities are also clearly recognized by their electron-dense material in immunogold experiments (Bergles et al. 2000). In electron micrographs, a single neuronal bouton often appears to contact both a postsynaptic spine and an NG2 cell (Fig. 1A, right; Bergles et al. 2000; Lin et al. 2005; Muller et al. 2009). This morphological feature

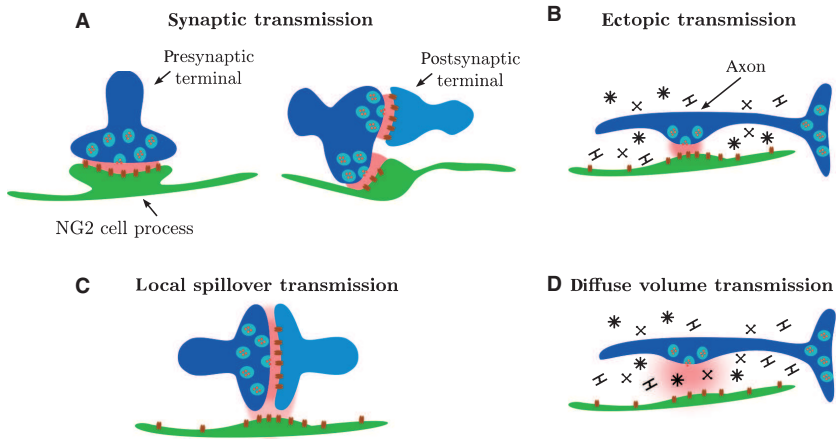

Fig. 1 Examples of different potential modes of transmission between neurones and NG2 cells. (A) Synaptic transmission. Vesicle-containing presynaptic compartments directly contact an NG2 cell process forming specialized synaptic junctions similar to those described in neurones (left). Released neurotransmitters diffuse across a narrow cleft to activate rapidly high densities of postsynaptic receptors. A single presynaptic bouton can also innervate simultaneously a neuronal spine and an NG2 cell process (right). (B) Ectopic transmission. Neurotransmitters could be found in small 'synaptic-like' vesicles located at varicosities along axons and released at non-synaptic sites. High densities of extrasynaptic receptors would be activated close to these release sites to induce fast rising quantal events in NG2 cells. These events, however, would have smaller amplitudes than those recorded at a genuine synapse. (C) Local spillover transmission. NG2 cell processes could enwrap or pass very close to neuronal synapses, allowing high densities of extrasynaptic receptors to sense locally neurotransmitters spilling out of the synaptic cleft. No miniature events would be detectable in this case. (D) Diffuse volume transmission. Diffuse transmission may occur at non-synaptic sites and, compared to other types of transmission modes, released neurotransmitters would have to cross large distances (typically > 1 μm) before reaching a targeted cell. Other modes of transmission are not excluded.

correlates with the occurrence of highly synchronized spontaneous glutamatergic synaptic currents between neurones and NG2 cells of the hippocampus and of the medial nucleus of trapezoid body (Mangin et al. 2008; Muller et al. 2009). Whether NG2 cells and neurones show synchronous GABAergic activity is unknown at present. Only a restricted description of functional and morphological GABAergic synaptic properties of NG2 cells exists (Lin & Bergles, 2004; Jabs et al. 2005; Karadottir et al. 2008; Velez-Fort et al. 2010). The GABAergic system of NG2 cells probably constitutes an interesting subject for future investigation.

Quantal events in white matter NG2 cells: synaptic or ectopic?

In white matter regions, quantal release of glutamate on NG2 cells has been described recently during postnatal development and after lysolecithin-induced demyelination in adult animals (Karadottir et al. 2005, 2008; Kukley et al. 2007; Ziskin et al. 2007; Etxeberria et al. 2010). This unexpected discovery supports the idea that white matter in the brain is not only a passive region where bundles of axons connect different brain regions, but a place where local information is precisely transferred at specialized sites from neurones to glia. Even so, a certain number of discrepancies exist regarding the physiological and morphological properties of axonal–NG2 cell junctions.

As for classical synaptic events, whole-cell currents of white matter NG2 cells are characterized by rise times in the submillisecond range and decay time constants of few milliseconds. Ca^{2+}-impermeable AMPA receptors mediate axonal–NG2 cell currents in the first postnatal weeks (Kukley et al. 2007; Ziskin et al. 2007), whereas Ca^{2+}-permeable receptors predominate in adult mice (Ziskin et al. 2007). Therefore, modifications of the subunit composition of AMPA receptors expressed at the membrane of NG2 cells probably occur during development. After lesion, immunostainings against GluR2/3 subunits confirmed the expression of AMPA receptors in migrating NG2 cells from the subventricular zone (Etxeberria et al. 2010). However, it was not possible, on the basis of these experiments, to establish the presence or absence of GluR2 subunits and thus to predict the Ca^{2+}-permeability of receptors during a demyelination/remyelination process. As Ca^{2+} could be an important intracellular transducer of neuronal signals in NG2 cells, it would be interesting to determine which AMPA receptor subtype predominates during remyelination of callosal axons.

Unmyelinated axons constitute the major source of axonal projections to white matter NG2 cells and their mechanisms of glutamate release exhibit many hallmarks of classical synaptic transmission, i.e. the presence of voltage-gated calcium channels as key mediators of Ca^{2+} entry into the axon, the existence of discrete Ca^{2+} microdomains, a highly sustained synchronous release of transmitter during intense stimulation and the presence of at least part of the machinery for synaptic vesicle exocytosis (Kukley et al. 2007; Ziskin et al. 2007; see also Alix et al. 2008 for the machinery). However, whether glutamate release in white matter regions occurs at true synaptic sites is still unclear. Ultrastructural analysis

reported by Ziskin et al. (2007) in corpus callosum showed NG2 cell processes opposed to nerve terminals containing VGLUT1$^+$ vesicles. The presence of discrete junctions characterized by a rigid parallel apposition of membranes and electron-dense material strongly suggests the existence of genuine synaptic contacts between axons and callosal NG2 cells (Fig. 1A, left; Ziskin et al. 2007). In contrast, in Kukley et al. (2007), electron microscopy analysis in corpus callosum and optic nerve revealed the presence of axonal varicosities in close contact with an NG2 cell process containing very few to a large number of small vesicles, showing clefts with irregular and relatively wide sizes and lacking electron-dense material. In addition, most putative vesicle release sites were not opposed to an NG2 cell membrane, suggesting that these structures are not specifically associated with NG2 cells. Another substantial discrepancy exists regarding the amplitudes of miniature currents and the estimated number of axonal fibres that contact a single callosal NG2 cell: −18 pA at a holding potential of −90 mV and ∼ 10 contacts in Ziskin et al. (2007) vs. −4 pA at a holding potential of −80 mV and hundreds of contacts in Kukley et al. (2007). Whereas data reported by Ziskin et al. (2007) are in favour of real glutamatergic synapses between axons and NG2 cells (Fig. 1A), those by Kukley et al. (2007) suggest the existence of an ectopic release of glutamate in white matter (Fig. 1B). Ectopic quantal release of glutamate outside active zones has already been described between neurones and Bergman glia of the cerebellum and thus exists between neurones and glial cells (Matsui & Jahr, 2003). If ectopic quantal release is the main mechanism governing axonal–NG2 cell communication in white matter, we can expect that its properties differ from those described for synapses of NG2 cells and neurones in grey matter. In keeping with this assumption, the inhibition of the amplitude of evoked currents by the low-affinity competitive antagonist of AMPA receptors γ-D-glutamylglycine (γ-DGG) was significantly greater in callosal NG2 cells than in CA1 pyramidal neurones as expected for a lower concentration of glutamate reaching NG2 cell receptors (Kukley et al. 2007). A similar observation was reported for ectopic release onto Bergman glia (Matsui & Jahr, 2003). It is noteworthy, however, that the effect of γ-DGG may be different between callosal NG2 cells and pyramidal neurones because of a different subunit AMPA receptor composition.

Quantal neurotransmitter release directly on NG2 cells seems to be a usual signalling pathway in different regions of the brain. However, quantal transmission on these cells may exist in two distinct forms according to the brain region: classical synaptic transmission in grey matter (Fig. 1A) and ectopic transmission in white matter (Fig. 1B). Substantial differences between ectopic and synaptic release mechanisms have been described in Bergman glia of the cerebellum and may be used, at least partly, for a comparative evaluation (Matsui & Jahr, 2004). Further detailed and comparative physiological analyses are thus needed to clarify the synaptic or extrasynaptic nature of neurotransmitter release from callosal axons. A revised axonal–NG2 and extended analysis of axonal–NG2 cell contact morphology should also help to resolve the controversy in white matter.

Which classes of NG2 cells respond to quantal vesicular release?

Most studies have established that virtually all NG2 cells in mice and rats receive glutamatergic input after the first postnatal week and in demyelinating lesions, suggesting that the presence of this input on NG2 cells is a general rule (Bergles et al. 2010; Etxeberria et al. 2010). In grey matter, the acquisition of synapses occurs during cell division, thus very early in NG2 cell development when cells are actively proliferating in the brain (Kukley et al. 2008; Ge et al. 2009). However, Karadottir et al. (2008) reported the existence of two classes of NG2 cells in the cerebellar white matter, defined by the presence or absence of Na^+ channels; only those expressing high levels of these channels are supposed to trigger action potential discharges and receive axonal input. Yet, the existence of two distinct subpopulations of NG2 cells, recognized by the levels of Na^+ channel expression, was contradicted in recent reports arguing that Karadottir et al. (2008) recorded from pre-oligodendrocytes, which progressively, but rapidly, lose both their functional Na^+ channels and neuronal inputs (De Biase et al. 2010; Kukley et al. 2010). The capacity of NG2 cells to elicit action potential discharges is also under intense debate.

If the question of which NG2 cells receive glutamatergic inputs in the brain is controversial, even less is known about NG2 cells contacted by GABAergic synapses. We recently reported that layer V NG2 cells in the barrel cortex receive GABAergic synaptic contacts in the second, but not in the fourth, postnatal week (Velez-Fort et al. 2010). To evaluate whether two distinct cortical NG2 cells can be identified during the period of loss of synaptic GABAergic activity, we studied the level of expression of Na^+ conductances at these two developmental stages. Whole-cell recordings of DsRed$^+$ NG2 cells were performed at a holding potential of −90 mV with a CsCl-based intracellular solution containing 4AP and tetraethylammonium (TEA) to inhibit voltage-gated K^+ channels and to better isolate Na^+ conductances (Fig. 2). Current responses elicited by voltage steps from −60 to +40 mV revealed the presence of an Na^+ conductance in 95% of recorded cells in the second postnatal week, but only in 40% in the fourth postnatal week (n = 57 and n = 67, respectively; Fig. 2A,C). However, we noticed that the loss of Na^+ currents in the fourth postnatal week was concomitant with a decrease of cell membrane resistance and an increase of a passive conductance expression that may mask Na^+ currents (Fig. 2A; Velez-Fort et al. 2010). An effective way to increase the membrane resistance in these cells is by adding extracellular Ba^{2+} in the perfusate (Velez-Fort et al. 2009). The presence of extracellular Ba^{2+}

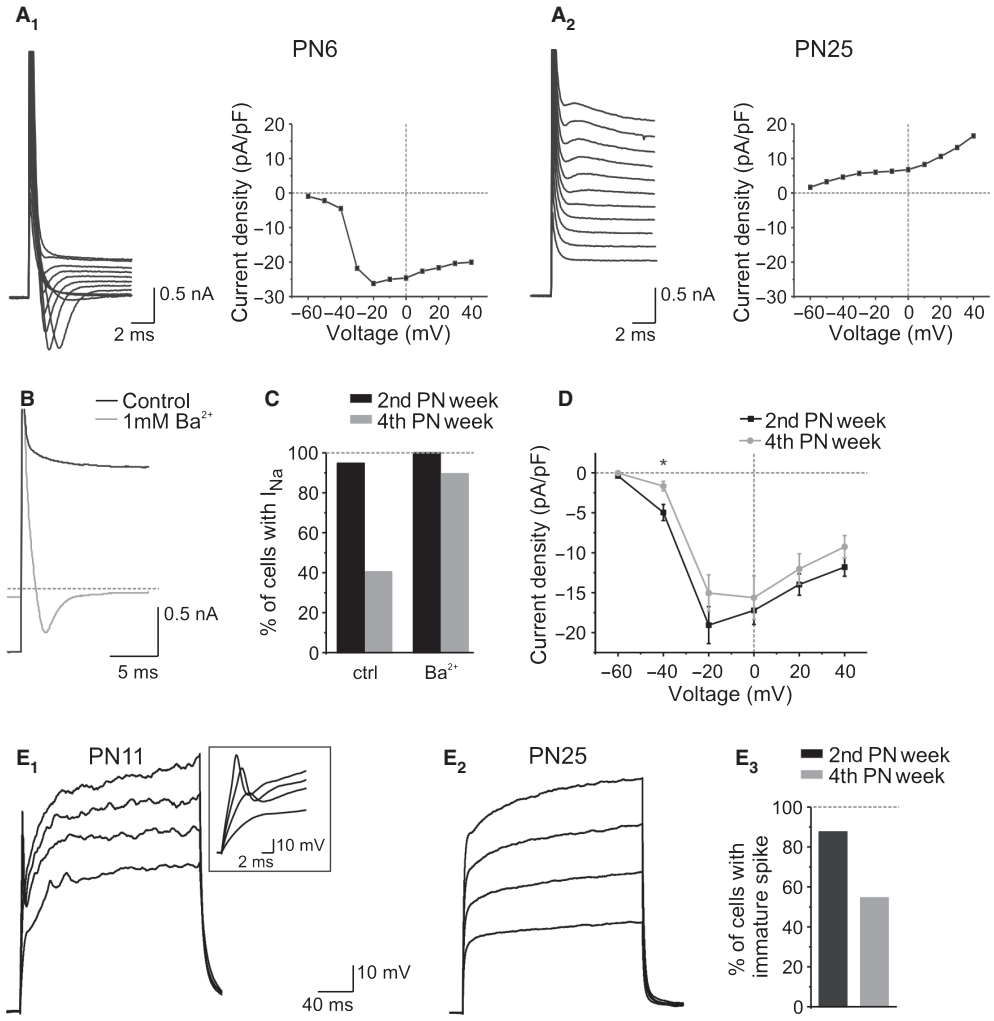

Fig. 2 NG2 cells of the barrel cortex express high levels of voltage-gated Na^+ channels, but do not elicit action potential discharges. (A) Currents induced by depolarizing steps from −60 to +40 mV in layer V cortical NG2 cells held at −90 mV and recorded in a CsCl-based intracellular solution containing TEA (10 mM) and 4AP (4 mM) at PN6 (A1, left) and PN25 (A2, left). Corresponding I–V curves (right) were obtained after leak subtraction. Note that in our recording conditions the reversal potential of Na^+ was +97 mV. Inward sodium currents (I_{Na^+}) at PN6 were observed at negative potentials and unmasked at positive potentials by leak subtraction (A1). Conversely, I_{Na^+} was not apparent using this procedure at PN25 (A2). (B) Recordings from a cortical NG2 cell during a voltage step from −90 to −20 mV at PN25, before (black trace) and after bath applications of 1 mM Ba^{2+} (grey trace). Note that extracellular Ba^{2+} revealed I_{Na^+}. (C) Histograms showing the percentage of cortical NG2 cells displaying voltage-gated Na^+ currents in the second (black) and fourth (grey) PN weeks, in control conditions and after bath application of Ba^{2+} (100 μM–1 mM). Note the large increase of the percentage of NG2 cells showing I_{Na^+} in the fourth postnatal week. (D) Comparison of I–V relationships of Na^+ conductances recorded at different voltage steps from −60 to +40 mV in the second (black) and fourth (grey) postnatal weeks. Note that the amplitudes of I_{Na^+} are similar between both postnatal stages, except at −40 mV (Mann–Whitney test, $*P < 0{,}01$). (E) Whole-cell current clamp recordings from cortical NG2 cells held at −70 mV at PN11 (E1) and PN25 (E2) with a KCl-based intracellular solution, during successive current injections from 200 pA. Less immature spikes were elicited in the fourth postnatal week (E3).

unmasked a Na^+ current in almost all tested cells (Fig. 2B,C). In addition, no significant changes in the Na^+ current density were observed between the second and fourth postnatal week in the presence of extracellular Ba^{2+}, confirming that Na^+ channel expression did not decrease with age (Fig. 2D). Only two of 17 cells recorded during the fourth postnatal week did not express an Na^+ current (Fig. 2C). To discard the possibility that DsRed is preferentially expressed in a subpopulation of cortical NG2 cells having Na^+ currents, we performed immunostainings against NG2 in perfused brains. We observed that virtually all $NG2^+$ cells of the cortex express DsRed, whereas most but not all of $DsRed^+$ cells were $NG2^+$ (100% and 73.4 ± 3.5%, respectively; $n = 2$ animals; Fig. 3A). It is also noteworthy that $DsRed^+/NG2^-$ cells expressed low levels of fluorescence (Fig. 3A, inset), suggesting that these cells are in a more mature state, as reported by Ziskin et al. (2007). It is thus likely that the two cells of our sample lacking Na^+ currents in Ba^{2+} were in a

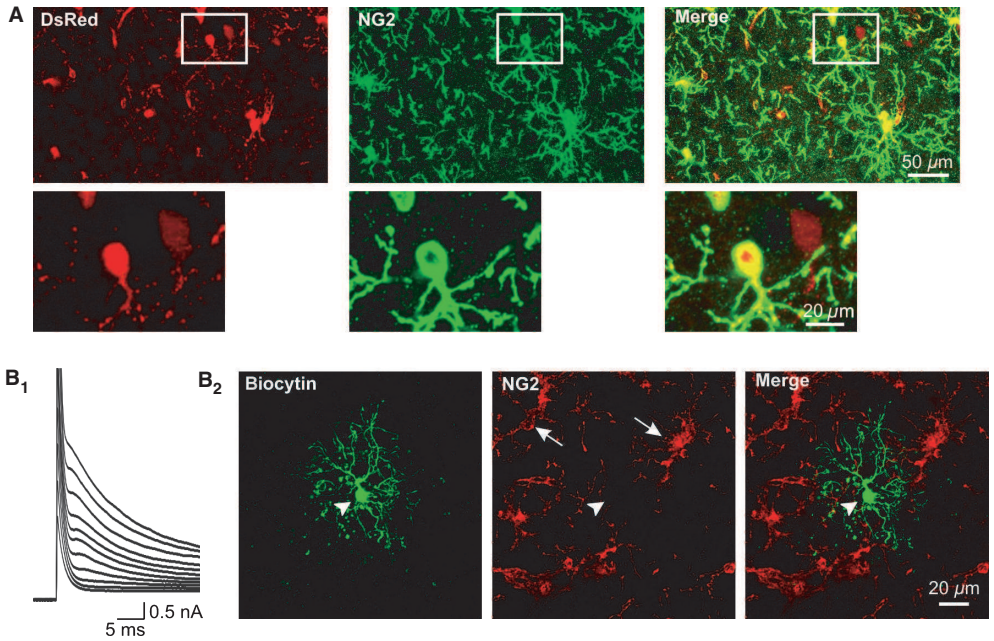

Fig. 3 Immunoreactivity of NG2 proteoglycan in NG2-DsRed transgenic mice in the fourth postnatal week. (A) Confocal images of NG2 in the somatosensory cortex of a perfused PN26 NG2-DsRed mouse (stack of seven z sections, each 2 μm). Note that all $NG2^+$ cells (green) are $DsRed^+$ (red) but that not all $DsRed^+$ cells are $NG2^+$. A $DsRed^+/NG2^+$ cell and a $DsRed^+/NG2^-$ cell are outlined in the white frame. These two cells are shown at higher magnification in the insets (lower panels). (B) Post-recording immunostaining of a $DsRed^+$ cell stained with biocytin at PN26. (B1) Currents induced by depolarizing steps from −60 to +40 mV in a $DsRed^+$ cell held at −90 mV and recorded in a CsCl-based intracellular solution containing 5.4 mM biocytin. Note the lack of Na^+ currents (this is also the case after leak subtraction). (B2) Confocal images of the same $DsRed^+$ cell after fixing the slice in 4% paraformaldehyde and immunostaining with both streptavidin-conjugated-Alexa488 (green) and NG2 revealed with a secondary antibody coupled to Alexa633 (red; stacks of 21 z sections, each 1 μm). In our confocal recording conditions, the DsRed is not visible. Note the lack of NG2 expression of the cell (arrowheads). Arrows show $NG2^+$ cells in the same slice.

transition state towards a more mature phenotype (Fig. 2C). To further test this hypothesis, we performed post-recording immunostainings against NG2 in $DsRed^+$ cells stained with biocytin during the fourth postnatal week. In these experiments, no Ba^{2+} was applied in the bath to preserve the quality of the slice. We observed that three of four $DsRed^+$ cells were positive for NG2 (not shown). However, one $DsRed^+$ cell with no detectable Na^+ currents after leak subtraction was $NG2^-$ (Fig. 3B). Taken together, our results indicate that the large majority, if not all, of NG2 cells of the somatosensory cortex express voltage-gated Na^+ channels regardless the age of the animal and the presence of GABAergic synaptic inputs. However, we cannot completely exclude that a small proportion of NG2 cells lacking Na^+ currents exist in other brain regions.

To test for the ability of NG2 cells to fire action potentials, we recorded the response to injections of depolarizing currents in a KCl-based intracellular solution. A single immature spike was elicited in a large proportion of NG2 cells; no discharge of action potentials in these cells was observed (Fig. 2E). When present, spikes were rudimentary in nature and resembled those described by others in NG2 cells of the neocortex (Chittajallu et al. 2004; Ge et al. 2009), i.e. they had a depolarized threshold potential, most often grew in size as the depolarization increased, and showed a small amplitude (Fig. 2E1, inset). In agreement with the apparent (but false) decrease of Na^+ currents during development, fewer cells showed immature spikes in the fourth than in the second postnatal week ($n = 11$ and $n = 24$ recorded cells, respectively, Fig. 2E). We can thus conclude that different classes of NG2 cells cannot be distinguished by the level of expression of Na^+ channels in the somatosensory cortex and that, even if Na^+ current amplitudes can reach 1 nA (mean: −600 ± 62 pA at −20 mV; from −133 pA to 1.17 nA; $n = 25$), NG2 cells are not able to elicit single or trains of genuine action potentials. This is in agreement with recent reports in other brain regions and using different transgenic mouse strains (De Biase et al. 2010; Etxeberria et al. 2010; Kukley et al. 2010). We could still argue that different electrophysiological properties reported for NG2 cells might be caused by the fact that observations come from different experimental models, i.e. transgenic mice vs. non-transgenic rats. Indeed, Clarke et al. (2010) recently showed that the mean size of this current in NG2 cells of rats is −0.9 nA and about 4.5-fold larger than in mouse NG2 cells. Yet, Kukley et al. (2007) reported in the same species, a mean Na^+ current amplitude of −0.3 nA. In addition, Chittajallu et al. (2004) showed in CNP-eGFP transgenic mice that the mean Na^+ current amplitude of cells eliciting immature spikes in the neocortex is around −0.9 nA (in our case, one-third of

cortical NG2 cells also reaches this amplitude regardless of the age of the animal in NG2-DsRed mice). Therefore, although different animals and brain regions may influence in some extent the size of Na^+ currents in NG2 cells, discrepancies regarding its amplitude and the ability of these cells to generate genuine action potentials cannot be explained solely by differences in the experimental model. Further experiments in which post-recording immunostainings against NG2 or PDGFαR are performed in each recorded cell are probably needed. Nevertheless, it has to be considered that NG2 cells do not have the same electrophysiological properties in young and adult mice (Kressin et al. 1995; Zhou et al. 2006; Velez-Fort et al. 2010), which strengthens the idea that distinct types of NG2 cells, probably playing different roles, emerge during postnatal development. Indeed, it is more and more likely that NG2 cells constitute a heterogeneous group of cells comprising distinct subpopulations that vary according to the postnatal developmental stage and brain region (Butt et al. 2002; Mallon et al. 2002; Nishiyama et al. 2009). The electrophysiological criteria that allow for a reliable identification of different NG2 cell classes are still unclear.

Different modes of spillover transmission between neurones and NG2 cells

In the last years, most of the studies on neurone-NG2 cell interactions in the brain have been focused on understanding the direct quantal transmission of glutamate on NG2 cells, leaving aside other neuronal signalling mechanisms that might be important or even predominant. In that sense, spillover transmission not only is a prevailed mode of communication between neurones and astrocytes (see Introduction) but also operates among neurones influencing neuronal network functioning (Szapiro & Barbour, 2009). Here we evaluate the existence of different modes of spillover transmission between neurones and NG2 cells.

Recently, we studied the GABAergic activity of NG2 cells in the barrel cortex during the first postnatal month (Velez-Fort et al. 2010), a period in which physiological myelination occurs in deep cortical layers. By using whole-cell recordings and classical calcium imaging at different postnatal stages, we demonstrated that more than 90% of fast spontaneous synaptic currents recorded in cortical NG2 cells are GABAergic and sensitive to $GABA_A$ receptor antagonists (Velez-Fort et al. 2010). Surprisingly, these functional synaptic inputs are completely lost after the second postnatal week, as revealed by the absence of spontaneous and miniature events. Despite the loss of functional GABAergic synapses, transient $GABA_A$-mediated currents are still detected in the adult upon low frequency stimulation of neuronal fibres. These evoked currents show very slow kinetics compared to those recorded in young animals, suggesting that they are not synaptic in the adult. Tanaka et al. (2009) recently reported similar slow transient GABAergic currents in $nestin^+/NG2^+$ cells of the adult neocortex, but the authors attributed these currents to genuine synaptic responses. Pharmacological experiments allowed us to establish that the concentration of GABA reaching $GABA_A$ receptors in NG2 cells of older mice is lower than that reaching synaptic receptors. By using the voltage jump technique, we also showed that slow kinetics of GABAergic responses in NG2 cells do not result from signal filtering, confirming that evoked currents are purely extrasynaptic. GABAergic transmission in the adult thus relies on pure GABA spillover (Fig. 1C). Because of its unique properties, this form of spillover transmission between interneurones and NG2 cells can be considered a novel mode of neurone-glia communication that allows for a transient and relatively fast communication compared to other forms of volume transmission. Interestingly, recent reports have also described the existence of a similar mode of communication in neurones of cerebellum, neocortex and hippocampus (Szapiro & Barbour, 2007; Markwardt et al. 2009; Olah et al. 2009). Therefore, this form of communication is not exclusive for glia, but also exists between different neuronal types and brain regions. This spillover transmission, which does not require direct synaptic junctions, implies that GABA diffuses over relatively short distances from neuronal synapses. The anatomical modifications occurring at interneurone–NG2 cell junctions during postnatal cortical development remain unresolved. These changes could be complex if they involve a transition from a synaptic (Fig. 1A) to an extrasynaptic junction (Fig. 1C) and may implicate a profound reorganization of NG2 cell processes in the extracellular environment. Confocal and ultrastructural analysis will thus be necessary to unravel developmental morphological changes.

In addition to AMPA and $GABA_A$ receptors, NG2 cells in tissue preparations are known to express other functional receptors on their membranes, such as NMDA, kainate, nicotinic and purinergic receptors (Karadottir et al. 2005; Kukley & Dietrich, 2009; Velez-Fort et al. 2009; Hamilton et al. 2010). As quantal currents in NG2 cells are mediated solely by either AMPA or $GABA_A$ receptors, these receptors are most probably activated at a location distant from direct quantal release sites. A relevant example of extrasynaptic receptors is that of NMDA receptors in white matter regions reported to be activated by high extrasynaptic levels of glutamate, as those reached during ischaemic conditions (Karadottir et al. 2005). NMDA receptors of NG2 cells have an unusual subunit composition containing NR1, NR2C and NR3 that is weakly blocked by extracellular Mg^{2+} and probably allows glutamate to evoke NMDA receptor-mediated currents at resting potentials, contributing to tissue damage during ischaemia (Karadottir et al. 2005). Therefore, these receptors must be specialized to discern changes in the ambient extracellular glutamate concentration, especially when the uptake glutamate system is overwhelmed and pathologically high levels of

glutamate are accumulated in the extracellular space. Kainate receptors are another case of glutamate receptors that are most likely expressed at extrasynaptic sites, as demonstrated in a recent report showing the functional expression of non-GluR5 kainate receptors in NG2 cells of the hippocampus (Kukley & Dietrich, 2009). NMDA and kainate receptors are therefore two glutamate receptor subtypes potentially activated by widespread diffusion of transmitters. However, the activation mode and the excitatory action of these receptors in NG2 cells under physiological conditions remain to be established.

Little is known about the expression and mode of activation of receptors for neurotransmitters other than glutamate and GABA in NG2 cells, but some examples exist in the literature. We recently demonstrated the functional expression of highly Ca^{2+}-permeable α7 nicotinic receptors in NG2 cells of the hippocampus, suggesting the existence of cholinergic neurone-to-NG2 cell signalling in the grey matter (Velez-Fort et al. 2009). However, the stimulation of neuronal hippocampal cholinergic afferents, in the presence of the anticholinesterase agent eserine, failed to induce any synaptic nicotinic receptor-mediated current in NG2 cells. Although the desensitization or the low density of receptors may prevent the detection of synaptic currents, the most plausible activation mode of nicotinic receptors in NG2 cells is by an extrasynaptic release of transmitter (Fig. 1D). Indeed, it is believed that a majority of hippocampal cholinergic release sites are non-synaptic and contribute to diffuse volume transmission in neurones (Dani & Bertrand, 2007). In addition, the immunolabelling of acetylcholinetransferase, the enzyme responsible for the production of ACh, reveals that varicosities containing ACh in the hippocampus may be in front of glial cell processes (Descarries et al. 1997). NG2 cells in an isolated optic nerve preparation respond to adenosine triphosphate (ATP) by elevations of the intracellular Ca^{2+} concentration mediated by P2Y1 and P2X7 purinergic receptors (Wigley et al. 2007; Hamilton et al. 2010). The release of ATP is triggered by nerve stimulation and the amplitude and duration of Ca^{2+} signals in NG2 cells increase in parallel with increased stimulus strength, following neuronal activity (Hamilton et al. 2010). It is possible that nerve axons release ATP by a non-synaptic mechanism at sites where axonal membranes are in close contact with NG2 cell processes (Fig. 1D; Hamilton et al. 2010). However, as axonal action potentials stimulate the release of ATP from astrocytes and NG2 cells enwrap short segments of astrocytic processes in the optic nerve (Hamilton et al. 2008, 2010), astrocytes constitute another potential source of ATP generating NG2 cell signals. This leaves open the interesting possibility that astrocytes are implicated in a tripartite communication system with neurones and NG2 cells in the brain. Indeed, ATP, glutamate and GABA are three major gliotransmitters released by astrocytes (Angulo et al. 2008; Halassa & Haydon, 2010) that could activate extrasynaptic receptors of NG2 cells and influence their cell function. NMDA and kainate receptors are potential targets of glutamate released by astrocytes, as these glial cells have been reported to maintain the ambient extracellular glutamate concentration (Jabaudon et al. 1999; Cavelier & Attwell, 2005; Le Meur et al. 2007).

In addition to functional receptors reported in NG2 cells, the expression of mGluR5 metabotropic glutamate receptors in O4-positive cells of the rat corpus callosum has been demonstrated by immunocytochemical analysis (Luyt et al. 2003). Considering that almost 80% of NG2 cells are labelled by O4 in this region (Kukley et al. 2007), we can infer that NG2 cells express the mGluR5 protein. The α1A and α1B adrenergic receptors also co-localize with NG2-positive cells in the mouse cerebral cortex (Papay et al. 2004, 2006). α1-Adrenergic and mGluR5 receptors are likely to be activated extrasynaptically by neurotransmitters spreading from neuronal synapses or from non-synaptic release sites. Many other receptors have been observed in cultured oligodendrocyte precursors (for instance, Belachew & Gallo, 2004), but their expression *in situ* has not been demonstrated as yet. It would be interesting to establish to what extent these receptors are functionally expressed in NG2 cells in brain slices and their mechanisms of activation.

Concluding remarks

Since the exciting discovery of functional synaptic contacts in NG2 cells, many efforts have been focused on understanding the functioning of these unique synapses of the brain. This research has motivated the study of signalling mechanisms between neurones and NG2 cells in pathophysiological conditions and increased the interest of physiologists working in neurone–glia interactions for this glial cell type. However, our present knowledge of neurone-to-NG2 cell communication in the brain remains relatively limited and the reasons why neurones signal to NG2 cells are still enigmatic. This communication appears as complex as for neurones with a variety of possible signalling mechanisms, from very local (synaptic) to a widespread diffusion of neurotransmitters (volume transmission). The answer to the question 'is neuronal communication with NG2 cells synaptic or extrasynaptic?' is that it is probably both. However, the predominance of synaptic over extrasynaptic transmission in distinct physiological situations and brain regions as well as the roles of different communication modes remain elusive.

Acknowledgements

We thank Etienne Audinat for helpful comments on the manuscript and Dwight E. Bergles for the gift of NG2-DsRed transgenic mice. We also thank Julia Montanaro and Andréa Virolle for technical assistance with immunostainings and the SCM Imaging Platform of the St-Pères Biomedical Sciences site of Paris Descartes University. This work was supported by grants

from Agence Nationale de la Recherche (ANR) and Fondation pour l'aide à la recherche sur la Sclérose en Plaques (ARSEP). P.P.M. was supported by a fellowship from Ecole des Neurosciences de Paris (ENP) and M.V.-F. by fellowships from Région Ile-de-France and Ligue Française contre la Sclérose en Plaques (LFSEP).

References

Alix JJ, Dolphin AC, Fern R (2008) Vesicular apparatus, including functional calcium channels, are present in developing rodent optic nerve axons and are required for normal node of Ranvier formation. *J Physiol* **586**, 4069–4089.

Angulo MC, Le Meur K, Kozlov AS, et al. (2008) GABA, a forgotten gliotransmitter. *Prog Neurobiol* **86**, 297–303.

Baracskay KL, Duchala CS, Miller RH, et al. (2002) Oligodendrogenesis is differentially regulated in gray and white matter of jimpy mice. *J Neurosci Res* **70**, 645–654.

Belachew S, Gallo V (2004) Synaptic and extrasynaptic neurotransmitter receptors in glial precursors' quest for identity. *Glia* **48**, 185–196.

Bergles DE, Roberts JD, Somogyi P, et al. (2000) Glutamatergic synapses on oligodendrocyte precursor cells in the hippocampus. *Nature* **405**, 187–191.

Bergles DE, Jabs R, Steinhauser C (2010) Neuron-glia synapses in the brain. *Brain Res Rev* **63**, 130–137.

Butt AM, Kiff J, Hubbard P, et al. (2002) Synantocytes: new functions for novel NG2 expressing glia. *J Neurocytol* **31**, 551–565.

Cavelier P, Attwell D (2005) Tonic release of glutamate by a DIDS-sensitive mechanism in rat hippocampal slices. *J Physiol* **564**, 397–410.

Chittajallu R, Aguirre A, Gallo V (2004) NG2-positive cells in the mouse white and grey matter display distinct physiological properties. *J Physiol* **561**, 109–122.

Clarke L, Hamilton NB, Young KM, et al. (2010) *The Distribution and Excitability of Two Types of Oligodendrocyte Precursor Cell in White and Grey Matter*. San Diego: Neuroscience 2010 (SfN).

Dani JA, Bertrand D (2007) Nicotinic acetylcholine receptors and nicotinic cholinergic mechanisms of the central nervous system. *Annu Rev Pharmacol Toxicol* **47**, 699–729.

De Biase LM, Nishiyama A, Bergles DE (2010) Excitability and synaptic communication within the oligodendrocyte lineage. *J Neurosci* **30**, 3600–3611.

Descarries L, Gisiger V, Steriade M (1997) Diffuse transmission by acetylcholine in the CNS. *Prog Neurobiol* **53**, 603–625.

Etxeberria A, Mangin JM, Aguirre A, et al. (2010) Adult-born SVZ progenitors receive transient synapses during remyelination in corpus callosum. *Nat Neurosci* **13**, 287–289.

Gallo V, Mangin JM, Kukley M, et al. (2008) Synapses on NG2-expressing progenitors in the brain: multiple functions? *J Physiol* **586**, 3767–3781.

Ge WP, Yang XJ, Zhang Z, et al. (2006) Long-term potentiation of neuron-glia synapses mediated by Ca^{2+}-permeable AMPA receptors. *Science* **312**, 1533–1537.

Ge WP, Zhou W, Luo Q, et al. (2009) Dividing glial cells maintain differentiated properties including complex morphology and functional synapses. *Proc Natl Acad Sci U S A* **106**, 328–333.

Halassa MM, Haydon PG (2010) Integrated brain circuits: astrocytic networks modulate neuronal activity and behavior. *Annu Rev Physiol* **72**, 335–355.

Hamilton N, Vayro S, Kirchhoff F, et al. (2008) Mechanisms of ATP- and glutamate-mediated calcium signaling in white matter astrocytes. *Glia* **56**, 734–749.

Hamilton N, Vayro S, Wigley R, et al. (2010) Axons and astrocytes release ATP and glutamate to evoke calcium signals in NG2-glia. *Glia* **58**, 66–79.

Jabaudon D, Shimamoto K, Yasuda-Kamatani Y, et al. (1999) Inhibition of uptake unmasks rapid extracellular turnover of glutamate of nonvesicular origin. *Proc Natl Acad Sci U S A* **96**, 8733–8738.

Jabs R, Pivneva T, Huttmann K, et al. (2005) Synaptic transmission onto hippocampal glial cells with hGFAP promoter activity. *J Cell Sci* **118**, 3791–3803.

Karadottir R, Cavelier P, Bergersen LH, et al. (2005) NMDA receptors are expressed in oligodendrocytes and activated in ischaemia. *Nature* **438**, 1162–1166.

Karadottir R, Hamilton NB, Bakiri Y, et al. (2008) Spiking and nonspiking classes of oligodendrocyte precursor glia in CNS white matter. *Nat Neurosci* **11**, 450–456.

Kressin K, Kuprijanova E, Jabs R, et al. (1995) Developmental regulation of Na^+ and K^+ conductances in glial cells of mouse hippocampal brain slices. *Glia* **15**, 173–187.

Kukley M, Dietrich D (2009) Kainate receptors and signal integration by NG2 glial cells. *Neuron Glia Biol* **5**, 13–20.

Kukley M, Capetillo-Zarate E, Dietrich D (2007) Vesicular glutamate release from axons in white matter. *Nat Neurosci* **10**, 311–320.

Kukley M, Kiladze M, Tognatta R, et al. (2008) Glial cells are born with synapses. *FASEB J* **22**, 2957–2969.

Kukley M, Nishiyama A, Dietrich D (2010) The fate of synaptic input to NG2 glial cells: neurons specifically downregulate transmitter release onto differentiating oligodendroglial cells. *J Neurosci* **30**, 8320–8331.

Le Meur K, Galante M, Angulo MC, et al. (2007) Tonic activation of NMDA receptors by ambient glutamate of non-synaptic origin in the rat hippocampus. *J Physiol* **580**, 373–383.

Lin SC, Bergles DE (2004) Synaptic signaling between GABAergic interneurons and oligodendrocyte precursor cells in the hippocampus. *Nat Neurosci* **7**, 24–32.

Lin SC, Huck JH, Roberts JD, et al. (2005) Climbing fibre innervation of NG2-expressing glia in the mammalian cerebellum. *Neuron* **46**, 773–785.

Luyt K, Varadi A, Molnar E (2003) Functional metabotropic glutamate receptors are expressed in oligodendrocyte progenitor cells. *J Neurochem* **84**, 1452–1464.

Mallon BS, Shick HE, Kidd GJ, et al. (2002) Proteolipid promoter activity distinguishes two populations of NG2-positive cells throughout neonatal cortical development. *J Neurosci* **22**, 876–885.

Mangin JM, Kunze A, Chittajallu R, et al. (2008) Satellite NG2 progenitor cells share common glutamatergic inputs with associated interneurons in the mouse dentate gyrus. *J Neurosci* **28**, 7610–7623.

Markwardt SJ, Wadiche JI, Overstreet-Wadiche LS (2009) Input-specific GABAergic signaling to newborn neurons in adult dentate gyrus. *J Neurosci* **29**, 15063–15072.

Matsui K, Jahr CE (2003) Ectopic release of synaptic vesicles. *Neuron* **40**, 1173–1183.

Matsui K, Jahr CE (2004) Differential control of synaptic and ectopic vesicular release of glutamate. *J Neurosci* **24**, 8932–8939.

Matsui K, Jahr CE, Rubio ME (2005) High-concentration rapid transients of glutamate mediate neural-glial communication via ectopic release. *J Neurosci* **25**, 7538–7547.

Muller J, Reyes-Haro D, Pivneva T, et al. (2009) The principal neurons of the medial nucleus of the trapezoid body and $NG2^+$ glial cells receive coordinated excitatory synaptic input. *J Gen Physiol* **134**, 115–127.

Nishiyama A, Komitova M, Suzuki R, et al. (2009) Polydendrocytes (NG2 cells): multifunctional cells with lineage plasticity. *Nat Rev Neurosci* **10**, 9–22.

Olah S, Fule M, Komlosi G, et al. (2009) Regulation of cortical microcircuits by unitary GABA-mediated volume transmission. *Nature* **461**, 1278–1281.

Papay R, Gaivin R, McCune DF, et al. (2004) Mouse alpha1B-adrenergic receptor is expressed in neurons and NG2 oligodendrocytes. *J Comp Neurol* **478**, 1–10.

Papay R, Gaivin R, Jha A, et al. (2006) Localization of the mouse alpha1A-adrenergic receptor (AR) in the brain: alpha1AAR is expressed in neurons, GABAergic interneurons, and NG2 oligodendrocyte progenitors. *J Comp Neurol* **497**, 209–222.

Pasti L, Volterra A, Pozzan T, et al. (1997) Intracellular calcium oscillations in astrocytes: a highly plastic, bidirectional form of communication between neurons and astrocytes *in situ*. *J Neurosci* **17**, 7817–7830.

Perea G, Araque A (2005) Glial calcium signaling and neuron-glia communication. *Cell Calcium* **38**, 375–382.

Schummers J, Yu H, Sur M (2008) Tuned responses of astrocytes and their influence on hemodynamic signals in the visual cortex. *Science* **320**, 1638–1643.

Szapiro G, Barbour B (2007) Multiple climbing fibres signal to molecular layer interneurons exclusively via glutamate spillover. *Nat Neurosci* **10**, 735–742.

Szapiro G, Barbour B (2009) Parasynaptic signalling by fast neurotransmitters: the cerebellar cortex. *Neuroscience* **162**, 644–655.

Tanaka Y, Tozuka Y, Takata T, et al. (2009) Excitatory GABAergic activation of cortical dividing glial cells. *Cereb Cortex* **19**, 2181–2195.

Velez-Fort M, Audinat E, Angulo MC (2009) Functional alpha 7-containing nicotinic receptors of NG2-expressing cells in the hippocampus. *Glia* **57**, 1104–1114.

Velez-Fort M, Maldonado PP, Butt AM, et al. (2010) Postnatal switch from synaptic to extrasynaptic transmission between interneurons and NG2 cells. *J Neurosci* **30**, 6921–6929.

Wang X, Lou N, Xu Q, et al. (2006) Astrocytic Ca^{2+} signaling evoked by sensory stimulation *in vivo*. *Nat Neurosci* **9**, 816–823.

Wigley R, Hamilton N, Nishiyama A, et al. (2007) Morphological and physiological interactions of NG2-glia with astrocytes and neurons. *J Anat* **210**, 661–670.

Zhou M, Schools GP, Kimelberg HK (2006) Development of $GLAST^+$ astrocytes and $NG2^+$ glia in rat hippocampus CA1: mature astrocytes are electrophysiologically passive. *J Neurophysiol* **95**, 134–143.

Ziskin JL, Nishiyama A, Rubio M, et al. (2007) Vesicular release of glutamate from unmyelinated axons in white matter. *Nat Neurosci* **10**, 321–330.

Alterations of synaptic connectivity of oligodendrocyte progenitor cells following central nervous system demyelination

Aurélia Sahel[1, 2, 3] *, Fernando C. Ortiz[4, 5, 6] *, Christophe Kerninon[1, 2, 3], Paloma P. Maldonado[4, 5, 6], Magali Frah[1, 2, 3], María Cecilia Angulo[4, 5, 6#], Brahim Nait Oumesmar[1, 2, 3, 7#]

[1] INSERM U.975, Centre de Recherche-Institut du Cerveau et de la Moelle Epinière, Paris, France, [2] UPMC, UMR-S975, Paris, France [3] CNRS UMR 7225, Paris, France [4] INSERM U603, Paris, France; [5] CNRS UMR 8154, Paris, France; [6] Université Paris Descartes, Sorbonne Paris Cité, Paris, France ; [7] AP-HP, Service de Neuropathologie, Hôpital Pitié-Salpêtrière, Paris, France.

Submitted to Proceedings of the National Academy of Sciences of the United States of America

Oligodendrocyte precursor cells (OPCs) are a major source of remyelinating oligodendrocytes. While OPCs are normally innervated by unmyelinated axons, the fate of such synaptic contacts in demyelinated lesions is still unclear. Using a model of lysolecithin (LPC)-induced focal demyelination of corpus callosum and mouse strains expressing fluorescent reporters, we show that newly generated OPCs inside the lesion are born without synapses during their active phase of proliferation, but gain synaptic inputs during remyelination. Patch-clamp recordings, electron microscopy and 3D confocal reconstructions of axon-OPC contacts immunostained with the vesicular glutamate transporter vGluT1 reveal a decrease in glutamatergic innervation of OPCs early after demyelination. Virtually all new-born OPCs stained with EdU (50-ethynyl-20 -deoxyuridine) lack synaptic contacts. At the end of the proliferation phase, the proportion of innervated OPCs rapidly recovered, although the frequency of spontaneous synaptic currents never reaches control levels. Once the phase of differentiation is advanced, a large number of vGluT1 immunopositive puncta per OPC highly increases while the frequency of synaptic activity was still low in the lesion, implying that not all vGluT1 positive axon-OPC contacts correspond to functional synapses at this stage of the remyelination process. Importantly, vGluT1 immunopositive puncta per OPC also increased in active regions of multiple sclerosis (MS) lesions. In conclusion, demyelination and remyelination are associated with major changes in functional synapses and axon-NG2 cell contacts with OPCs in a mouse model of demyelination and in MS disease.

NG2 cells | Oligodendrocyte | Synapses | Demyelination | Multiple Sclerosis

Significance Statement

Myelinating oligodendrocytes derive from oligodendrocyte precursor cells (OPCs) during development of the central nervous system. OPCs also persist in the adult, where they constitute the major source of remyelinating oligodendrocytes after demyelination. These non-neuronal cells are unique in the brain by their ability to receive functional synaptic inputs from neurons under normal conditions. However, whether neuron-OPC synapses are regulated following demyelination remains unclear. Here, we showed that newly-generated OPCs are born without synapses during their active proliferation after demyelination, but gain synapses during remyelination. We also demonstrated a regulation of neuronal-OPC contacts in multiple slcerosis lesions. Hence, major alterations of the synaptic connectivity between neurons and OPCs occur following demyelination, which could have a therapeutic relevance in demyelinating diseases.

INTRODUCTION

Myelinating oligodendrocytes in the brain are derived from oligodendrocyte precursor cells (OPCs) expressing the proteoglycan NG2 (NG2 cells). OPCs are highly abundant at birth, but also persist in the adult where they represent the main proliferating cell type (1). OPCs in both grey and white matter receive functional GABAergic and glutamatergic synapses from neurons but their role remains unclear (2, 3). Initial studies in culture demonstrated that prolonged AMPA receptor activation greatly reduced the number of proliferative OPCs (4). Consistent with a role of glutamate in inhibiting OPC proliferation, sensory deprivation of whiskers reduces thalamocortical synaptic inputs of OPCs and increases their proliferation in the developing barrel cortex (5). These studies might suggest that glutamatergic synapses between neurons on OPCs inhibit proliferation. However, glutamatergic innervation of mitotic OPCs during development is maintained and transferred to their progeny during cell division (6, 7).

In the *corpus callosum*, unmyelinated axons establish glutamatergic synapses with OPCs as early as the first postnatal week and connectivity increases in the adult (3, 8, 9). After a demyelinating injury, demyelinated axons also form functional synapses with a minor pool of OPCs derived from the subventricular zone (SVZ) that contribute to oligodendrocyte regeneration (10). However, whether all OPCs within demyelinated lesions, are contacted by synapses remains elusive. The regulation and relevance of axon-OPC synapses after demyelination is also unknown. Here we use a model of lysolecithin (LPC)-induced

Significance

Myelinating oligodendrocytes derive from oligodendrocyte precursor cells (OPCs) during development of the central nervous system. OPCs also persist in the adult, where they constitute the major source of remyelinating oligodendrocytes after demyelination. These non-neuronal cells are unique in the brain by their ability to receive functional synaptic inputs from neurons under normal conditions. However, whether neuron-OPC synapses are regulated following demyelination remains unclear. Here, we showed that newly-generated OPCs are born without synapses during their active proliferation after demyelination, but gain synapses during remyelination. We also demonstrated a regulation of neuronal-OPC contacts in multiple slcerosis lesions. Hence, major alterations of the synaptic connectivity between neurons and OPCs occur following demyelination, which could have a therapeutic relevance in demyelinating diseases.

Reserved for Publication Footnotes

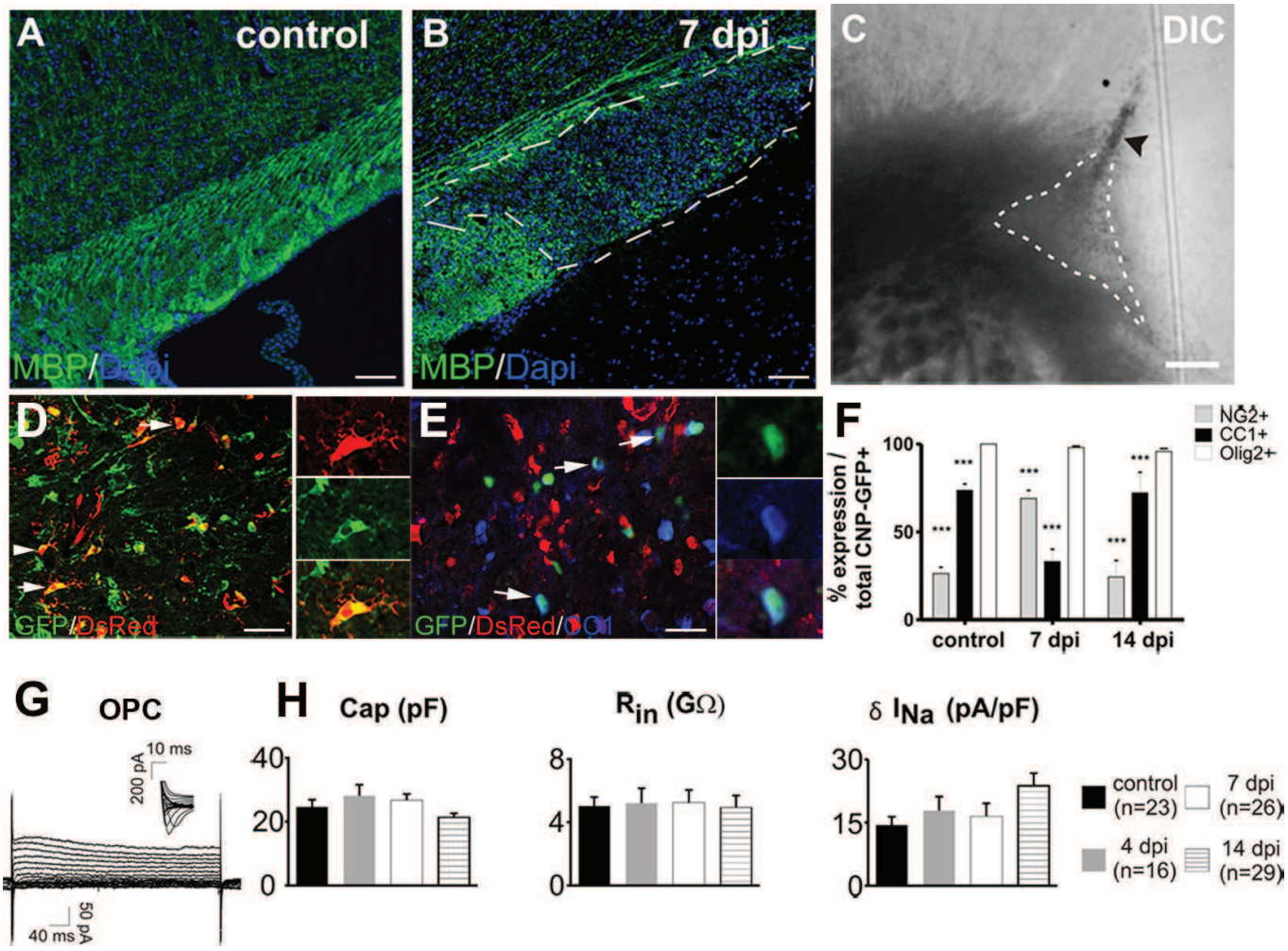

Fig. 1. Identification of OPCs in demyelinated lesions by using different transgenic mice.A-B. Sagittal slices of a healthy control brain (**A**) and an LPC-induced lesion in the mouse *corpus callosum* at 7dpi (**B**) stained with MBP (green) and DAPI (blue). **C**. DIC videomicroscopy of the LPC-induced lesion at 7dpi in a coronal acute *corpus callosum* slice. Note the trace of the injection pipette (arrowhead). **D**. OPCs were identified as DsRed+/GFP+ cells (**D**, arrows) in the NG2-DsRed;CNPase-GFP double transgenic mouse. **E**. Mature oligodendrocytes were identified as CC1+ cells (blue) and also expressed GFP (arrows) but not DsRed. **F**. Histogram showing the percentage of NG2+ and CC1+ cells within control and lesioned *corpus callosum* in CNPase-GFP animals (n≥ 4), ***p<0.001 with respect to Olig2 expression. **G**. Currents elicited in OPCs by voltage steps from +40 mV to -120 mV. Note the presence of I_{Na+} (inset). **H**. Capacitance, input resistance and Na^+ current density of OPCs recorded in control conditions and in lesions at different time points after LPC injection. Scale bars: (A, B), 50 µm; (**C**), 500 µm; (D, E), 20µm.

focal demyelination of the *corpus callosum* in mice expressing specific fluorescent reporters to assess the glutamatergic connectivity of OPCs. Our data show a drastic regulation of functional glutamatergic synapses and vGluT1 immunostained axon-OPC contacts in mouse LPC-induced demyelinating lesions and in MS disease.

RESULTS

Transgenic mouse strategy to identify OPCs in acute slices of the healthy and demyelinated mouse *corpus callosum*

Demyelinating lesions, induced by stereotaxic injection of LPC into the adult mouse *corpus callosum* of NG2-DsRed mice, were defined by the loss of myelin (Fig. 1A, B) and by an increased number of inflammatory cells. LPC-induced lesions were spontaneously remyelinated by OPCs, remyelination being almost complete at 30 days post-injection (dpi) (11). DIC videomicroscopy of acute brain slices, revealed the demyelinated area in the *corpus callosum* as a brighter region than the normal white matter surrounding it (Fig. 1C). Patch-clamp recordings of DsRed+ cells (excluding pericytes) in lesioned *corpus callosum* slices of these mice showed that half of DsRed+ cells showed a current profile characteristic of OPCs with outwardly rectifying steady-state currents and inward Na^+ currents (Fig. 1G and Fig. S1G), while the other half expressed a time and voltage-dependent outward current and lacked inward Na^+ currents, typical of activated microglia in cell culture (Fig. S1B and G) (12). To further investigate the expression of DsRed by microglia/macrophages in LPC-induced lesions, we confirmed the co-expression of the marker of microglia Iba1 with the DsRed by immunohistochemistry (Fig. S1A). We also performed patch-clamp recordings of DsRed+/GFP+ microglial cells on brain slices of NG2-DsRed;Cx3CR1-GFP mice (Fig. S1B).

To circumvent the expression of DsRed in microglia cells and therefore unambiguously identify OPCs in lesioned slices, we crossed the NG2-DsRed strain with the CNPase-GFP mouse line in which all cells of the oligodendroglial lineage express GFP (13). In double transgenic mice, patch-clamp recordings of DsRed+/GFP+ cells in demyelinating lesions revealed a current profile characteristic of OPCs with outwardly rectifying steady-state currents and inward Na^+ currents in more than 90% of recorded cells (Fig. 1G and Fig. S1G) (9, 14). The large majority of DsRed+/GFP+ cells in the lesion had the immunohistochem-

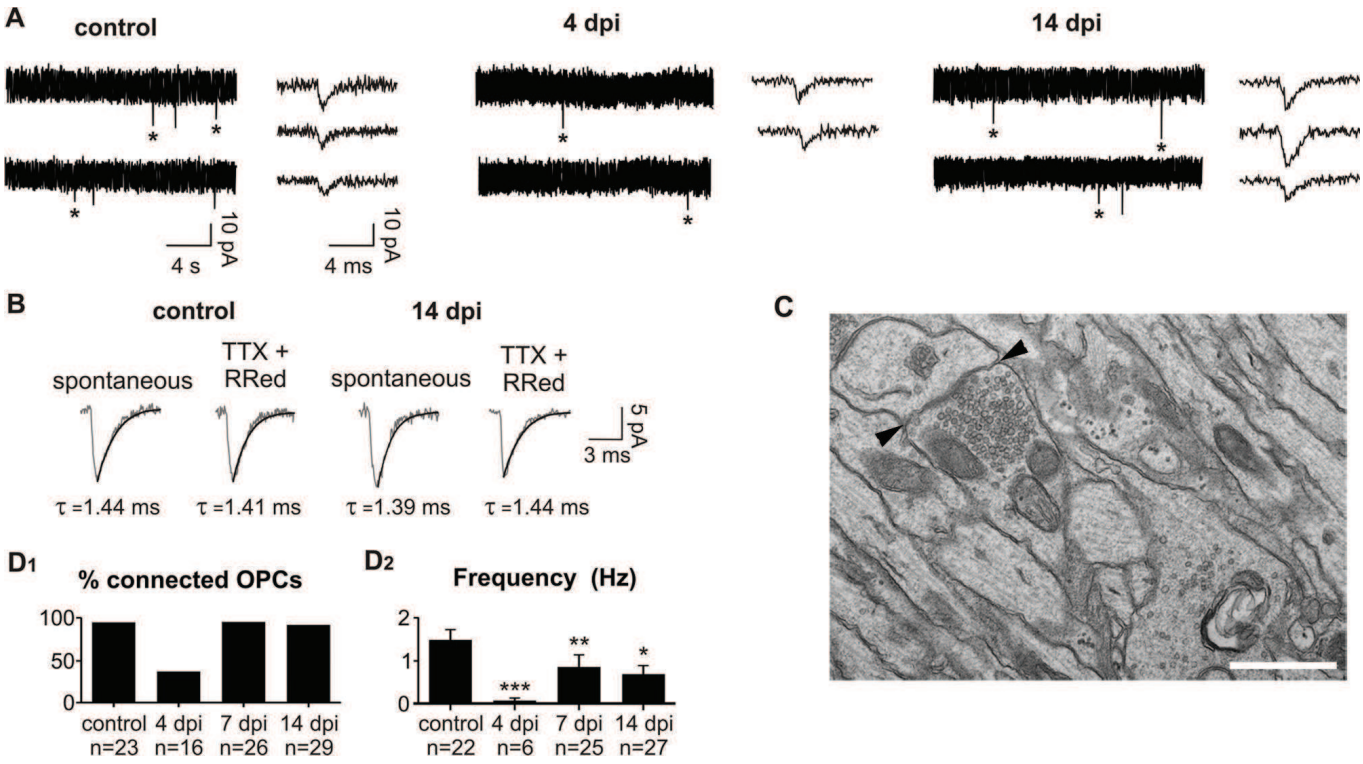

Fig. 2. Spontaneous glutamatergic synaptic currents of OPCs in demyelinated lesions.A. Spontaneous synaptic currents recorded at -90 mV from DsRed+/GFP+ OPCs from a control and at 4 and 14 dpi. Note the fast rise and decay times of individual currents (*) in all conditions (insets). **B**. Averaged time course of spontaneous and miniature synaptic events in OPCs held at -90 mV in a control and at 14 dpi. Miniature synaptic currents were recorded in the presence of 1 μM TTX and 75 μM ruthenium red as previously described (21). **C**. Electron-micrograph of a LPC lesion at 14 dpi, illustrating a typical synaptic contact between an axon and a putative OPC process, characterized by a rigid parallel apposition of membranes, electron-dense material and an accumulation of pre-synaptic vesicles (arrowheads). Note that this process lacks gliofilaments and lipofuscin granules, two typical features of astrocytes and microglia respectively. **D1**. Histrogram of the percentage of synaptically connected OPCs in control and at 4, 7 and 14 dpi. **D2**. Histrogram of the frequency of spontaneous synaptic currents observed in connected OPCs in control and at 4, 7 and 14 dpi. Cells without synaptic currents were excluded. *p<0.05, **p<0.01, ***p<0.001 respect to the control. Scale bar for C, 1 μm

ical phenotype of NG2+ OPCs (Fig. 1D) while DsRed-/GFP+ cells were labeled for CC1, a specific marker of differentiated oligodendrocytes (Fig. 1E). As expected, following LPC-induced demyelination (15), the population of DsRed+/GFP+ OPCs was largely increased at 7 dpi whereas a clear increase in differentiated DsRed-/GFP+/CC1+ oligodendrocytes was detected at 14 dpi (Fig. 1F). Hence, in LPC-induced lesions, the NG2-DsRed;CNPase-GFP mouse line allows the unequivocal identification of OPCs from microglia and mature oligodendrocytes by the simultaneous expression of both DsRed and GFP.

However in healthy adult brain of NG2-DsRed mouse, only pericytes expresses DsRed, thus preventing the use of this line to clearly identify OPCs in control (Fig S2). To by-pass this limitation, we used the PDGFRα-GFP mouse line. Patch-clamp recordings from the non-demyelinated *corpus callosum* of PDGFRα-GFP mice revealed that 52% of recorded GFP+ cells had the typical current profile of OPCs; the remaining 48% showing the classical linear phenotype of mature oligodendrocytes (Fig. S1D and G). In addition, immunohostochemical analysis showed that only 50% of GFP+ cells expressed NG2 (Fig. S1C and F), while the remaining cells were mature CC1+ oligodendrocytes (Fig. S1F) (16). Nevertheless, patch-clamp recordings in the demyelinated *corpus callosum* revealed current profiles typical of mature oligodendrocytes in 17 of 18 GFP+ cells recorded. Thus, this mouse line cannot be used to identify OPCs with accuracy following demyelination.

Our strategy was therefore to use NG2-DsRed;CNPase-GFP line for LPC-induced demyelination and the PDGFRα-GFP line as controls for electrophysiological experiments. Comparison of the capacitance, input resistance and sodium current density of OPCs in these mice between controls and at 4, 7 and 14 dpi showed no differences induced by LPC (Fig. 1H). Overall, our results indicate that appropriate transgenic lines are needed to overcome difficulties in OPC identification under normal and pathological conditions.

Regulation of axon-OPC contacts in LPC-induced demyelinating lesions

To study whether synaptic properties of reactivated OPCs are modified in the lesion, we recorded spontaneous and miniature currents of OPCs in slices from control animals and at 4, 7 and 14 dpi (Fig 2A). The averaged amplitude and kinetics of spontaneous synaptic events were similar at all time points (Fig. 2B and Fig. S3A). They were sensitive to the AMPA/Kainate receptor antagonist NBQX (Fig. S4A) and equally similar to those of miniature synaptic events recorded in the presence of TTX and ruthenium red (Fig. 2B and Fig. S3A). This implies that spontaneous synaptic events correspond to currents generated by release of single vesicles. Estimated quantal size was around -10 pA at a holding potential of -90 mV in both the control and lesioned brains (Fig. 2B and Fig. S3A1). Synaptic currents were never detected in either DsRed+/GFP- microglia or DsRed-/GFP+ oligodendrocytes (Fig. S4B). The existence of synaptic junctions in the lesioned tissue was corroborated by electron microscopy. Figure 2C illustrates the ultra-structural anatomy of a synaptic contact between an axon and a putative OPC process.

The proportion of innervated OPCs in control brain slices was 97% (Fig. 2D1). At 4 dpi this proportion fell to 38% and recovered to more than 90% at 7 and 14 dpi (Fig. 2D1). The

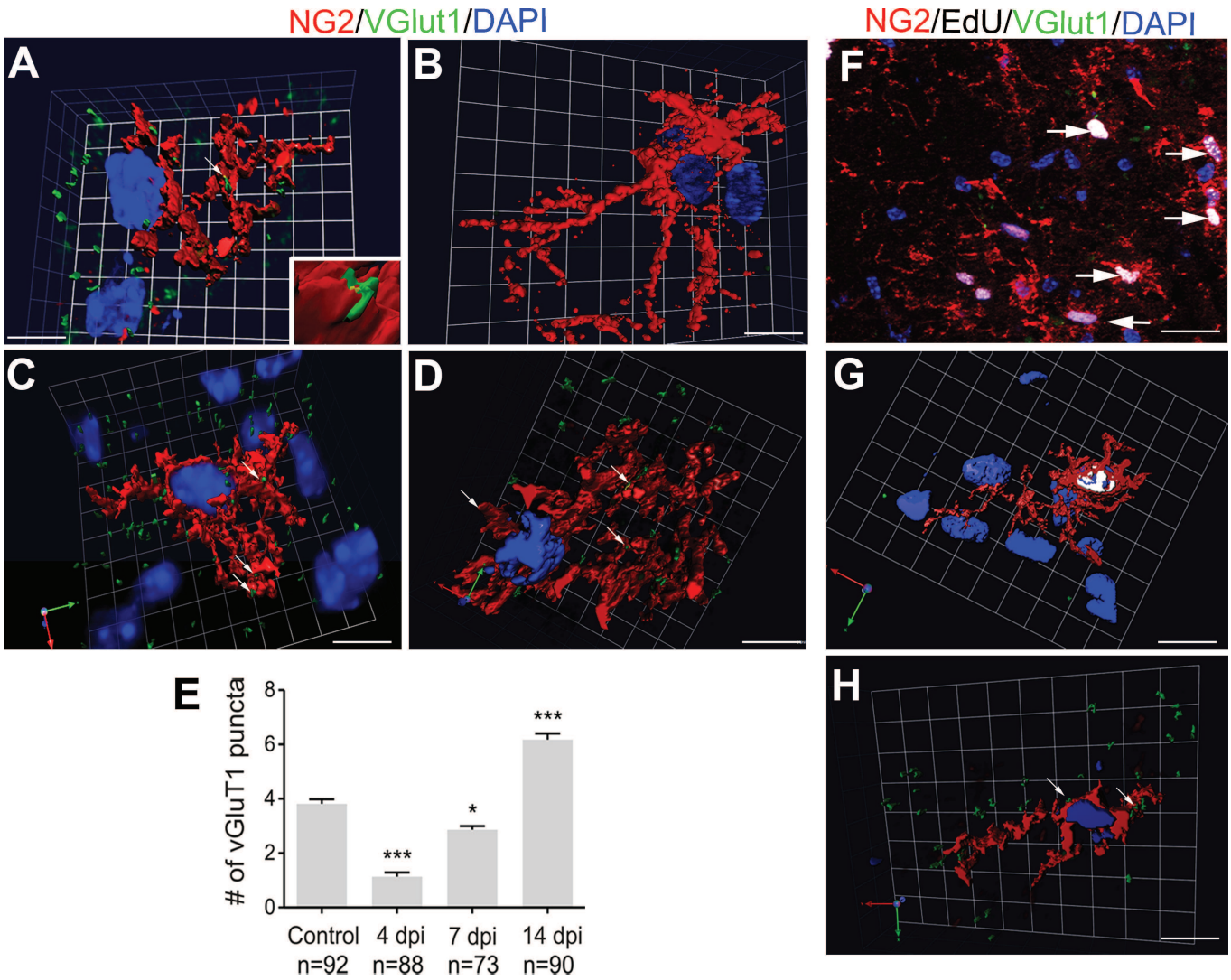

Fig. 3. Regulation of glutamatergic axon-OPC contacts in demyelinated lesions.A-D. 3D reconstruction of NG2 (red) and vGluT1 (green) labeling in control (**A**) and LPC-induced lesions at 4 (**B**), 7 (**C**), and 14 (**D**) dpi. Contacts are indicated by arrows. **E**. Histogram of the numbers of vGluT1+ puncta per OPC in controls and lesions at different time points after demyelination. *p<0.05; ***p<0.001 with respect to control. **F**. Triple immunolabeling for NG2 (red, arrows), EdU (white) and vGluT1 (green) in LPC lesion at 4 dpi. **G**. 3D reconstruction of a typical NG2+ (red), EdU+ (white) cell lacking vGlut1 contacts (green) within the lesion at 4 dpi. **H**. 3D reconstruction of an NG2+ EdU- cell in the non-demyelinated area of the *corpus callosum*. **p<0.01; ***p<0.001 with respect to control. Scale bars for A-D, H, I, 10 µm; G, 50 m; F, 2 µm. Nuclei were stained with Dapi in panels A-D, F-H.

frequency of spontaneous synaptic events recorded in innervated OPCs at 4 dpi was also greatly reduced (Fig. 2D2). Even though the proportion of connected OPCs recovered at 7 and 14 dpi, their frequency of synaptic currents did not increase back to control levels (Fig. 2D1 and 2D2). We asked whether this deficit might result from a lack of axonal conduction in the lesion after demyelination by analyzing extracellular compound action potentials (CAPs). Callosal simulation in control tissue elicited field responses characterized by two waves corresponding to myelinated and unmyelinated fibers (conduction velocities of 0.55±0.04 $m.s^{-1}$ and 0.24±0.02 $m.s^{-1}$, respectively; Fig. S3B). As expected for a lesion, only the CAP peak corresponding to unmyelinated and demyelinated axons could be detected at 4, 7 and 14 dpi (conduction velocity: 0.27±0.02 $m.s^{-1}$; Fig. S3B). These data demonstrate major changes in glutamatergic synaptic connectivity with OPCs in demyelinated lesions.

Anatomical studies were made to complement our physiological data. We quantified synaptic contacts in 3D confocal images of tissue co-labeled with vGluT1 and NG2. NG2+ microglial cells with a typical amoeboid morphology were excluded from the analysis (Fig. S1A). This data showed a drastic decrease in the number of axon-OPC contacts at 4 dpi and only a partial recovery at 7 dpi with respect to control (Fig 3A-D and E). OPCs proliferate massively in the lesion during the first days after injection (Fig. 1F). At this stage, most cells are weakly or not connected, suggesting that newly generated OPCs may receive few or no synaptic contacts (Fig. 2B1 and B2). We attempted to confirm our hypothesis, by injecting lesioned mice with EdU (5 injections of EdU at 2 hours intervals) before sacrifice at 4 dpi, in order to label actively proliferating cells in the lesion. Our results show that all EdU+/NG2+ OPCs within the lesion at 4 dpi virtually lacked vGluT1+ contacts (Fig. 3F and G). In contrast, NG2+ OPCs with vGluT1 puncta detected in the normal appearing white matter were not labeled with EdU (Fig. 3H). Finally, the number of vGluT1+ puncta per OPC highly increased at 14 dpi when the proportion of connected OPCs was similar to that of controls, but the frequency of synaptic activity was as low as that at 7 dpi in the lesion (Fig. 3D and E vs Fig. 2B2),

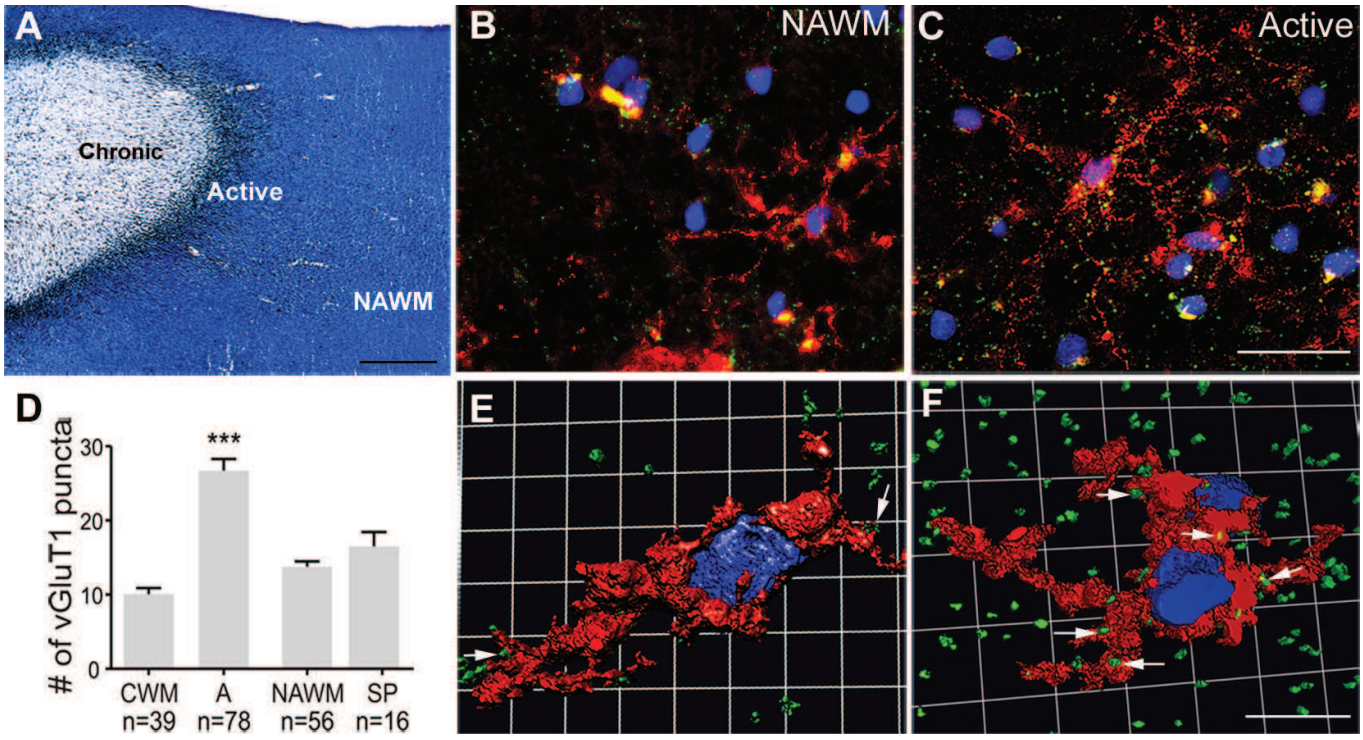

Fig. 4. Glutamatergic axon-OPC contacts in MS tissue.A. MS brain section stained with Luxol fast blue/MHCII (black), illustrating a typical chronic active lesion in the subcortical white matter. The different areas of the lesion were classified as active, chronic silent and normal appearing white matter (NAWM). Active borders of chronic active lesions were filled with MHCII+ macrophages/microglia, while chronic silent cores were devoid of labeling. **B, C**. NG2 (red) and vGluT1 (green) staining in the NAWM and in active border of a chronic active lesion. **D**. Histogram of the numbers of vGluT1+ puncta per NG2+ cells in control white matter (CWM) from non-neurological cases, in active borders of MS lesions, NAWM and shadow plaques. ***p<0.001 with respect to CWM. **E, F**. 3D reconstruction of NG2 cells (red) with vGluT1 puncta (green, arrows). Nuclei were stained with Dapi (blue) in B, C, E, F. Note the large number of vGluT1 puncta at active borders of the lesion. Scale bars for A, 1 mm; B, C, 50 µm; E, F, 10 µm. A, active lesions; SP, shadow plaques.

suggesting that not all vGluT1+ contacts with OPCs correspond to functional synapses at this stage.

In summary, these results show that reactivated OPCs in demyelinated lesions are not born with synapses, but gain synaptic inputs at the end of the active phase of rapid OPC proliferation. Once the differentiation phase is advanced, new vGluT1$^+$ contacts on OPCs, emerge in the lesion despite the lack of increase in synaptic activity.

Axon-OPC contacts are present in MS lesions

To assess a potential relevance of glutamatergic axon-OPC contacts in demyelinating human diseases, we analyzed vGluT1 and NG2 expression on post-mortem MS brain samples and non-neurological controls. MS lesions were first classed as active, chronic active, chronic silent, shadow plaques and normal appearing white matter (NAWM) according to Luxol-fast blue/MHCII staining. Figure 4A illustrates a typical chronic active lesion in the subcortical white matter with a typical silent core and an active border filled with MHCII+ microglia/macrophages. We found that vGluT1 puncta on OPCs were present in all regions of MS lesions (Fig. 4B and C). Using 3D reconstruction imaging of vGluT1 and NG2 staining, we quantified glutamatergic contacts per OPC in different types of MS lesions with respect to control white matter in non-neurological controls (Fig. 4E and F). Our data also revealed a significantly increased number of vGluT1 punctas per OPCs in active borders of MS lesions (Fig. 4D), correlating with increased differentiation of OPCs in these areas as previously reported (17).

DISCUSSSION

Sensory experience has recently been shown to control thalamic innervation of OPCs during early postnatal development of the barrel cortex (5). Here we show that synaptic connections with OPCs are also highly regulated after demyelination in the adult. This work was facilitated by our use of transgenic mouse lines permitting an unequivocal identification of reactivated OPCs in demyelinated lesions. Thus OPC innervation is a dynamic feature that changes according to neuronal activity and cell environment in different brain regions of adult animals. In line with the effect of sensory deprivation on the reduction of thalamocortical inputs and the increase in cortical OPC proliferation (5), our data show reactivated OPCs are poorly connected at 4 dpi during the active phase of proliferation in demyelinated lesions. Therefore, synaptic loss is concomitant with OPC proliferation in different conditions. A role for glutamatergic synaptic activity in preventing proliferation has been shown in organotypic slice cultures (4). However, dividing OPCs appear to retain afferent synapses and share them with daughter cells during postnatal development (6, 7). While mitotic OPCs have a reduced synaptic activity compared to non-mitotic cells (6), this discrepancy seems paradoxical. We also showed reactivated OPCs in LPC-induced lesions are not born with glutamatergic synapses, but gain synaptic inputs after their active phase of proliferation. Therefore, even if glutamatergic inputs to OPCs do not function exclusively to inhibiting proliferation, they seem likely to influence the process *via* glutamate release.

In addition to the early regulation of functional synapses of OPCs after demyelination, we showed that a large number of vGluT1+ puncta emerges during the phase of massive OPC differentiation in LPC lesions and active regions of MS lesions. The role of these new-formed vGluT1+ puncta on OPCs is unclear, but they may correspond to either non-functional synaptic junctions or non-synaptic release sites. Interestingly, Wake et al. (2011) recently showed that axonal glutamate release along OPC processes in culture regulates initial events in myelin formation *via* actions at metabotropic and NMDA glutamate receptors

(18), which are both present at non-synaptic sites on OPCs (see discussion in (19)). *In vivo*, glutamate release from non-synaptic axonal sites may contribute to induce the massive OPC differentiation and myelin regeneration in the lesion. A drastic increase in vGluT1+ puncta per OPC is also observed in active zones of MS lesions, characterized by a pronounced OPC differentiation (17), suggesting a regulation of axon-OPC contacts relevant for human OPC development in clinical MS. Further work will be needed to understand the functional role of these junctions and how they are involved in the human pathology.

MATERIALS AND METHODS

LPC-induced demyelination and EdU treatment. All experiments followed European Union and institutional guidelines for the care and use of laboratory animals. Histochemical and electrophysiological experiments were performed with transgenic mice used at adult heterozygous stages: NG2-DsRed (3), PDGFRα-GFP (20) and the CNPase-GFP (13). Wild-type C57BL/6 adult mice were also used for histological analysis. Focal demyelinating lesions were induced by a stereotaxic injection of 2 µl lysolecithin solution (LPC, Sigma, 1% LPC in 0.9% NaCl) in the *corpus callosum* in single or double adult (PN40-P70) transgenic mice anesthetized with Ketamine (0.1mg/g) and Xylazine (0.01mg/g) as previously described (coordinates: 1mm lateral, 1.3mm rostral to Bregma, and 1.7 mm depth to brain surface; Tepavcevic et al., 2011). Control mice were injected with saline solution only. Brains were analyzed at 4, 7 and 14 dpi. Edu (Invitrogen), a BrdU analogue, was injected intraperitoneally (75 mg/kg) every two hours for 10 hours before sacrifice at 4 dpi.

Acute slice preparation and electrophysiology. Acute coronal slices of LPC-injected *corpus callosum* (300 µm) were prepared from different mouse strains following previously described procedures (21). Patch-clamp recordings were performed at 33°C using an extracellular solution containing (in mM): 126 NaCl, 2.5 KCl, 1.25 NaH_2PO_4, 26 $NaHCO_3$, 20 glucose, 5 pyruvate, 2 $CaCl_2$ and 1 $MgCl_2$ (95% O_2, 5% CO_2). The intracellular solution contained (in mM): 130 Cs-gluconate, 10 4-aminopyridine, 5 tetraethylammonium chloride, 5 EGTA, 0.5 $CaCl_2$, 2 $MgCl_2$, 10 HEPES, 2 Na_2-ATP, 0.2 Na-GTP and 10 Na_2-phosphocreatine (pH ≈ 7.4, 296 mOsm). Potentials were corrected for a junction potential of -10mV. Whole-cell recordings of OPCs were obtained using Multiclamp 700B, filtered at 4 kHz and digitized at 20 kHz. Digitized data were analyzed off-line using pClamp10.1 software (Molecular Devices) and Spacan, a collection of IGOR Pro functions (22). The Na^+ current density for each cell was calculated by dividing the Na^+ current amplitude obtained after leak subtraction at –10 mV by its capacitance. Spontaneous and miniature synaptic currents were recorded at a holding potential of -90 mV and detected with a detection threshold of 3 times the noise standard deviation during a time window of 2 min for controls, 7 and 14 dpi and of 5 min for 4 dpi. Compound action potentials (CAPs) were obtained by stimulating with a monopolar tungsten electrode while a recording electrode (glass pipette) was placed in the lesion core (100 µs stimulations; Iso-Stim 01D, npi electronic GmbH, Tamm, Germany).

Immunohistochemistry and Electron Microscopy. Adult mice were anesthetized and transcardially perfused with 2% paraformaldehyde. Brains were dissected and postfixed for 2-4 h, cryoprotected in 20% sucrose and stained using standard protocols. The following primary antibodies were used: rabbit anti-NG2 (1:200; Chemicon), rabbit anti-Olig2 (1:200; Millipore), mouse anti-CC1 (1:100; Abcam), mouse anti-vGluT-1 (1:500; Millipore), rabbit anti-Iba1 (1:100; Millipore), rat anti-PDGFRα (1:200; Santa Cruz) and rabbit anti-MBP (1:100; Millipore). EdU labelling was detected with the Click-It™ Kit (Invitrogen). For electron microscopy analysis, brains were processed at 14 dpi as previously described (23) and imaged using a Siemens Electron Microscope.

Confocal microscopy analysis. Images were acquired using an Olympus confocal microscope, or a Zeiss apotome system (AxoVision LE Rel 4.5) and processed using Axovision, ImageJ, Adobe Photoshop/Illustrator (Adobe Systems) and Volocity (3D images; PerkinElmer) softwares. For quantitative analysis, the number or reporter+ cells, positive for each oligodendroglial stage specific marker, was counted and expressed as a percentage of reporter+ cells. To measure co-localization between vGluT1 puncta and NG2 labelling, 4-6 sections were analyzed in each animal (n=4-6 animals). For each section, a z-stack of 6 µm (0.2 µm z-step) was analysed using 3D reconstructions. Single OPCs were isolated and vGluT1 puncta were filtered according to a size ranging from 0.3-0.7 µm in diameter. We quantified the number of vGluT1+ puncta per OPC considering as contacting punctas, those that were at least 80% co-localized with NG2.

MS tissue samples. Post-mortem, snap-frozen, brain samples were obtained from the British MS Tissue Bank (collaboration with Dr R. Reynolds, London), including primary progressive (PP, 1 case), secondary progressive (SP, 6 cases), and relapsing progressive cases (RP, 1 case). All MS lesions were characterized using Luxol fast blue/MHCII (macrophages/microglia) staining and classified according to their inflammatory activity and on the basis of histological criteria of acute (active demyelination, myelin vacuolation, inflammation or edema, minor gliosis and vague margin), chronic lesions (no myelin vacuolation, absence of inflammation, gliosis, axonal loss and sharp margin) and shadow plaques (myelin pallor; (24). Immunohistochemistry of NG2 and vGluT1 was analysed as described above.

Statistical Analysis. All values are expressed as mean±SEM. Each data group was first subject to D'Agostino & Pearson normality Test. According to the data structure, multiple group comparisons were done using one way ANOVA or Kruskal-Wallis. Bonferroni or Dunn's multiple comparison post-hoc tests were used respectively. All statistical tests were performed with GraphPad Prism 5.00 software (GraphPad Software Inc., USA).

Acknowledgments.

We thank Richard Miles and Etienne Audinat for their helpful comments on the manuscript. This study was supported by grants from Agence Nationale de la Recherche (ANR), Fondation pour l'Aide à la Recherche sur la Sclérose en Plaques (ARSEP) and Fédération pour la recherche sur le cerveau (FRC). A.S. and P.P.M. were recipients of fellowships from the Ecole des Neurosciences de Paris (ENP). A.S. was also recipient of a fellowship from Fondation pour la Recherche Médicale (FRM). The team of B.N.O. is part of the ENP-Ile-de-France network. We thank the Salpêtrière Imaging PIPCS core facility for their fruitful advises on electron microscopy experiments and the "Investissements d'avenir" ANR-10-IAIHU-06. **Conflict of Interest**: None

1. Nishiyama A, Komitova M, Suzuki R, & Zhu X (2009) Polydendrocytes (NG2 cells): multifunctional cells with lineage plasticity. *Nat Rev Neurosci* 10, 9-22.
2. Bergles DE, Roberts JD, Somogyi P, & Jahr CE (2000) Glutamatergic synapses on oligodendrocyte precursor cells in the hippocampus. *Nature* 405, 187-191.
3. Ziskin JL, Nishiyama A, Rubio M, Fukaya M, & Bergles DE (2007) Vesicular release of glutamate from unmyelinated axons in white matter. *Nat Neurosci* 10, 321-330.
4. Yuan X, Eisen AM, McBain CJ, & Gallo V (1998) A role for glutamate and its receptors in the regulation of oligodendrocyte development in cerebellar tissue slices. *Development* 125, 2901-2914.
5. Mangin JM, Li P, Scafidi J, & Gallo V (2012) Experience-dependent regulation of NG2 progenitors in the developing barrel cortex. *Nat Neurosci* 15, 1192-1194.
6. Kukley M, Kiladze M, Tognatta R, Hans M, Swandulla D, Schramm J, & Dietrich D (2008) Glial cells are born with synapses. *Faseb J* 22, 2957-2969.
7. Ge WP, Zhou W, Luo Q, Jan LY, & Jan YN (2009) Dividing glial cells maintain differentiated properties including complex morphology and functional synapses. *Proc Natl Acad Sci U S A* 106, 328-333.
8. Kukley M, Capetillo-Zarate E, & Dietrich D (2007) Vesicular glutamate release from axons in white matter. *Nat Neurosci* 10, 311-320.
9. De Biase LM, Nishiyama A, & Bergles DE (2010) Excitability and synaptic communication within the oligodendrocyte lineage. *J Neurosci* 30, 3600-3611.
10. Etxeberria A, Mangin JM, Aguirre A, & Gallo V (2010) Adult-born SVZ progenitors receive transient synapses during remyelination in corpus callosum. *Nat Neurosci* 13, 287-289.
11. Nait-Oumesmar B, Decker L, Lachapelle F, Avellana-Adalid V, Bachelin C, & Van Evercooren AB (1999) Progenitor cells of the adult mouse subventricular zone proliferate, migrate and differentiate into oligodendrocytes after demyelination. *Eur J Neurosci* 11, 4357-4366.
12. Klee R, Heinemann U, & Eder C (1999) Voltage-gated proton currents in microglia of distinct morphology and functional state. *Neuroscience* 91, 1415-1424.
13. Yuan X, Chittajallu R, Belachew S, Anderson S, McBain CJ, & Gallo V (2002) Expression of the green fluorescent protein in the oligodendrocyte lineage: a transgenic mouse for developmental and physiological studies. *J Neurosci Res* 70, 529-545.
14. Kukley M, Nishiyama A, & Dietrich D (2010) The fate of synaptic input to NG2 glial cells: neurons specifically downregulate transmitter release onto differentiating oligodendroglial cells. *J Neurosci* 30, 8320-8331.
15. Watanabe M, Toyama Y, & Nishiyama A (2002) Differentiation of proliferated NG2-positive glial progenitor cells in a remyelinating lesion. *J Neurosci Res* 69, 826-836.
16. Clarke LE, Young KM, Hamilton NB, Li H, Richardson WD, & Attwell D (2012) Properties and fate of oligodendrocyte progenitor cells in the corpus callosum, motor cortex, and piriform cortex of the mouse. *J Neurosci* 32, 8173-8185.
17. Moll NM, Hong E, Fauveau M, Naruse M, Kerninon C, Tepavcevic V, Klopstein A, Seilhean D, Chew L-J, Gallo V, *et al.* (2013) SOX17 is Expressed in Regenerating Oligodendrocytes in Experimental Models of Demyelination and in Multiple Sclerosis. *Glia* In Press.
18. Wake H, Moorhouse AJ, Jinno S, Kohsaka S, & Nabekura J (2009) Resting microglia directly monitor the functional state of synapses in vivo and determine the fate of ischemic terminals. *J Neurosci* 29, 3974-3980.
19. Maldonado PP, Velez-Fort M, & Angulo MC (2011) Is neuronal communication with NG2 cells synaptic or extrasynaptic? *J Anat* 219, 8-17.
20. Hamilton TG, Klinghoffer RA, Corrin PD, & Soriano P (2003) Evolutionary divergence of platelet-derived growth factor alpha receptor signaling mechanisms. *Mol Cell Biol* 23, 4013-4025.
21. Vélez-Fort M, Maldonado PP, Butt AM, Audinat E, & Angulo MC (2010) Postnatal switch from synaptic to extrasynaptic transmission between interneurons and NG2 cells. *J Neurosci* 30, 6921-6929.
22. Dugue GP, Brunel N, Hakim V, Schwartz E, Chat M, Levesque M, Courtemanche R, Lena C, & Dieudonne S (2009) Electrical coupling mediates tunable low-frequency oscillations and resonance in the cerebellar Golgi cell network. *Neuron* 61, 126-139.
23. Tepavcevic V, Lazarini F, Alfaro-Cervello C, Kerninon C, Yoshikawa K, Garcia-Verdugo JM, Lledo PM, Nait-Oumesmar B, & Baron-Van Evercooren A (2011) Inflammation-induced subventricular zone dysfunction leads to olfactory deficits in a targeted mouse model of multiple sclerosis. *J Clin Invest* 121, 4722-4734.
24. Lassmann H (1998) Neuropathology in multiple sclerosis: new concepts. *Mult Scler* 4, 93-98.

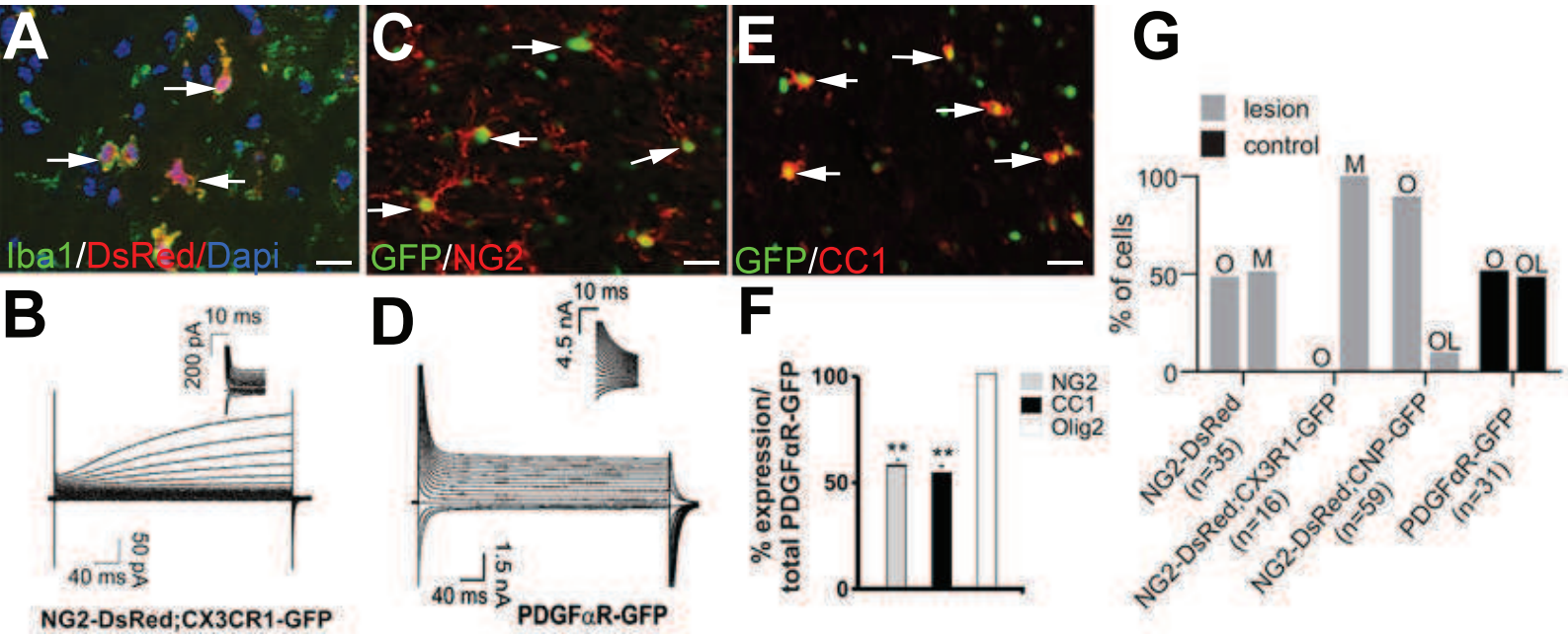
A
Iba1/DsRed/Dapi
C
GFP/NG2
E
GFP/CC1
G
lesion
control
% of cells
100
50
0
O
M
O
M
O
O
OL
O
OL
NG2-DsRed (n=35)
NG2-DsRed;CX3R1-GFP (n=16)
NG2-DsRed;CNP-GFP (n=59)
PDGFαR-GFP (n=31)
B
10 ms
200 pA
50 pA
40 ms
NG2-DsRed;CX3CR1-GFP
D
10 ms
4.5 nA
1.5 nA
40 ms
PDGFαR-GFP
F
% expression/ total PDGFαR-GFP
100
50
0
**
**
NG2
CC1
Olig2

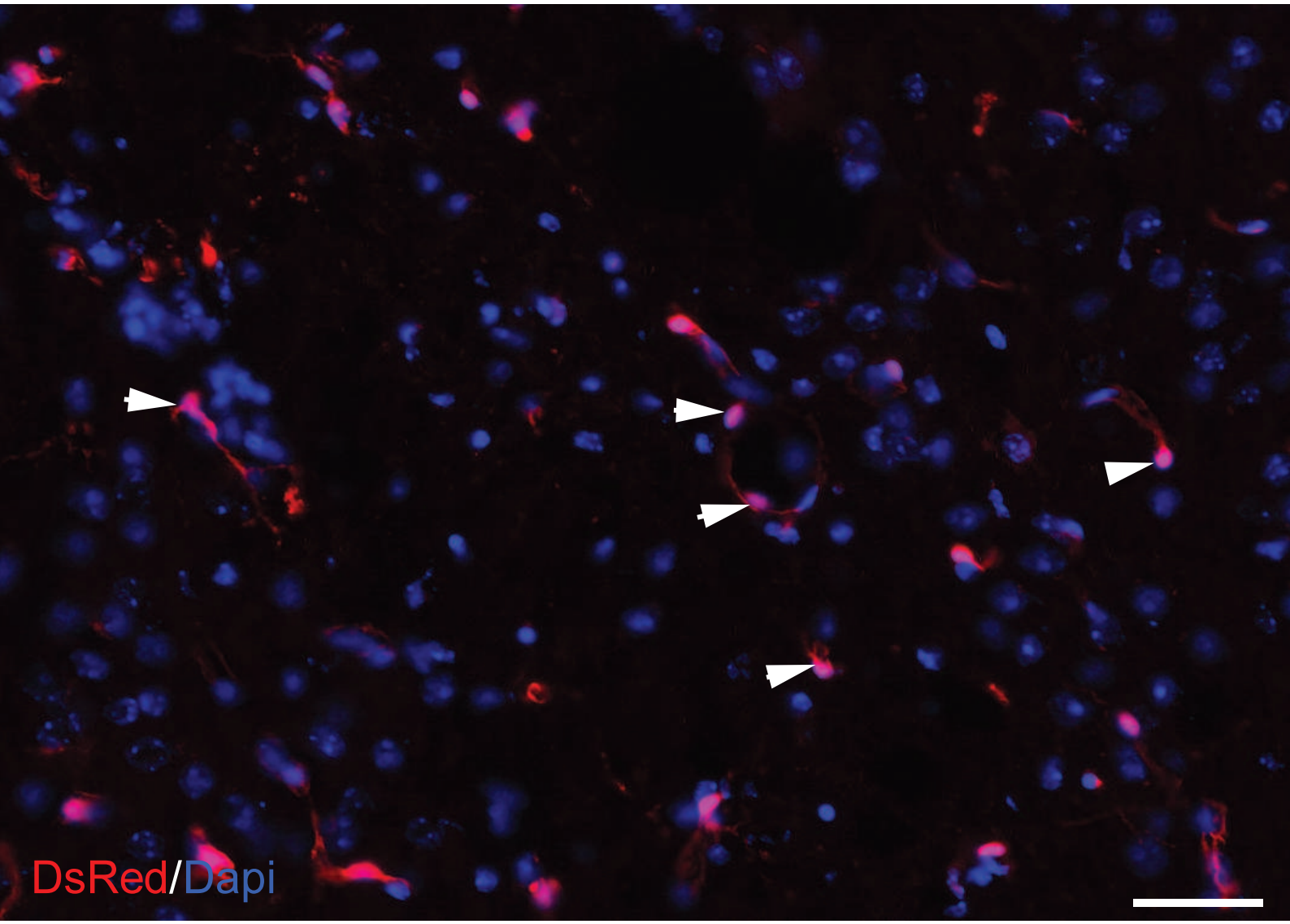
DsRed/Dapi

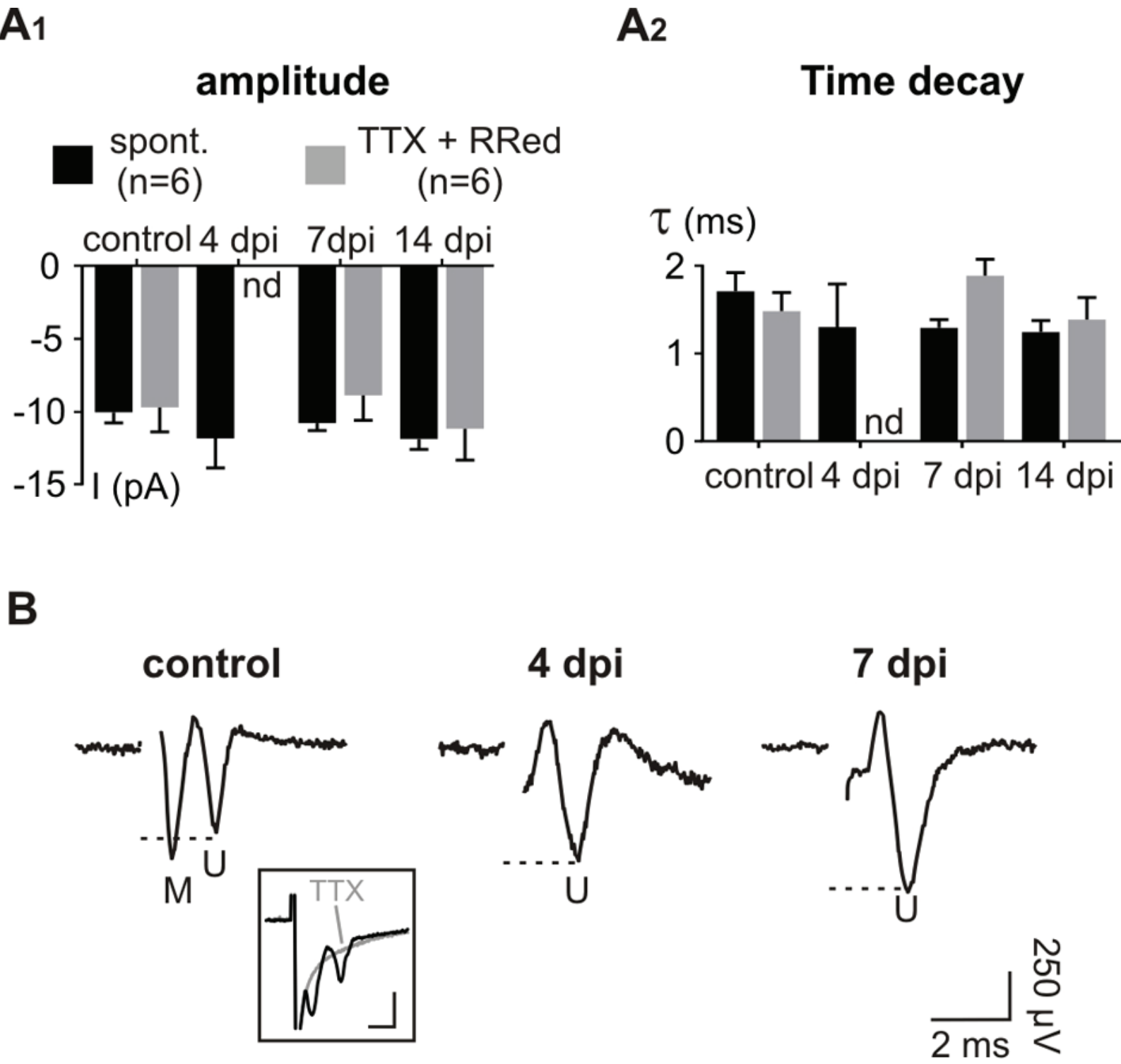
A1
amplitude
spont.
(n=6)
TTX + RRed
(n=6)
control
4 dpi
7dpi
14 dpi
0
-5
-10
-15
nd
I (pA)
A2
Time decay
τ (ms)
2
1
0
nd
control
4 dpi
7 dpi
14 dpi
B
control
4 dpi
7 dpi
M
U
TTX
U
U
250 µV
2 ms

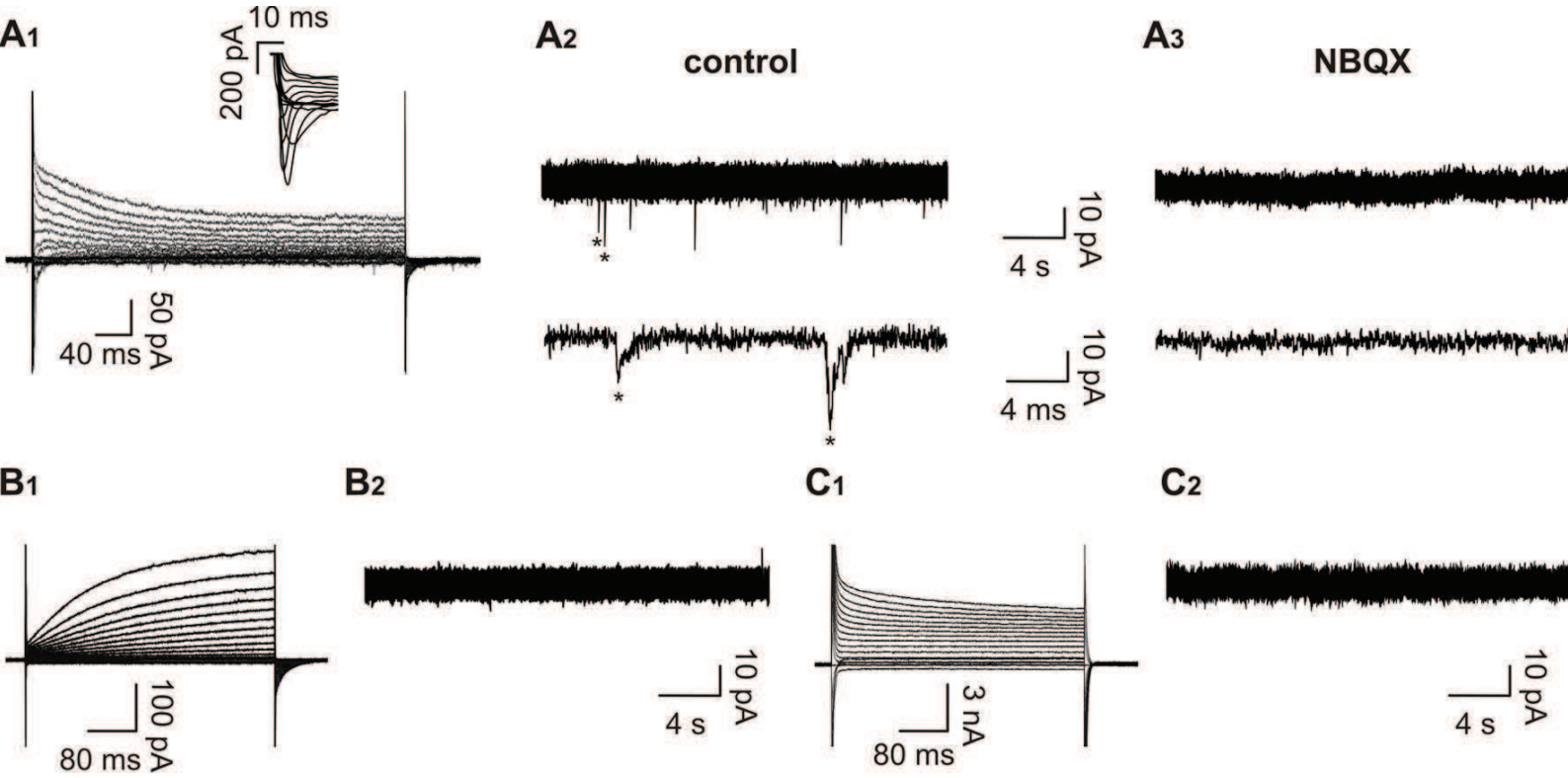
A1
10 ms
200 pA
50 pA
40 ms
A2
control
10 pA
4 s
10 pA
4 ms
A3
NBQX
B1
100 pA
80 ms
B2
10 pA
4 s
C1
3 nA
80 ms
C2
10 pA
4 s

SUPPLEMENTARY INFORMATIONS

Figure S1. Immuno-characterization and electrophysiological properties of fluorescent cells in different transgenic lines.

A. Iba1+ resident microglia/macrophage expressing DsRed in NG2-DsRed mouse strain. **B**. Currents induced by voltage steps from +40 mV to -120 mV in a $DsRed^{+}$ microglia held at -90 mV. Note the absence of I_{Na+} (inset). We confirmed that DsRed was expressed in activated microglia inside lesions by crossing NG2-DsRed line with the CX3CR1-EGFP strain in which microglia/macrophages express GFP (1). All DsRed+/GFP+ cells recorded from this double transgenic mouse had an electrophysiological phenotype of cultured activated microglia (**B**). Our data show that activated microglia/macrophages express the NG2 proteoglycan under pathological conditions as recently suggested (2). **C, E**. NG2+ OPCs (**C**, arrows) and CC1+ differentiated oligodendrocytes (**E**, arrows) in PDGFRα-GFP mouse strain. **D**. Currents induced by voltage steps from +40 mV to -120 mV in an oligodendrocyte held at -90 mV in a PDGFRαR-GFP mouse. Note the absence of I_{Na+} (inset). **F**. Histograms showing the percentage of NG2+ and CC1+ cells within control and lesioned corpus callosum in the PDGFRα-GFP strains (n≥ 4). **p<0.01 with respect to Olig2 expression. **G**. Histogram of the proportion of OPCs (O), microglia (M) and oligodendrocyte (OL) identified by their electrophysiological profiles and recorded in different mouse strains. Scale bars for A, C, E, 20 µm.

Figure S2. Expression of DsRed in a healthy adult NG2-Red mouse brain.

Sagittal brain section through the *corpus callosum* of 2 month-old control NG2-DsRed mouse. At the adult stage, the expression of DsRed is only detected in pericytes around blood vessels (arrowheads). Scale bar, 50 μm.

Figure S3. Properties of spontaneous and miniature events of OPCs and CAPs in demyelinated lesions.

A1, A2. Comparison of the amplitude (**A1**) and decay time (**A2**) of spontaneous and miniature synaptic currents. The large decrease of connected OPCs and the low frequency of connected cells at 4 dpi precluded the detection of miniature events at this time point (nd, see Fig. 2). **B**. CAPs in control and in lesions at 4 and 7 dpi obtained after subtracting averaged traces before and after application of 1 μM TTX (3-5 sweeps; inset). Note that the first peak corresponding to myelinated fibers (M) is lost in early stages of remyelination. CAPs produced by unmyelinated fibers (U) are distinguished in lesions by their slower conduction velocity. Inset scale bar: 1 ms; 500 μs.

Figure S4. OPCs display NBQX-sensitive spontaneous synaptic activity while microglia and oligodendrocytes completely lack synaptic events.

A1. Currents elicited in a OPC at 7 dpi by voltage steps from +40 mV to -120 mV. Note the presence of I_{Na+} (inset). **A2, A3**.Spontaneous synaptic currents recorded at -90 mV from the same OPC in control (**A2**, frequency: 1.34 Hz) and after bath applying 10 μM NBQX (**A3**, frequency: 0 Hz). **B1, C1**. Currents induced by voltage steps from +40 mV to -120 mV in a microglia at 7 dpi (**B1**) and an oligodendrocyte at

14 dpi (**C1**) held at -90 mV. **B2, C2**. Currents recorded at -90 mV from the same cells. Note the lack of synaptic events in both cells types (n=12 and n=14 for microglia and oligodendrocytes, respectively).

SUPPLEMENTARY REFERENCES

1. Avignone E, Ulmann L, Levavasseur F, Rassendren F, & Audinat E (2008) Status epilepticus induces a particular microglial activation state characterized by enhanced purinergic signaling. *J Neurosci* 28, 9133-9144.
2. Zhu L, Xiang P, Guo K, Wang A, Lu J, Tay SS, Jiang H, & He BP (2012) Microglia/monocytes with NG2 expression have no phagocytic function in the cortex after LPS focal injection into the rat brain. *Glia* 60, 1417-1426.